

# **Mechanical Characterisation and Computational Modelling of Spinal Ligaments**

Miss Ayesha Bint-E-Siddiq

Submitted in accordance with the requirements for the degree of  
**Doctor of Philosophy**

The University of Leeds  
Institute of Medical and Biological Engineering  
School of Mechanical Engineering

July, 2019

The candidate confirms that the work submitted is her own and that appropriate credit has been given where reference has been made to the work of others.

This copy has been supplied on the understanding that it is copyright material and that no quotation from the thesis may be published without proper acknowledgement.

The right of Miss Ayesha Bint-E-Siddiq to be identified as Author of this work has been asserted by her in accordance with the Copyright, Designs and Patents Act 1988.

© 2019 The University of Leeds and Miss Ayesha Bint-E-Siddiq

For my Mum & Dad, Samina & Siddiq

## Acknowledgements

Over the course of my PhD, I have had the honour of working with some incredible people without whom I would not be here today. It is an acknowledgement to these people, who have supported me throughout this journey with their continuous advice, help and guidance. I would also like to express my gratitude towards people without whom I would not have come this far.

First and foremost, I would like to thank my primary supervisor Professor Ruth Wilcox, who has always been ever so helpful. Her cheerful and kind personality has lifted my morale on many occasions. Every time I needed some help or advice, she was just an email away. She has always had something constructive to add to even the most 'naïve' and 'silly' questions I have had and hence why I never hesitated in raising any concerns. I would also like to thank my co-supervisors Dr Alison Jones and Dr Marlène Mengoni who have also contributed immensely to my progress and have always given very thorough and timely feedback. Thank you all for your help and patience throughout the years. Words cannot do justice to the amount of gratitude I have, I could not have asked for a better team. It has been an incredible journey and your support is much appreciated.

I would like to extend my thanks to Phil Wood, Irvin Homan and Lee Whetherill and the rest of the technical staff within the School of Mechanical Engineering for their support and guidance. Special thanks to Dr Nagitha Wijayathunga without his help the human tissue work would not have been possible. His willingness to make time to help me when asked is commendable. Thanks to all my researcher friends for not only providing good office banter but also extending a helping hand whenever needed.

I sincerely thank my family without whom I would not be here today. In particular, my Mum and Dad, Samina and Siddiq, I have no words to acknowledge the sacrifices you made to make me successful. Your hard work and can-do attitude has always been an inspiration to me. Mum, your belief in me has kept me going even at difficult times. Thanks to my wonderful sister, Ajwa, for your patience and willingness to lend an ear whenever I needed a sounding board. Thanks to my lovely sisters Fozia and Aisha for your constant entertainment and support that helped me through low-moments. Special thanks to my amazing brothers Omar, Salman and Zaid for always believing in me. Your support and encouragement has lifted my spirits on many occasions.

Sincere and heart-felt gratitude to Ma (Shirin), Pa (Rashid) and Yasir for being ever so kind and thoughtful. And last but not the least, my wonderful husband, Yasiin, who have provided me with a listening ear whenever needed and have helped me get through hard times. This journey would not have been possible without you all and for that I am grateful to you all from the bottom of my heart.

## Abstract

Low back pain is a common complaint in people of all ages. The long-term success rates of many surgical devices to treat the spine have been relatively low and improved methods of pre-clinical testing of these devices are therefore needed. Sheep spine models are commonly employed in pre-clinical research studies for the evaluation of spinal devices. The anterior and posterior longitudinal ligaments (ALL and PLL) provide passive stability to the spine, however, limited studies have been conducted to characterise the mechanical properties of the ovine longitudinal ligaments or compare them to the human. Moreover, previous studies have derived material properties for the human ALL and PLL directly from force-displacement data, assuming uniform cross sectional area and length, and these values have been used extensively in finite element models of the spine for the analysis of clinical interventions.

The aim of this study was to develop a methodology to test and compare the stiffness of human and ovine spinal longitudinal ligaments and to uniquely combine experimental and specimen-specific finite element (FE) modelling approaches to determine the ligament mechanical properties.

The methodology was developed on ovine thoracic spines and then applied to human thoracic spines. The spines were dissected into functional spinal units (FSUs) with the posterior elements removed and imaged under micro computed tomography ( $\mu$ CT). The specimens were sectioned through the disc to leave only either the ALL or PLL intact and tested in tension to determine the stiffness. The  $\mu$ CT images from each FSU were used to build specimen-specific FE models of the ligaments and bony attachments. Hyper-elastic material models were used to represent the ligament behaviour. Initial values for the material model were derived using mean cross sectional area (CSA) and length (L), with the assumption that ligament was uniaxially loaded. The parameters were then iteratively changed until a best fit to the corresponding experimental load-displacement data was found for each specimen.

The stiffness of the ligaments for the ovine specimens were found to be higher than for the human specimens. This may have implications for the use of ovine FSUs for preclinical testing of devices. There was poor agreement between the material parameters derived from FE models and the initial values derived by assuming a mean CSA and L. This work demonstrates that a specimen-specific image-based approach needs to be applied to derive the elastic properties of the ligaments due to their non-uniform shape and cross-sectional area.

## Table of Contents

<b>Acknowledgements .....</b>	<b>i</b>
<b>Abstract .....</b>	<b>iii</b>
<b>Abbreviations .....</b>	<b>xix</b>
<b>Chapter 1 Introduction and Literature Review .....</b>	<b>1</b>
1.1 Introduction.....	1
1.2 Literature Review .....	3
1.2.1 Biomechanically Relevant Human Spinal Anatomy.....	3
1.2.2 Comparison of Human and Ovine Spine Anatomy.....	15
1.2.3 Biomechanics of Spine.....	18
1.2.4 Biomechanics of Spinal Ligaments .....	19
1.2.5 Experimental Testing of Spinal Ligaments .....	23
1.2.6 Finite Element Modelling of Ligaments .....	42
1.2.7 Material models for soft tissue modelling .....	52
1.3 Study Motivation, Aim and Objectives .....	57
<b>Chapter 2 Experimental Methods Development and Results for Ovine     Longitudinal Ligaments .....</b>	<b>60</b>
2.1 Introduction.....	60
2.2 Ovine Ligament Anatomy .....	60
2.2.1 Introduction .....	60
2.2.2 Methods .....	60
2.2.3 Results .....	61
2.2.4 Discussion.....	62
2.3 General Materials and Methods .....	64
2.3.1 Specimens .....	64
2.3.2 Dissection.....	64
2.3.3 Potting of Specimens .....	65
2.3.4 Mechanical Testing Setup.....	66
2.3.5 Load and Displacement Limits .....	67
2.4 Testing Protocol .....	68
2.4.1 Introduction .....	68
2.4.2 Method Development .....	69
2.4.3 Method Adopted.....	75
2.5 Methods of Data Analysis.....	77

2.6	Results and Analysis .....	80
2.7	Discussion .....	84
2.7.1	Discussion of testing methods and results .....	84
2.7.2	Comparison to published human data.....	86
2.7.3	Summary.....	87
<b>Chapter 3 Computational Methods Development and Results for Ovine Longitudinal Ligaments .....</b>		<b>88</b>
3.1	Introduction.....	88
3.2	Imaging Specimens.....	88
3.2.1	Introduction .....	88
3.2.2	Imaging Protocol .....	89
3.2.3	Use of Radiopaque Gel.....	90
3.3	Determination of Ligament Thickness over Disc .....	92
3.3.1	Introduction .....	92
3.3.2	Needle Indentation Test .....	92
3.3.3	Photographic Image Analysis.....	95
3.3.4	Discussion.....	97
3.4	Image Segmentation .....	97
3.4.1	Images Pre-processing .....	97
3.4.2	Segmentation of the Bone.....	98
3.4.3	Segmentation of the Ligament .....	99
3.5	Image Downsampling .....	101
3.6	Finite Element Method Development .....	105
3.6.1	Sensitivity Analysis.....	105
3.6.2	Summary.....	122
3.7	Final Methods of FE Modelling.....	123
3.7.1	FE Modelling of the ALL.....	123
3.7.2	FE Modelling of the PLL.....	124
3.8	Initial Results for the ALL Model with Material Data derived by Assuming Uniform Uniaxial Conditions.....	125
3.9	Method of Tuning the Material Properties.....	127
3.9.1	Theoretical Considerations.....	128
3.9.2	Effect of Varying Input Parameters .....	130
3.9.3	Parameter Tuning Methods.....	131
3.9.4	Parameter Tuning Results .....	135
3.10	Discussion .....	137



<b>Chapter 4 Application of Experimental &amp; Computational Methods to Human Longitudinal Ligaments</b> .....	<b>141</b>
4.1 Introduction.....	141
4.2 Methodology.....	141
4.2.1 Magnetic Resonance Imaging.....	141
4.2.2 Dissection.....	142
4.2.3 Specimen preparation and testing.....	142
4.2.4 Computational Modelling.....	143
4.3 Results .....	144
4.3.1 Comparison of Human and Ovine Thoracic Spine .....	144
4.3.2 Visual Observations, MRI and Photographic Images .....	147
4.3.3 Mechanical Testing .....	149
4.3.4 FE modelling and material parameter tuning .....	152
4.3.5 Comparison of Material Models.....	155
4.3.6 Comparison between Coefficients.....	157
4.3.7 Comparison by spine and by level .....	158
4.3.8 Comparison with other computational data .....	162
4.4 Discussion .....	165
4.4.1 Discussion of Experimental Results and Visual Observations 165	
4.4.2 Discussion of Finite Element Modelling.....	167
4.4.3 Comparison and Analysis of Material Parameters .....	168
4.4.4 Variability across Individual Spines and Spinal Levels.....	170
4.4.5 Comparison with Published Human Data.....	171
4.4.6 Conclusion .....	176
<b>Chapter 5 Discussion</b> .....	<b>177</b>
5.1 Introduction.....	177
5.2 Comparison of the stiffness values for human and ovine longitudinal ligaments .....	178
5.3 Comparison of the material parameters of human and ovine ligaments .....	181
5.4 Comparison with the literature on other ligaments .....	183
5.5 Limitations and future work.....	186
5.5.1 Limitations .....	186
5.5.2 Future recommendations .....	187
5.6 Conclusion.....	188

**List of References.....190**

## List of Tables

<b>Table 1.1: Comparison of Human and Ovine Spine Vertebrae (Adapted from Wilke, et al., 1997).</b> .....	<b>17</b>
<b>Table 1.2: Mechanical properties of anterior longitudinal ligament (ALL).</b> .....	<b>34</b>
<b>Table 1.3: Mechanical properties of posterior longitudinal ligament (PLL)</b> .....	<b>35</b>
<b>Table 1.4: Mechanical properties of ligamentum flavum (LF)</b> .....	<b>36</b>
<b>Table 1.5: Mechanical properties of intertransverse ligament (ITL)</b> .....	<b>37</b>
<b>Table 1.6: Mechanical properties of interspinous ligament (ISL)</b> .....	<b>38</b>
<b>Table 1.7: Mechanical properties of supraspinous ligament (SSL)</b> .....	<b>39</b>
<b>Table 1.8: Mechanical properties of joint capsular ligament (JCL)</b> .....	<b>39</b>
<b>Table 1.9: Material properties used by researchers in FE studies including the cross sectional area (CSA), Young's moduli (E) and transition strains (<math>\epsilon</math>). where, E1, E2 and E3 represent the Young's moduli of the polygonal stress-strain function while <math>\epsilon_1</math>, <math>\epsilon_2</math> and <math>\epsilon_3</math> are the corresponding transitions strains separating the Young's moduli with <math>\epsilon_3</math> being the maximum strain of the physiological range.</b> .....	<b>45</b>
<b>Table 1.10: Comparison of different elements types used by researchers in FE modelling of lumbar spine</b> .....	<b>49</b>
<b>Table 1.11: List of various hyperelastic material models and their respective Abaqus implementation strain energy potentials which can be used for FE modelling of ligaments. (ABAQUS, 2011)</b> .....	<b>55</b>
<b>Table 2.1: Initial ovine spine dissection comparing images of the ligaments identified in both lumbar and thoracic region with the cranial end on the right side of all the images.</b> .....	<b>62</b>
<b>Table 2.2: The 'toe region' (<math>k_1</math>) and final 'linear region' (<math>k_2</math>) stiffness values, calculated by fitting least squares slopes to the post-processed load displacement curves of ALL, alongside the level and the spine the specimen was obtained from. The whole group mean and standard deviation (S.D.) are also shown.</b> .....	<b>82</b>
<b>Table 2.3: The 'toe region' (<math>k_1</math>) and final 'linear region' (<math>k_2</math>) stiffness values, calculated by fitting least squares slopes to the post-processed load displacement curves of PLL, alongside the level and the spine the specimen was obtained from. The whole group mean and standard deviation (S.D.) are also shown.</b> .....	<b>83</b>
<b>Table 3.1: <math>\mu</math>CT scanner settings used on a SCANCO <math>\mu</math>CT100 device to image FSUs with the ligaments intact</b> .....	<b>89</b>

<b>Table 3.2: Thickness values of a ligament obtained after conversion from pixels to millimetres over disc and corresponding bone regions.....</b>	<b>96</b>
<b>Table 3.3: An example of image downsampling from original resolution of 0.074mm to how the optimum of 0.6mm was arrived at.....</b>	<b>102</b>
<b>Table 3.4: The various downsampling algorithms along with the volume of ligament and the final model generated by each.....</b>	<b>103</b>
<b>Table 3.5: Geometric parameters used for the development of idealised rectangular models of ligament.....</b>	<b>106</b>
<b>Table 3.6: Contour plots obtained for Rec_A, Rec_B and Real_A alongside the scale in mm showing displacement in the direction of stretch (U3) .....</b>	<b>109</b>
<b>Table 3.7: The displacements in the x (U1), y (U2) and z (U3) directions obtained for Rec_C and Rec_D showing that the greatest variation occurs over the section corresponding to the disc region.....</b>	<b>114</b>
<b>Table 3.8: Material coefficient values obtained for the various material models used for modelling ALL. ....</b>	<b>127</b>
<b>Table 3.9: The final material coefficients obtained as a result of material tuning.....</b>	<b>136</b>
<b>Table 4.1: List of specimens according to the level of the spine and the ligament tested alongside the gender and age for each donor. ...</b>	<b>143</b>
<b>Table 4.2: Differences in the thickness of the ALL across the three spines with white lines drawn over the images of specimens (row 1) to highlight the edges of the ligament while the unaltered images are presented in 2<sup>nd</sup> row showing that Spine 3 have the thickest and Spine 1 the thinnest ALL. ....</b>	<b>148</b>
<b>Table 4.3: The ‘toe region’ (k1) and ‘linear region’ (k2) stiffness values calculated by fitting least squares slopes to the post-processed load displacement curves of the ALL specimens. The level and the spine the specimen was obtained from are indicated in the specimen name.....</b>	<b>150</b>
<b>Table 4.4: The ‘toe region’ (k1) and ‘linear region’ (k2) stiffness values calculated by fitting least squares slopes to the post-processed load displacement curves of the PLL. The level and the spine the specimen was obtained from are indicated in the specimen name. ....</b>	<b>151</b>
<b>Table 4.5: Percentage difference between experimental input and specimen-specific FE-output using material parameters derived by the in-built Abaqus calibration code assuming mean cross-sectional area and length for all the specimens of ALL and PLL. ....</b>	<b>153</b>
<b>Table 4.6: Calibrated material parameters for Ogden (N=1) and hyperfoam material models obtained as a result of the material optimisation procedure undertaken on the specimen-specific FE models by the author.....</b>	<b>155</b>

<b>Table 4.7: Estimated values of the stress-strain gradient at 12% strain (E) from the material parameters for all the specimens of ALL (n=7).</b> .....	<b>163</b>
<b>Table 4.8: Estimated values of the stress-strain gradient at 20% strain (E) from the material parameters for all the specimens of PLL (n=7).</b> .....	<b>164</b>
<b>Table 5.1: Results of ANOVA performed to compare the stiffness between human and ovine ALL and PLL specimens separately for the toe-region (K1) and linear-region (K2) stiffness.</b> .....	<b>180</b>

## List of Figures

<b>Figure 1.1: Schematic representation of three views of the vertebral column; Anterior view (left) posterior view (middle) lateral view (right) showing cervical, thoracic, lumbar, sacrum and coccyx regions, both the lordosis in the cervical and lumbar region and the kyphosis in the thoracic and sacrum region are noticeable. (Adapted from Micheau &amp; Hoa, 2009). .....</b>	<b>4</b>
<b>Figure 1.2: A typical lumbar vertebrae showing (a) top view and (b) lateral view. (Adapted from Emory University, 1997).....</b>	<b>5</b>
<b>Figure 1.3: The structure of trabeculae. (a) Sagittal section of a lumbar vertebral body with its vertical (VT) and transverse (TT) trabeculae seen in white. (b) Schematic representation of the internal structure (c) shows the ability of the structure to withhold its shape under loading. (Adapted from Bogduk, 2005).....</b>	<b>6</b>
<b>Figure 1.4: The motion of intervertebral joints in flexion and extension. (Adapted from PainNeck.com, 2010).....</b>	<b>7</b>
<b>Figure 1.5: Schematic representations of the intervertebral disc. (a) The anatomical regions in a mid-sagittal cross-section. (b) A three dimensional view of the disc illustrating annulus fibrosus lamellar structure. (Adapted from Smith et al. 2011).....</b>	<b>8</b>
<b>Figure 1.6: A view of spinal ligaments from the front of the vertebral bodies with the top body excised (adapted from Eidelson, 2012). ..</b>	<b>10</b>
<b>Figure 1.7: A schematic of micro to macro level structure of a typical ligament (adapted from Panagos, 2015). .....</b>	<b>13</b>
<b>Figure 1.8: Microradiograph image of sagittal decalcified section through a neonate lumbar spine with anterior side on the left. Image shows short fibres of ALL (open arrows), long fibres of ALL (solid arrows), penetration into annulus fibrosus (AF), and cartilaginous endplates (C). (Adapted from Francois, 1975). .....</b>	<b>15</b>
<b>Figure 1.9: The range of motion exhibited by cervical spine or spine in general. (Adapted from Banton, 2012). .....</b>	<b>18</b>
<b>Figure 1.10: A typical load-deformation curve of a ligament illustrating the three regions: the neutral zone (NZ), the elastic zone (EZ) and the plastic zone (PZ). (Adapted from White III &amp; Panjabi, 1990). ...</b>	<b>20</b>
<b>Figure 1.11: Force deformation curve for spinal ligaments of lumbar region (Adapted from White III &amp; Panjabi, 1990). .....</b>	<b>21</b>
<b>Figure 1.12: A comparison of purely elastic (a) and viscoelastic (b) material showing hysteresis presented by the viscoelastic material.....</b>	<b>22</b>
<b>Figure 1.13: Schematic representation of specimen fixation (Adapted from Myklebust, et al., 1988) .....</b>	<b>31</b>
<b>Figure 1.14: Photograph of the FSU in the metal cup (Adapted from Dumas, et al., 1987) .....</b>	<b>31</b>

<b>Figure 1.15: Graph showing stress-strain relationship for PLL used by different researchers in their FE models .....</b>	<b>46</b>
<b>Figure 1.16: Typical tensile stress-strain curve of a foam (adapted from ABAQUS, 2011). .....</b>	<b>56</b>
<b>Figure 2.1: Photographs of the ovine thoracic FSU with all the ligaments intact. (a) Lateral view: interspinous and supraspinous ligaments are visible, (b) Anterior view: anterior longitudinal ligament (longitudinal band) and intervertebral disc can be seen. ....</b>	<b>64</b>
<b>Figure 2.2: The process of attaching cement endcaps to the specimen: (a) the specimen is held in place within a mould, using a steel rod through the spinal canal to locate the specimen; (b) cement is then poured into the mould and allowed to set; (c) the other end of the FSU is cemented, the pots are aligned using metal guides and spirit level; (d) the FSU with cement endcaps ready for mechanical testing. ....</b>	<b>66</b>
<b>Figure 2.3: Load-displacement graph of a specimen tested to failure to obtain maximum limits for load and displacement to be used in future testing. ....</b>	<b>68</b>
<b>Figure 2.4: Experimental setup: Initial testing (left); Testing after ISL transection (right). ....</b>	<b>69</b>
<b>Figure 2.5: Load-displacement curves for the entire set of experiments in Test I from the specimen in the intact state through to the transection of the IVD. The initial pre-conditioning step (dark-blue curve) was undertaken to remove any loosening in the set-up, then the loading regime was repeated for the specimen in the intact state (red curve) and following removal of the ligaments and disc in subsequent steps. ....</b>	<b>70</b>
<b>Figure 2.6: Load-displacement curves obtained from Test II from the specimen in the intact state (with transected IVD) through to the transection of the PLL. ....</b>	<b>71</b>
<b>Figure 2.7: A comparison of the load-displacement behaviour for the PLL from both Test I and Test II. The curves exhibit completely different shapes but very similar linear slopes (black lines in the graph).....</b>	<b>72</b>
<b>Figure 2.8: Photographs of the FSU in Test II after the transection of all the ligaments. Anterior view (left image) and lateral view (right image) both show the presence of fibres keeping the vertebrae attached. ....</b>	<b>72</b>
<b>Figure 2.9: An ovine FSU (lateral view) divided into an anterior (top-anterior view) and posterior (lateral view) section with the anterior section used for testing. ....</b>	<b>73</b>
<b>Figure 2.10: An example of a typical hysteresis observed on specimens after five cycles of pre-loading to 1mm. ....</b>	<b>74</b>

- Figure 2.11: Load-displacement curves obtained from Test III from the specimen in the intact state through to the transection of the IVD to test the behaviour of ALL alone (only Positive displacements are shown). The initial pre-conditioning cycle (dark-blue curve) was undertaken to remove any loosening in the set-up, then the cycle was repeated for the specimen in the intact state (red curve) and following transection of the PLL and IVD in subsequent steps. The thicker regions on red, purple and orange curves are the five cycles of pre-loading that were undertaken to ensure the behaviour was repeatable.....75**
- Figure 2.12: Anterior view (a) and posterior view (b) of the vertebral bodies after the removal of posterior elements. ....76**
- Figure 2.13: An example of 1st and 2nd derivative of a load-displacement curve. (a) & (c) shows the raw data, (b) & (d) filtered data after performing the smoothing operation.....78**
- Figure 2.14: An example of how systematic data analysis method is used to calculate ‘toe region’ (k1) and ‘linear region’ (k2) stiffness values.....80**
- Figure 2.15: An example of load-extension slopes of all the steps followed for a specimen showing repeated hysteresis in pre-loading cycles. The thicker area of the slopes is the five cycles of pre-loading performed up to 1mm extension before the final loading step.....81**
- Figure 2.16: The trimmed load-extension curves for all ALL specimens. The level and the spine the specimen was obtained from are indicated in the specimen name.....82**
- Figure 2.17: The trimmed load-extension curves for all PLL specimens. The level and the spine the specimen was obtained from are indicated in the specimen name.....83**
- Figure 2.18: Comparison of ovine and human (Pintar, et al., 1992) linear-region stiffness for both ALL and PLL showing mean stiffness values. Error bars depict standard deviation values. ....84**
- Figure 3.1: sagittal view taken from a  $\mu$ CT scan of an ovine vertebra, including the ALL and PLL, without contrast agent. ....90**
- Figure 3.2: Different concentrations of Nal gel in relation to the bone as seen on  $\mu$ CT scans with concentrations of (a) 0.2 mol, (b) 0.4 mol, (c) 0.6 mol. ....91**
- Figure 3.3: Cross-sections through a vertebral sample (a) without and (b) with Nal gel showing the difference in ALL appearance after the application of gel. In these images, the contrast has been increased and the bone has been segmented (red region) in order to provide a better contrast between the ligament and background for comparison.....92**
- Figure 3.4: Needle-Indentation test (a) over the bone region and (b) over the disc region (b) to measure the thickness of (a) ALL and (b) PLL in both regions.....93**



- Figure 3.5: Examples of force-displacement graphs of needle indentation into different tissues. (a) For the ligament-bone region: the transition from ligament to bone is apparent and could be used to calculate the thickness of ligament. (b) For the ligament-disc region: there is no transition of gradients, showing the similarity in the response from both ligament and disc.....94**
- Figure 3.6: Process of measuring the ligament thickness: (a) sagittal view of the disc section (left) and PMMA-cemented-bone section (right), (b) calibration of the image from pixels to mm, (c) measurement of the ligament thickness over the disc region, (d) measurement of the ligament thickness over the bone region. ....96**
- Figure 3.7: (a)  $\mu$ CT sagittal view of an FSU with the PMMA cement on each end, (b) cropped image of (a) following removal of the cement and unwanted regions leaving the image area only covering the ligament to be segmented and small sections of attaching bones and disc.....98**
- Figure 3.8: Segmentation of bone (a) after the use of thresholding to capture the bone tissue only, and (b) after the use of floodfill, to separate inferior and superior vertebra masks, and after closing all the respective holes and gaps.....98**
- Figure 3.9: ligament mask manually painted over every 5th slice of bone region only.....99**
- Figure 3.10: segmentation of ligament (a) before and (b) after the application of 'Boolean operations' whereby the yellow regions show the overlapping regions between the bones and the ligament.....100**
- Figure 3.11: (a) creation of an oval shape between the superior and inferior vertebrae to represent disc, (b) the overlapping region (blue area) between the disc and the ligament, (c) final ligament mask after using 'Boolean operations' to remove the unwanted region.....101**
- Figure 3.12: Discontinuities in the ligament mask as a result of downsampling.....104**
- Figure 3.13: Final 3-D volume of the masks after dilate and smoothing tools have been applied, showing (a) the ALL, superior vertebra, inferior vertebra and disc, (b) the PLL with superior and inferior vertebrae.....104**
- Figure 3.14: Sagittal view through segmented microCT image showing the measurements used for the development of the equivalent rectangular models ( $L_n$  = length,  $t_{max}$  = maximum thickness,  $t_{min}$  = minimum thickness). .....106**
- Figure 3.15: Final meshed model of ALL ready to be exported. ....107**
- Figure 3.16: Boundary conditions and loads applied to models (a) Rec\_A, (b) Rec\_B and, (c) Real\_A. ....108**

- Figure 3.17: Expressions to theoretically calculate the approximate length of ligament (a) post-stretching, assuming it to be part of a circle. ....110**
- Figure 3.18: Lateral view of a meshed ligament in Abaqus to measure the curved distance between top and bottom of ligament i.e. length of ligament (c) and difference between the ends and middle of the ligament (perpendicular distance between lines) i.e. curve (h) of ligament. The green region shows the meshed anterior side of the ligament. ....110**
- Figure 3.19: Schematic of the Rec\_C model boundary conditions. (a) Ligament with bone and disc attachment regions identified, (b) image of model with side-plate tied to the top region, (c) front view of model with BCs and load.....112**
- Figure 3.20: Mesh convergence study on simple rectangular model, showing the predicted U3 displacement (note: U3 scale does not start at zero) for models using hexahedral and tetrahedral elements. ....117**
- Figure 3.21: (a) Schematic of ligament with idealised rectangular bone to represent superior-vertebra. (b) Rec\_E model with load applied to the reference point on top via a rigid plate and encastre BCs on the inferior vertebra and the restriction of the reference point at the top to move in the directions of the stretch only.....119**
- Figure 3.22: Curve-fitting of different material models using the Abaqus software applied to data from an experimental specimen (Chapter 2). Both Ogden and Mooney-Rivlin models depicted similar behaviour to the experimental input. Neo Hookean behaved like a linear-elastic material and hence was discarded as an option for modelling the ligament behaviour.....121**
- Figure 3.23: Comparison of FE force-displacement curves from all material models with the experimental force-displacement curve. ....122**
- Figure 3.24: shows (a) anterior and (b) posterior view of a realistic ligament (ALL) model in Abaqus with the load and boundary conditions highlighted. ....124**
- Figure 3.25: (a) Anterior and (b) posterior view of the PLL model in Abaqus with the load and boundary conditions highlighted.....125**
- Figure 3.26: Comparison between experimental input for a specimen of ALL (ALL1) and FE model results from all three material models in the form of force-displacement curves in the direction of the stretch.....126**
- Figure 3.27: Comparison between experimental input for a specimen of ALL (ALL1) and FE models results for a single element in the form of stress-strain curves in the direction of the stretch. The stress-strain curves were obtained from the same element in all three models located on the surface of the middle section the ligament i.e. the section covering the disc region.....126**

<b>Figure 3.28: Comparison between the experimental input and FE model results with the variation of <math>\alpha</math> in increments of 10% from its original value of 4.22. ....</b>	<b>130</b>
<b>Figure 3.29: Comparison between the experimental input and FE model results with the variation of <math>\mu</math> from its original value of 0.00375 GPa. ....</b>	<b>131</b>
<b>Figure 3.30: Flowchart describing the general process for material tuning.....</b>	<b>132</b>
<b>Figure 3.31: The visually-best-matched force-displacement curve for Ogden (N=1) material tuning for the ALL model. ....</b>	<b>133</b>
<b>Figure 3.32: The method of finding the error between experimental input and FE output. ....</b>	<b>133</b>
<b>Figure 3.33: (a) example of plots obtained from matlab comparing the input and closest matched output along with (b) a plot of mean percentage difference between inputs and outputs for a model of ALL.....</b>	<b>134</b>
<b>Figure 3.34: Plots obtained from matlab comparing the input and closest matched output for PLL, stating the mean percentage difference for (a) Ogden (N=1) and (b) hyperfoam material models. ....</b>	<b>136</b>
<b>Figure 4.1: Examples of the ovine (a) and human (b) cemented FSU illustrating the difference in height (cm).....</b>	<b>145</b>
<b>Figure 4.2: Examples of the (a) ovine and (b) human disc illustrating the difference in colour and appearance. ....</b>	<b>146</b>
<b>Figure 4.3: Photographs of the anterior spine following dissection through the spinal canal showing the differences in the appearance of the (a) ovine and (b) human PLL. ....</b>	<b>146</b>
<b>Figure 4.4: Photographs of the anterior spine showing differences in the appearance of (a) ovine and (b) human ALL.....</b>	<b>146</b>
<b>Figure 4.5: Comparison of (a) photographic (anterior view) and (b) MRI image (sagittal view) showing the damage to the specimen (circled area) as well as cuts in the ALL (superimposed arrows) for a specimen (2:T10-11) chosen to be tested for the PLL.....</b>	<b>147</b>
<b>Figure 4.6: Sagittal view of three specimens of Spine 1 showing bone and disc protrusion in specimen (a) T2-3 and (b) T4-5 leading to stretching of the ALL, and specimen (c) T10-11 showing the fusion of disc and bone on the anterior side as a result of ossification.</b>	<b>148</b>
<b>Figure 4.7: (a) Anterior and (b) top-anterior view of the FSU (Spine 1:T6-7) showing bone compression leading to disc protrusion and bony infusion with the disc. ....</b>	<b>149</b>
<b>Figure 4.8: Post-processed load-displacement slopes for all the seven human specimens tested for ALL. ....</b>	<b>150</b>
<b>Figure 4.9: Post-processed load-displacement slopes for all the seven human specimens tested for PLL. ....</b>	<b>151</b>

- Figure 4.10: An example of a comparison between the experimental input and resulting FE predicted force-extension behaviour using the Ogden material model for specimen 1:T2-3. The FE material parameters were determined using a mean cross-sectional area and length under the assumption of a uniaxial stress. The disparity in the resulting curves demonstrates that these assumptions were incorrect. ....153**
- Figure 4.11: An example of a comparison of experimental input with pre-optimised and post-optimised FE outputs illustrating the effect of material calibration on Ogden material model for specimen 1:T2-3. ....154**
- Figure 4.12: Graphical comparison of the material coefficient  $\mu$  for both (a) ALL and (b) PLL derived using the two material models, showing that they are very similar hence either material model could be used for further analysis. ....156**
- Figure 4.13: Graphical comparison of the material coefficient  $\alpha$  for both (a) ALL and (b) PLL derived using the two material models showing that they are related hence either material model could be used for further analysis. ....157**
- Figure 4.14: Material coefficients plotted against each other for Ogden (N=1) material model. The figure illustrates that both coefficients are not related and hence both have to be discussed in further analysis.....158**
- Figure 4.15: Comparison of  $\mu$  for Ogden (N=1) for (a) ALL and (b) PLL specimens by spine (left to right is from upper to lower levels). In the case of the ALL, there were bigger differences between spines than within each spine. ....159**
- Figure 4.16: Comparison of  $\alpha$  for Ogden (N=1) for (a) ALL and (b) PLL specimens by spine (left to right is from upper to lower levels). In the case of the PLL, there are bigger differences between spines than within each spine. ....160**
- Figure 4.17: Comparison of  $\mu$  for Ogden (N=1) for (a) ALL and (b) PLL specimens by level showing big differences across individuals but no clear trends between levels are evident. ....161**
- Figure 4.18: comparison of  $\alpha$  for Ogden (N=1) for (a) ALL and (b) PLL specimens by level showing big differences across individuals in the case of PLL but no clear trends between levels are evident. 162**
- Figure 4.19: Comparison of Young's modulus (E) between the average value of ALL from the current study and the data cited by computational studies. \*others include; Lee & Teo (2005), Polikeit et al. (2003), Lee & Teo (2004), Sylvestre et al. (2007), Bowden et al. (2008), Tsuang et al. (2009), Moramarco et al. (2010) .....164**

<b>Figure 4.20: Comparison of Young's modulus (E) between the average value of PLL from the current study and the data cited by computational studies. *others include; Lee &amp; Teo (2005), Tsuang et al. (2009) **others include; Lee &amp; Teo (2004), Sylvestre et al. (2007), Bowden et al. (2008).....</b>	<b>165</b>
<b>Figure 4.21: A schematic illustration of anterior flexion in healthy FSU and in degenerated FSU due to anterior ossification. (a) illustrates an FSU of an healthy individual in a resting state with posterior (P) and anterior (A) side labelled; (b) illustrates the same healthy FSU when the individual bends forward; there would be anterior disc compression with the centre of rotation located towards the middle of the disc; (c) illustrates an individual with anterior ossification that leads to anterior pivoting of the vertebra during forward flexion, resulting in greater stretching of the structures at the posterior.....</b>	<b>166</b>
<b>Figure 5.1: Comparison of mean bilinear stiffness for human (n=7x2) and ovine (n=6x2) ALL and PLL. ....</b>	<b>179</b>
<b>Figure 5.2: Comparison of material parameter <math>\mu</math> between human (n=7x2) and ovine ALL and PLL with the standard deviation error bars. ....</b>	<b>182</b>
<b>Figure 5.3: Comparison of material parameter <math>\alpha</math> between human (n=7x2) and ovine ALL and PLL. ....</b>	<b>183</b>

## Abbreviations

AF	–	Annulus fibrosus
ACL	–	Anterior cruciate ligament
ALL	–	Anterior longitudinal ligament
C	–	Cervical
CL	–	Capsular ligament
CMC	–	Carboxymethylcellulose
CSA	–	Cross sectional area
CT	–	Computed tomography
DICOM	–	Digital Imaging and Communications in Medicine
EPD	–	Endplate depth
EPW	–	Endplate width
EZ	–	Elastic zone
FCH	–	Facet capsule height
FE	–	Finite element
FEA	–	Finite element analysis
FEM	–	Finite element model
FSU	–	Functional spinal unit
GAG	–	Glycosaminoglycan
gof	–	Goodness of fit
ISL	–	Interspinous ligament
ITL	–	Intertransverse ligament
IVD	–	Intervertebral disc
IW	–	Intermediate weight
JC	–	Joint capsule
JCL	–	Joint capsular ligament
L	–	Lumbar
LF	–	Ligamentum flavum
Lit.	–	Literature
MRI	–	Magnetic resonance imaging
NAI	–	Sodium iodide
NZ	–	Neutral zone
PDW	–	Pedicle width
PLL	–	Posterior longitudinal ligament
PMMA	–	Polymethylacrylate

PZ	–	Plastic zone
Rec_A	–	Rectangular model A
Rec_B	–	Rectangular model B
Rec_C	–	Rectangular model C
Rec_D	–	Rectangular model D
Rec_E	–	Rectangular model E
ROM	–	Range of motion
S.D.	–	Standard deviation
RMSE	–	Root mean square error
Sag	–	Sagittal
SEM	–	Scanning electron microscopy
SLR	–	Single lens reflex
SPL	–	Spinous process length
SSE	–	Sum of the squares due to error
SSL	–	Supraspinous ligament
SST	–	Sum of squares total
T	–	Thoracic
TIFF	–	Tagged image file format
TPW	–	Transverse process width
TSE	–	Turbo spin echo
TT	–	Transverse trabeculae
UK	–	United Kingdom
UKAS	–	UK's National Accreditation Body
USA	–	United States of America
VBHp	–	Posterior vertebral body height
VT	–	Vertical trabeculae
W/O	–	Without
XRD	–	X-ray diffraction
μCT	–	Micro computed tomography
1D	–	One dimensional
2D	–	Two dimensional
3D	–	Three dimensional

## Chapter 1 Introduction and Literature Review

### 1.1 Introduction

Low back pain is a common complaint in people of all ages. It is a major cause of absence from work and one of the leading reasons for early retirement and long term incapacity (van Tulder, et al., 2004). Half of the European population is estimated to suffer back pain at some time in their lives (Bevan, 2012). For some, the pain will ease after a few weeks but for others it becomes chronic, with the risk of reoccurrence being as high as 85%. The etiology of low back pain is still not well understood. Degeneration of intervertebral discs and the lumbar zygapophysial joints (facet joints) is one of the major causes of low back pain (Bogduk, 2005). A number of surgical interventions such as total disc replacement, nucleus augmentation and lumbar facet replacement devices have been introduced to treat disc and facet degeneration but their long term success rates have proven to be relatively low (Blumenthal, et al., 2005; Freeman & Davenport, 2006; Coric & Mummaneni, 2007). Improved methods of pre-clinical testing of these devices are therefore needed.

Physical and computational models are often employed to test new techniques in order to check the restoration of natural function of the spine with the insertion of artificial replacements. Such models require physical and mechanical parameters of the bones and soft tissues involved. The mechanical properties of the vertebrae, intervertebral disc and ligaments must therefore be established. The disc has received considerable attention due to its important role in load bearing and its clinical relevance with disc herniation (Urban & Roberts, 2003). In addition, the vertebrae have been studied extensively due to their relation to osteoporosis and trauma (Dumas, et al., 1987; Panjabi, et al., 1982). The spinal ligaments may also play a major role in the biomechanics of the spine and several of them have been shown to be innervated (mainly the longitudinal, spinous and capsular ligaments); hence, they could be potential sources of back pain (Pederson, et al., 1956; Stillwell, 1956; Hirsch, et al., 1963; Jackson & Winkelmann, 1966; Edgar & Ghadially, 1976). However, the role of the ligaments is not well understood, both in the etiology of back pain and in providing the stability to the spinal column.

Ovine spine models are commonly employed in research studies as a precursor to clinical trials. These models have been used for *in vivo*



experiments to study disc problems (Moore, et al., 1992; Gunzburg, et al., 1993) or spinal fusion processes (Nagel, et al., 1991; Vazquez-Seoane, et al., 1993; Kotani, et al., 1996; Slater, et al., 1988) and also in *in vitro* spinal research (Yamamuro, et al., 1990; Wilke, et al., 1997) because fresh human specimens are difficult to obtain. Anatomically, the vertebral geometry of the ovine cervical spine has been shown to be favourably comparable with that of the human spine (Kandziora, et al., 2001). However, to the author's knowledge no study has been conducted to characterise the mechanical properties of ovine spinal ligaments to justify the use of the ovine spine as an alternative model for the human spine.

The overall aim of the work presented in this thesis was to characterise the ligamentous spinal structures using both experimental and computational approaches and examine the suitability of using the ovine spine as model for the human, in terms of the ligamentous behaviour.

This chapter presents an extensive literature review that was undertaken to understand how ligaments have been tested and modelled previously. The literature review begins with the anatomy and biomechanics of the spine and individual vertebrae and ligaments. This is followed by a section on the analysis of literature for experimental testing of spinal ligaments, including the description of methods used and the results obtained followed by a discussion on what can be adapted from these methods. The last section of the literature review focusses on the finite element modelling of spinal ligaments and ligaments in general. The material models, the type of elements and replication of the attachment sites used by researchers are explored, followed by a discussion on what can be deduced from the research to date. The literature review leads to the development of the set of objectives to guide both the experimental and computational work and the predicted outcomes of the study.

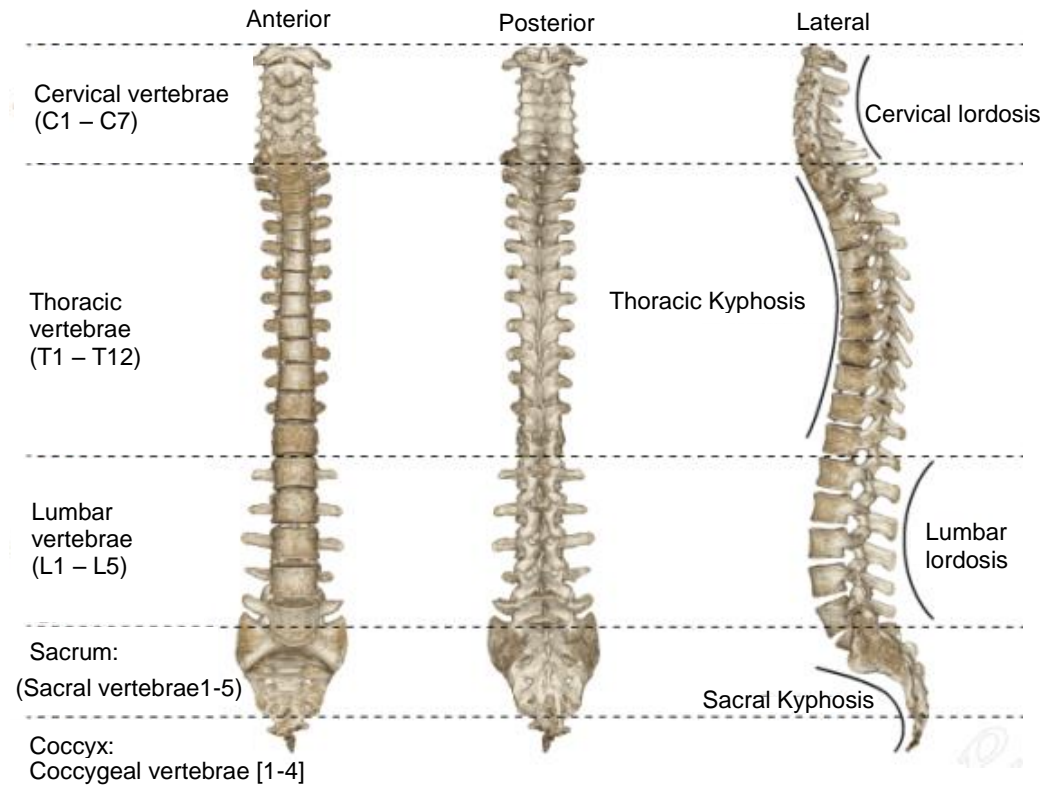
## **1.2 Literature Review**

### **1.2.1 Biomechanically Relevant Human Spinal Anatomy**

#### **1.2.1.1 Introduction**

The spine is the main structure of the axial skeleton that protects the spinal cord and spinal nerve roots, supports the body under various loads and postures and allows the movement of the trunk simultaneously owing to its strength and flexibility (Putz & Müller-Gerbl, 1996). Spinal dysfunction leads to pain or disability and has a number of socioeconomic impacts. A detailed knowledge of anatomy and mechanical behaviour of the spine is essential for understanding the disease mechanism or the changes in the anatomical structures that may lead to dysfunction. The human spine is composed of 24 moveable vertebrae spread across three sections: cervical (7), thoracic (12) and lumbar (5), and between 8-10 fused vertebrae including sacrum (5) and coccyx (3-5) (Figure 1.1). Intervertebral discs are present between all the articulating vertebrae, apart from between occiput and C1 and C1 to C2, and also present between the inferior most lumbar vertebrae (L5) and the superior most sacral vertebrae (S1).

The cervical region (C1-7) is the most distinct region of spine as it connects the head to the thorax, however cervical lordosis (anteriorly convex curvature) is the least distinct amongst the spinal curves. The thoracic region is the longest of the moveable regions of the spine with the most vertebrae (T1-12). Due to its anatomical relationship with the ribs, attaching to the sternum anteriorly, this region has very little movement. The size of the thoracic vertebrae increases from the cranial to the caudal corresponding to the increasing weight it has to carry down its length. This increasing dimension of the posterior portion of the thoracic vertebrae from top to bottom results in kyphosis, a posteriorly convex curvature (Masharawi, et al., 2008). The lumbar region has the lowest number of vertebrae of the articulating regions of the vertebral column consisting of five vertebrae (L1-L5). It is usually referred to as the lower back where the spine is convex anteriorly, giving its characteristic shape (lumbar lordosis). The sacral region has fused vertebrae which are also curved in the same way as the thoracic region (convex posteriorly). These characteristic curves of the spine not only increase its flexibility and shock-absorbing capacity but also maintain adequate stiffness and stability at the intervertebral joint level (White III & Panjabi, 1990).

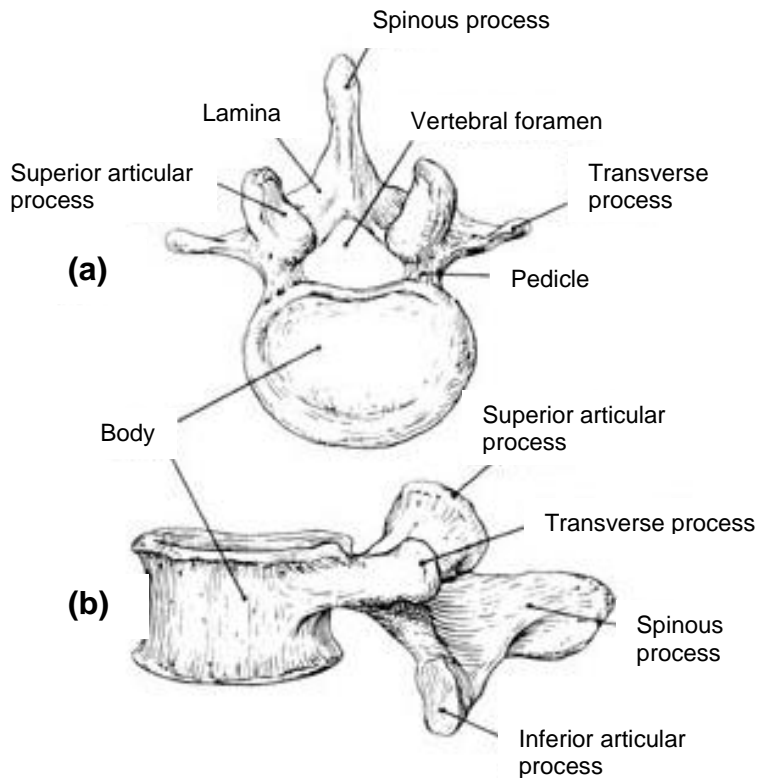


**Figure 1.1: Schematic representation of three views of the vertebral column; Anterior view (left) posterior view (middle) lateral view (right) showing cervical, thoracic, lumbar, sacrum and coccyx regions, both the lordosis in the cervical and lumbar region and the kyphosis in the thoracic and sacrum region are noticeable. (Adapted from Micheau & Hoa, 2009).**

### 1.2.1.2 Anatomy of a Typical Vertebra

Typically a vertebra is made up of two basic sections, a vertebral body and a vertebral arch (the pedicles and posterior elements). Both regions are composed of bone with an interior core of trabecular bone (also known as cancellous or spongy bone) and an outer layer of compact or cortical bone.

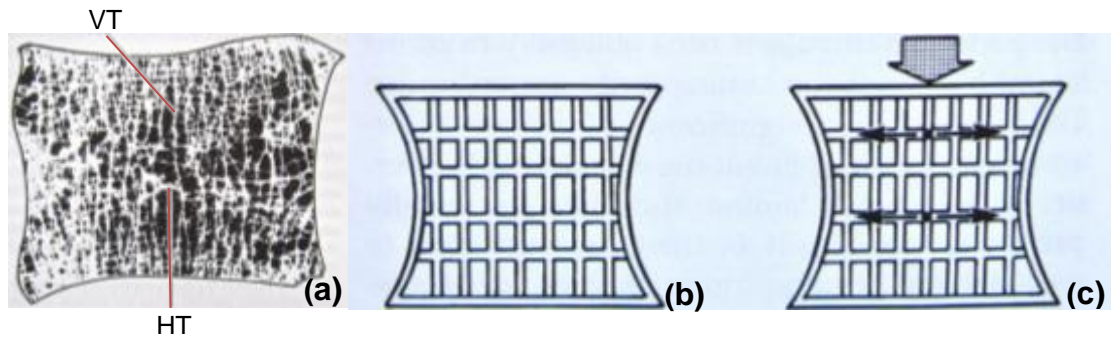
The different sections of spine (i.e. cervical, thoracic and lumbar region) have some differences in the shape of the vertebrae due to their varying functions, but each has the same general features. An image of a typical lumbar vertebra is shown in Figure 1.2. The following sections discuss the individual functions of each component of the vertebrae along with its integrated function as a whole.



**Figure 1.2: A typical lumbar vertebrae showing (a) top view and (b) lateral view. (Adapted from Emory University, 1997).**

#### 1.2.1.2.1 Vertebral Body

The vertebral body can withstand very large axial loads due to its structural composition. The cortical shell of the vertebrae is thought to be made up of thin porous membrane of fused trabeculae up to 0.6 mm in thickness (Silva, et al., 1994; Mosekilde, 1993). The anterior shell is found to be significantly thicker than the posterior one, 0.5 mm compared to 0.2 mm, respectively (Silva, et al., 1994). The trabeculae provide weight bearing strength and resilience to the vertebral body as it fills the internal region of the vertebral body with a structure in the form of vertical struts and horizontal cross-beams, known as vertical and transverse trabeculae respectively. The vertical struts brace the structure while the transverse connections develop tension when a load is applied and keep the vertical struts from bowing (Figure 1.3). The spaces between these trabeculae are used for blood supply and venous drainage. This presence of blood in the intertrabecular spaces further endows vertebral body with weight-bearing capability and ability to withstand force.



**Figure 1.3: The structure of trabeculae. (a) Sagittal section of a lumbar vertebral body with its vertical (VT) and transverse (TT) trabeculae seen in white. (b) Schematic representation of the internal structure (c) shows the ability of the structure to withhold its shape under loading. (Adapted from Bogduk, 2005).**

#### 1.2.1.2.2 Posterior Elements

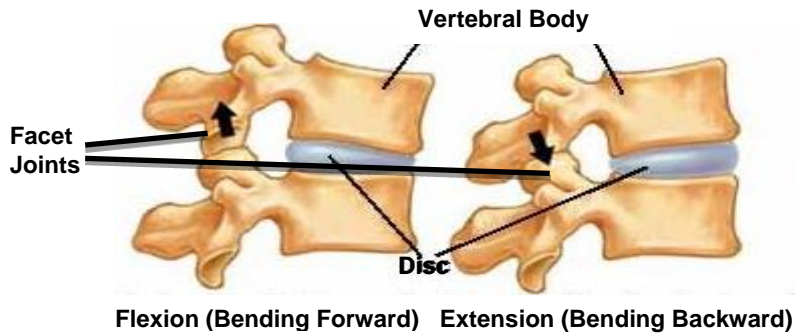
A typical vertebra has seven processes arising from its posterior portion. Transverse processes (a pair) are lateral projections while the spinous process is a midline structure directed posteriorly and somewhat inferiorly (Figure 1.2). The remaining four processes are articular processes, present in pairs; one inferior to the vertebra and one superior. The spinous and transverse processes have long protruding shapes which are ideal for attachment of ligaments and muscles. These processes act as levers enhancing the action of muscles on the spine. The articular processes provide a locking mechanism against rotations and forward sliding.

#### 1.2.1.2.3 Pedicles

Pedicles connect the vertebral bodies to the posterior elements, in turn, transmitting the forces, both tension and bending, that are sustained by the posterior elements to the vertebral bodies. These structures have a high bone density and are composed of bundles of trabeculae, closely packed together. Their main function is to transmit the loads exerted by the muscles on the posterior processes in order to move the spine.

#### 1.2.1.3 The Intervertebral Joints

Articulation of any two consecutive vertebrae form three joints, one between the vertebral bodies known as interbody joint, provided by the intervertebral disc, and the other two between the articular processes of the vertebrae known as zygapophysial joints (Figure 1.4). The zygapophysial joints are also known as facet joints and are formed by the articulation of the superior articular process of one vertebra with the inferior articular processes of the vertebra above (Bogduk, 2005).



**Figure 1.4: The motion of intervertebral joints in flexion and extension. (Adapted from PainNeck.com, 2010).**

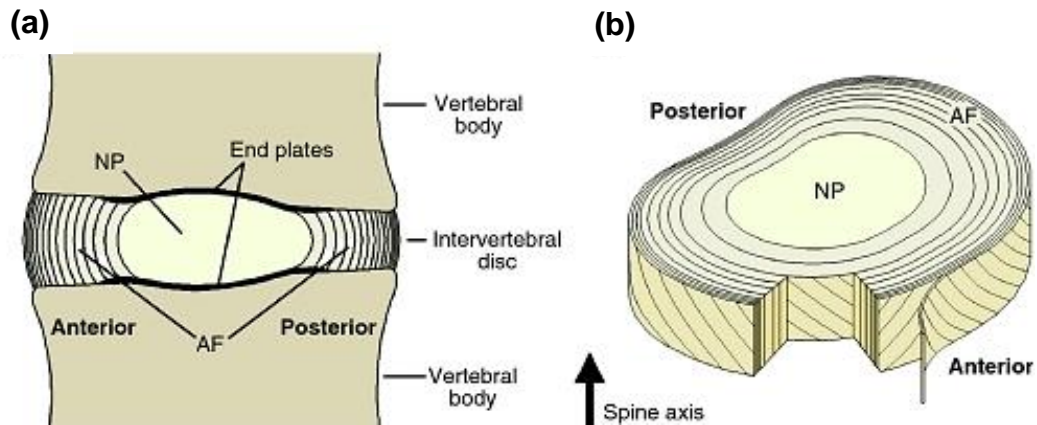
#### **1.2.1.4 Intervertebral Disc (IVD)**

The intervertebral disc forms a layer of strong but soft deformable tissue separating two consecutive vertebral bodies (Bogduk, 2005) constituting 20-33% of the entire height of the vertebral column (White III & Panjabi, 1990). The disc, along with facet joints, carries the entire compressive loads that the trunk is subjected to (Hirsch, 1955) (Prasad, et al., 1974). The weight on a lumbar disc during sitting position has been shown to be three times the weight of the trunk (Nachemson & Morris, 1964). During flexion, extension and lateral bending the disc is partially subjected to tensile stresses. Lumbar discs are subjected to torsional loads during axial rotation of torso with respect to pelvis resulting in shear stresses in the disc.

The intervertebral disc comprises three distinct components: the nucleus pulposus located centrally, surrounded by the annulus fibrosus located at its periphery and the vertebral (cartilaginous) end-plates located at the top and bottom of each disc (Figure 1.5).

##### **1.2.1.4.1 Nucleus Pulposus**

The nucleus pulposus is a semifluid centre of the disc composed of a mucoprotein gel containing a loose network of fine collagen fibres and various mucopolysaccharides (glycosaminoglycan, GAGs). It comprises of 70-90% water content which is reduced with age (Panagiotacopoulos, et al., 1987). In lumbar discs the nucleus lies more posteriorly than centrally and fills 30-50% of the total disc area in cross section (White III & Panjabi, 1990).



**Figure 1.5: Schematic representations of the intervertebral disc. (a) The anatomical regions in a mid-sagittal cross-section. (b) A three dimensional view of the disc illustrating annulus fibrosus lamellar structure. (Adapted from Smith et al. 2011)**

#### 1.2.1.4.2 Annulus Fibrosus

The annulus fibrosus gradually differentiates from the periphery of the nucleus and forms the outer boundary of the disc. This structure consists of highly organised pattern of fibrous tissue, arranged in concentric sheets (bands) of lamellae. The collagen fibres run in approximately the same direction in one sheet but in the opposite direction in the adjacent sheet (Figure 1.5). Just like the nucleus pulposus, water constitutes a large proportion of the weight of annulus fibrosus with proteoglycans making up one fifth of its dry weight (Bogduk, 2005). The sites of attachment of annulus fibrosus to the vertebral endplates appears to be highly concentrated with elastic fibres. These fibres reinforce the collagen lamellae and help them to recoil after deformation (Yu, et al., 2007). The collagen fibres of the lamellae are attached directly to the endplates in the inner zone, however in the outer zone where the endplates do not cover the peripheries of the annulus fibrosus, the fibres directly attach to the bone of the vertebral body (White III & Panjabi, 1990).

#### 1.2.1.4.3 Vertebral Endplates

The vertebral endplates are a layer of hyaline cartilage, between approximately 0.2 and 0.5 mm thick (Silva, et al., 1994), which separates the inner components of the disc from vertebral body encircled by the ring apophysis. It has been shown that with age the cartilage is replaced by bone (fibrocartilage) (Bernick & Cailliet, 1982). The endplates are strongly bound to the intervertebral discs due to their attachment with the annulus fibrosus but loosely bound to the vertebral bodies and can be fully detached from vertebral bodies under certain spinal trauma (Bogduk, 2005).

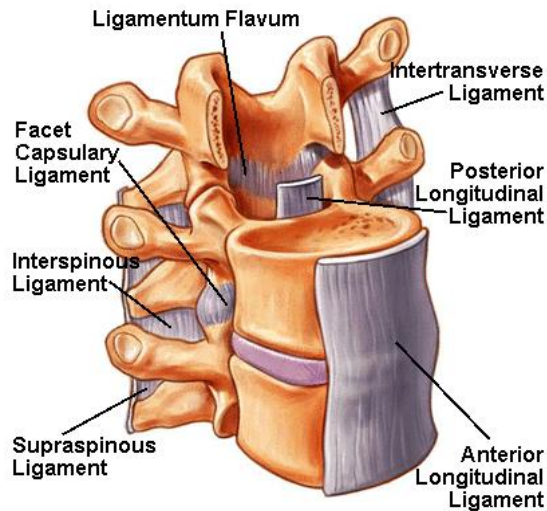
### 1.2.1.5 Spinal Ligaments

Ligaments are the soft tissue structures that provide stability to the spine. They protect the spine from injury by controlling movement during hyperextension and hyperflexion. The ligaments are relatively uniaxial structures effectively carrying loads in the directions in which the fibres run. They resist tensile forces but buckle when subjected to compression. The ligaments are mainly composed of collagen fibres and elastin embedded in a proteoglycan gel substance (Aspden, 1992). Ligaments have more rounded cells near the insertions to the bones whereas interconnected, elongated fibroblastic cells are found in their midsubstance. The cells have an important function of maintaining the collagen scaffold. Collagen is the primary component of ligament in tension as it resists tensile stresses and it is also capable of reinforcing the proteoglycan gel, if orientated appropriately (Hukins & Aspden, 1985). The direction in which the ligamentous tissue sustains tensile forces defines the orientation of the collagen fibres with the fibres preferentially aligned parallel to the axis of the spine. In un-stretched ligaments, the orientation is found to be quite broad however stretching the ligaments makes the fibres highly aligned (Hukins, et al., 1990). During complex motions, ligamentous structures develop tension in order to provide tensile resistance to external loads. The basic functions of the ligaments are:

- To provide stability to the spine within its physiological ranges of motion
- To allow the vertebrae to move in a physiological manner with fixed postural attitudes with minimum use of muscular energy
- To protect the spinal cord by not only restricting the motions in safe limits but also in absorbing the large amounts of energy that are suddenly applied to the spine in highly dynamic traumatic situations.

There are seven ligaments of the spine (Figure 1.6) that run over the region from C2 to sacrum. The upper cervical region (above C2) is quite different from the rest of the spine and hence will not be discussed here. A description of each of the ligaments from anterior to posterior of the spine follows. The longitudinal ligaments are discussed in more detail, compared to others, as they are the main focus of this work.





**Figure 1.6: A view of spinal ligaments from the front of the vertebral bodies with the top body excised (adapted from Eidelson, 2012).**

#### **1.2.1.5.1 Anterior Longitudinal Ligament (ALL)**

The anterior longitudinal ligament (ALL) is a long band of fibrous tissue covering the anterior aspect of the entire vertebral column longitudinally from the sacrum all the way up to the cervical region. The ligament attaches firmly to the anterior edges of the vertebral bodies but is loosely attached to the annular fibres of the disc with loose areolar tissue. Due to its longitudinal disposition, it resists the vertical separation of the anterior ends of the vertebral bodies (Bogduk, 2005), effectively resisting bowing of the lumbar spine and the neck in the anterior direction. The ALL consists of sets of short and long collagen fibres (Williams, 1995). The shorter fibres are deep and unisegmental spanning each interbody joint, attaching to the anterior margins of vertebral bodies, to the bone or the periosteum (Francois, 1975), while covering the IVD. The shorter fibres are covered by several layers of longer fibres that can span up to five interbody joints attaching into the upper and lower ends of the vertebral bodies. The width of fibre bundles is very thin at the level of disc but thicker elsewhere (White III & Panjabi, 1990). The main function of the ALL is to prevent hyperextension of the vertebral column and provide stability for the intervertebral joints (Moore & Dalley, 1999).

#### **1.2.1.5.2 Posterior Longitudinal Ligament (PLL)**

The posterior longitudinal ligament (PLL) is described to be narrower and thinner than the ALL and covers the entire length of the vertebral column longitudinally, like the ALL. It runs over the posterior surface of all the vertebral bodies in a serrated manner, as a narrow band over the vertebral bodies but expanding laterally over the posterior surface of the IVDs. Its fibres interweave

with the posterior annular fibres of the IVD. Unlike the ALL, it is thicker at the vertebral body level and thinner at the disc level. The shortest, deepest fibres of the PLL span two IVDs while the more superficial, longer fibres span up to five vertebrae. The main function of the PLL is to prevent the posterior ends of the vertebral bodies from separation. It acts over several interbody joints due to its polysegmental disposition (Bogduk, 2005). The main function of PLL is to prevent hyperflexion of the vertebral column. Due to its location between the intervertebral disc and the spinal cord, it also serves to prevent herniation; where a large bending force or compression force is applied to the spine which leads to posterior bulging of disc due to the increased pressure in the nucleus pulposus, and risks making contact with and injuring the spinal cord.

#### **1.2.1.5.3 Ligamentum Flavum (LF)**

The ligamentum flavum (LF) is a thick but short ligament that joins consecutive vertebrae through their laminae (White III & Panjabi, 1990). It is identified by its characteristic yellow colour and its paired structure with a symmetrical representation on both left and right sides. The LF is described as an 'elastic ligament', meaning it has a relatively low stiffness, unlike other ligaments in the spine. Its elastic nature allows it to aid in restoration of flexed spine to its extended position and reduces the risk of spinal cord encroaching as the ligament does not buckle. It also prevents excess separation of vertebral laminae.

#### **1.2.1.5.4 Interspinous Ligament (ISL)**

The interspinous ligament (ISL) connects adjacent vertebrae by connecting their spinous processes with attachments extending from the root to the apex of each process. The ISL is broader and thicker in the lumbar region, narrow and elongated in the thoracic region and only slightly developed in the cervical region. Like most other ligaments, the ISL is mainly composed of collagen fibres, however, the ventral part of ligament, where it meets LF, is denser in elastin fibres. X-ray diffraction studies have shown that most fibres of ISL run parallel to the spinous processes making it less capable of resisting forward bending movements of spine (Hukins, et al., 1990).

#### **1.2.1.5.5 Supraspinous Ligament (SSL)**

The supraspinous ligament (SSL) bridges the interspinous spaces by posteriorly attaching to the posterior edges of the spinous processes. The ligament originates from C7 vertebrae and terminates at the sacrum. It is well defined only in the upper lumbar region with very little or no presence in lower

regions of certain individuals. It is almost always absent at L5-S1 level (Levangie & Norkin , 2011). It appears broader and thicker in the lumbar region as compared to thoracic region. The SSL is not considered a true ligament due to its dense structure of tendinous fibres derived from back muscles (Bogduk, 2005).

#### **1.2.1.5.6 Intertransverse Ligament (ITL)**

The intertransverse ligament (ITL) is characterised as rounded cords connecting transverse processes, intimately connected to deep or intrinsic back muscles. It appears like a membrane, comprising of sheets of connective tissue that runs from lower end of one transverse process to the upper end of the transverse process below. The collagen fibres in the ITL are not as regularly oriented and as densely packed as the fibres of other ligaments. The ligament serves to separate the anterior and posterior musculature of the spine. The ITL appear as scattered fibres in the cervical region whereas in the thoracic region, the ligaments are fibrous chords. It has negligible cross-sectional area in the lumbar region therefore it is considered to have no mechanical significance in this region (Bogduk, 2012).

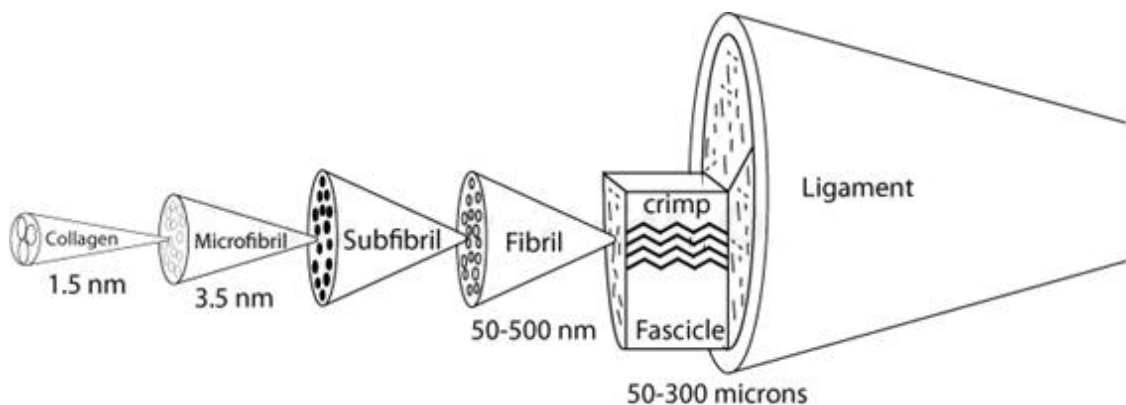
#### **1.2.1.5.7 Joint Capsular Ligament (JCL)**

The joint capsular ligament (JCL) consists of fibres running perpendicular to the plane of the facet joints, attaching beyond the margins of the adjacent articular processes (White III & Panjabi, 1990). The collagen fibres of the JCL are oriented along a medial lateral axis (Yamashita, et al., 1996). The capsule is found to have greater strength parallel to the collagen fibres (Little & Khalsa, 2005). These ligaments are generally perpendicular to the joint line. The facet joint capsule is one of the structures of spine that constrains the motions of vertebrae during physiological loading (Little & Khalsa, 2005).

#### **1.2.1.5.8 Microstructure of Ligaments**

All ligaments have a hierarchical structure with the collagen component ordered into micro-fibril, sub-fibril, fibril and subsequently fibres that make up the ligament (Figure 1.7). Kirby et al. (1989) explored the structure of the ALL, PLL and LF alongside their mechanical properties. Light microscopy, X-ray Diffraction (XRD) and Scanning Electron Microscopy (SEM) were employed to study the structure of ligaments at various stages of the investigation. The composition of the ligaments was also investigated using histological techniques. The ligaments were obtained from frozen lumbar sections of pig spines. Light microscopy showed that the longitudinal ligaments had a crimped

structure, as shown in Figure 1.7, which straightened on the application of strain. Therefore during the initial application of strain the ligament was less stiff, but as the extension increased so did the stiffness, as the crimps disappeared after a strain of about 0.12. Polarised light microscopy also revealed that the crimp of the longitudinal ligaments was not planar as the rotation of unstrained ligament about its own axis did not have any effect on the appearance of crimps. The LF structure showed no evidence of gross crimping under light microscope. XRD demonstrated that the collagen fibrils were almost randomly oriented about their axial direction in unstrained ligaments but as the ligaments were stretched, the fibrils gradually aligned about their preferred orientation, parallel to the axis of the spine. In the case of the longitudinal ligaments, little alignment occurred after the crimp was removed and an almost constant stiffness was attained by the ligaments. However, in the case of the LF, a gradual alignment of fibrils occurred on stretching, allowing the elastin to play a role in the extensibility of ligament. SEM further confirmed the interpretation of XRD and showed crimped fibres in longitudinal ligaments but not in the LF. The higher elastin content in the LF was also reported by Nachemson & Evans (1968) who performed biochemical assay and histological studies on the tissue and found a content of 80%. Chazal et al. (1985) performed histological studies on supraspinous and interspinous ligaments during tensile tests which showed that in these ligaments, the collagen fibres lost their zig-zag pattern at the rupture limit.



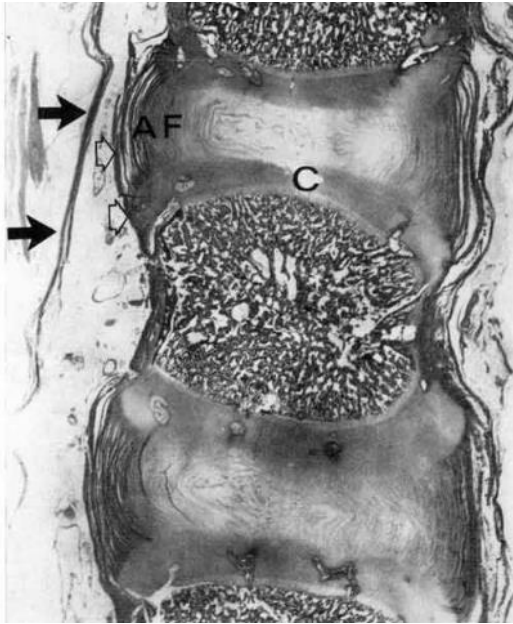
**Figure 1.7: A schematic of micro to macro level structure of a typical ligament (adapted from Panagos, 2015).**

#### 1.2.1.5.9 Attachment Sites

Attachment sites, also known as the insertion sites or entheses, are the sites where loads are transferred across the ligament-bone interface. They are designed to reduce stress concentrations that would otherwise occur at this complex junction between soft tissue of ligaments and hard tissue of bones.

This junction not only varies greatly from ligament to ligament but also varies between the two ends of the same ligament. These attachment sites could either be direct or indirect depending on the tissue microstructure at the junction.

If the boundary between bone and ligament is quite sharp occurring over a distance of less than 1mm then the attachment site is defined as direct (Woo & Buckwalter, 1988). In these areas, the deep collagen fibrils quickly come out from the ground substance matrix of ligament and carry on through fibrocartilage, mineralised fibrocartilage and then finally enter bone (Cooper & Misol, 1970), mostly meeting the bone at approximately right angles. On the other hand, indirect attachment sites have more gradual transition between soft tissue and hard tissue, making the area of attachment to the bone broader. The attachment is mainly through the superficial fibres of the ligament usually attaching to the periosteum of the bone. Unlike the direct insertion, the deep fibres meet the bone at acute angles without the transition through fibrocartilage zone (Benjamin, et al., 1986). Francois (1975) found the short fibres of ALL and PLL to be attached to the vertebral body via indirect attachment sites. These short fibres were also found to penetrate the annulus fibrosus of the disc (Francois, 1975). The long fibres of both the ALL and the PLL were found to cross several discs and are separated from the short fibres by a loose connective tissue with fats and blood vessels (Figure 1.8). Both the ISL and the SSL were found to be attached to the spinous processes via direct attachment sites (Gray, 1944; Scapinelli, 1989) and so is the LF (Niepel & Sitaj, 1979; Yoshida, et al., 1992).



**Figure 1.8: Microradiograph image of sagittal decalcified section through a neonate lumbar spine with anterior side on the left. Image shows short fibres of ALL (open arrows), long fibres of ALL (solid arrows), penetration into annulus fibrosus (AF), and cartilaginous endplates (C). (Adapted from Francois, 1975).**

The attachment sites have been shown to be often the site of injuries especially during skeletal maturation and joint immobilisation (Noyes, et al., 1974; Woo, et al., 1987). The difference in the microtissues present at the site of attachment leads to inhomogeneous deformations throughout ligaments. The strains near the attachments sites are also found to be different to the strains observed in the mid-substance of ligaments (Woo, et al., 1983; Noyes, et al., 1984).

Moreover, the ligaments wrap around the surface of the bones and are found to be subjected to compressive contact stresses (Matyan, et al., 1995; Weiss, et al., 1996; Giori, et al., 1993). The location of these sites also determines the orientation of the forces when the loads are transferred from the ligament to the bone.

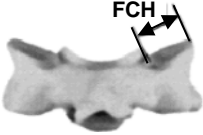

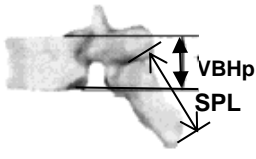
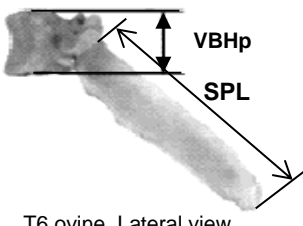
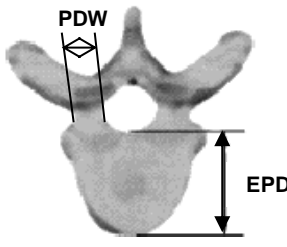
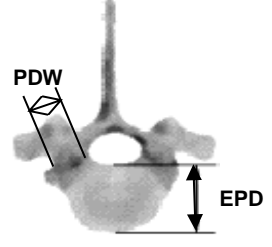
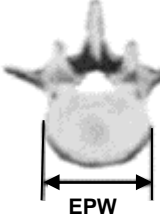
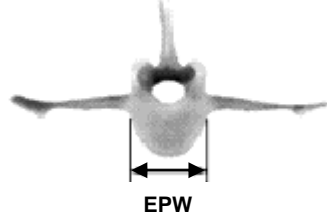
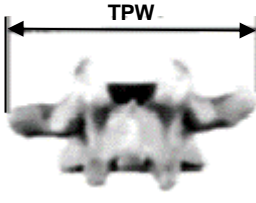
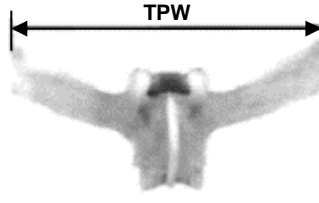
### **1.2.2 Comparison of Human and Ovine Spine Anatomy**

Ovine models are used commonly for *in vivo* experiments to study disc pathologies (Moore, et al., 1992; Gunzberg, et al., 1993; Asazuma, et al., 1990) or spinal fusion processes (Nagel, et al., 1991; Vazquez-Seonae, et al., 1993; Kotani, et al., 1996). The tissue is also used in *in vitro* spinal research (Slater, et al., 1988; Yamamuro, et al., 1990), because fresh human specimens are increasingly difficult to obtain. The ovine spine is larger than the human spine especially in vertebral body height (Sheng, et al., 2010). The mean vertebral body width and depth is found to be higher in the human spine than the ovine

spine (Sheng, et al., 2010). Wilke et al. (1997) compared cervical, thoracic and lumbar regions of five fresh ovine spines with reported values of the human spine. It was found that ovine vertebral bodies were taller than wide, unlike human vertebral bodies which are wider than tall. The ovine pedicles were also found to be taller than they are wide, unlike human, however the width of the pedicle is found to be similar between the two species. Overall, it was reported that the experiments related to the gross structure of both ovine thoracic and ovine lumbar spines had better correlations to humans than the cervical spine. However, Kandziora et al. (2001) compared ovine cervical spines with 20 fresh human cadaver cervical spines and encouraged the use of the ovine cervical spine as a model for cervical spine research based on their results. A comparison of human and ovine spine in pictorial form is tabulated below (Table 1.1).

In terms of biomechanical parameters, Wilke et al. (1997) determined the mechanical properties of ovine spines and compared them with published *in vitro* and *in vivo* results from various studies on human spines. They reported that the craniocaudal variations in range of motion were qualitatively similar between ovine spines and values reported for human spines in literature in all load directions. For both species, the range of motion (ROM) was found to be small for axial rotation in the lumbar region and for flexion/extension in the upper thoracic region. Similarly, lateral bending over the entire length, axial rotation in the thoracic region and all three directions in middle cervical spines were found to have a large ranges of motion for both species. Likewise, for both human and ovine spines the stiffness was almost zero in lateral bending. These similarities led Wilke et al. to state that “the use of ovine spine, which already includes evaluation of surgical techniques and bone healing processes, might be extended to spinal implants” (Wilke, et al., 1997). Due to the strongest similarities in the major dimensions and the biomechanical parameters across both species in the thoracic and lumbar regions, and the association of the ligaments in general to the biomechanics of the spine, one may conclude that the ovine spine would be a reasonable model to represent ligament behaviour in spinal biomechanics investigations.

**Table 1.1: Comparison of Human and Ovine Spine Vertebrae (Adapted from Wilke, et al., 1997).**

Region of Spine	Equal Scale Vertebrae Images		Abbreviations
	Human Spine	Ovine Spine	
Cervical	 C4 human, Dorsal view	 C4 ovine, Dorsal view	<b>FCH</b> – Facet Capsule Height
Thoracic	 T6 human, Lateral view	 T6 ovine, Lateral view	<b>VBHp</b> - Posterior vertebral body height
	 T6 human, Cranial view	 T6 ovine, Cranial view	<b>EPD</b> – Caudal Endplate Depth
Lumbar	 L4 human, Cranial view	 L4 ovine, Cranial view	<b>EPW</b> – Caudal Endplate Width
	 L4 human, Dorsal view	 L4 ovine, Dorsal view	<b>TPW</b> – Transverse Process width



### 1.2.3 Biomechanics of Spine

As discussed earlier, the human spine is a complex structure comprising of a tri-joint structure consisting of vertebrae-disc-vertebrae complex and two facet joints held in place by ligaments and muscles, providing structural integrity and passive stability to the spine. The tri-joint structure allows both rotational and translational movements of vertebrae. For each spinal segment, the movement is restricted by anatomical structures such as intervertebral discs, facet joints and ligaments. These structures cause the motion to be coupled i.e. rotational and translational movements occur simultaneously. This allows for increased mobility without having to compromise on stability. The healthy human spine allows three-dimensional coupled movements present in flexion/extension, axial rotation, translation and lateral bending (Figure 1.9). As the anatomical structures vary regionally, the exact pattern of coupling depends on the region and on the first movement. For example, if lateral bending is the first movement then it will be coupled with axial rotation in the same direction. However, if the first movement is axial rotation then it will be coupled with lateral bending in the opposite direction. Abnormal coupling patterns will lead to instability in the spine (Banton, 2012).



**Figure 1.9: The range of motion exhibited by cervical spine or spine in general. (Adapted from Banton, 2012).**

The cervical spine is considered to be the most mobile section of spine which allows axial rotation and side bend of the head in opposite directions. The lower cervical segment has higher incidences of cervical spondylosis (age related degeneration of soft tissues and bones), due to the largest range of motion in this region. The facet joints in the lumbar region are oriented in such a way that they allow more extension and flexion than rotation, therefore degeneration of facets or bone in general adversely affects the functioning of lumbar region of spine. Lumbar disc degeneration has been shown to increase translation in the lumbar spine which in turn is linked to lower back pain (White & Panjabi, 1990).

## 1.2.4 Biomechanics of Spinal Ligaments

The biomechanical functions of the spine are partly accomplished by the mechanical behaviour of the individual ligaments. These ligaments have been shown to provide passive stability to the spine and play a major mechanical role within the physiological range of motion (Bowden, et al., 2008). The physical characteristics i.e. the locations and orientations of all the ligaments have been discussed in detail previously (Section 1.2.1.5). The functional role of ligaments is described in the following section.

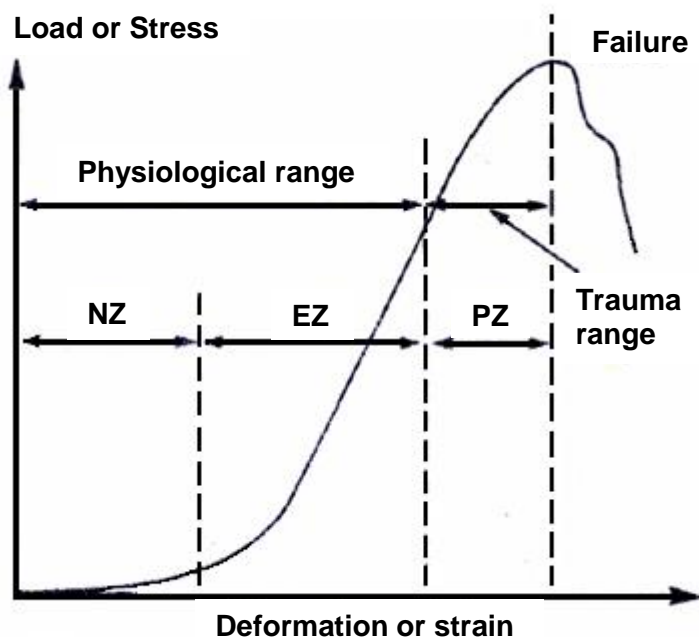
### 1.2.4.1 Non-Linear Behaviour

The stiffness and strength of the ligaments are important factors in spinal biomechanics, especially during trauma to the spine. One of the characteristics of a ligament that helps provide its physiological function is the nonlinearity of the load-displacement curve. Figure 1.10 shows a typical load-displacement curve of a spinal ligament (White III & Panjabi, 1990). The curve is divided into three regions:

- I. The neutral zone (NZ) – shows an increase in strain beyond the neutral position without a corresponding significant increase in stress. This is due to the uncoiling of the crimp pattern of the collagen fibres which stretches until the fibres reach a straightened condition.
- II. The elastic zone (EZ) – shows a rise in stress with corresponding strain, stretching the collagen fibres further, beyond the NZ and up to the physiological limit. This elastic zone is divided into two regions: (i) a non-linear active zone where the stress starts to increase significantly with the corresponding strain, and, (ii) an active linear zone where the stress increases proportionally to the strain (Dumas, et al., 1987).
- III. The plastic zone (PZ) – is the region of increasing trauma whereby a non-linear rise in stress is evident with corresponding strain, stretching the fibres beyond the physiological limit and until failure occurs. The fibres are arranged in a ligament in such a manner that loading on the entire ligament results in some fibres being loaded more than the others and hence they begin to fail early under increasing load. The plastic zone represents this behaviour. Progressive loading of a ligament would eventually result in complete rupture, corresponding to the failure region on the graph.

The non-linear active zone of the EZ and the NZ, collectively, are commonly known as the toe-region, whereas the linear active zone is commonly known as

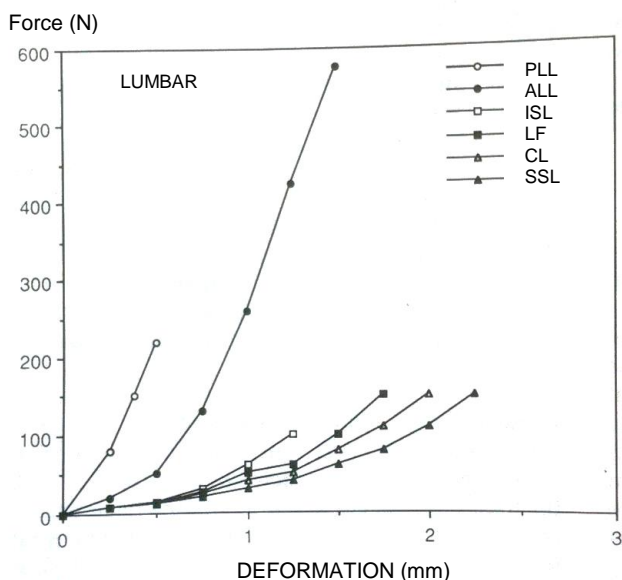
the linear-region (Chazal, et al., 1985; Dumas, et al., 1987; Panjabi, et al., 1982).



**Figure 1.10: A typical load-deformation curve of a ligament illustrating the three regions: the neutral zone (NZ), the elastic zone (EZ) and the plastic zone (PZ). (Adapted from White III & Panjabi, 1990).**

Spinal ligaments all follow a similar behaviour, when loaded, to the load-displacement curve shown in Figure 1.10. White III & Panjabi (1990) plotted physiological load-displacement curves for the most significant ligaments of lumbar region using the data from Panjabi et al. (1982) (Figure 1.11). All curves show non-linearity, characterised by their unique combination of stiffness, maximum deformation and failure load. The variations in their behaviour are a reflection of the role of each of the ligaments. Chazal et al. (1985) established a correlation between stress and strain values for spinal ligaments. It was found that the ALL exhibited largest deformations for lowest loads while the ITL exhibited smallest deformation for highest loads. The difference in the behaviour of the ALL observed between Panjabi et al. (1982) and Chazal et al. (1985) is due to the difference in testing. Chazal et al. (1985) performed the testing on ligaments in isolation whereas Panjabi et al. (1982) performed the testing in-situ, i.e. within a whole functional spinal unit, by applying physiological loads and moments. Kirby et al. (1989) has shown that the stiffness of the longitudinal ligaments increases for strain of up to about 0.12, after that it becomes constant until the signs of failure are visible. The longitudinal ligaments were found to require higher stress to induce a given strain, up to a value of 1.5, as compared to the LF. The LF showed no signs of

failure up to a strain value of 1.5. Myklebust et al. (1988) tested individual ligaments, in situ, in isolation. It was generally concluded that as the distance from the vertebral centre of rotation is increased, the deflection at failure also tended to increase because these far ligaments must functionally withstand more force and deflection.

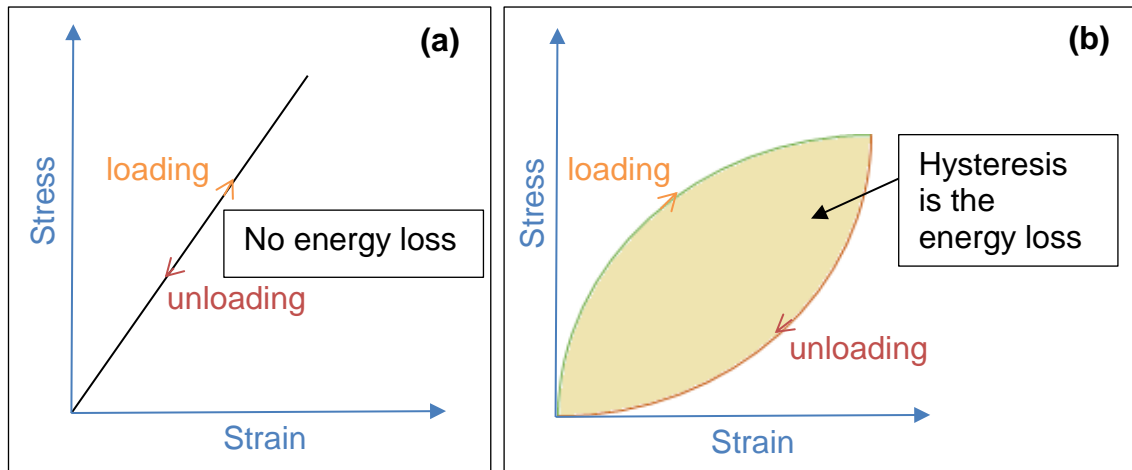


**Figure 1.11: Force deformation curve for spinal ligaments of lumbar region (Adapted from White III & Panjabi, 1990).**

#### 1.2.4.2 Viscoelastic Nature

Viscoelastic materials are characterised by both viscous and elastic properties when undergoing deformation. Because of the viscosity factor they have a time dependant behaviour even when they are subjected to constant loads. Unlike elastic materials, when a load is applied to viscoelastic materials and then removed, some of the energy stored is recovered while the remainder is dissipated in the form of heat. This dissipation of energy is known as hysteresis and is defined by the area between the loading and unloading curve (see Figure 1.12). Chazal et al. (1985) observed all spinal ligaments exhibited hysteresis during the loading-unloading curve owing to their viscoelastic nature. When viscoelastic materials like ligaments are loaded and unloaded a few times in a cyclic manner, the hysteresis, i.e. the energy lost in each respective cycle, is reduced with each consecutive cycle. An equilibrium, close to zero energy lost, is usually reached whereby the loading and unloading curves become repeatable, indicating the importance of preconditioning before experimental testing. Pre-conditioning reduces the effect of the viscous part of the material behaviour as it can be dependent on the hydration level of the material whereas the elastic part is easily characterised and repeatable.

Ligaments display time and history dependant viscoelasticity when undergoing deformation due to the presence of both a viscous proteoglycan gel substance and elastic collagen fibres and elastin. This means they would provide increased stiffness with increasing loading rate compared to when the loads are applied slowly (Hukins, et al., 1990). If kept within the physiological range, they would retrieve their original shape once the load is removed but the recovery would take longer than an elastic structure. These are important characteristics responsible for their shock-absorbing capacity.



**Figure 1.12: A comparison of purely elastic (a) and viscoelastic (b) material showing hysteresis presented by the viscoelastic material.**

#### 1.2.4.3 Pre-tension/Pre-strain

Connective tissues such as ligaments, tendons and skeletal muscles are known to retract when excised from the body. This behaviour is attributed to the in situ strains that exists in vivo in the absence of any loading and is usually considered as a reference state from which different motions can be simulated. Removing the tissue from the body yields a relatively stress-free configuration, relieving the strains and associated stress hence the retracting. This in-situ strain (i.e. pre-strain) for ligaments has been shown to contribute to the stability of the joints (Ellis, et al., 2006). Spinal ligaments have also been shown to be pre-strained in a spine from which all the muscles have been removed. This behaviour is shown by the retracting of the ligaments when cut (Hukins, et al., 1990; Tkaczuk, 1968). The ALL and PLL have been shown to have a pre-strain of up to 10% and 13% respectively (Tkaczuk, 1968) in the parallel fibre direction and it not only affects their own stress and strain state but the overall biomechanics of the spine (Hukins, et al., 1990; Nachemson & Evans, 1968; Tkaczuk, 1968; Petter, 1933). Pre-strain is reported to significantly decrease with age (Nachemson & Evans, 1968; Tkaczuk, 1968) with the LF shown to

buckle into the spinal canal on physiologic extension (Penning & Wilmink, 1986).

### **1.2.5 Experimental Testing of Spinal Ligaments**

This section provides a review of the experimental testing procedures previously used to investigate properties of the spinal ligaments. This includes specimen preparation, mechanical test design and investigation of microstructures. Two distinct methods of testing have been cited in literature: individual ligament testing and whole functional spinal unit testing. This section of the literature review discusses the two methods and highlights the procedures along with their merits and demerits. The various studies have different loading techniques, rates, and magnitudes which provide a great deal of information but is challenging for comparison purposes. The values of the mechanical properties of the ligaments obtained as a result of both methods of testing are presented in tabular form at the end of this section (Tables 1.2 to 1.8).

#### **1.2.5.1 Individual Ligament Testing**

Studies by Tkaczuk (1968), Nachemson & Evans (1968), Waters & Morris (1973), Chazal et al. (1985) and Kirby et al. (1988) have all focused on experimental biomechanical characterisation of individual ligaments. These studies have all used various techniques and testing protocols to extract and load ligaments. An extensive amount of data has been accumulated, however, comparison of data obtained as a result of these various studies shows considerable differences in the values obtained.

##### **1.2.5.1.1 Specimen Preparation, Fixation and Maintenance**

###### *Storage*

The method of storage of connective tissue could bring about changes in its mechanical properties (Waters & Morris, 1973) hence it is an important consideration during the planning of an experiment. There are a number of different methods used by researchers for storage of ligaments in biomechanical investigations including: testing fresh, freezing and storage at room temperature or refrigerator, in sealed bags or in a fluid. The methods used will be described in more detail in the following paragraphs.

Tkaczuk (1968) and Nachemson & Evans (1968) both obtained specimens from fresh cadavers and tested them either on the day of autopsy or within 48 hours of retrieval. Wherever delayed, Nachemson & Evans (1968) stored the samples at -29°C, in sealed plastic bags, and used within 3 days. Kirby et al.

(1988) froze the specimens, obtained from frozen pigs, immediately in liquid nitrogen (-196 °C) and stored in a deep freezer at (-20 °C). Waters & Morris (1973) stored the specimens at 10°C in watertight plastic bags, to maintain constant hydration without the use of humidity chamber, and tested within 48 hours of retrieval. Chazal et al. (1985) also maintained proper hydration by keeping the ligaments obtained from fresh cadavers or living subjects in a solution of water, alcohol and glycerine when the testing was delayed for few hours or the ligaments were placed in Ringer's solution when tested within one hour. The authors did not make any comparison between the two methods. Nachemson & Evans (1968) showed that this method of storing ligaments (LF) in immersed conditions even for an hour increases the weight of tissue by 7-10%. This will also have an effect on the respective geometric properties of the tissues.

Water content in the tissue is generally attributed to cause artefacts due to the freezing process. Volumetric changes of 6.2% for human muscle tissue were reported by Pech et al. (1987) (Pech, et al., 1987). However, the muscle tissue has much higher water content than the ligament therefore as long as such connective tissues are frozen at sufficiently low temperatures; their tensile properties appear to remain unaffected (Mathews & Ellis, 1968; Nordwall, 1973). Viidik et al. (1965) used sealed containers to store rabbit ligaments at 20°C for 96 hours and found the collagen bundles to still be preserved for this time period. Although the collagen fibre bundles were found to be swollen at 2 hours with autolysis of cell nuclei beginning at 24 hours and completing at 96 hours, the tensile characteristics of the ligaments were found to be unaltered until after 96 hours. Specifically for spinal ligaments, Tkaczuk (1968) has found that rapid freezing to -60°C and thawing of ALL & PLL does not have any effect on the mechanical properties of tissue samples. Hickey & Hukins (1979) also demonstrated that freezing does not have any effect on the orientation of the collagen fibrils in connective tissues.

None of the storage temperatures discussed above were shown to cause any adverse effect on the structure or state of the specimens. These studies show that specimens can either be tested on the day of retrieval or within 48 hours by keeping them moist and storing in refrigerator or, if need be, the specimens can be frozen on the day of retrieval and then tested on a later date. However, storing in a fluid will cause the tissue to swell and will affect the corresponding geometric properties; therefore tissue should be stored in airtight bags to avoid it drying out.

### *Specimen Geometry*

Being able to measure the geometry of ligaments (length and cross sectional area) accurately is an important consideration for planning the tests to work out the mechanical properties of ligaments. An error in the cross-sectional area measurement has been cited as the single greatest source of technical error in this type of experiments (Waters & Morris, 1973). The method of measurement has to be accurate to detect possible small differences in mechanical properties of different ligaments or sections of ligaments. Various methods of determining the geometric parameters of the ligaments have been used in literature including: direct measurement using displacement gauges, microtomes or palpators and indirect measurement using masses and densities or graphic methods.

In terms of direct measurement, Tkaczuk (1968), Nachemson & Evans (1968) and Chazal et al. (1985) all used measuring instruments for determining the length and cross-sectional area of ligaments. Tkaczuk (1968) tested whole individual ligaments as well as samples of identical sizes. The samples of ALL and PLL were cut into segments and subsequently frozen to allow cutting sheets of 0.5 mm thickness using a freezing microtome. A dial displacement gauge was used to measure the thickness of samples whereby the sample was placed between two metal plates. The 0.5 mm thick sheets were then used to obtain identical samples of uniform width of 2 mm, this was achieved by using pressing stamp method to stamp a soft plastic material placed under the sheet and subsequently cutting the ligaments parallel to the orientation of the collagen fibres. The dial displacement gauge and the pressing stamp method appeared to be a good way of obtaining specimens of identical sizes.

Nachemson & Evans (1968) tested LF attached to their laminae with the vertebral bodies and articular processes removed. The dimensions were measured using a micrometre and callipers. This method of measuring dimensions may not be accurate because the specimen might be deformed by the micrometer during measurement. The authors did not mention if they took measurements at one position or at many locations to take an average to avoid the inaccuracy in values obtained due to the inhomogeneity in ligament structure over the entire length.

Chazal et al. (1985) also conducted a study on the LF with bony attachments at each side to include both the short and long fibres in order to gain accurate mechanical properties, dependant on anatomical integrity of the ligament. A palpator was used to measure cross section of ligaments every 2 mm on the entire length with the tracing being obtained on a graph paper using an



amplifier. The lowest cross-section was used to calculate stress. The length was measured at rest using a micrometer, however, since the length was measured at rest in isolation it would not be a true representation of the actual length of ligament under its normal state of pre-tension in situ.

Several groups used a variety of indirect methods for measuring the dimensions of ligaments including Water & Morris (1973) and Kirby et al. (1989). Waters & Morris (1973) obtained the cross sectional areas of the specimens by first clamping the ligament under slight tension and freezing it rapidly with liquid nitrogen. The ligaments were then sectioned in 2 mm segments and were allowed to thaw under a concave coverslip that prevented water loss without touching the specimen. The specimen was then placed on a projector, a thin cross section of ligament was magnified and projected on a screen, and the area of the magnified image was determined by a graphical method. This method provides a simple approach however it does not take into account the variability in the thickness of ligaments across the entire length.

Kirby et al. (1989) determined the cross-sectional areas from masses and densities of the specimens by mixing carbon tetra-chloride and xylene to produce a liquid in which they neither floated nor sank (Sikoryn & Hukins, 1988). This method relies heavily on getting the consistency of the mixture accurate each time and also the pre-tension in ligaments is not accounted for.

In summary, various methods of measuring the length and cross sectional areas of the ligaments have been established, however, each method has its own shortcoming as described above. The ideal method would incorporate both the pre-tension in the ligaments to obtain accurate length and the variability in the cross-section of ligaments through their entire length.

### *Fixation*

Tkaczuk (1968) and Kirby et al. (1989) tested ligaments individually without any bony attachments by firmly attaching a clamp to the ends of the ligaments. Chazal et al. (1985), Nachemson & Evans (1968) and Waters & Morris (1973) clamped the bones, attached to ligaments to preserve their anatomical and mechanical integrity. The method of testing ligaments attached to their bones is better due to its ease of fixation and also because it avoids the damage to the structure of ligament due to clamping. However, when only sections of ligaments are to be tested, it is not possible to have bones on either end and hence the use of specialised holders is recommended which would minimise the effects of slippage and surface damage.

### *Test Environment*

The physical properties of connective tissues can be greatly affected by their state of hydration (Waters & Morris, 1973). Stromberg and Wiederheilm (1969) found the mouse tail tendon dried rapidly when exposed to room temperature with shrinkage and shortening within seconds of exposure. Tkaczuk (1968) also observed similar patterns during testing of ALL and PLL from fresh cadavers. He noted drying of specimens at room air of 60-70% humidity while excessive uptake of water by the specimens when tested in Ringer's or other solutions. The tests were performed in high humidity chamber (100%) to prevent water loss from the tissues that can affect their physical properties. Waters & Morris (1973) performed the tests in a heat-sealed tubular plastic sleeve at either end to maintain constant hydration. Nachemson & Evans (1968) performed tests on samples immersed in Ringer's solution hence the stress-strain values obtained were thought to be slightly inaccurate due to small changes in dimensions by the swelling of tissue, however, the results were used only for comparison within the study. Kirby et al. (1989) decided to conduct the tests at room temperature by constantly spraying the specimens with saline; to avoid drying off of the specimens. Studies on some ligaments have shown the stress-strain curves at 20°C and at body temperature to be indistinguishable (Dorlot, et al., 1980) (Hasberry & Pearcy, 1986).

From above, it can be concluded that the tissue should be kept moist throughout the procedure but it must not be placed in a solution otherwise it would swell and exhibit inaccurate mechanical properties, and that testing at room temperate is acceptable.

#### **1.2.5.1.2 Test Design and Loading Regime**

##### *Preliminary or Calibration Tests*

Various authors (Tkaczuk, 1968; Waters & Morris, 1973) have undertaken initial tests to determine the most appropriate loading regime e.g. by testing initial specimens to failure (tearing of ligament) to check maximum loads that should be applied in subsequent experiments. Tkaczuk (1968) suggested using maximum loads of about 30% of the failure load of weakest sample used. This is useful as structures do not return to their original state after they have gone past their elastic limit therefore it is crucial to test them well within the elastic range if further tests are to be undertaken.

### *Actual Tests*

A displacement control was mostly used by researchers to test the ligaments. Nachemson & Evan (1968) conducted tests on LF at a constant strain rate of  $0.0055 \text{ s}^{-1}$  which is of the same order as the strain rate of  $0.003 \text{ s}^{-1}$  used by Kirby et al. (1989) to test both the LF and the longitudinal ligaments. Chazal et al. (1985) also used a slow constant rate of  $1 \text{ mm/min}$  ( $\sim 0.017 \text{ mm/s}$ ) to test the specimens in tension. Since multiple ligament types from various levels of spines were tested in these studies, the lengths (hence strains) will be very different, so it is hard to make meaningful comparisons. It has been shown previously that the loading rate has a significant effect on the stiffness such that stiffness increased linearly with the logarithm of the loading rate (Yoganandan, et al., 1989). Moreover, increased loading rate has been shown to shorten the toe region, increase stress and reduce failure elongation (Shim, et al., 2005). Therefore loading rate of the test should be selected to replicate the loading rate of interest *in vivo*. Furthermore, different ligaments of the spinal motion segment tend to undergo different amounts of strain in different motions. For example, the PLL has been shown to have a physiological maximum strain of about 13% in extension whereas SSL has been found to have maximum strain of about 31% in the same motion (Panjabi, et al., 1982). Therefore, it is not surprising that different strain rates have been used depending on the type of motion under consideration and the type of ligament under test. However, the strain rates used by Kirby et al. (1989) and Nachemson & Evan (1968) appear low for physiological movement, for example, at a strain rate of  $0.003 \text{ s}^{-1}$  ligament would take over 40 seconds to reach a physiological stretch of 13%. Preloading (Tkaczuk, 1968) or resting-stress (Nachemson & Morris, 1964) values were also determined. Nachemson & Evan (1968) determined the resting stress from the contractional strain that occurred when the vertebral arches were separated from vertebral bodies. In both studies, the resting strain was found to be dependent on the IVD condition and on the condition of spine in general. It was found that the results varied markedly across samples since pre-stress values are dependent on dimensions of the ligaments, the pressures within the nucleus pulposus and the elasticity of annulus fibrosus.

The effect of repeated loading was also determined by Tkaczuk (1968) and Nachemson & Evan (1968) by cyclically loading all the samples. Tkaczuk (1968) performed three loading cycles on both ALL and PLL specimens and found significant differences between the parameters obtained from both the ligaments although these differences were found to decrease in the 2<sup>nd</sup> and 3<sup>rd</sup> load cycles. Moreover, similar proportional change of mean parameters was

found between each load cycle for both the ligaments. Nachemson & Evan (1968) established that LF deforms elastically over much of its deformation range; owing to the elastin fibres which account for approximately 65% of its dry weight, and that the time-dependant properties of ligament increase in magnitude with increase in stress but are negligible at very low stresses. Nachemson & Evan (1968) also demonstrated that strains of less than 30-60% on the LF were fully recoverable on removal of the stress.

### **1.2.5.2 In-situ Ligament Testing**

Panjabi et al. (1982), Dumas et al. (1987), Myklebust et al. (1988), and Heuer et al. (2007) all tested ligaments in situ, intact with the spinal canal or the functional spinal unit. The studies analysed the changes in the range of motion of the spinal segments, by sequentially cutting the ligaments, in order to assess the role of each ligament in spine kinematics. These studies, just like those in the previous section, have their merits and shortcomings which are discussed in the following section.

#### **1.2.5.2.1 Specimen Preparation, Fixation and Maintenance**

##### *Storage*

The storage methods used by the aforementioned studies on in situ ligament testing are quite similar to the ones used in individual ligaments testing. Dumas et al. (1987) left some muscle tissue on the specimens during preparation, before storage, in order to keep the ligaments moist by protecting the contact with the air. Pintar et al. (1992) froze specimens in the intact state with sandbags placed in appropriate position to maintain normal spinal curvature.

##### *Specimen Type*

There are two types of specimens used in such in situ ligament testing studies:

- I. A whole functional spinal unit with all the ligaments intact, transecting ligaments in turn until only the bones and discs remain.
- II. Individual ligaments, in situ, in isolation i.e. removing all other ligaments, disc and supporting structures from the vertebral body except the one under study.

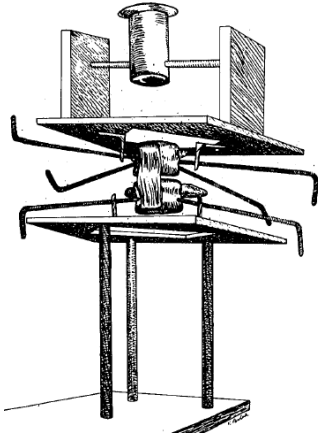
Dumas et al. (1987), Panjabi et al. (1982) and Heuer et al. (2007) all used the first type of specimen in order to test either the biomechanical behaviour of ligaments (Panjabi, et al., 1982; Dumas, et al., 1987) or to study the biomechanical effect of stepwise anatomy reduction for various loading directions and magnitudes (Heuer, et al., 2007).

Myklebust et al. (1988) used the second type of specimen to test ALL, PLL, both joint capsule (JC), ISL and LF at each spinal level from C2-S1. The SSL was also evaluated but only in the lumbar and thoracic regions. The fibres of the ALL and PLL are normally interwoven with the disc and it is difficult to draw a clear boundary between these longitudinal ligaments and the disc. The investigators solved this issue by differentiating the fibres based on their orientation. The ones belonging to the ligament were noted to be vertical while the ones of the disc were found to be oblique. Similarly, the testing of JCL is impossible without keeping the facet joints intact; therefore, the JCs were tested as a bilateral unit, comprising of both the JCLs and the facet joints. The LF was distinguished from the ISL due to its characteristic yellow colour while the SSL was differentiated from the ISL by defining the end of spinous process to be the division between the two.

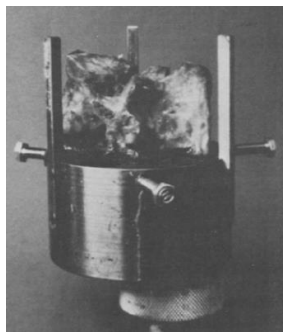
Pintar et al. (1992) also used the second type of specimen to test ligaments. They focussed on keeping the proper alignment of the spinal column. The specimens were frozen and marked under computed tomography (CT) to maintain alignment and photographed to obtain the dimensions.

### *Fixation*

These in situ studies face fewer issues in terms of fixation as it is easier to fix hard structures i.e. bones in the testing apparatus than soft tissue structures such a ligaments which are prone to slippage and deformation/damage from the site of fixation. The general approach followed in these studies was to fix one vertebra, usually the bottom one and attach the loading frame or testing rig to the top vertebrae and apply different types of forces/moments to it. Panjabi et al. (1982) and Myklebust et al. (1988) rigidly fixed the vertebral bodies attached to the top and bottom of ligament under consideration, as illustrated in Figure 1.13. Others have used potting methods to hold the vertebrae in place. Dumas et al. (1987) employed cylindrical metal cups with three screws to hold vertebrae in place before pouring fast setting epoxy resin (Figure 1.14). Metal guides were used to assure parallelism of cups. Heuer et al. (2007) embedded the FSU in PMMA from both sides with radio-translucent screws placed in the vertebrae prior to potting to provide better fixation. The potting method has advantages over the direct attachment to the testing machine as several specimens can be pre-prepared using the pots and stored in the refrigerator/freezer and tested one after another, saving time spent on preparation and potting in between tests.



**Figure 1.13: Schematic representation of specimen fixation (Adapted from Myklebust, et al., 1988)**



**Figure 1.14: Photograph of the FSU in the metal cup (Adapted from Dumas, et al., 1987)**

#### *Test Environment*

Dissection for in-situ ligament testing was performed at room temperature in 90-100% humidity chamber (Panjabi, et al., 1982; Dumas, et al., 1987) or using Ringers solution (Myklebust, et al., 1988). After dissection, Dumas et al. (1987) kept the ligaments covered until the testing with a commercial jelly, Lubafax, in order to prevent dehydration. Heuer et al. (2007) used a different approach to other studies and kept the specimens moist by wrapping them with 0.9% saline gauzes throughout the entire testing. This is a more practical way of keeping the tissue moist because testing within a high humidity chamber requires specialised equipment or a chamber to be built. Also working in high humidity chambers would be difficult for manipulating the specimens into the testing apparatus.

#### **1.2.5.2.2 Mechanical Test Design**

##### *Preliminary or Calibration Tests*

Dumas et al. (1987) performed preliminary tests to measure the stiffness of resin used to fix the vertebrae into the metal cups. The resin was found to have

higher stiffness by an order of magnitude than the ligaments stiffness. Therefore its deformation was considered to be negligible compared to ligament deformation for testing. The maximum loads used in the experiments were predetermined so that no permanent damage to the ligaments could occur. The investigators also determined the order of resecting the ligaments to choose the one which gave well separated curves, i.e. where the ligament with the most effect is cut first in order to avoid overriding the effects of other ligaments. This order was found to be from anterior to posterior. In order to reduce the water content of the specimens, Heuer et al. (2007) exposed the specimens to 500 N axial compression for 15 minutes.

#### *Actual Tests/ Measurements Taken*

Panjabi et al. (1982) conducted a study to determine physiological strains in each of the lumbar spinal ligaments during spine movement in three dimensions. They applied 12 different types of physiological loads at the geometric centre of the upper vertebral body and measured the deflection of this vertebra under load. The locations of the spinal ligaments for the neutral position of the FSU were determined by measuring the coordinates of various ligament attachment points. The flexion extension curves (on motion versus moment plots) were found to not meet each other at the origin, implying that there exists a zone for the neutral position of spine. The spine can lie anywhere within this zone on the application of smaller loads. This zone was named as the "neutral zone (NZ)". To move the spine outside the neutral zone, higher loads were required. These regions of increasing resistance, both on the negative and positive side of neutral zone, were termed as active zones. This increasing resistance to motion involves the elastic deformation of the soft tissues produced by the activation of muscles. In degenerated specimens the neutral zones were found to be generally wider indicating a higher probability of over-stretching the ligaments in a degenerated state.

Myklebust et al. (1988) used an M.T.S. (Minneapolis, MN) electrohydraulic system to apply direct axial tension to the specimens at 10 mm/s and obtained force versus deflection curves. Failure loads alongside failure deflections were also obtained. A similar method of measuring the displacement to Panjabi, et al. (1982) was used. Pintar et al. (1992) used the same testing procedure in order to determine the mechanical properties of spinal ligaments for direct incorporation into mathematical or finite element model.

Dumas et al. (1987) and Heuer et al. (2007) both performed preconditioning on the ligaments by submitting the specimens to several loading cycles in order to make the final response repeatable (see Section 1.2.4.2) hence minimising the

effect of viscoelasticity by capturing the reproducible elastic behaviour in the ligament. Preconditioning of the ligaments is important as it removes any crimping in the ligaments as a result of being stored in a frozen and fixed position by returning the structural collagen fibres to proper physiological conditions (Hashemi, et al., 2005). This results in a response that is repeatable and a better representative of normal physiological response (Van Ee et al., 2000). The last loading cycle was recorded to collect data for evaluation. Subsequently the specimens were reduced in structures by transecting the ligaments in turn. This way, a set of curves were obtained for each specimen. In order to compare the curves across different specimens, Dumas et al. (1987) calculated force at the linearity point i.e. the point where non-linear curve and linear curve differ significantly, and the rigidity which is defined as the slope of the linear portion of the curve (K).

Dumas et al. (1987) and Heuer et al. (2007), both, also measured the pre-tension exerted by the ligaments. Dumas et al. (1987) used a conventional method of resecting the ligaments and noting the force created as the pre-tension exerted by the ligaments. Whereas, Heuer et al. (2007) established pre-tension by introducing a concept of lordosis angle (the angle at the unloaded posture).

#### **1.2.5.3 Mechanical Properties of Ligaments from Experimental Studies**

The following section lays out the spread of experimental data on various aspects of lumbar spinal ligaments properties. The results are tabulated for comparison purposes both amongst the studies and with the result of the current study.



**Table 1.2: Mechanical properties of anterior longitudinal ligament (ALL).**

Author	Mechanical Properties								
	Pre-strain (%)	Pre-loading (N)	Failure Strain (%)	Failure stress (N/mm <sup>2</sup> )	Failure Load (N)	Failure Deflection (mm)	Mean strain at limits of NZ (%)	Maximum Strain (%)	Stiffness (N/mm)
Tkaczuk (1968) <sup>1</sup>	10.9	1.77		20.8	330				
Panjabi et al. (1984)							6		
Chazal et al. (1985) <sup>2</sup>			28	10.6	437		25	12.85 (extension)	
Myklebust et al. (1988)					209±196 – 676±359	11.5±12.1 – 20.4±3.5			
Pintar et al. (1992)			28.1±18.3 – 49±31.7	8.2±2.5 – 16.1±6.2					33±15.7

**Notes:**<sup>1</sup>Tkaczuk et al. (1968):

- ALL shortened less than PLL on removal.
- Degenerative changes in disc shown to effect the subsequent shortening of ligament.
- Exact pre-stress in a ligament was difficult to determine as it depended on the dimensions of ligaments and the pressure within nucleus pulposus and on the elasticity of annulus fibrosus.

<sup>2</sup>Chazal et al. (1985):

- Stress and strain at linearity point (start of linear region) on the load-deformation curve were reported as 1.15 N/mm<sup>2</sup> and 25% respectively.
- Stress and strain at plasticity point (end of linear region) on the load-deformation curve were reported as 9.11 N/mm<sup>2</sup> and 18.1% respectively.

**Table 1.3: Mechanical properties of posterior longitudinal ligament (PLL)**

Author	Mechanical Properties								
	Pre-strain (%)	Pre-loading (N)	Failure strain (%)	Failure stress (N/mm <sup>2</sup> )	Failure Load (N)	Failure Deflection (mm)	Mean strain at limits of NZ (%)	Maximum Strain (%)	Stiffness (N/mm)
Tkaczuk (1968)	13.4	2.94		19.42					
Panjabi et al. (1984)							5.75		
Chazal et al. (1985) <sup>1</sup>			29.5	20.8			45	13.5 (flexion)	
Myklebust et al. (1988)					38±15 – 160±82	4.2±0.1 – 7±3.2			
Pintar et al. (1992)			11.3±0.2 – 16.2±9.3	7.2±4.1 – 28.4±11.3					20.4±11.9

**Notes:**<sup>1</sup>Chazal et al. (1985)

- Stress and strain at linearity point (start of linear region) on the load-deformation curve were reported as 2.04 N/mm<sup>2</sup> and 45% respectively.
- Stress and strain at plasticity point (end of linear region) on the load-deformation curve were reported as 16.2 N/mm<sup>2</sup> and 0.34% respectively.

**Table 1.4: Mechanical properties of ligamentum flavum (LF)**

Author	Mechanical Properties								
	Modulus of Elasticity (N/mm <sup>2</sup> )	Force at linearity point (N)	Failure Strain (%)	Failure Stress (N/mm <sup>2</sup> )	Failure Load (N)	Failure Deflection (mm)	Mean strain at limits of NZ (%)	Maximum Strain (%)	Stiffness/K (N/mm)
Nachemson & Evan (1968) <sup>1</sup>	19.6(elderly) – 98(young)	277*	30(elderly) – 70(young)	1.96(elderly) – 9.8(young)	315			16.20 (flexion)	133 (old) – 665(young)*
Panjabi et al. (1984)		150 – 200*					7.1 & 7.2		310*
Chazal et al. (1985) <sup>2</sup>			19	15.2			16.6		
Dumas et al. (1987)		170							358
Myklebust (1988)					133±41 – 334±158	4.5±1.3 – 14.5±3.4			
Pintar et al. (1992)			28.8±8.2 – 102±2.9	1.3±0.4 – 4.1±0.5					27.2±9.2

**Notes:**

\*Values were estimated by Dumas et al. (1987)

<sup>1</sup>Nachmenson & Evans (1968)

- Tests conducted at a constant strain rate of 0.33/min.
- LF remained elastic in the physiological stress range; strains of 30-60% were found to be fully recoverable on removal of stress.
- Stress relaxation tests showed that the LF does behave in a non-linear viscoelastic manner although its time-dependent behaviour is not much significant at very low stresses but increase in magnitude with increasing stress.
- Found to pre-stress disc by a force ranging from 1.5kg in young to 0.4kg in old causing intradiscal pressures of 0.7kg/cm<sup>2</sup>.

<sup>2</sup>Chazal et al. (1985)

- Stress and strain at linearity point (start of linear region) on the load-deformation curve were reported as 3.17N/mm<sup>2</sup> and 16.6% respectively.
- Stress and strain at plasticity point (end of linear region) on the load-deformation curve were reported as 13.57N/mm<sup>2</sup> and 18.7% respectively.

**Table 1.5: Mechanical properties of intertransverse ligament (ITL)**

Author	Mechanical Properties			
	Failure Strain (%)	Failure Stress (N/mm <sup>2</sup> )	Mean strain at limits of NZ (%)	Maximum Strain (%)
Panjabi et al. (1984) <sup>1</sup>			13.5	25.50 in lateral bending
Chazal et al. (1985)	4.2	51	8.2	

**Notes:**<sup>1</sup>Panjabi et al. (1984)

- Stress and strain at linearity point (start of linear region) on the load-deformation curve were reported as 10.85N/mm<sup>2</sup> and 8.2% respectively.
- Stress and strain at plasticity point (end of linear region) on the load-deformation curve were reported as 47N/mm<sup>2</sup> and 0.15 respectively.
- ITL was found to have highest mean stress value with lowest mean strain value amongst other ligaments, showing its high resistance.

**Table 1.6: Mechanical properties of interspinous ligament (ISL)**

Author	Mechanical Properties							
	Force at linearity point (N)	Failure Strain (%)	Failure Stress (N/mm <sup>2</sup> )	Failure Load (N)	Failure Deflection (mm)	Mean Strain at limits of NZ (%)	Maximum Strain (%)	Stiffness/K (N/mm)
Waters & Morris (1973)	341*	18-34						1530*
<sup>1</sup> Chazal et al. (1985) (tested ISL with SSL)		38.5	8.71	80-300		41.6		
Myklebust et al. (1988)				95±22 – 185±41	7.4±3.3 – 17.8±0.6			
Panjabi et al. (1984)	50-100*					10.9	27.90 (flexion)	218*
Pintar et.al (1992)		51.5±2.9 – 119.7±14.7	1.8±0.1 – 5.9±1.8					11.5±6.6
*Dumas et al. (1987)	82							80

**Notes:**

\*Values were estimated by Dumas et al. (1987)

<sup>1</sup>Chazal et al. (1985)

- Stress and strain at linearity point (start of linear region) on the load-deformation curve were reported as 1.75N/mm<sup>2</sup> and 41.6% respectively
- Stress and strain at plasticity point (end of linear region) on the load-deformation curve were reported as 7.92N/mm<sup>2</sup> and 30.5% respectively

**Table 1.7: Mechanical properties of supraspinous ligament (SSL)**

Author	Mechanical Properties						
	Force at linearity point (N)	Failure Strain (%)	Failure Stress (N/mm <sup>2</sup> )	Failure Load (N)	Failure Deflection (N)	Maximum Strain (%)	Stiffness/K (N/mm)
Panjabi et al. (1984)	50-100*					31.95 (flexion)	100*
*Dumas et al. (1987)	66						75
Myklebust et al. (1988)				226 – 750±159	21.1 – 29.2		
Pintar et al. (1992)		70.6 ± 45 – 115.1 ± 49.1	8.9±3.2 – 15.5±5.1				23.7±10.9

**Note:** \*Values were estimated by Dumas et al. (1987)

**Table 1.8: Mechanical properties of joint capsular ligament (JCL)**

Author	Mechanical Properties					
	Failure Strain (%)	Failure Stress (N/mm <sup>2</sup> )	Failure Load (N)	Failure Deflection (mm)	Maximum Strain (%)	Stiffness (N/mm)
*Panjabi et al. (1984)					19.25 (rotation)	
Myklebust et al. (1988)			252±22 – 429±122	9.8±1.6 – 12.8±2.5		
Pintar et al. (1992)	47.9±5.4 – 90.4±17.7	3.5±1.2 – 4.4±1.4				33.9±10.7

**Notes:**

\*Panjabi et al. (1984)

- Only ligament that was found to resist axial rotation.
- When the CL on one side was stretched the one on the other side was found to be shortened.

#### 1.2.5.4 Discussion

The above mentioned studies all give considerable amount of data on biomechanical parameters and mechanical properties of ligaments, however the results are quite varied. Although the geometric parameters were calculated and presented, there is huge amount of variability across studies due to differences in the measurement procedures, for the individual ligament testing studies. Based on these results, it is difficult to determine which method is the most accurate for measuring geometric properties. Although dissection is never raised as an issue in any of the aforementioned studies, it is one of the most challenging parts of mechanical testing of individual ligaments. The ligaments do not follow the same pattern within a specimen or across different specimens. The fibres run in all directions and interweave with fibres of other tissues, such as the discs, making the distinction between the two difficult. They also tend to have different width and thickness across the entire length making it even harder to predict their boundary for accurate dissection of the entire structure. The removal of ligaments from the spinal column for testing often results in damage to the ligament. Pre-tension in the ligament is another important consideration which is often neglected in most of the studies apart from Tkaczuk (1968). When the ligaments are removed for individual testing, they lose the constant pre-tension they are under, in the intact state, in the spine. Hence, the stress-strain curves derived would start at a different point to that if a pre-strain were applied first. This makes it harder to compare between studies. Another disadvantage of individual ligament testing is the difficulty of fixation, the ligaments either have to be removed with the bony attachments or specialised clamping systems have to be employed to avoid slippage of the specimen and damage of the specimen from the areas of contact in the clamp. The technique is also unable to define the role of ligaments in relation to other spinal components. Despite all its disadvantages, the technique still has an advantage of being able to produce individual load-displacement curves for each ligament and is useful when one wants to study the internal structure of ligaments.

The in situ ligament testing method resolves most of the difficulties stated above. As the ligaments were tested in the anatomical position in relation to other structures, their geometry was not needed to obtain the overall mechanical parameters (e.g. stiffness and strength) hence avoiding the issues of inaccurate measure of length and cross-sectional area. The challenge of dissection and extraction of the ligament without damaging its fibres was also

avoided by keeping them intact and transecting in steps, when needed. Keeping the ligaments in situ, in the intact state, will keep them in a more normal state hence the results better reflect the true behaviour. The problem of fixation is also resolved as it is easier to fix the vertebrae in the testing apparatus without the need for designing specialised clamping systems for each ligament.

The studies reviewed in this chapter have highlighted some useful pointers for future in situ testing of ligaments, summarised as follows:

- The ligaments can be stored in sealed plastic bags at  $-20^{\circ}\text{C}$  to  $-30^{\circ}\text{C}$  after retrieval and used later without experiencing any change in their behaviour.
- The tissue can be thawed in a refrigerator rather than at room temperature and kept moist during testing with saline gauzes to prevent it from drying out.
- The transection can use the distinction between the fibres and orientation of interconnected ligaments.
- The order of the transection of ligaments should be considered as it is shown to affect the behaviour of ligaments and hence the properties obtained. In a particular motion, if the ligaments which are higher contributors to the whole ligament complex behaviour in the FSU are saved until the end, then the behaviour of all other ligaments will be dominated by their presence and the resulting stress-strain curves will be superimposed until those dominating ligaments are transected.
- The specimen can be kept in place by holding it between screws in the pot before pouring in the potting material.
- Preconditioning should be considered in order to minimise the effect of viscoelastic response.
- The stiffness of the surrounding materials and holders should be checked to make sure their deformation would be negligible compared to ligament deformation for testing.
- The maximum loads that will be used in the actual experiments should be predetermined so that no permanent damage to the ligaments could occur during testing.



All the advantages discussed above makes in situ ligament testing a better method of evaluating the mechanical properties of spinal ligaments and hence will be the method of choice of experimental testing for this study. All the points raised above will be useful considerations when developing the protocol for the actual study plan. The only disadvantage of in situ ligament testing is to decide on the motions and devise methods of creating the movements and controlling them. All the in situ studies above described the role of each ligament in relation to other structures and gathered substantial amount of data, however, its comparison and validity is hard to establish as all the studies used different methods.

## **1.2.6 Finite Element Modelling of Ligaments**

### **1.2.6.1 Introduction**

As discussed in the previous section, a number of studies have been performed to establish the physical and biomechanical properties of ligaments. The large variability in outcomes mean that either a large number of experimental studies have to be performed to gather the full behaviour of each ligament in the functional spinal unit model or other avenues must be explored. Computational modelling, using finite element (FE) methods makes it possible to simulate the complex behaviour of the FSU. Such models can include detailed representations of the bone and soft tissue structures and their non-linear material properties. Physical and mechanical properties of ligaments are required to be able to represent these tissues in the models. The ligaments have been represented in these models using a number of different types of finite elements, with different geometries, material properties and initial conditions.

As discussed above, to develop material models of ligaments, detailed experimental measurements of the material structure and mechanical behaviour are needed. The various experimental studies performed on isolated ligaments as well as in situ ligaments generated useful data describing the mechanical behaviour of ligaments (Section 1.2.5) and have been used by researchers to develop FE models of ligaments or of spine in general. Based on these experimental studies, ligaments have been described as inhomogeneous, non-linear, anisotropic and viscoelastic structures that undergo large deformations during elongation (Weiss & Gardiner, 2001). They have been shown to exhibit a non-linear load-displacement (stress-strain) behaviour (Section 1.2.4.1) with a neutral zone (NZ), elastic zone (EZ) and plastic zone (PZ). For the accurate representation of ligaments this non-linear behaviour must be taken into account in the FE model. In addition, their contact

with other tissues and in-situ pre-tension makes the accurate modelling of the mechanical behaviour of ligaments a challenging task. But these types of models can also potentially be used to derive the properties (i.e. by reverse engineering) in a more reliable way than the methods reported in Section 1.2.5 where the ligaments had to be either extracted out or assumptions had to be made about the geometry.

The following section reviews the literature on a selection of recent finite element studies that incorporate the spinal ligaments in models. Their application of in-vitro experimental values such as Young's modulus, width, thickness and pre-tension and their choices of finite element type, material model and attachment sites are explored.

#### **1.2.6.2 Geometry, Material Properties and Material Model**

The quantitative information on geometry and material properties of the human lumbar ligaments, used in FE studies, comes primarily from a limited number of experimental studies (Tkaczuk, 1968; Chazal, et al., 1985; Pintar, et al., 1992). The raw data obtained by these primary experimental studies for each of the spinal ligaments is tabulated in the previous section (Tables 1.2 to 1.8). The majority of FE studies have used the average value of Young's modulus for each of the ligaments while a limited number have used values towards the lower and upper extremes of the experimental range (Table 1.9). A Poisson's ratio of 0.3 has been almost universally chosen for all of the ligaments without much justification of the choice.

The in-vitro studies mentioned in Section 1.2.5 were mainly focussed on the material properties of the ligaments. However, most have also recorded information on the ligament geometry as the material properties have primarily been derived from the geometry. As discussed previously, the methods used to determine the geometry have varied and the values obtained are quite different from each other. Although finite element studies require these dimensions to be translated into their investigations, the geometric values used are not reported consistently. For example, Lee & Teo (2005) report only the elastic modulus and not the cross-sectional area in their study, so it is not possible to derive the ligament stiffness to make comparisons with the values reported by the in-vitro studies such as Pintar et al. (1992).

The material properties and cross-sectional area (CSA) used by different researchers are compared in Table 1.9. As can be seen from the table, the properties used are quite varied and cross sectional area is not given in all cases. Some studies did not publish any material property data used. As an example, the variation in the stress-strain behaviour of the PLL used by

different groups is shown in Figure 1.15 using the information summarised in Table 1.9. The graph clearly shows the variability in model behaviour.

Furthermore, a variety of material models have been used to represent the ligament behaviour including elastic, viscoelastic and hyperelastic models. The use of an elastic model by researchers is due partly to the relative insensitivity of ligaments material behaviour to strain rate over several orders of variations (Fung, 1993) and partly to the “preconditioned” state that the tissue reach after repeated loading with minimal amount of hysteresis (Weiss & Gardiner, 2001).

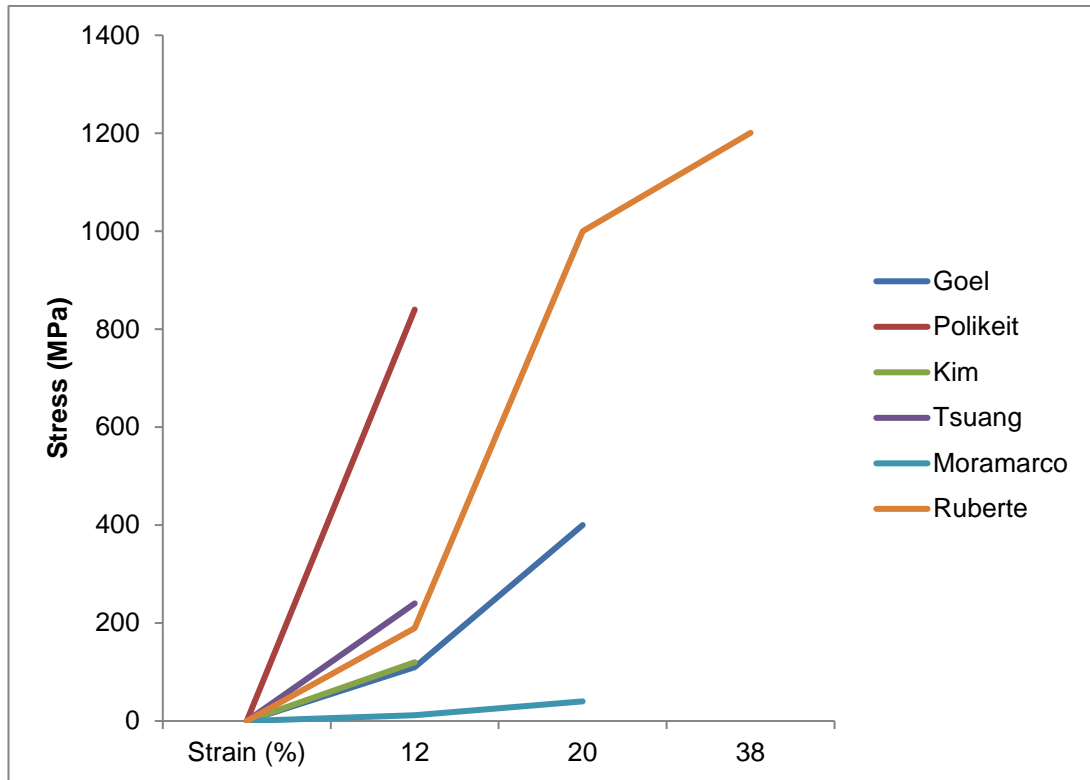
In a review by Weiss & Gardiner (2001) on computational modelling of ligaments, the methods of modelling the toe-region to represent elastic behaviour of ligaments were divided into two approaches. Both of these approaches describe the uniaxial response of ligaments by relating the toe region to the collagen structure. Uniaxial response refers to the load-carrying ability of the ligaments along their preferential axis i.e. along the direction of collagen fibres.

One approach represents non-linear, elastic behaviour by sequentially recruiting numerous individual linearly elastic elements. These individual elements represent collagen fibrils in their crimped and unloaded form with different initial lengths. To begin with, only a few collagen fibrils are recruited, but as the ligaments are loaded, more and more fibrils are recruited to represent the non-linear behaviour characteristic of the toe-region. With this method, linear behaviour is demonstrated at higher loads where all the fibrils are loaded, causing the stress-strain curve to become linear. The other approach directly models a representation of the amalgamated collagen fibrils, by using non-linear spring elements, in order to describe the uniaxial behaviour and the corresponding toe-region. The discrete elements used in these studies are either single-line or multiple-line, to represent different fibre bundles (Li, et al., 1999).

**Table 1.9: Material properties used by researchers in FE studies including the cross sectional area (CSA), Young's moduli (E) and transition strains ( $\epsilon$ ). where, E1, E2 and E3 represent the Young's moduli of the polygonal stress-strain function while  $\epsilon_1$ ,  $\epsilon_2$  and  $\epsilon_3$  are the corresponding transitions strains separating the Young's moduli with  $\epsilon_3$  being the maximum strain of the physiological range.**

Authors	Ligament	CSA (mm <sup>2</sup> )	E1 (MPa)	$\epsilon_1$ (%)	E2 (MPa)	$\epsilon_2$ (%)	E3 (MPa)	$\epsilon_3$ (%)
Goel et al. (1995) Lee & Teo (2005)*	ALL	63.7	7.8	12	20			
	PLL	20	10	11	20			
	LF	40	15	6.2	19			
	ITL	1.8	10	18	59			
	CL	30	7.5	25	33			
	ISL	40	10	14	12			
	SSL	30	8	20	15			
Polikeit et al. (2003) Lee & Teo (2004)* Sylvestre et al. (2007) Bowden et al. (2008)	ALL	38	20					
	PLL	20	70					
	LF	60	50					
	ITL	10	50					
	CL	40	20					
	ISL	35.5	28					
	SSL	35.5	28					
Kim (2007)	ALL	22.4	7.8					
	PLL	7	10					
	LF	14.1	17					
	ITL	0.6	10					
	CL	10.5	7.5					
	ISL	14.1	10					
	SSL	10.5	8					
Tsuang et al. (2009)	ALL		20					
	PLL		20					
	LF		19.5					
	ITL		59					
	CL		32.9					
	ISL		12					
	SSL		15					
Moramarco et al. (2010)	ALL	32.4	7.8	12	20			
	PLL	5.2	1	11	2			
	LF	84.2	1.5	6.2	1.9			
	ITL	1.8	10	18	59			
	CL	43.8						
	ISL	35.1						
	SSL	25.2	3	20	5			
Ruberte et al.(2009)	ALL	32.5	12.6	8	15.6			
	PLL	5	27.1	7	40	25	31.6	38
	LF	91.6	24	8	40	20	36	25
	ITL	2	125	8	313			
	CL	51.2	7.5	25	12.7			
	ISL	34	4.15	20	11.4			
	SSL	34	4.15	20	11.4			
Hortin & Bowden (2016)	ALL	65.6	9.58		24.9		9.15	
	PLL	25.7	18.5		61.5		46.1	
	LF	39	29.1		59.2		20.7	
	CL		0.3					
	ISL	15.1	5.59		23.4		5.19	
	SSL	15.1	5.59		23.4		5.19	

\*No CSA



**Figure 1.15: Graph showing stress-strain relationship for PLL used by different researchers in their FE models**

In the finite element models of spine to date, a number of researchers have taken the second approach to simulate the non-linear stress-strain behaviour of ligaments (Rohlmann, et al., 2006; Schmidt, et al., 2007; Bellini, et al., 2007). However, a large number of studies have adopted a similar approach and assigned a linear elastic model by assuming that the ligaments mostly function within the linear region (Polikeit, et al., 2003; Guan, et al., 2006; Sylvestre, et al., 2007; Chen, et al., 2009; Tsuang, et al., 2009). However, attempts have also been made to represent the toe-region as well as the linear region of stress-strain curve and for this purpose a bilinear model has been used (Goel, et al., 1995a; Goel, et al., 1995b; Moramarco, et al., 2010; Lee & Teo, 2005; Ivanov, et al., 2009). Trilinear approaches have also been used to model some ligaments (Ruberte, et al., 2009).

Viscoelastic models of ligaments have also been developed (Lee & Teo, 2004) which mainly represent the time-dependant or strain-rate dependant behaviour of ligaments at higher loads or in impact scenarios. These models can be useful if considering the cyclic loading (Yahia & Drouin, 1990), creep or stress relaxation (Hughes, et al., 1990).

### 1.2.6.3 Attachments Sites

Apart from material behaviour modelling, another aspect which is important in modelling ligaments is the attachment site replication. A close representation of these attachment sites in FE studies is crucial (Section 1.2.1.5.9). In the literature, very few studies describe the attachments (Sylvestre, et al., 2007; Tsuang, et al., 2009; Lee & Teo, 2005; Lee & Teo, 2004). Other studies, although the ligaments have been attached in the models, do not give any description of the attachment site. Sylvestre et al. (2009) developed a five-vertebra lumbar spine model. They modelled the ALL and PLL with ten and six tension only cable elements attaching respectively the anterior and posterior sections of the IVD to corresponding sections of the vertebral endplates. The LF was modelled as three elements attached to the lamina, the ITL as two elements joining adjacent transverse processes while the SSL and ISL as three and four elements attaching adjacent spinous processes respectively. Lee & Teo (2004, 2005) and Tsuang et al. (2009) both stated the use of bony landmarks as attachment site based on the description given in anatomy books but do not give any description of how the attachment were translated into the model.

### 1.2.6.4 Elements Type

In the FE modelling of the lumbar spine, ligaments have always been incorporated in the model with the geometry of other structures such as vertebrae and disc primarily derived from some imaging source, such as a CT scan. Different studies use different types of elements to define the geometry of ligaments. The vast majority of short spinal segment studies have used one-dimensional elements such as 2-node axial elements (Guan, et al., 2006; Zhang, et al., 2010; Moramarco, et al., 2010; Goel, et al., 1995a; Goel, et al., 1995b; Wong, et al., 2003; Polikeit, et al., 2003; Sylvestre, et al., 2007; Kim, 2007; Ivanov, et al., 2009), although some studies have used two-dimensional thin shell elements (Bowden, et al., 2008) and some three-dimensional elements such as spring or tetrahedral elements (Rohlmann, et al., 2006; Schmidt, et al., 2007; Bellini, et al., 2007; Tsuang, et al., 2009). Table 1.10 summarises the different types of elements used by different studies and the justification of choice, if any given.

### 1.2.6.5 Pre-strain/Pre-tension

Ligaments have been observed to be under a certain amount of tension in situ (Section 1.2.4.3). This property of spinal ligaments is rarely included in the FE models, and it is unclear what, if any, influence this parameter may have on the results. In a study by Kim (2007) the LF was assumed to have a pre-strain of

3.5% which was assumed to be ignorable under compression. No consideration was given to pre-tension in other studies. The reason for this omission/exclusion is the difficulty in establishing a definitive value for pre-stress due to the dependence of pre-stress on various factors including the state of the intervertebral discs and the annulus fibrosis, age, and, vertebral level of the spine (Tkaczuk, 1968). Moreover, if the experimental data came from the study which was carried out on ligaments in their close-to-natural state such as in-situ ligament testing, then the ligaments will be in a state of pre-stress and the deformation would be representative of testing beyond the pre-stress. However, in cases where the data came from testing carried out on individual ligaments, inclusion of pre-stress would be important in clinical cases for instance when simulating spinal replacement devices or new interventions that are being tested for their performance within the body. In these cases it is important to note that the physiological range starts beyond the pre-stress and so the testing range should be large enough to go above and beyond it and to also appreciate the point where the change in stress starts making a difference physiologically. In high impact scenarios inclusion/exclusion of pre-stress would not make much difference to the results as the performances at such low stresses would not add much to the high stresses being experienced.

**Table 1.10: Comparison of different elements types used by researchers in FE modelling of lumbar spine**

<b>Author</b>	<b>Ligament Modelled</b>	<b>Type of Element</b>	<b>Justification of Choice</b>
Goel et al. (1995)	All	Cable - tension only (1D)	These elements resist tension producing forces – representing physiologic conditions experienced by ligaments
Polikeit et al. (2003)	All	Truss - tension only (1D)	Ligaments oriented along the same direction as given in text books
Wong et al. (2003)		2-node Truss (1D)	
Lee & Teo (2004, 2005)	All		
Rohlmann et al. (2006)	All	Spring - tension only (3D)	
Kim (2007)	All	Cable - tension only (1D)	Ligament fibres are described as bilinear, isotropic elastic materials have large resistance in tension but are very compliant in compressions
Schmidt et al. (2007)	Six (no ITL)	3-D uniaxial Spring elements (3D)	
Bellini et al. (2007)	All	Nonlinear spring – tension only (3D)	
Sylvestre et al. (2007)	All	Bi-linear cable-tension only (1D)	
Bowden et al. (2008)		2D Fabric representation – tension only (2D)	More complex than spring elements- support complex loading patterns with non-uniform stress concentrations
Tsuang et al. (2009)	All	Tetrahedral- linear properties (3D)	
Moramarco et al. (2010)		Nonlinear truss elements - tension only (1D)	



### **1.2.6.6 Boundary and Load Conditions**

Boundary conditions and loads applied in FE studies are usually problem-specific. The studies mainly focus on defining a problem, showcasing diseased scenarios or testing the stability with the insertion of a surgical device. The ligaments have usually been added as the structures that help in maintaining and providing the stability to the overall segment, therefore the loads and boundary conditions are usually applied to the entire segment and not just to the ligaments separately.

### **1.2.6.7 Discussion**

A number of finite element models (FEMs) have been developed over the years to simulate spinal injury scenarios or to predict the onset or risk of injuries in healthy or degenerated spines (Cheung, et al., 2003; Whyne, et al., 2003; Wilcox, et al., 2004; Wang, et al., 2005; Qiu, et al., 2006). In the FEMs of the lumbar spine, ligaments have usually been modelled using one-dimensional single-line elements or multiple-line elements with simplified load-displacement behaviour, whereby line elements are straight lines representing a collection of fibre bundles in the ligament. More sophisticated approaches have been taken, especially in modelling the knee. Mommersteeg et al. (1996) simulated tensile tests performed on isolated knee ligaments (bone-ligament-bone preparation) with a numerical model. The use of three or fewer non-linear elastic line elements per ligament in human knee ligaments model was shown to be very sensitive to geometrical parameters used, whereas using seven or more line elements was shown to be mathematically redundant in this case (Mommersteeg, et al., 1996). Therefore, a compromise will have to be found which is specific to the model, the geometry being represented, any interactions with features and loading conditions. This means performing a mesh refinement study to obtain the optimum number of elements used for each ligament.

In terms of modelling the dimensions of the ligaments, all studies manually created the ligaments based on the values generated by in-vitro experimental studies. Since the experimental studies used different techniques for obtaining these geometric parameters, the values obtained are quite varied and it is difficult to determine the most appropriate values from the list as all the methods have their own shortcomings as discussed previously (Section 1.2.5.4). Therefore, a better way of modelling these ligaments is required which closely replicate the real geometry and scenario. The most ideal method would be to scan the ligaments in situ and export the geometric data to the model directly for meshing and subsequent analysis. As the rest of the mesh

geometry i.e. the bones and disc are usually obtained from CT scans of FSU, this would require a method to be devised to either scan the ligaments in CT or using other soft tissue scanning modalities such as MRI.

The material properties, especially the range of Young's modulus values, taken from literature also spanned several testing methodologies with various testing equipment. Moreover, the amount of post mortem time, preservation methods and testing conditions were quite varied (Section 1.2.5). Furthermore, these studies have used values that were derived directly from force-displacement data, using mean values for cross sectional area (CSA) and length in order to derive linear (Tsuang, et al., 2009) or bilinear (Moramarco, et al., 2010) material properties for the ligaments. This could have implications as the ligaments are heterogeneous with an irregular shape and hence have a varying cross-sectional area across its length which cannot be captured by a mean value. These differences in testing protocols affect the outcome and hence have led to a large range of values being used for each ligament. A better approach could be to perform experiments to gather the in situ behaviour of ligaments and then calibrate the FE model to the experimental study. This will result in a specimen-specific model which represents the actual mechanical behaviour of each ligament more closely for that specimen. Such an approach has been undertaken for the knee ligaments in a study by Harris, et al. (2016) on natural knee joint with all the tissues intact. They combined experimental tests and subject-specific FE models to accurately simulate the behaviour of ligaments by having a one-to-one experiment to model calibration. The ligaments material parameter were tuned and perturbed until the output matched the experimental behaviour.

As described previously, some studies do represent the non-linear or bi-linear behaviour of ligaments in their FE models. It would be ideal to capture the non-linear behaviour of the ligament; however, it may be that the ligaments act predominantly in the linearly elastic range of strains, so starting off with an elastic linear model and then examining the strains in the ligament would indicate if a bi-linear or other more complex material model was necessary. Similarly, starting off with an elastic model and building up to a viscoelastic model would be ideal only if a time-dependant model is needed.

A number of FE studies have been one-dimensional and have successfully described the uniaxial behaviour of ligaments (Weiss & Gardiner, 2001). However, their predictive values (outcome) cannot be tested as there are no independent tests that can predict one-dimensional behaviour of ligaments. Also these one-dimensional models cannot describe or predict the three

dimensional, anisotropic (due to collagen-reinforced structure) behaviour of ligaments. The shear and transverse loading experienced by ligaments *in vivo* also cannot be described by the one-dimensional model. The material properties for ligaments have usually been taken from in-vitro experimental studies performed in low-strain rate conditions. These studies predict the behaviour of the model under the application of external loads, however, are still limited in predicting non-uniform three-dimensional (3D) stresses and strains (Weiss, et al., 2005). The models are also limited in that they do not represent the strain inhomogeneities that occur across individual ligaments *in situ* (Woo, et al., 1990).

The attachment site replication, as discussed above, is not really described in previous FE studies. There are two ways the ligaments could be attached to the rest of the geometry. It could either be completely bound over a surface or the ligament can be attached at a line of points. In any case, proper interaction conditions have to be applied to stop the elements of the ligaments and other geometry protruding into each other during simulation.

Although the pre-tension in ligaments is not widely modelled across FE studies, it is considered to be responsible for joint stability in the absence of muscle and tendon forces (Weiss & Gardiner, 2001). Therefore, its inclusion in FE models is imperative to avoid the underestimation of the real stresses in ligaments.

### **1.2.7 Material models for soft tissue modelling**

From the previous section, it can be seen that, in spinal modelling, various assumptions have been made about ligaments; mostly that it has either a linear, bi-linear or even a tri-linear behaviour. The most basic form is a linear elastic relationship between stress and strain that is often employed in simpler cases. More sophisticated models have been used in other joints to model the ligaments using FE analysis which have demonstrated a significant increase in accuracy with more realistic constitutive models, especially when a three-dimensional representation of ligaments is used (Park, et al., 2010). In the knee for example, hyperelastic material models are widely used (Kiapour, et al., 2014; Limbert, et al., 2004; Dai, et al., 2015; Dhaher, et al., 2010; Mootanah, et al., 2014; Pena, et al., 2005; Liu & Zhang, 2013) to model the ligaments.

The finite element solution for structural problems is usually based on the fact that the structural potential energy has to be minimised; one of the energy components is the strain energy within the structure as it deforms. The strain energy potential,  $U(\epsilon)$ , defines the strain energy stored in a material per unit of reference volume as a function of strain ( $\epsilon$ ) at that point in the material. The strain energy potential for an elastic material is the area under the stress strain

curve. For more complex material behaviour, the strain energy is non-linear and the stress can be related to strain with a hyperelastic material model. The strain energy potentials for various isotropic hyperelastic material models which will be explored in this study are outlined in Table 1.11, in the form in which they are implemented in a commercial finite element package (Abaqus). Hyperelastic material models were initially developed to predict the stress-strain behaviour of materials such as polymers and rubbers, but due to the similarity in the mechanical behaviour of soft tissues such as ligaments, the models have also been implemented to represent these tissues.

The Neo-Hookean model is one of the simplest hyperelastic models which provides good approximation of stress-strain behaviour of materials at relatively small strains but is unable to capture the upturn (stiffening) of the stress-strain curve (Shahzad, et al., 2015). It behaves more like a linear elastic model having a working strain range of 30% (Kumar & Venkateswara Rao, 2016) and is known for not being able to predict accurate phenomena at large strains. The Mooney Rivlin model has a strain range of 30% in compression and 200% in tension depending on the order, however it also cannot capture the upturn of force-extension relation in uniaxial tests. The Ogden model captures the stiffening of the stress-strain curve and model the material accurately for large ranges of deformation, up to 700% (Kumar & Venkateswara Rao, 2016; Beomkeun, et al., 2012). Martins et al. (2006) performed a comparative study of several hyperelastic material models for prediction of hyperelastic properties for materials with non-linear behaviour and found the Ogden material model to be amongst the best representations of the behaviour, whereas the Neo-Hookean model was found to be the worst as it was unable to capture the nonlinearity of the mechanical behaviour (Martins, et al., 2006). In the analysis of the behaviour of rubber component, the Ogden model (especially 3<sup>rd</sup> order) was found to have better flexibility in describing the non-linear stress-strain curve than the Mooney-Rivlin model since the stretch ratio's exponents of the Ogden model are composed of any real numbers whereas for Mooney-Rivlin model they are composed of integers (Beomkeun, et al., 2012).

From the above, it can be deduced that the Neo-Hookean and Mooney-Rivlin models could be used for initial studies of hyperelastic materials as they are simple and easy to implement, but they will only make good approximations at relatively small strain rates. For large deformation in rubber-like materials, more advanced models would be better suited.

The Neo-Hookean form and the Mooney-Rivlin form have both been used in knee ligaments modelling (Abraham, et al., 2011). The Ogden form has also

been successfully implemented to model ligaments of the human ear (Cheng & Gan, 2008; Gan, et al., 2011). The Holzapfel-Gasser-Ogden model that captures the anisotropic behaviour of soft tissues has been used in multiple studies to model anterior cruciate ligaments in the knee joint and has been very recently employed in the spine for the first time to represent the ALL, ISL and SSL (Hortin & Bowden, 2016).

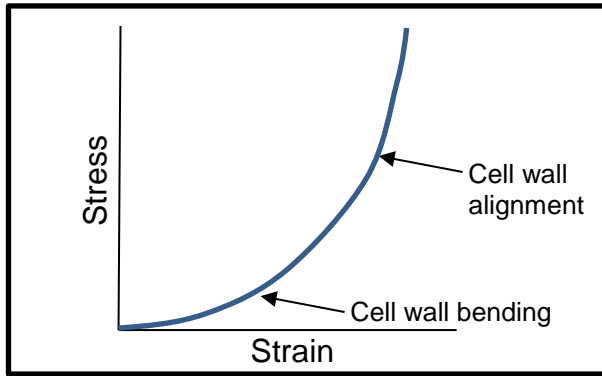
The hyperfoam model is a type of hyperelastic model that can represent cellular solids whose porosity permits large volumetric change (Poisson's ratio  $< 0.5$ ) as the cells deform and collapse. The structure of the foam has some similarities to that of the ligaments i.e. it is composed of polyhedral cells packed in three dimensions. The cells have interconnected networks of solid struts that form the edges of the cells similar to the collagen fibres. The response of a hyperfoam model under tension is very similar to ligaments (see Figure 1.16) but it behaves differently under compression, so this model is only appropriate when the full tissue is in tension (ABAQUS, 2011). At small strains, it deforms in a linear, elastic manner due to cell wall bending similar to the uncoiling of the crimp pattern of the collagen fibres in the neutral zone of ligaments. This is followed by the rise in stiffness due to the rotation and alignment of the cell walls similar to the elastic zone in ligaments whereby a rise in stress with corresponding strain is evident due to the stretching of the collagen fibres further, beyond the NZ and up to the physiological limit.

In conclusion, although current models of the spine have generally used linear elastic constitutive models, more accurate representations of the non-linear behaviour have been adopted for other ligaments. These provide some useful indicators of models that could be employed for the spine in future studies.

**Table 1.11: List of various hyperelastic material models and their respective Abaqus implementation strain energy potentials which can be used for FE modelling of ligaments. (ABAQUS, 2011)**

<b>Material model</b>	<b>Strain energy potential</b> (where $I_k$ , $\lambda_k$ and $J^{el}$ are related to the strain tensor)
Neo-Hookean  (adapted from Rivlin, 1948)	$U = C_{10}(\bar{I}_1 - 3) + \frac{1}{D_1}(J^{el} - 1)^2$ <p>Where <math>C_{10}</math> and <math>D_1</math> are model parameters such that  <math>\mu_0 = 2C_{10}</math> is the initial shear modulus  <math>K_0 = \frac{2}{D_1}</math> is the initial bulk modulus</p>
Mooney-Rivlin  (adapted from Mooney, 1940 & Rivlin, 1948)	$U = C_{10}(\bar{I}_1 - 3) + C_{01}(\bar{I}_2 - 3) + \frac{1}{D_1}(J^{el} - 1)^2$ <p>Where <math>C_{10}</math>, <math>C_{01}</math> and <math>D_1</math> are model parameters such that  <math>\mu_0 = 2(C_{10} + C_{01})</math> is the initial shear modulus  <math>K_0 = \frac{2}{D_1}</math> is the initial bulk modulus</p>
Ogden  (adapted from Ogden, 1972)	$U = \sum_{i=1}^N \frac{2\mu_i}{\alpha_i^2} (\bar{\lambda}_1^{\alpha_i} + \bar{\lambda}_2^{\alpha_i} + \bar{\lambda}_3^{\alpha_i} - 3) + \sum_{i=1}^N \frac{1}{D_i} (J^{el} - 1)^{2i}$ <p>Where <math>\mu_i</math>, <math>\alpha_i</math> and <math>D_i</math> are model parameters such that  <math>\mu_0 = \sum_{i=1}^N \mu_i</math> is the initial shear modulus  <math>K_0 = \frac{2}{D_1}</math> is the initial bulk modulus  <math>\alpha_i</math> is a unit less coefficient that defines the non-linearity of the curve</p>
Hyperfoam  (adapted from Jemiolo & Turtleaub, 2000)	$U = \sum_{i=1}^N \frac{2\mu_i}{\alpha_i^2} \left[ \hat{\lambda}_1^{\alpha_i} + \hat{\lambda}_2^{\alpha_i} + \hat{\lambda}_3^{\alpha_i} - 3 + \frac{1}{\beta_i} (J^{el})^{-\alpha_i \beta_i} - 1 \right]$ <p>Where <math>\mu_i</math>, <math>\alpha_i</math> and <math>\beta_i</math> are model parameters such that  <math>\mu_0 = \sum_{i=1}^N \mu_i</math> is the initial shear modulus  <math>K_0 = \sum_{i=1}^N 2\mu_i \left( \frac{1}{3} + \beta_i \right)</math> is the initial bulk modulus  <math>\alpha_i</math> is a unit less coefficient that defines the non-linearity of the curve  <math>\beta_i</math> is related to the Poisson's ratio, <math>\nu_i</math>, by the expressions  <math display="block">\beta_i = \frac{\nu_i}{1 - 2\nu_i}, \quad \nu_i = \frac{\beta_i}{1 + 2\beta_i}</math></p>

N.B. The models are phenomenological models and as such the resulting model parameters have no discernible physical association.



**Figure 1.16: Typical tensile stress-strain curve of a foam (adapted from ABAQUS, 2011).**

### 1.3 Study Motivation, Aim and Objectives

#### Motivation

The extensive literature review carried out and presented in this chapter helped identify the gaps in the current literature. The various experimental studies carried out to test the spinal ligaments have produced a considerable amount of data on the mechanical properties of ligaments. However, due to the variability in the methods of dissection and retrieval of the ligaments and measurement of geometric parameters, as well as the various testing regimes and associated motions applied, there is a large amount of inconsistency in the outcomes. This makes it impossible to compare the results or to make any meaningful conclusions.

Although a comparison of human and ovine spines has been undertaken to examine the vertebrae, no studies have been found that examine and compare the structure and mechanical properties of human and ovine spinal ligaments. As the ovine spine is often used as an alternative model for the human spine in research studies, and since the spinal ligaments are known to play a major mechanical role in the stability of the spine, there is a need to compare the mechanical behaviour of ovine spinal ligaments to human to establish if the ovine spine is a suitable alternative for human spine in terms of ligamentous behaviour.

Similarly, finite element models of spine are regularly employed in studies to examine new interventions and devices. Over the years, the computational power and simulation expertise have increased. This has resulted in the development of very sophisticated and complex models of the human spine, which include detailed representations of the bone and soft tissue architecture, and non-linear material properties of the tissues. However, within these models, the ligaments have usually been represented as simple linear elastic uniaxial structures with uniform geometric properties. Where a non-linear behaviour is considered, as a bi-linear or tri-linear response, little attention has been given to the realistic geometry of the ligaments. Since ligaments are three dimensional entities with a non-uniform structure, it is important to establish the sensitivity of the models to the geometric parameters of the ligaments. Moreover, the quantitative information on geometry and material properties used in these studies came primarily from a limited number of experimental studies. There has been little justification given to the choice of ligament data used, and this makes it difficult for the reader to evaluate why and how the data has been implemented. Although bi-linear or tri-linear mechanical behaviour



has been implemented in some FE studies, the non-linear behaviour of the spinal ligaments has not yet been well characterised.

In this study, the focus of the research will be on the anterior and posterior longitudinal ligament. While each spinal ligament plays a role in the spinal biomechanics under different motions, the ALL and PLL provide stability over wide range of motions and are of particular interest for studies of the disc. Although the main focus is ALL and PLL, the aim is to develop methods that could be adapted to study other ligaments in the future. The overall aim and objectives are presented in the next section.

### **Aim**

The overall aim of the work presented in this thesis was to establish the non-linear behaviour of the spinal longitudinal ligaments using a combined experimental and computational approach, and to examine the suitability of using the ovine spine as a model for the human spine, in terms of the ligamentous behaviour.

### **Objectives**

The following objectives were established to achieve the above aim:

- Develop a methodology to test and compare the stiffness of ovine and human spinal ligaments.
  - Develop a protocol to test the mechanical properties of ovine spinal ligaments
  - Adapt the protocol developed and apply it to human spinal ligaments.
  - Examine the mechanical differences between human and ovine spinal ligaments and compare with the published human data.
- Devise a methodology to determine the material properties of the ligaments using specimen-specific finite element models
  - Develop a protocol to build specimen specific computational models of the ovine longitudinal ligaments and surrounding tissue where needed
  - Establish the sensitivity of the model behaviour to the ligament parameters
  - Gain an understanding of the most appropriate way to represent the ligaments and their attachments within the FE model

- Establish a method for comparing the outputs of the models to experimental test data for model calibration (i.e. for tuning the ligament properties) and validation.
- Adapt the protocols developed for the ovine spine and apply to the human longitudinal ligaments.

The methodology for testing ovine spinal ligaments is presented in Chapter 2. The methodology for developing the specimen-specific finite element models of the ovine spinal ligaments computationally using an image-based approach is presented in Chapter 3. The methodology devised in these two chapters is then applied to human specimens and presented in Chapter 4 alongside the results. The final chapter, Chapter 5, highlights the important results and presents a comparison of human and ovine spinal ligaments stiffness and material parameters. Limitations of the current study and some recommendations for future work are also presented in the final chapter, concluding the thesis with the key outcomes.

## **Chapter 2**

### **Experimental Methods Development and Results for Ovine Longitudinal Ligaments**

#### **2.1 Introduction**

This chapter presents the procedures that were used to develop a methodology for mechanical testing of the spinal ligaments with the aim of deriving their mechanical properties. The methodology was developed on the ovine spine in such a way that the techniques would be transferrable to the human spine. Initial testing that was carried out over the functional spinal unit as a whole is presented first, including an approach that was developed to keep the ligaments in as natural a state as possible. This is followed by a detailed description of the experimental procedures and data analysis that were carried out on the anterior section of the spine to test the two longitudinal ligaments. This includes the dissection, tissue preparation, experimental setup and methods of mechanical testing.

The results are then presented and the longitudinal ligament stiffness values compared with the literature to examine if the ovine spine could be used for testing surgical interventions as an alternative to the human spine, and also to see if similar differences between the two ligaments are observed in both species.

#### **2.2 Ovine Ligament Anatomy**

##### **2.2.1 Introduction**

As described in Chapter 1, Section 1.2.2, the ovine model is commonly used for biomechanical testing and provides a more readily available source of tissue than human, hence it was used for the method development. However, there is little documented information in the literature on the ovine spinal ligamentous structures, an initial visual examination was therefore made of the ovine spinal ligaments in the thoracic and lumbar regions. Comparisons were made to data from the literature on human spinal ligaments to establish the similarities and differences between the two.

##### **2.2.2 Methods**

An ovine spine of age approximately two years was obtained from a local abattoir (John Penny and Sons, Leeds, UK). It was dissected and both the

thoracic and lumbar region were photographed. A visual examination was undertaken to identify the ligament structures present in the two regions of the ovine spine, and comparisons made to the reported anatomy of the human spine.

### **2.2.3 Results**

The ovine lumbar vertebral anatomy was visually found to be quite similar to the human in terms of the location of the landmarks (Wilke, et al., 1997). The only obvious difference was that the ovine vertebrae were larger than corresponding human ones. All the seven ligaments appeared similar in structure and location to the human spine (Gray, 1944) (See Table 2.1). The ovine lumbar region was found to have six vertebrae as opposed to human which usually has five vertebrae.

The thoracic region also appeared to have had similar anatomical features and ligamentous structures to lumbar spine (Table 2.1). There were thirteen thoracic vertebra found in ovine spine as opposed to twelve in humans. The transverse processes in the thoracic region of the ovine spine were very small, almost non-existent; the intertransverse ligaments were also missing. Both the ALL and PLL appeared similar in structure and location to that described for the human spine. The ALL was found to be a thick band of fibers covering the anterior aspect of the vertebral column with some short fibers running in parallel covering most of the vertebral bodies and the disc anteriorly. The PLL appeared narrower and thinner than the ALL and covered the entirety of the vertebral column longitudinally, like ALL. It ran over the posterior surface of all the vertebral bodies in a serrated manner. It was a narrow band over the vertebral bodies but expanded laterally over the posterior surface of the IVDs. Unlike the ALL, the PLL was found to be thicker at the vertebral body level and thinner at the disc level.

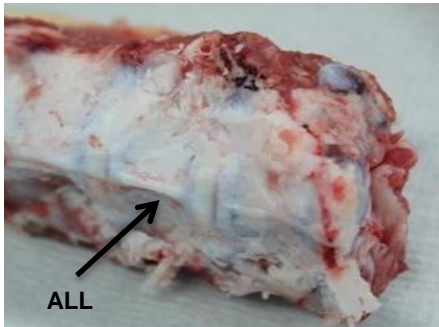
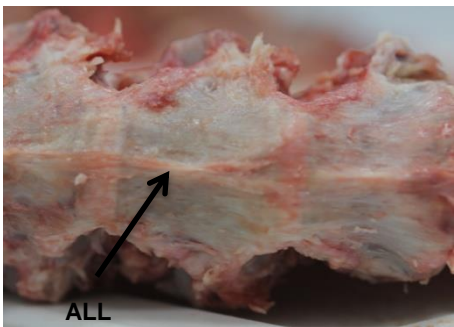
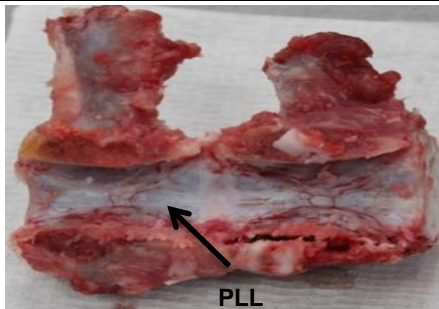
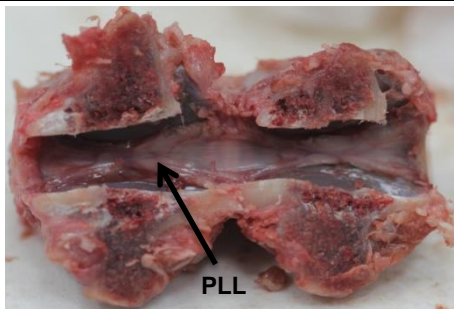
In both the lumbar and thoracic regions, the ALL and PLL were found to be very thin and especially in the case of ALL, the fibres dispersed over the surface of the surrounding structures and hence were difficult to unpick in their entirety. Similarly, the SSL and ISL were found to intermingle and it was difficult to draw a clear boundary between the two. The ITL, ISL and IF were found to be too small in length to be extracted and tested individually because there would not be enough length to clamp the ligament from both sides in order to perform a tensile test.

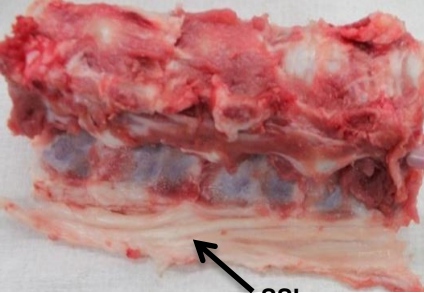
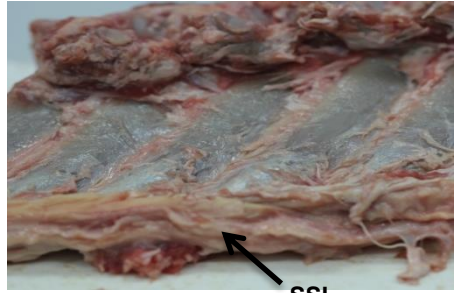
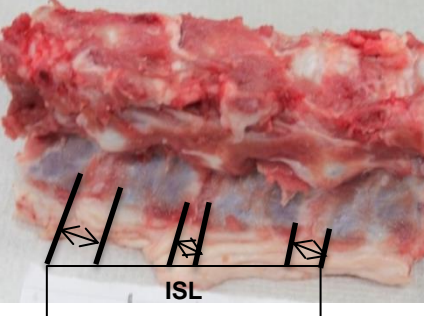
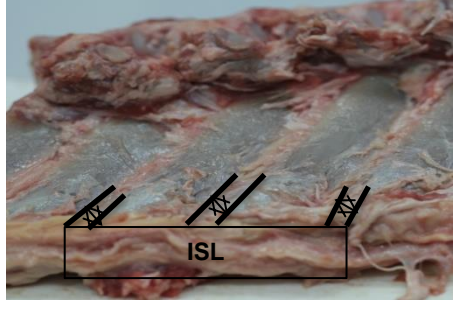
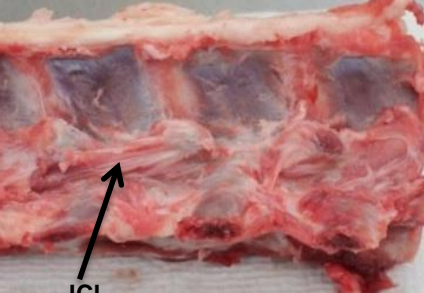

## 2.2.4 Discussion

This initial dissection further confirmed the use of in-situ testing regime (previously described in Section 1.2.5.2 and discussed in Section 1.2.5.4) as the abstract structure of ligament fibres and the small thickness would make it very difficult to extract entire individual ligaments without damaging their fibres. Also the fixation of such soft and moist structures for mechanical testing would be challenging.

Since both thoracic and lumbar regions of the ovine spine were found to be very similar to the human, the thoracic was used for subsequent testing since a longer region of similar types of vertebrae could be obtained due to the attachment of ribs to the thoracic region. A higher number of specimens per spine could be obtained from the thoracic region, which was important in the case of the human tissue (Chapter 3) where the number of spines was limited. Therefore, it was more economical to use the thoracic spine instead of the lumbar and provided more capacity to make comparisons along the length. Also the methodology developed was devised such that it could be transferrable to any section of the spine and not just the thoracic section.

**Table 2.1: Initial ovine spine dissection comparing images of the ligaments identified in both lumbar and thoracic region with the cranial end on the right side of all the images.**

Ligament	Lumbar	Thoracic
Anterior Longitudinal ligament (ALL)		
Posterior Longitudinal ligament (PLL)		

Ligament	Lumbar	Thoracic
Supraspinous Ligament (SSL)		
Interspinous Ligament (ISL)		
Joint Capsular Ligament (JCL)		<p>Not possible to image the JCL because the facet capsules are located directly underneath (between) the articular processes, unlike in the lumbar region, where the facet capsules are protruding to the side, hence unable to reveal without separating the two processes</p>
Intertransverse Ligament (ITL)		<p>transverse processes very small →no ITL</p>
Ligamentum Flavum (LF)	<p>Difficult to capture LF photographically because it is a very small ligament that lies between the spinous processes. It appeared thicker in the thoracic region.</p>	

## 2.3 General Materials and Methods

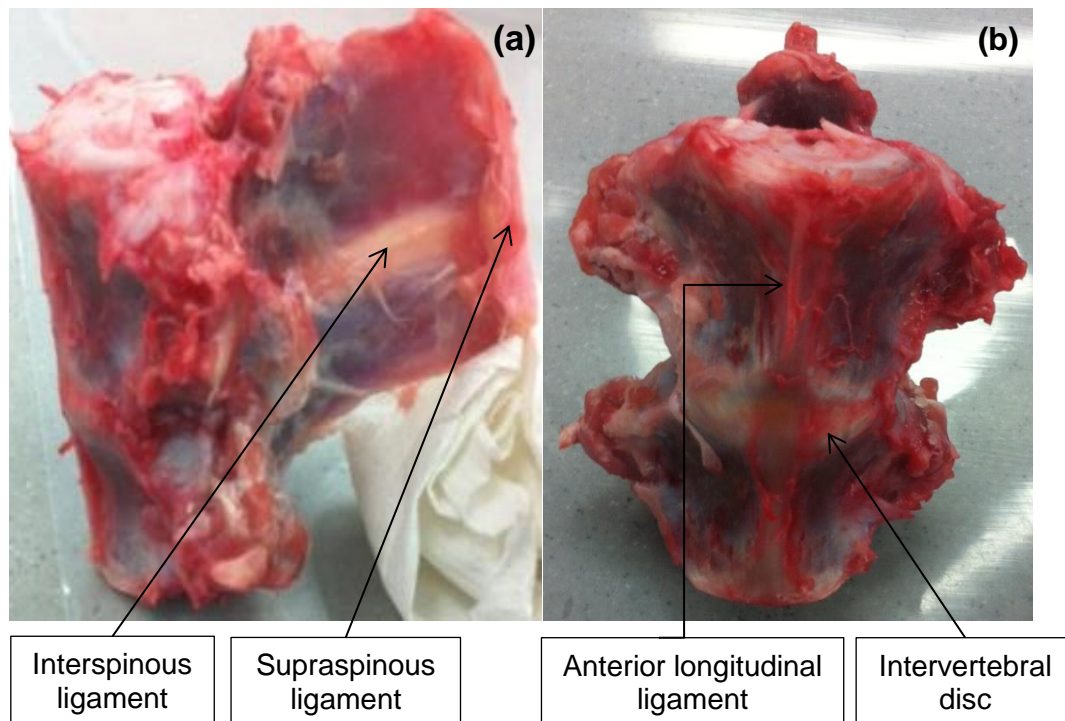
This section describes the work which was carried out in order to develop a methodology to test the ovine longitudinal ligaments under tension using a materials testing machine.

### 2.3.1 Specimens

The specimens were sourced from ovine spines of age approximately two years to ensure that the tissue was mature such that the bony structures were strong enough to withstand the tensile testing. The specimens were obtained within a few hours of slaughter from a local abattoir (John Penny and Sons, Leeds, UK) and the thoracic region was extracted for this study.

### 2.3.2 Dissection

The fresh thoracic spine was cut into sections to obtain functional spinal units (FSUs) comprising a vertebra-disc-vertebra section with all the ligaments intact. A typical FSU is shown in Figure 2.1. It was difficult to obtain just the vertebrae on each side of the central disc because they were strongly attached to the discs via the end plates; therefore, the sections were made through the disc tissue, leaving half a disc below the inferior vertebra and half a disc above the superior vertebra.



**Figure 2.1: Photographs of the ovine thoracic FSU with all the ligaments intact. (a) Lateral view: interspinous and supraspinous ligaments are visible, (b) Anterior view: anterior longitudinal ligament (longitudinal band) and intervertebral disc can be seen.**

### 2.3.3 Potting of Specimens

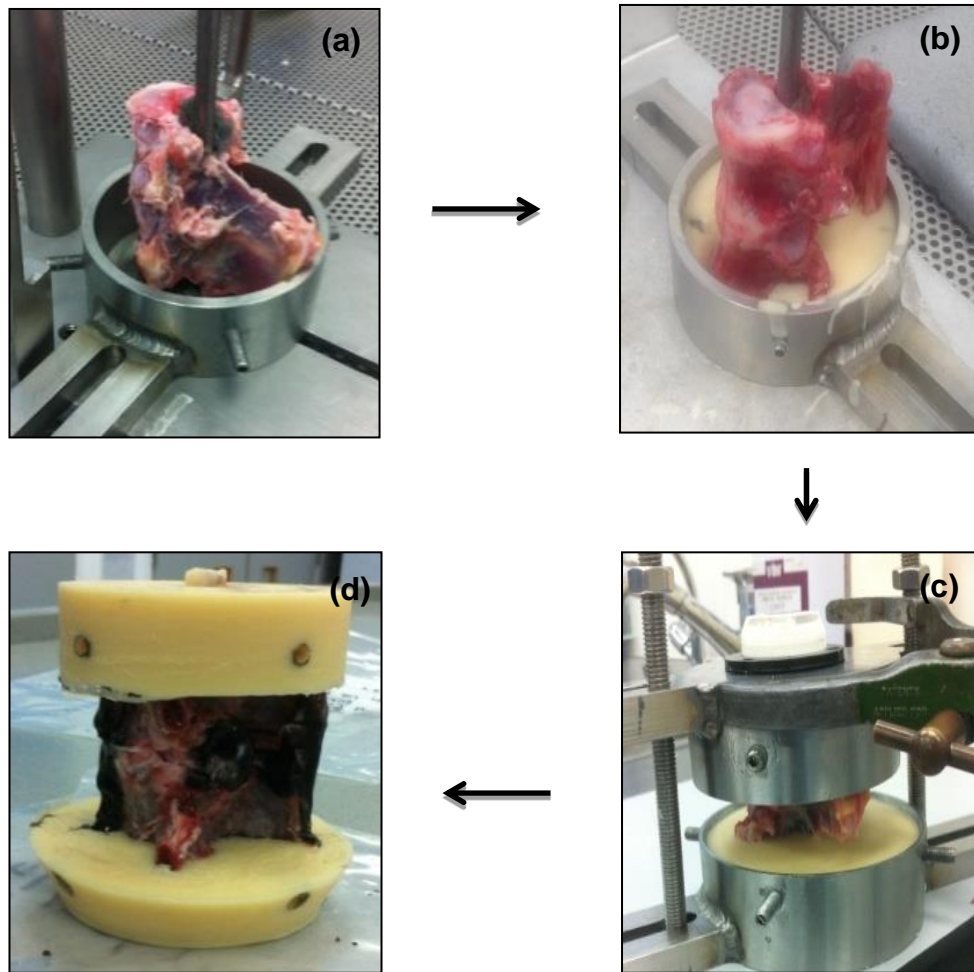
The process of cementing the FSU is shown in Figure 2.2. In order to house the specimens in the materials testing machine for tensile loading, steel pots were used that could be bolted to the testing machine fixtures. The specimens were fixed into the pots using polymethylacrylate (PMMA) cement to provide grip around the whole of the vertebral surface and prevent localised stress concentrations. PMMA cement is frequently used in orthopaedic procedures to aid the fixation of artificial prostheses. Screws were inserted through the pots into the cement to secure the cement to the pot. The following procedure was used:

First the specimen was held in place over a stainless steel pot by a steel rod carefully inserted into the spinal canal so that it was in contact with the anterior wall of the canal, making sure PLL was not damaged. Screws were inserted through holes in the pot to keep the cemented vertebrae fixed in the pots.

Then, PMMA cement (Cold Cure, WHW Plastics, Hull, UK) was prepared by mixing a pre-polymerised cold cure powder with a liquid monomer using a powder to liquid component ratio of 2:1, according to the manufacturer's instructions. The powder and liquid were mixed on a downdraft table and poured into the pot to a marked level above the screws. A tissue soaked in saline was wrapped around the areas of the FSU not being cemented to reduce the risk of any damage that could have been caused by the increasing temperature of the cement as it hardens. The superior vertebra was cemented first and the cement was allowed to set for a minimum of 20 minutes (Figure 2.2 (b)), then the inferior vertebrae was cemented by placing the potted FSU on top of a second metal cup. Metal guides were used to ensure parallelism of the cups and a spirit level was placed on the top metal pot to make sure it was levelled with the bottom one (Figure 2.2 (c)).

Once the cement had set, the screws and specimens were removed from the pots and frozen. Since the process of dissection and subsequent cementing took nearly a whole day, this enabled the mechanical testing to be conducted at a later date.





**Figure 2.2: The process of attaching cement endcaps to the specimen: (a) the specimen is held in place within a mould, using a steel rod through the spinal canal to locate the specimen; (b) cement is then poured into the mould and allowed to set; (c) the other end of the FSU is cemented, the pots are aligned using metal guides and spirit level; (d) the FSU with cement endcaps ready for mechanical testing.**

### 2.3.4 Mechanical Testing Setup

The cemented FSU specimens were tested using a materials testing machine ( $\pm 500$  N load cell, model 3365, Instron, UK). The machine is externally calibrated annually to ISO 7500-1:2015 standards, using an independent UKAS-accredited company. Calibration certificates covering the period of testing showed that the documented error was less than 1% over the range of the load cell used. A visual inspection of the machine was also carried out prior to testing to ensure there are no warning or error messages displaying.

The samples were attached to the machine via the steel pots to test under uniaxial tension. Extending the FSU in this manner is not physiological, however, this will allow the ligaments to be stretched. This usually occurs when FSU is under bending e.g. during forward flexion, the posterior ligaments are

stretched whereas the anterior ligaments are stretched during backward extension.

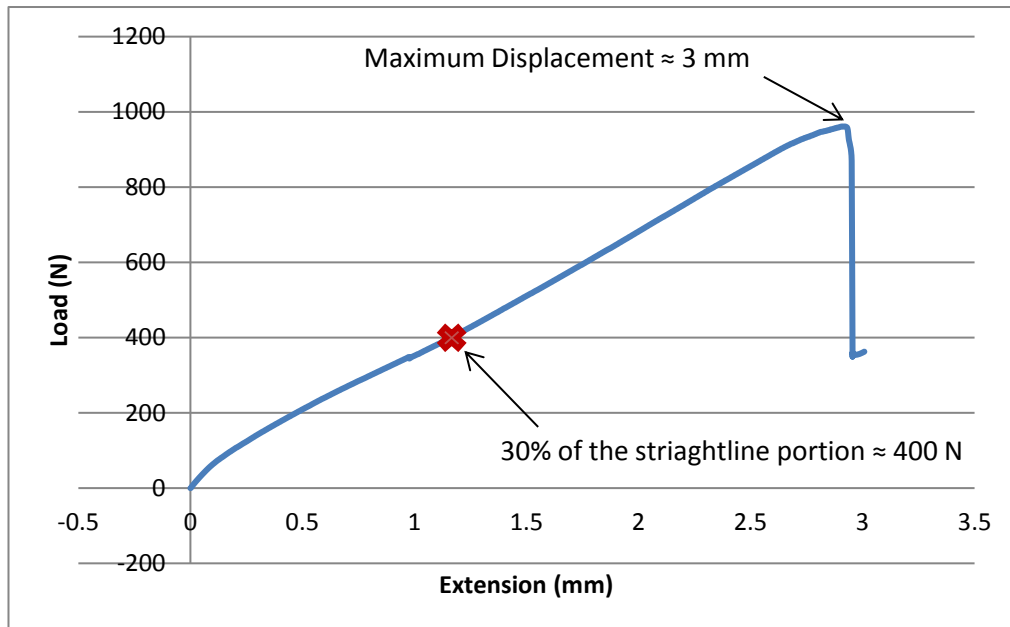
The pot on the caudal end of the FSU was fixed to the machine baseplate while the cranial pot was attached to the crosshead which allows the cranial end to move in order to extend the ligaments (Figure 2.4).

The load output was first set to zero without any contact to the specimen. The caudal end was fixed first and the crosshead was brought down until it was touching the top of the fixture without putting the specimen under any compression. The cranial end of the fixture and the crosshead were screwed in and the crosshead was raised or lowered manually to remove any compression/tension experienced by the specimen due to the attachment to the crosshead (i.e. to return the load reading to zero). The load was allowed to settle in between any crosshead movement before any adjustments were made. Once the cranial end had been attached, the displacement was also set to zero and this cross-head position was defined as the 'zero' point for the tests to follow. Each time a test was completed, the machine was returned to this 'zero' point, ready for the next test, to keep the tests consistent. Each time the machine was returned to 'zero' point, the load was also reset to zero before commencing the following test. A displacement control was used and the crosshead was moved at a rate of 1 mm/min (Chazal et al. 1985). A fixed displacement rate instead of a strain rate was used as it was difficult to measure an accurate length of ligament to determine strain. Also the length of the ligament was different from specimen to specimen because the disc is different height each time, however, an approximate range of lengths between 3-6 mm was used which gives an approximate strain rate of 0.0028-0.0055 s<sup>-1</sup> which is very similar to the strain rates of 0.0055 s<sup>-1</sup> (Nachemson & Evans, 1968) and 0.003 s<sup>-1</sup> (Kirby, et al., 1989) used by other researchers.

### **2.3.5 Load and Displacement Limits**

Preliminary tests were conducted to pre-determine the maximum load and/or displacement which would be used in future experiments, such that there was no damage to the ligaments during the tests i.e. the ligaments stayed within the elastic region. For the preliminary tests, a specimen was tested until failure using displacement control, by gradually increasing displacement until rupture or damage in the specimen was observed. For this preliminary test, a load cell of 5 kN was used. From the resulting load-displacement curve, the maximum load was taken as 30% of the straight-line portion of slope (Tckazuk, 1969) whereas, the displacement at which permanent damage to the vertebrae was observed was taken as the maximum displacement. An example is presented

in Figure 2.3. This was repeated for three different specimens and the average was calculated to obtain a limit to be used in future experiments. From these results, all subsequent tests were halted when either a limit of 400 N load or 3 mm extension was reached.



**Figure 2.3: Load-displacement graph of a specimen tested to failure to obtain maximum limits for load and displacement to be used in future testing.**

## 2.4 Testing Protocol

### 2.4.1 Introduction

Several methodologies were initially investigated, each with the methods adapted based on the outcome of the previous one in order to derive the most appropriate method for determining the mechanical properties of ligaments. The final method adopted for testing is then presented in more detail. The original premise was to test the full FSU and sequentially remove one tissue at a time and retest, such that the contribution of each tissue could then be determined.

## 2.4.2 Method Development

### 2.4.2.1 Development Test I

The aim of this study was to examine if a sequential testing and removal of ligaments could be carried out on the cemented thoracic FSU as a whole and adapted for ligament testing in other specimens.

#### *Methods*

One specimen was used and prepared as described in Section 2.3. The specimen was pre-conditioned by loading it for one loading cycle. The specimen was then further loaded one more time to record the intact behaviour followed by subsequent reduction in anatomical structures starting from the posterior side and recording the behaviour each time. This way, each time the specimen was loaded and the corresponding behaviour was recorded, the machine was brought back down to the 'zero' position (see Section 2.3.4) and a ligament was transected using a scalpel. In order to characterise the contribution of each structure, the specimen was loaded with the same loading method after transection of each of the structures. The order of transection followed was SSL which was followed by ISL, ALL and then the IVD.



**Figure 2.4: Experimental setup: Initial testing (left); Testing after ISL transection (right).**

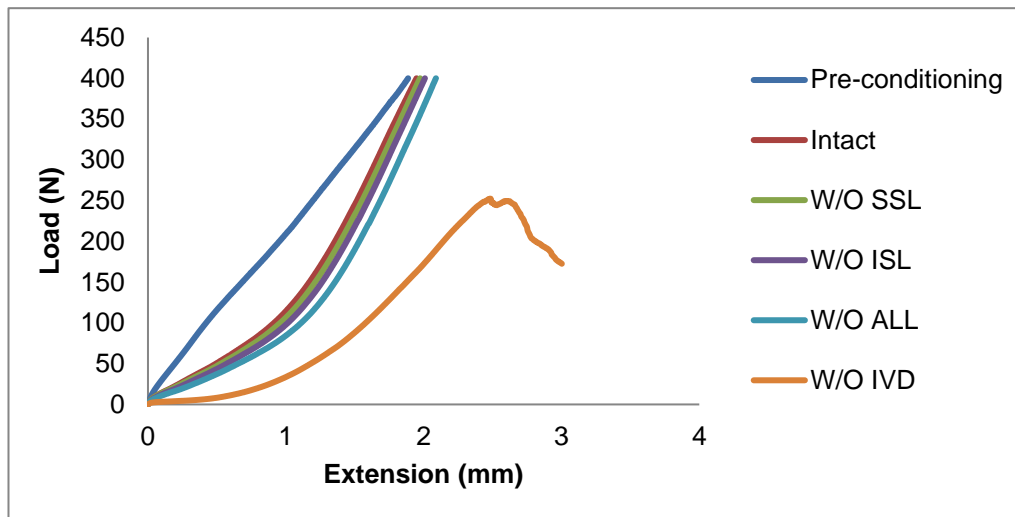
#### *Results*

The load-displacement curves obtained as a result of Test I were all plotted on the same graph for comparison (Figure 2.5). As can be seen from the graph the pre-conditioning prepared the specimen for testing because the remaining load-displacement curves all followed similar characteristic behaviour. Each curve has similar shape to the characteristic load-displacement curve for ligaments seen in literature (see Chapter 1, Figure 1.10).

A typical toe-region was evident beyond the neutral position which corresponds to the region of increasing strain without a corresponding significant increase in

stress. This was followed by a linear region with a linear rise in force with corresponding displacement. The non-elastic zone and the failure region were only evident in the curve which represented the specimen without IVD (W/O IVD). This corresponds to the behaviour of the PLL because after transecting all other ligaments and disc the only ligament still intact was the PLL.

During transection of disc, some fibres of the PLL might have been damaged or even transected as it was difficult to judge a clear boundary between the disc and PLL, which may explain why the failure occurred at such a low force. All the curves apart from the one without the IVD (W/O IVD) were almost superimposed, especially in the toe region. This was attributed to the dominance of the IVD, because once the disc was transected a distinct difference between the first set of curves and the last one was evident.



**Figure 2.5: Load-displacement curves for the entire set of experiments in Test I from the specimen in the intact state through to the transection of the IVD. The initial pre-conditioning step (dark-blue curve) was undertaken to remove any loosening in the set-up, then the loading regime was repeated for the specimen in the intact state (red curve) and following removal of the ligaments and disc in subsequent steps.**

#### 2.4.2.2 Development Test II

##### *Methods*

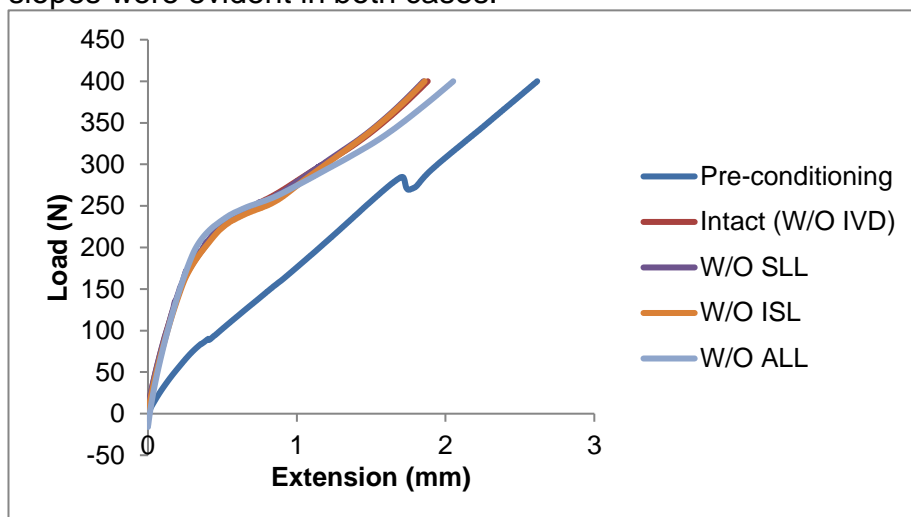
The aim of this study was to test the FSU without any effect from the IVD in order to neutralise the effect observed in Test I. One specimen was used and prepared as described in Section 2.3. The disc was then damaged by making cuts through the annulus laterally from both sides, keeping the anterior and posterior aspects of the FSU intact in order to save the ALL and PLL. A similar procedure to the first experiment was followed, starting with the intact specimen and transecting ligaments in steps down to the ALL. This time, since the IVD

was already damaged, a further cut was made through the disc all the way through the neural canal to the posterior elements.

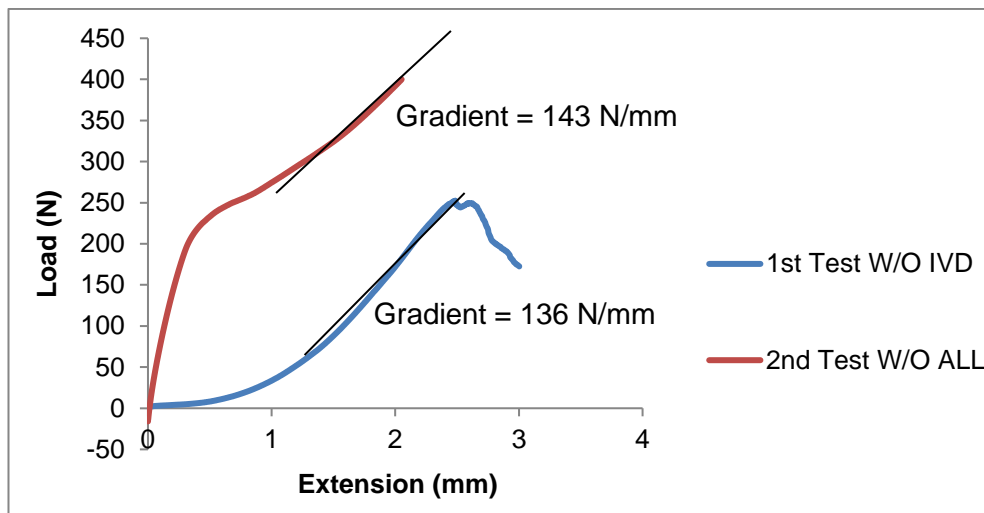
### Results

The results obtained (Figure 2.6) exhibited a completely different pattern than the set of curves obtained as a result of the first test. There was a dip evident in the pre-conditioning step which is probably due to a loosening in the setup. The pots were tightened at the end of this step to avoid any further slippage. The load-displacement curves for all the other steps did not exhibit the characteristic features of a typical curve for a ligament. Instead, the behaviour appeared very similar to how a rubber would behave under tension. There was no toe-region; the curves all appeared to start in the linear region, followed by a non-linear region which could be considered as the plastic zone (trauma region) however, this was not followed by a failure zone and the curves carried on increasing in stress again with corresponding strain. The curves were still almost superimposed as was previously observed in the first study.

For both Test I and Test II the load-displacement curve which corresponds to the behaviour of the PLL (W/O IVD in Test I and W/O ALL in Test II) were both plotted on the same graph for comparison (Figure 2.7). The comparison should exhibit similar behaviour, since there is no effect of IVD in both these cases and all other ligaments had been transected. However, as can be seen from the Figure 2.7 the curves exhibited very different shapes although similar linear slopes were evident in both cases.



**Figure 2.6: Load-displacement curves obtained from Test II from the specimen in the intact state (with transected IVD) through to the transection of the PLL.**



**Figure 2.7: A comparison of the load-displacement behaviour for the PLL from both Test I and Test II. The curves exhibit completely different shapes but very similar linear slopes (black lines in the graph).**

At the end of the second test, the PLL was sectioned and the specimen was loaded again to separate the two vertebrae. However, the extension exposed some fibres that were still holding the two vertebrae together (Figure 2.8). These fibres were mainly on the lateral sides of vertebral bodies towards the back. These could have been fibres of the disc or the ALL spreading to the sides and mistaken as muscle tissue. After further investigation on other specimens, the fibres were mainly attributed to the CL which had been left intact because reaching them before transection of both the ALL and PLL was not possible.

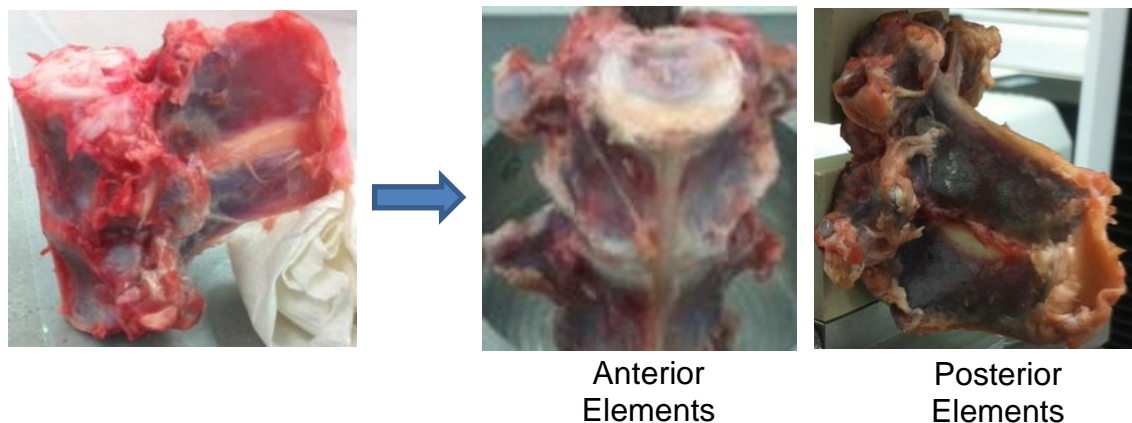


**Figure 2.8: Photographs of the FSU in Test II after the transection of all the ligaments. Anterior view (left image) and lateral view (right image) both show the presence of fibres keeping the vertebrae attached.**

### 2.4.2.3 Development Test III

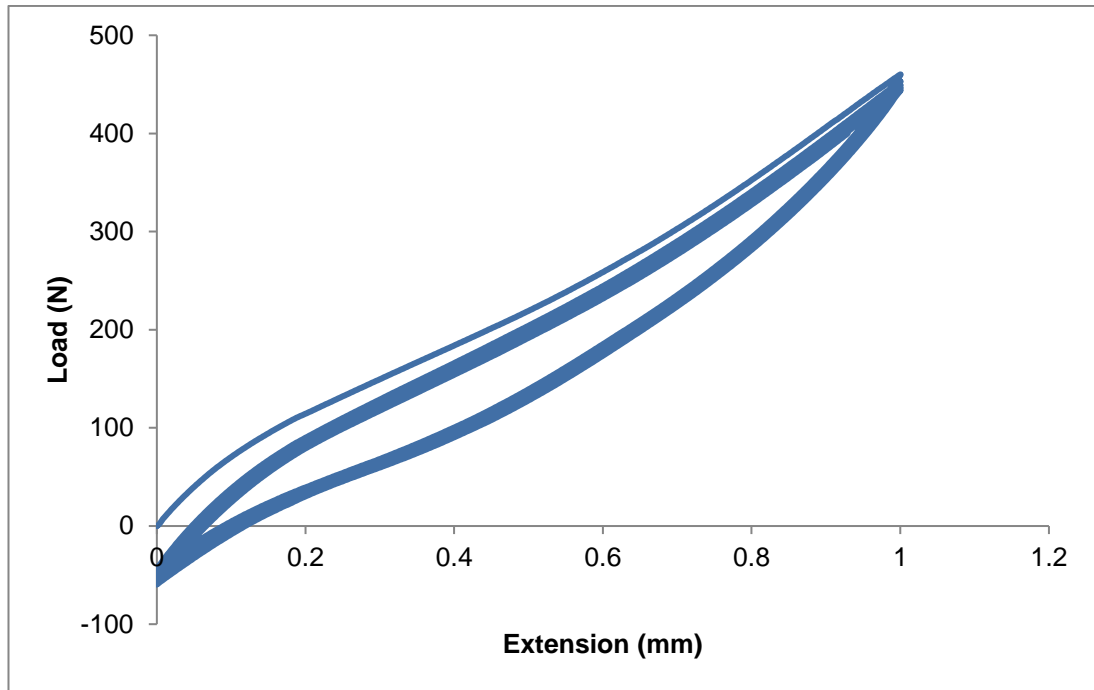
#### *Methods*

The aim of this study was to test the ligaments without any effect from the facet capsules in order to obtain the true behaviour of each ligament involved. One specimen was used and prepared as described in Section 2.3. The FSU was further divided in two subsections, the anterior section and the posterior section (Figure 2.9). Both ALL and PLL were retained in the anterior section, and testing was carried out on this section alone. The section was cemented, potted and tested in the same manner as the full FSU, starting with the intact specimen and then transecting the PLL, followed by disc so that the final test was on the ALL only. After each consecutive step, five cycles of pre-loading were undertaken to ensure the behaviour was repeatable. Three cycles of pre-loading were initially carried out because it was found that it took three cycles for the slope to become steady, then two more cycles were included to obtain a repeatable hysteresis (see Figure 2.10).



**Figure 2.9: An ovine FSU (lateral view) divided into an anterior (top-anterior view) and posterior (lateral view) section with the anterior section used for testing.**





**Figure 2.10: An example of a typical hysteresis observed on specimens after five cycles of pre-loading to 1mm.**

### *Results*

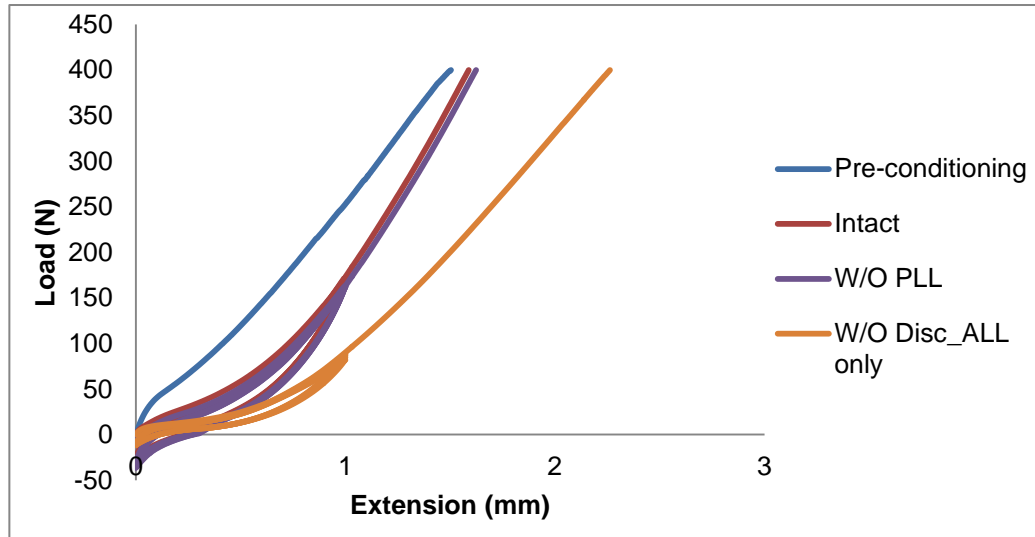
The resulting curves (Figure 2.11) still presented an initial stiffer region, however, the curves were not superimposed anymore. This confirms the behaviour was heavily controlled by the presence of facet capsules as removing the capsules resulted in each ligament and the disc exhibiting its own respective behaviour. This final method of testing only the anterior section with ALL and PLL was adopted for further testing.

#### **2.4.2.4 Discussion**

The method development studies presented in this section showed that the disc dominates the behaviour and so masks any changes due to removal of the ligaments while it is intact. It was also established that testing the full FSU is problematic because it is difficult to reliably remove full tissue structures at each step, especially due to the complex architecture and tissue structure in the posterior elements. Therefore the initial aim was modified to consider only the anterior section of the spine and focus on the behaviour of the PLL and ALL only.

An initial stiffer region was observed in the load-displacement curves obtained in these preliminary tests. There could be a few possible reasons for this behavior; it could have been a specimen-specific issue, or a machine artefact, or it could be the true behavior of the ligaments themselves. Checks were made on the machine without a specimen in place to make sure it was not due

to restriction in the crosshead or similar, and no detectable load was recorded, suggesting it was not a machine artefact. Subsequent tests were modified to increase the number of pre-conditioning cycles, and examine the behaviour across the neutral zone in more detail, as described in the following section.

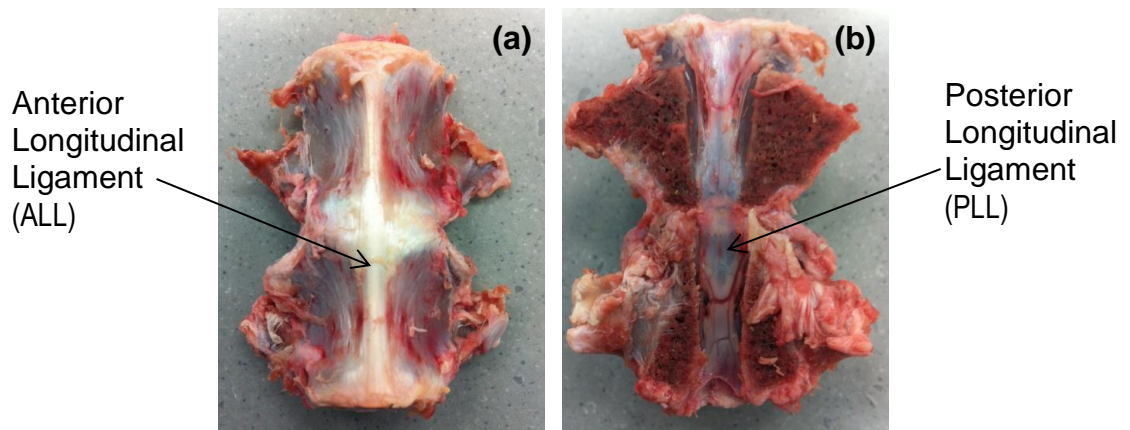


**Figure 2.11: Load-displacement curves obtained from Test III from the specimen in the intact state through to the transection of the IVD to test the behaviour of ALL alone (only Positive displacements are shown). The initial pre-conditioning cycle (dark-blue curve) was undertaken to remove any loosening in the set-up, then the cycle was repeated for the specimen in the intact state (red curve) and following transection of the PLL and IVD in subsequent steps. The thicker regions on red, purple and orange curves are the five cycles of pre-loading that were undertaken to ensure the behaviour was repeatable.**

## 2.4.3 Method Adopted

### 2.4.3.1 Specimens

Twelve FSUs from the thoracic region were extracted from three fresh ovine spines as described in Section 2.3. The vertebral bodies were separated from the posterior elements such that each FSU contained just the anterior elements comprising a superior vertebral body, an intervertebral disc and an inferior vertebral body with the anterior and posterior longitudinal ligaments attached (Figure 2.12). Care was taken during the separation of vertebral bodies to ensure that both the ligaments and the disc were kept intact before the start of the test. The specimens were divided into two groups (N=6 each): one which was tested for the ALL i.e. the PLL was transected first and the other was tested for the PLL i.e. the ALL was transected first.



**Figure 2.12: Anterior view (a) and posterior view (b) of the vertebral bodies after the removal of posterior elements.**

#### **2.4.3.2 Mechanical Testing**

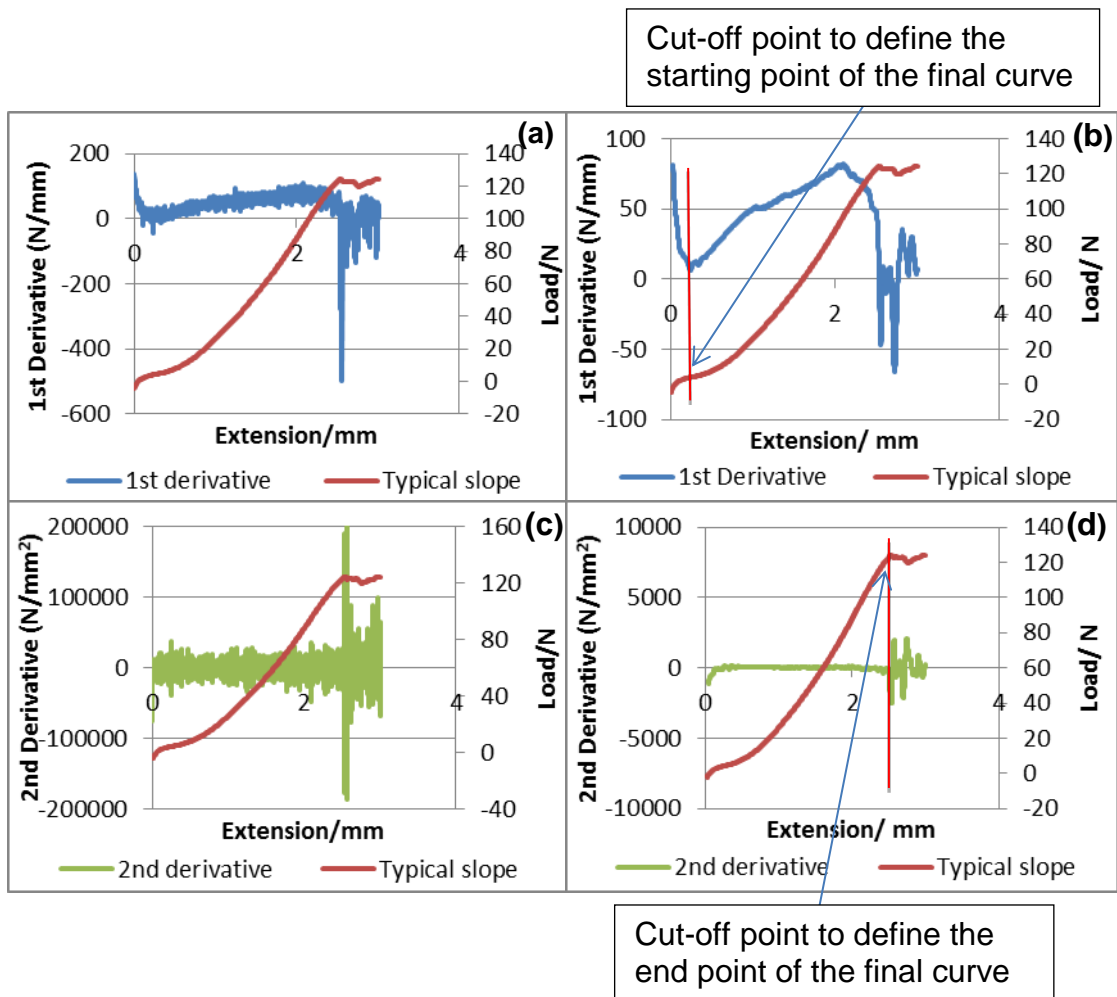
To further examine the apparent high stiffness at very low load, the specimens were put into a small amount of compression (0.01 mm) first before the displacement was zeroed and the test started, to observe if this behavior initiated only after tensile force was applied. Each specimen was then preconditioned by loading it to 1mm for three loading cycles at the same loading rate as the actual test.

The specimen was then further loaded to record the intact behavior followed by subsequent removal of the anatomical structures starting from either the posterior (for testing the behavior of the ALL alone) or the anterior side (for testing the behavior of the PLL alone) and recording the behavior each time. This way, each time the specimen was loaded and the corresponding behavior was recorded, the machine was brought back down to 'zero' (the starting crosshead position for the first test where the specimen was under 0.01mm compression) and the ligament/disc was transacted using a scalpel. The specimen was loaded again and the corresponding behavior was recorded. The behaviour of the ALL and PLL was measured in alternate specimens down the levels of each spine.

## 2.5 Methods of Data Analysis

Although load-displacement data was recorded for each loading step, only the final step (i.e. when only either the ALL or PLL remained for each respective specimen) was examined in this study.

Due to the difficulty in obtaining a consistent zero strain point in the experiment, there was considerable variation in the shape and length of the toe region of the load-displacement curves obtained for both the ALL and PLL from different specimens. The initial stiffer region at very low strains reported previously was again observed. Since physiologically, there would be greater pre-strain caused by the disc swelling pressure, it could be that the ligaments would not be operating at these very low strains in vivo, so this region of the curve was not considered. In addition, failure started to occur towards the end of some tests, especially in the case of the PLL. Therefore, it was necessary to define a criteria to trim the data for all the specimens consistently in order to obtain the curves which all have the same starting and ending points for comparison. The 1<sup>st</sup> and 2<sup>nd</sup> derivatives of the load-displacement curves were computed for this reason (an example is shown in Figure 2.13 (a) and (c)). A nine-kernel moving average smoothing operation was then performed to filter the noise in the derivative data (Figure 2.13 (b) and (d)). A moving average operation smooths out short-term fluctuations. The 1<sup>st</sup> derivative was used to define a starting point at the minimum stiffness or when the gradient was closest to zero, this defined a 'zero strain' point cutting off the initial steep rise in the data. The 2<sup>nd</sup> derivative was used to define the end of the linear region because it was necessary to remove the parts of the curve that represented damage or failure of the specimen, which would be characterised by a drop in the load-displacement gradient. This is shown in Figure 2.13 (b), where the value of the first derivative starts to reduce at ~2 mm. If the load-displacement gradient is dropping, this means the 2<sup>nd</sup> derivative becomes negative (Figure 2.13 (d)). It was therefore necessary to select an appropriate negative value as a cut-off. The 2<sup>nd</sup> derivative values were examined across all of the specimens and a suitable cut-off value was selected after which the slope visibly started to become non-linear in all cases. This cut-off value was then applied to all the specimen load-displacement data.



**Figure 2.13: An example of 1st and 2nd derivative of a load-displacement curve. (a) & (c) shows the raw data, (b) & (d) filtered data after performing the smoothing operation.**

In order to make a comparison across different specimens, the curves obtained after trimming the data were all quantified using a systematic data analysis method (Herbert, et al., 2016) to consistently extract the stiffness of the ligaments. This involved fitting the data to a bilinear model using non-linear least squares regression with an in-house Matlab script (Matlab (R2014a), MathWorks, USA) (Herbert, et al., 2016). The stiffness values were defined as the slopes of the least-squares fit lines in the two portions of the force-deformation curve: the initial 'toe region' ( $k_1$ ) and subsequent 'linear region' ( $k_2$ ). The script used a *fit* function with the type *piecewiseLine* using the NonLinearLeastSquares option available in Matlab (R2014a) for fitting a bilinear curve to the non-linear slope. A *piecewiseLine* is a line made of two or more pieces (in this case two) that is continuous. The point where the two lines met was computed by defining the intersection between the two lines and solving the linear system for it. The intersection point is defined in the algorithm to automatically get the best fit. The *gof* (goodness-of-fit) function was then

called which calculates the root mean square error (RMSE) and an  $R^2$  value between the observed non-linear slope and the predicted bi-linear data in order to quantitatively demonstrate the difference between them. The RMSE (Equation 2.1) is a function of the sum of the squares due to error (SSE) which measures the deviation of the response values from the model's predicted values. Whereas,  $R^2$  (Equation 2.2) is a function of the sum of squares total (SST), which measures the deviation of the response values from the mean. The  $R^2$  is scaled between 0 and 1 with value being closer to 1 indicates that the model accounts for a greater proportion of variance, whereas RMSE is not scaled. Although  $R^2$  is easily interpreted due to it being scaled, however, RMSE explicitly shows how much the predicted values deviate, on average, from the observed values in the dataset and hence is a better indicator of how good the fit is.

$$RMSE = \sqrt{\frac{SSE}{V}} \quad [\text{eq. 2.1}]$$

Where,

SSE is the total deviation of the response values ( $y_i$ ) from the fit to the response values ( $\hat{y}_i$ ) given by:

$$SSE = \sum_{i=1}^n (y_i - \hat{y}_i)^2$$

and  $V$  is the residual degrees of freedom - the number of response values minus the number of fitted coefficients estimated from the response values.

$$R^2 = 1 - \frac{SSE}{SST} \quad [\text{eq. 2.2}]$$

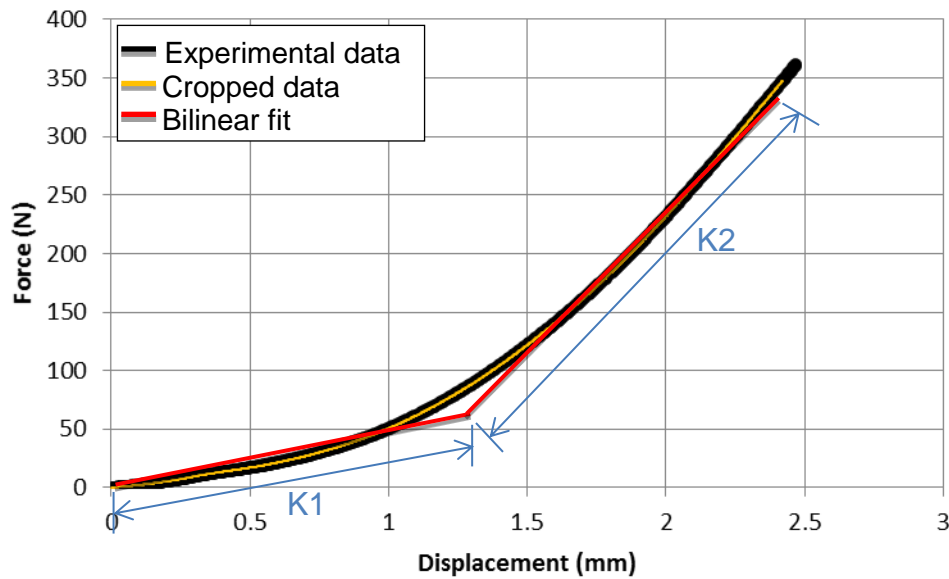
Where,

SST measures the total deviation of the response values ( $y_i$ ) from the mean ( $\bar{y}$ );

$$SST = \sum_{i=1}^n (y_i - \bar{y})^2$$

(Maths Work Inc., 1994-2018)

An example of how the stiffness values were calculated using the method described above is shown in Figure 2.14. The  $k_2$  values were compared with the stiffness values of the linear region cited in literature for human spinal ligaments.

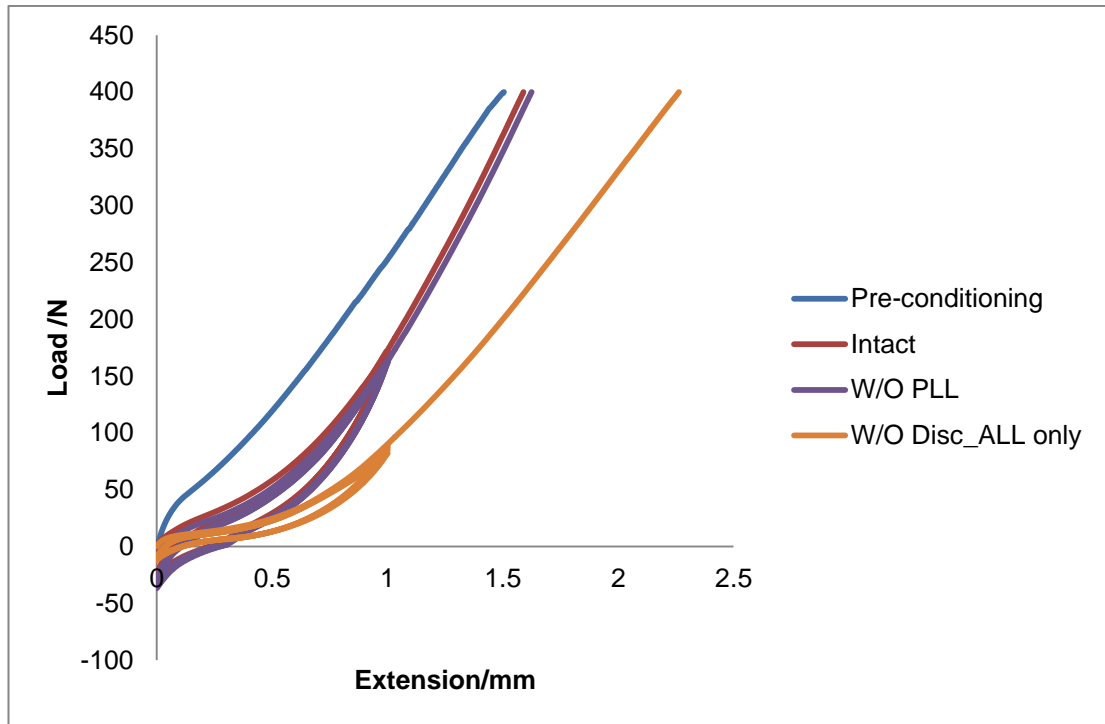


**Figure 2.14: An example of how systematic data analysis method is used to calculate ‘toe region’ ( $k_1$ ) and ‘linear region’ ( $k_2$ ) stiffness values.**

## 2.6 Results and Analysis

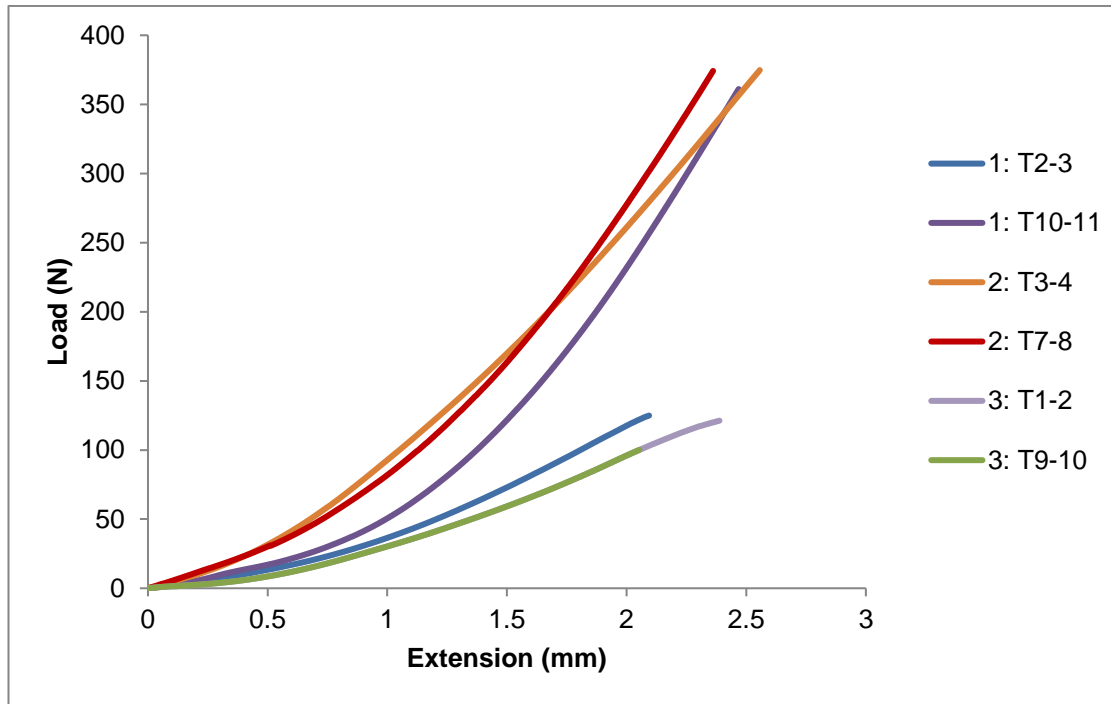
For all specimens tested, the pre-loading cycles showed a repeatable hysteresis similar to that shown in Figure 2.10. A typical full dataset is shown in Figure 2.15. The repeatability of the hysteresis loops and lack of sudden jumps in the output load increased confidence in the testing setup i.e. that there was no slippage in the testing machine. The raw final load-displacement behavior obtained for both ligaments, ALL and PLL, had an initial stiffer region followed by the typical toe region and a final linear elastic region before failure. The initial stiffer region and failure regions (where required) were removed from all the respective curves using the method described previously in Section 2.5. The final curves obtained after the trimming procedure for both ligaments are plotted in Figure 2.16 and Figure 2.17. The level and the spine, the specimen was obtained from, are indicated in the specimen name.

The experimental load-displacement data showed the characteristic non-linear behaviour of ligaments for both the ALL and the PLL. This post-processed data was then used to obtain  $k_1$  and  $k_2$  for both the ALL and PLL by fitting the experimental data to the bi-linear model described in Section 2.5. The  $k_1$  and  $k_2$  values obtained are presented in Table 2.2 and Table 2.3 alongside the RMSE in each case. The mean stiffness of the linear regions for both ligaments were compared with the published mean stiffness for the linear regions of human ligaments respectively (Pintar et al., 1992) (Figure 2.18).



**Figure 2.15: An example of load-extension slopes of all the steps followed for a specimen showing repeated hysteresis in pre-loading cycles. The thicker area of the slopes is the five cycles of pre-loading performed up to 1mm extension before the final loading step.**

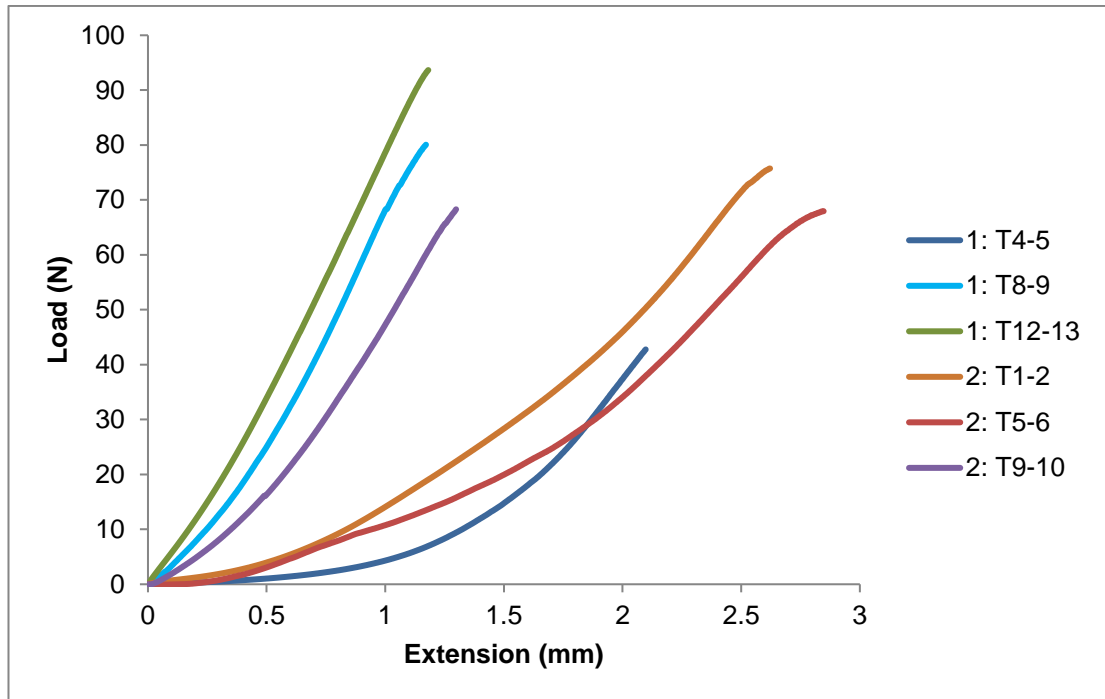




**Figure 2.16: The trimmed load-extension curves for all ALL specimens. The level and the spine the specimen was obtained from are indicated in the specimen name.**

**Table 2.2: The ‘toe region’ (k1) and final ‘linear region’ (k2) stiffness values, calculated by fitting least squares slopes to the post-processed load displacement curves of ALL, alongside the level and the spine the specimen was obtained from. The whole group mean and standard deviation (S.D.) are also shown.**

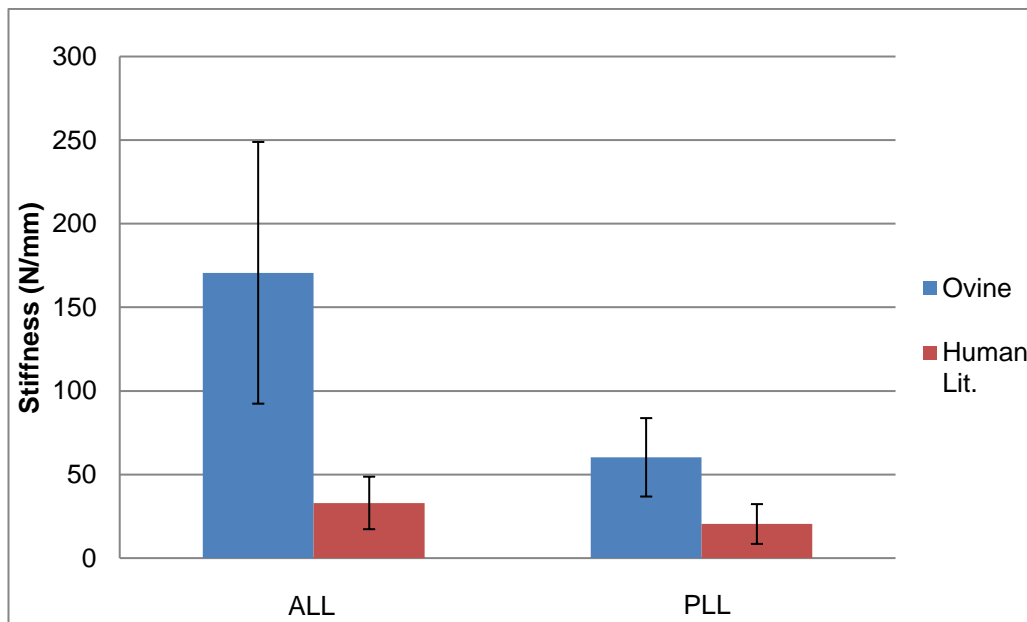
Specimen	Stiffness values for ALL (N/mm)		RMSE	R <sup>2</sup>
	k1	k2		
1: T2-3	30	82	1.64	0.998
1: T10-11	49	230	7.15	0.995
2: T3-4	73	179	5.19	0.998
2: T7-8	75	224	6.27	0.997
3: T1-2	20	66	1.99	0.997
3: T9-10	64	243	5.27	0.998
<b>Mean ± S.D.</b>	<b>52 ± 23</b>	<b>171 ± 78</b>		



**Figure 2.17: The trimmed load-extension curves for all PLL specimens. The level and the spine the specimen was obtained from are indicated in the specimen name.**

**Table 2.3: The ‘toe region’ (k1) and final ‘linear region’ (k2) stiffness values, calculated by fitting least squares slopes to the post-processed load displacement curves of PLL, alongside the level and the spine the specimen was obtained from. The whole group mean and standard deviation (S.D.) are also shown.**

Specimen	Stiffness values for PLL (N/mm)		RMSE	R <sup>2</sup>
	k1	k2		
1: T4-5	4	41	1.24	0.989
1: T8-9	43	85	0.78	0.999
1: T12-13	61	89	0.38	1.000
2: T1-2	12	40	1.89	0.993
2: T5-6	11	39	1.61	0.993
2: T9-10	30	67	0.82	0.998
<b>Mean ± S.D.</b>	<b>27 ± 22</b>	<b>60 ± 23</b>		



**Figure 2.18: Comparison of ovine and human (Pintar, et al., 1992) linear-region stiffness for both ALL and PLL showing mean stiffness values. Error bars depict standard deviation values.**

## 2.7 Discussion

### 2.7.1 Discussion of testing methods and results

The published experimental studies (Chapter 1, Section 1.2.5) on mechanical testing of ligaments provide a considerable amount of data on the biomechanical parameters and mechanical properties of ligaments, however the results are quite varied. Although the geometric parameters have been calculated and presented, there is huge amount of variability across studies due to difference in measurement procedures. Based on these results, it is difficult to decide which method is the most accurate for testing. Although dissection is never raised as an issue in any of these studies, based on the observation and experience of this study, it is one of the most challenging parts of mechanical testing of individual ligaments. The structure of the ligaments do not follow the same pattern in the same specimen or across different specimens. The fibres run in differing directions and interweave with fibres of other tissues, such as discs, making the distinction between the two difficult. They also tend to have different widths and thicknesses along the length making it even harder to predict their boundary for accurate dissection of the entire structure. The removal of ligaments from the spinal column for testing often results in damage to the ligament.

Pre-tension in the ligament is another important consideration which is often neglected in these studies. When the ligaments are removed for individual

testing, they lose the constant pre-tension they are under, in the intact state, in spine which would make them retract and shorten (Tkaczuk, 1968). The ALL and PLL have been shown to have a pre-strain of up to 10% and 13% respectively (Tkaczuk, 1968). Therefore, keeping them in situ is essential to obtain physiological behaviour, otherwise the stress-strain curves derived would start at a different point to that if a pre-strain were applied first. Moreover, the pre-strain is different for every specimen as it is shown to be dependent on dimensions of the ligaments, the pressures within the nucleus pulposus and the elasticity of annulus fibrosus (Tkaczuk, 1968), hence presenting data together would not be comparable. Another disadvantage of individual ligament testing is the difficulty of fixation, the ligaments either have to be removed with the bony attachments or specialised clamping systems have to be employed to avoid slippage of the specimen and damage of the specimen from the areas of contact in the clamp. The technique is also unable to define the role of ligaments in relation to other spinal components.

An in situ ligament testing method resolves most of the difficulties stated above and was therefore the method of choice for this particular study. However, the results obtained using this method showed quite a variability in initial load-displacement behaviour at low strains. The load-displacement data recorded was broadly compared to the published literature for ligaments to ensure the loads obtained are reasonable and not due to a machine artefact. The initial shape of the load-displacement curve appeared to be different to the shape that is been published in literature, with a steep initial section prior to the toe and linear region. This could have been due to the state of the disc, i.e. how hydrated it was for a particular specimen, because both extension and load were zeroed before starting the test. Different levels of disc hydration would have affected the initial height of the specimen, and once the disc was sliced through, there would be a change in the strain in the ligaments, so they are potentially starting from different initial conditions hence the variation in results. If the disc was compressed i.e. under-hydrated then it would push the vertebral bodies to draw more water in but if it was overhydrated then it would pull on the attaching structures. Although this initial high stiffness region does not tie in with literature, it is difficult to make direct comparisons because authors have not published their full load-displacement profile. Since this occurred at very low strains, and was highly variable from one specimen to another, this region was not considered in this analysis. Therefore, in order to make a comparison across the specimens and with the published human data, the data was consistently trimmed to remove the initial stiffer region and to define a 'zero' point that is consistent from one specimen to another.

The curves obtained after trimming the data all showed a characteristic shape (Fig. 2.16 & Fig. 2.17), however, there was still quite a spread in the results which is perhaps due to the natural variation in the specimens. Visually, the ligaments tended to appear thicker and well defined towards the inferior of the spine and the level is therefore also likely to affect the result. This is supported by the stiffness results that generally showed a trend of increasing stiffness with increasing level down the spine (see Table 2.2 and Table 2.3), although this was not conclusive due to the small sample size. Most previous researchers did not find a trend in spinal level and stiffness due to limited sample size, however, Chazal et al. (1985) found each ligament at lower thoracic or thoracolumbar level to be more resistant than the ligament of same variety at any other level. Pintar et al. (1986) performed a histological study to examine the composition of spinal ligaments in human. It was found that a sample of LF from the upper cervical spine had very few elastin fibres compared to the otherwise very high composition (50-60%) of elastin fibres in the LF in other levels. This suggests that composition varies between spinal levels, which might lead to different mechanical properties at different spinal levels. Myklebust et al. (1984) studied spinal ligaments from 41 fresh human cadavers and found the variation in strength and distensibility to be apparently related to spinal geometry as they observed the strongest ligaments at atlanto-occipital (C0-C1) and lumbar levels. Moreover, the size of the vertebrae (Gray, 1944) as well as the cross-sectional area of both ALL and PLL (Chazal, et al., 1985) is found to be higher in the lumbar region of the spine. This indicates that if size is considered to be the main factor affecting stiffness, then the stiffness of the ligaments might be higher in the lumbar region. Also the natural variation from one animal to another due to variances in weight, age and size is unavoidable and might affect the stiffness outcome. Care was taken to choose animals over 2 years old which would at least be fully mature for this study, but further controls on variability were not possible.

The ALL appeared to be thicker than the PLL which was reflected in the mean stiffness of ALL ( $171 \pm 78$  N/mm) being almost double to that of PLL ( $60 \pm 23$  N/mm).

### **2.7.2 Comparison to published human data**

The main aim of this study was not only to characterise the ovine spinal ligaments but also to compare the stiffness data obtained with published data on human longitudinal ligaments. The stiffness data published in the literature is mainly of the linear region of the force-displacement curve i.e. the k2 stiffness. The k2 stiffness obtained for both the ovine ALL ( $171 \pm 78$  N/mm) and

ovine PLL ( $60 \pm 23$  N/mm) of the thoracic region were both found to be stiffer than published human ALL ( $33 \pm 15.7$  N/mm) and PLL ( $20.4 \pm 11.9$  N/mm) of the lumbar spine (Pintar et al. 1992). In both these cases the ligaments were tested in situ and in isolation and all supporting structures except the ligament to be evaluated were sectioned. However, the loading rates in both cases were very different with Pintar et al. (1992) using data that was tested at a faster rate of 600mm/min as opposed to 1mm/min used for this study. An increase in loading rate has been shown to increase the stiffness in cervical spinal ligaments in similar isolated bone-ligament-bone samples (Butler, et al., 1988; Mattucci, et al., 2012; Trajkovski, et al., 2014). If the same is true for the lumbar spine, then the published stiffness by Pintar et al. (1992) would be lower if the tests were to be carried out at a slower loading rate of 1mm/min. Also, as described earlier, the stiffness appeared to change with the spinal level and if the speculation above about stiffness of ligaments being higher in the lumbar region holds true, then the stiffness for the human thoracic specimens would be even lower than that stated above for human lumbar spine and hence certainly lower than the ovine thoracic spine used in this study.

This potentially has repercussions if researchers are using the ovine spine as an experimental animal model for spine research. For example, spinal stabilization devices have been tested in ovine models to evaluate their performance (Gunzburg, et al., 2009). If the ligaments are stiffer, then they are likely to help with the stabilization, restricting the range of motion much better than in the human spine. This means the spinal components which are approved for clinical trial as a result of the success of testing in an ovine model could fail in human as the stabilizing forces provided by human spinal ligaments will be smaller. Therefore, the differences in the mechanical properties between human and ovine ligaments should be borne in mind when making a transition from the ovine model to the human.

### **2.7.3 Summary**

In conclusion, a methodology for characterizing the mechanical properties of spinal ligaments was developed and applied to ovine FSUs. Whilst there was considerable variation in the results, the stiffness of both the ALL and PLL were found to be higher than for human specimens, which may have implications for the use of ovine FSUs for preclinical testing. The methodology developed in this study will be used to test and extract the stiffness data for human spinal ligaments (Chapter 4), enabling direct comparison between the ovine and human data by removing the differences due to different testing regimes.

## **Chapter 3**

# **Computational Methods Development and Results for Ovine Longitudinal Ligaments**

### **3.1 Introduction**

This chapter presents the procedures that were used to devise a methodology for developing specimen-specific computational models of the ovine spinal ligaments using an image-based approach. The methods for micro-CT imaging the specimens used in Chapter 2 are described, including an approach that was developed to visualise the ligament clearly in the image data. The methods for estimating the thickness of the ligaments over the disc region for the purpose of segmentation as well as for the development of simplified-geometry models are also presented. The image processing steps and generation of the finite element models are then reported, with a particular focus on the development of a methodology to best represent the experimental setup in the computational model, to allow for a direct comparison of the model predictions with the experimental outputs. An account of the sensitivity analysis to understand the effect of varying geometric parameters, boundary conditions, mesh size and material models is also given. The representation of the ligament behaviour using various material models are described, starting with a simple linear elastic model and building up to more complex material models. The iterative approach used to determine the material model parameters for each specimen are explained. The resulting material model parameters are presented alongside the initial parameters derived by assuming uniaxial behaviour.

### **3.2 Imaging Specimens**

#### **3.2.1 Introduction**

Micro-computed tomography ( $\mu CT$ ) is usually used in clinical or other research studies for imaging bones. It provides high resolution volumetric information on the internal microstructure of the sample by x-ray imaging taken at a series of different projections. Computer algorithms are used to automatically reconstruct the images as 2D image stacks or 3D volumes. The bone absorbs more x-ray radiation than the soft tissues and the software by default assigns a brighter colour to the pixels (or voxels in 3D) where the most energy is absorbed. Hence, the bone appears brighter in the image while the soft tissue structures

such as discs, muscles and ligaments appear darker. As these soft tissues have low X-ray attenuation in their native state, this makes their 3D imaging challenging, especially when high resolution is required (Naveh, et al., 2014). Contrast agents are often used to improve the visibility of soft tissue structures and hence increase their contrast in  $\mu$ CT scans.

### 3.2.2 Imaging Protocol

Each specimen with PMMA plates on both sides was scanned using a  $\mu$ CT system (SCANCO  $\mu$ CT100; Scanco Medical, Bassersdorf, Switzerland) to provide images for the development of specimen-specific computational models. The scanner settings used were as shown in Table 3.1. These settings are the in-house standard for imaging spinal segments and have been shown to consistently provide sufficient contrast between the bone and soft tissue for image segmentation across a range of bone densities (Zapata-Cornelio, et al., 2017). Using these settings meant there was the capacity to use greyscale-derived bone properties in the FE models (Zapata-Cornelio, et al., 2017), although it was not subsequently found necessary in this study. A good contrast between different soft tissues is difficult to attain with the in-house CT scanners and hence it was decided to use settings that were suitable for the spinal bone and then use a separate protocol to visualise the ligament structures of interest described in the following section.

**Table 3.1:  $\mu$ CT scanner settings used on a SCANCO  $\mu$ CT100 device to image FSUs with the ligaments intact.**

Energy (kVp)	70
Current ( $\mu$ A)	114
Integration time (ms)	300
Resolution ( $\mu$ m)	74

The machine is calibrated monthly using a proprietary hydroxyapatite phantom. The greyscales of the different concentrations of hydroxyapatite in the phantom are compared to a calibration curve provided by the scanner manufacturer (Scanco Medical, Bassersdorf, Switzerland). Any change in X-ray tube performance will cause a drift the calibration and require the tube to be replaced; this did not occur over the course of this study.

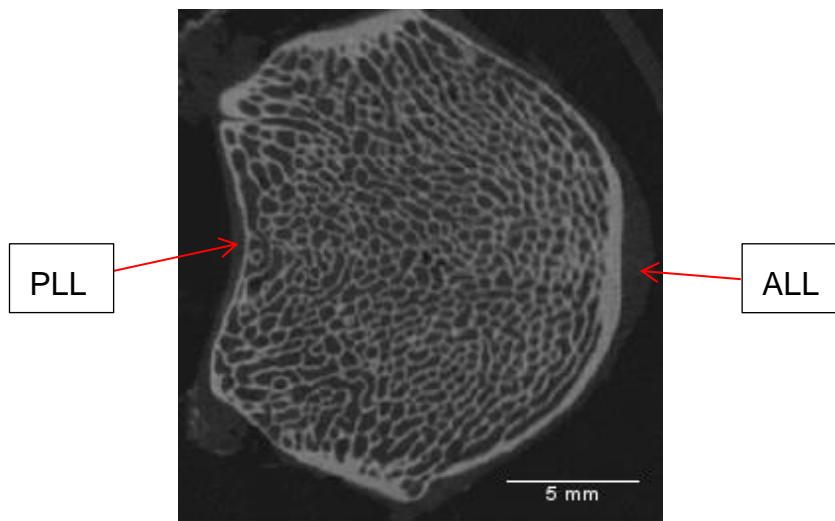


### 3.2.3 Use of Radiopaque Gel

#### 3.2.3.1 Introduction

Initial scans were undertaken on the native tissue, however it was observed that there was little contrast between the ligament and the background (air) (Figure 3.1), therefore the use of a contrast agent was investigated to establish if the contrast between ligament and background could be sufficiently improved to allow clear visualisation of the ligament geometry.

The contrast agent used for this purpose was a radiopaque sodium iodide (NaI) gel following successful preliminary trials of an in-house technique used to visualise other soft tissues (personal communication with Dr Sami Tarsuslugil). The gel used in previous projects was prepared with 0.2mol solution of NaI (containing NaI powder and PBS solution) and low viscosity carboxymethylcellulose sodium salt (CMC). The iodide ions have the ability to be absorbed by the soft tissue and help improve their visibility on  $\mu$ CT because of the improved x-ray attenuation. The improved visibility of the soft tissue gives a better contrast with the background. The CMC component is used as a gelling agent which give the solution sufficient viscosity to stay in place.



**Figure 3.1: sagittal view taken from a  $\mu$ CT scan of an ovine vertebra, including the ALL and PLL, without contrast agent.**

#### 3.2.3.2 Method

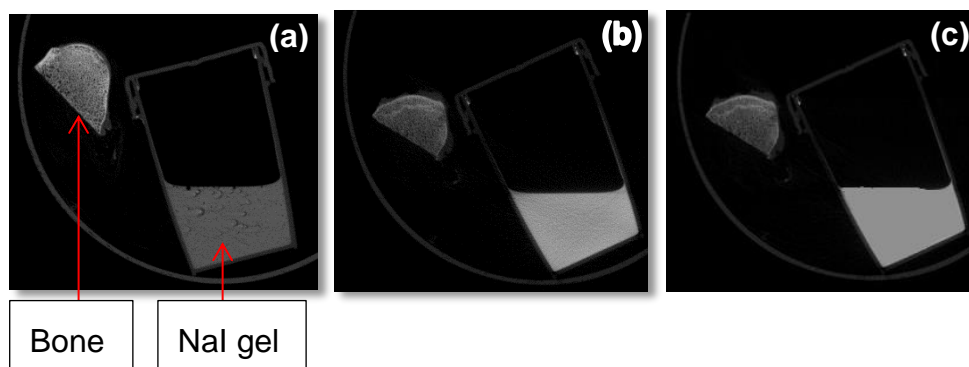
In order to increase the contrast between the background and the ligament, a study was designed to test the concentration of NaI gel such that the resulting image had a greyscale halfway between the background and the bone. If it were too dark, then the NaI greyscale distribution would overlap the background greyscale distribution, making it difficult to segment the two using image processing tools. Similarly if it were too bright, then the NaI greyscale

distribution would overlap the bone greyscale distribution, again making it difficult to segment the two using image processing tools. Mixtures with three different concentrations of the Nal gel (0.2 mol, 0.4 mol and 0.6 mol solutions) were prepared with an adequate amount of CMC so that the gel was sufficiently thick to be able to stay in place when applied to a specimen. A few drops of Indian ink were also added to the gel to make it distinguishable from the specimen so it could be easily removed after application. The mixtures were imaged individually alongside a small piece of vertebrae in the  $\mu$ CT scanner and their contrast against the bone was observed (Figure 3.2).

The optimum concentration of Nal gel was then applied to a specimen to verify that the gel provided sufficient contrast between the ligament and the background. For this purpose, an FSU was fully cleaned, with as much as possible of the muscle tissue removed carefully, leaving the ligaments intact. The cleaned FSU was initially scanned under  $\mu$ CT without the contrast agent. The ligaments were then painted with the Nal gel and left to rest for 20 minutes so the iodide could be absorbed by the ligament tissue. The gel was then wiped off so that there was no gel layer remaining on the surface of the ligament, because such a layer would make it difficult to distinguish between the soft tissue and the gel itself. The specimen was then rescanned.

### 3.2.3.3 Results

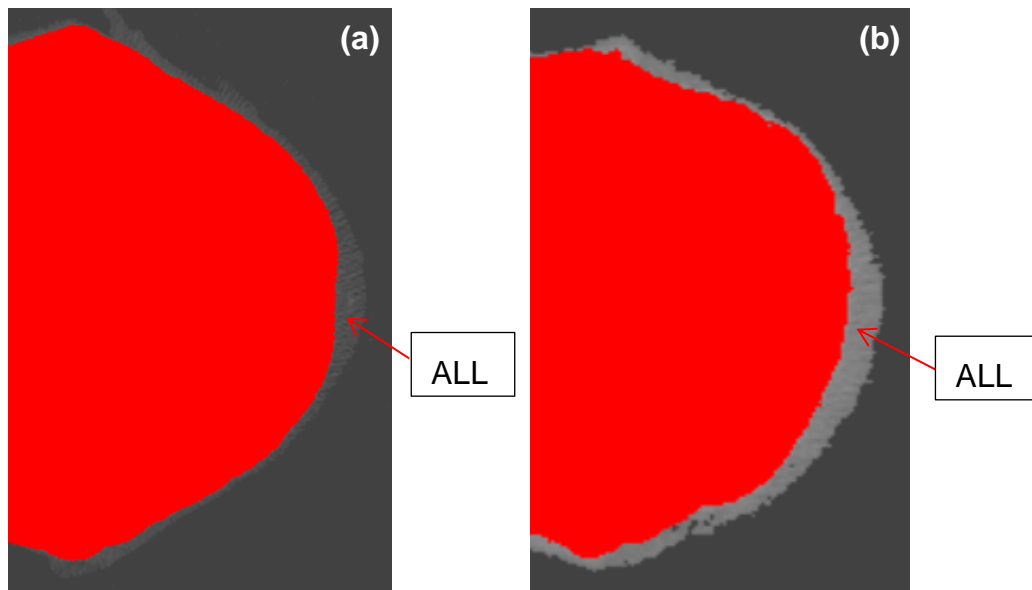
The results obtained for the study designed to test the concentration of Nal gel are presented in Figure 3.2. The gel with 0.4 mol concentration solution was found to give the optimum contrast.



**Figure 3.2: Different concentrations of Nal gel in relation to the bone as seen on  $\mu$ CT scans with concentrations of (a) 0.2 mol, (b) 0.4 mol, (c) 0.6 mol.**

After the application of the radiopaque gel with this optimum concentration to a test specimen, it was found that the ligaments were distinguishable from both the bone and the background. Figure 3.3 shows cross-sections through a

vertebral sample without (Figure 3.3(a)) and with NaI gel (Figure 3.3(b)) to visualise the difference in ALL contrast post-application.



**Figure 3.3: Cross-sections through a vertebral sample (a) without and (b) with NaI gel showing the difference in ALL appearance after the application of gel. In these images, the contrast has been increased and the bone has been segmented (red region) in order to provide a better contrast between the ligament and background for comparison.**

#### 3.2.3.4 Conclusion

The optimum concentration of 0.4mol was therefore used in subsequent studies.

### 3.3 Determination of Ligament Thickness over Disc

#### 3.3.1 Introduction

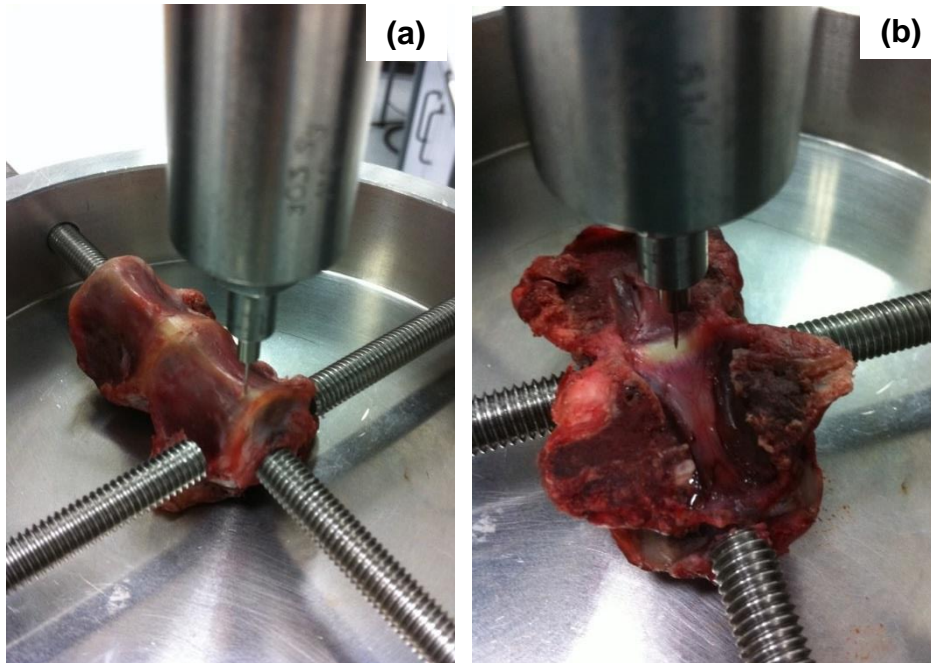
Although the application of contrast agent was useful in capturing the entirety of the ligament, it was still difficult to draw a distinct boundary between ligament and the disc from the  $\mu$ CT images. Thus it was not possible either to segment the ligament over the disc region or to obtain a measure of the ligament thickness that was required for the later development of a simplified-geometry FE model. Two methods were explored in order to measure the thickness of the ligament over the disc region.

#### 3.3.2 Needle Indentation Test

The aim of this preliminary study was to measure the thickness of the ligament over the disc as well as the bone regions to deduce if there was a difference in thickness across the two regions.

### **Method**

In this method, a needle was used to pierce through the tissues and the applied force measured to detect the change in response as the needle goes from one medium to another, which in this case was from ligament to bone or from ligament to disc (see Figure 3.4).



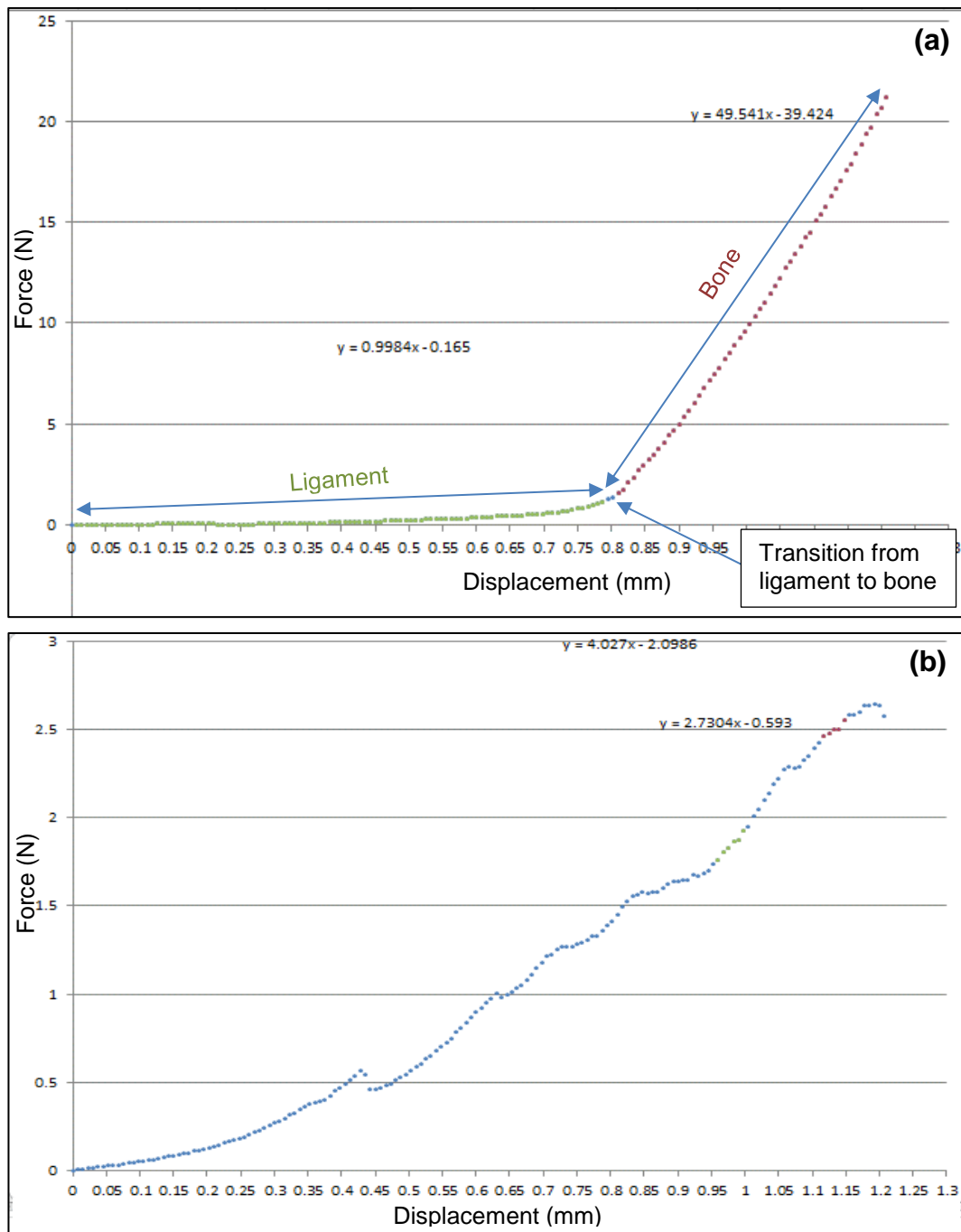
**Figure 3.4: Needle-Indentation test (a) over the bone region and (b) over the disc region (b) to measure the thickness of (a) ALL and (b) PLL in both regions.**

### **Results**

The force-displacement response through ligament and through the bone was found to have different gradients (Figure 3.5 (a)). Using this change in gradient from one medium to another and from the initial point where the tip of the needle touched the ligament, the thickness of the ligament could be derived. However, this was not found to be the case with the ligament over the disc region. Since the ligament and the disc have similar structure, a transition from ligament to disc was not evident and a curve with an almost consistent gradient throughout both tissues was obtained (Figure 3.5 (b)).

### **Conclusion**

The thickness over the disc region could not be evaluated using the needle indentation method and hence this method was discarded.



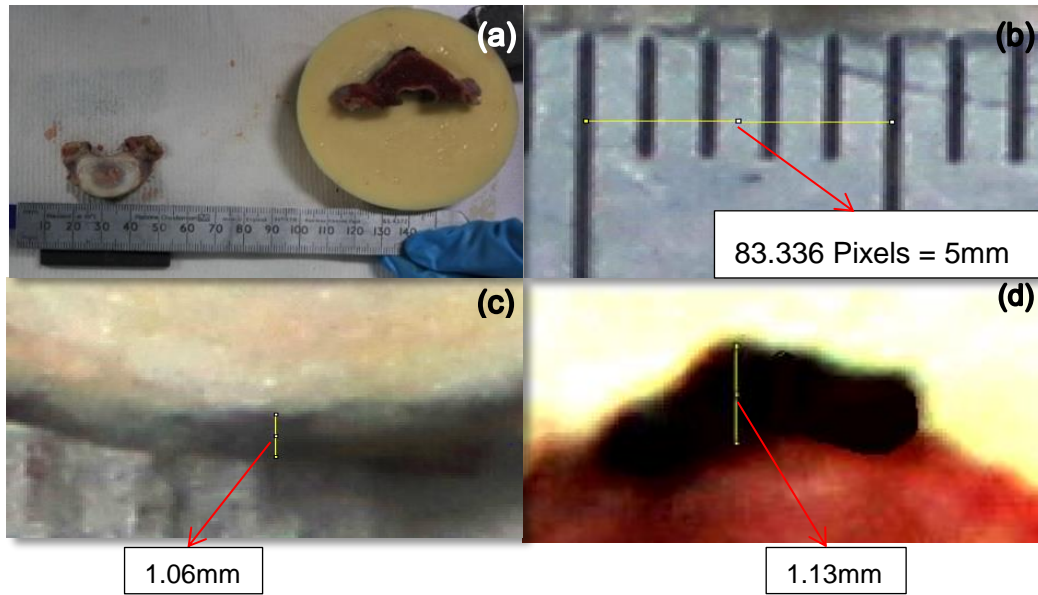
**Figure 3.5: Examples of force-displacement graphs of needle indentation into different tissues. (a) For the ligament-bone region: the transition from ligament to bone is apparent and could be used to calculate the thickness of ligament. (b) For the ligament-disc region: there is no transition of gradients, showing the similarity in the response from both ligament and disc.**

### 3.3.3 Photographic Image Analysis

The aim of this preliminary study was to measure the thickness of ligament over the disc as well as the bone region using pixels in photographic images to deduce if there is difference in thickness across the two regions.

#### ***Methods***

An FSU specimen was sectioned in such a way that the disc was separated from the vertebrae from one side i.e. by cutting through from the edge of the disc. A photograph of the vertebra as well as the disc with the ligament attached was captured with an aligned ruler using a SLR camera (Canon EOS 550D) with a high resolution lens (Canon 100 mm macro lens) (Figure 3.6 (a)). A resolution of at least 14 pixels/mm was achieved. The ligaments on each section were carefully tinted with a fine-nibbed black marker pen, prior to capturing the image, so it could be easily differentiated from the attaching disc or bone. An image analysis tool (ImageJ 1.41, Wayne Rasband, National Institutes of Health, USA) was used to measure the thickness from the pixels in the pictures. The images were imported to the software and the pixels in the image were calibrated using the reference scale in the photograph. The thickness was measured in pixels sagittally over six different regions of the disc section as well as over the corresponding bone section. The pixels were converted into respective values in millimetres and mean values were calculated and compared across both the disc and the bone region. An example of the process is illustrated in Figure 3.6.



**Figure 3.6: Process of measuring the ligament thickness: (a) sagittal view of the disc section (left) and PMMA-cemented-bone section (right), (b) calibration of the image from pixels to mm, (c) measurement of the ligament thickness over the disc region, (d) measurement of the ligament thickness over the bone region.**

### **Results**

The results for the photographic analysis of the ligament thickness are presented in Table 3.2. The mean thickness value of the ligament over the disc ( $1.05 \pm 0.05$  mm) was found to be very similar to the mean thickness of the ligament over the bone ( $1.04 \pm 0.07$  mm).

**Table 3.2: Thickness values of a ligament obtained after conversion from pixels to millimetres over disc and corresponding bone regions.**

Measurement Region	I	II	III	IV	V	VI	Mean
Thickness Over Bone (mm)	1.13	1.04	1.01	1.11	1.01	1.02	$1.05 \pm 0.05$
Thickness Over Disc (mm)	1.09	0.99	1.06	1.14	1.02	0.95	$1.04 \pm 0.07$

### **Conclusion**

The results indicated that there was little difference in the thickness along the length of the ligament and therefore the measureable thickness in the vertebral region could be used for the disc region where the thickness could not be measured directly from the CT images.

### **3.3.4 Discussion**

Two studies were carried out to deduce the thickness of the ligament over the disc region from the vertebra-bone region. The needle indentation test failed to output the thickness over the disc region due to similar fibrous composition of disc and ligament, hence this method could not be adopted. The photographic image analysis method showed very little difference in the thickness of the ligament across the two regions. This method was likely prone to some human error and the accuracy with which the edge of the marker pen line could be lined up with the observed ligament boundary. Experiments were undertaken to quantify this error by using the same marker pen to follow a given line on a piece of paper. It was found that the deviation from the line was less than 0.06 mm, indicating the likely accuracy of this technique. To further develop confidence in this method of image analysis, the thickness of the ligament from the FSU used in this study was also measured from a sagittal cross-section of its microCT image close to the disc using an image processing package (Scan IP version 7.0, Simpleware, UK). The average thickness over the disc section, measured from ScanIP, was compared with the thickness obtained from the photographic image analysis method (Table 3.2) and it was found to be less than 0.032 mm. This provided further confidence in the photographic method and in the conclusion that there was little change in ligament thickness between bone and disc regions.

## **3.4 Image Segmentation**

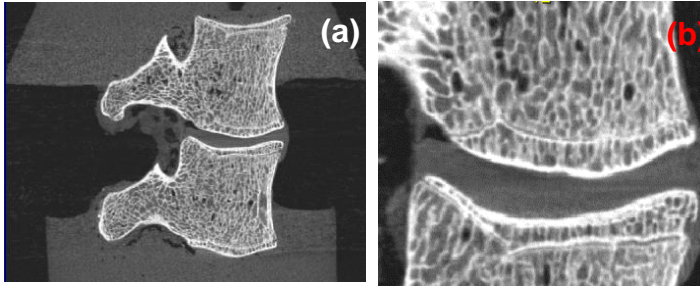
### **3.4.1 Images Pre-processing**

The reconstructed  $\mu$ CT images of the specimens were subjected to some preliminary preparations before being segmented. This included conversion of the images from the  $\mu$ CT scanner format (\*.DICOM) at the same resolution (74 $\mu$ m) to an alternative format (\*.TIFF) using a code developed in-house (Matlab 7.9, MathWorks, USA; Jones and Wilcox 2007). This reduced the number of greyscale values present in the images from 64,000 (Hounsfield units) to 256, i.e. reducing the number of grey shade variations in the greyscale spectrum.

The image data in \*.TIFF format was then exported to an image processing package (Scan IP version 7.0, Simpleware, UK) (Figure 3.7 (a)). The software enabled the images to be segmented and the vertebra and the morphology of the ligaments to be identified. The image data was first cropped to remove both the side plates leaving the image area only covering the ligament to be



segmented i.e. either the ALL or PLL and small sections of attaching superior and inferior bones and disc (Figure 3.7 (b)).

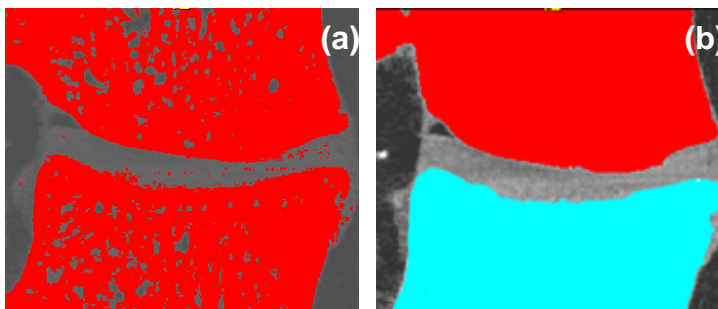


**Figure 3.7: (a)  $\mu$ CT sagittal view of an FSU with the PMMA cement on each end, (b) cropped image of (a) following removal of the cement and unwanted regions leaving the image area only covering the ligament to be segmented and small sections of attaching bones and disc.**

The following segmentation procedure was adopted to create segmented images (referred to here as ‘masks’) of the vertebral bone and ligament of interest.

### 3.4.2 Segmentation of the Bone

An iterative method was used to find the optimum upper and lower threshold values to capture the bone by visual comparison between the mask and the underlying image. These values were then used with an active thresholding tool (‘paint with threshold’) on all the image slices to create a mask capturing the bones of both the superior and inferior vertebra (Figure 3.8 (a)). A floodfill tool was then used to remove unwanted islands and to separate the superior and inferior vertebra into separate masks (Figure 3.8 (b)). Further segmentation methods including morphological close, cavity fill and floodfill, were performed as required to obtain fully closed bone masks with no holes and or gaps.

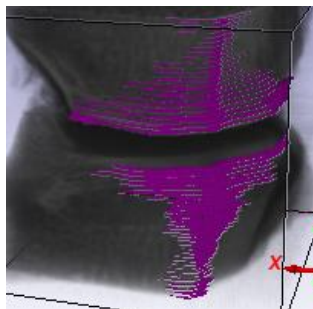


**Figure 3.8: Segmentation of bone (a) after the use of thresholding to capture the bone tissue only, and (b) after the use of floodfill, to separate inferior and superior vertebra masks, and after closing all the respective holes and gaps.**

### 3.4.3 Segmentation of the Ligament

The segmentation of the ligament using automated tools was found not to be possible because the greyscale distribution of the ligaments overlapped those of the disc, the trabecular bone spaces and also some background noise. Therefore, a semi-manual approach was required to segment the ligament. One potential option was to use the 'paint with threshold' tool manually on all individual slices. However, this was found to be an immensely time-consuming and labour-intensive process as each specimen contained over 250 slices in the vertical direction. After some iterations, the procedure below was found to be the optimum for segmenting the ligaments efficiently with the fewest manual procedures:

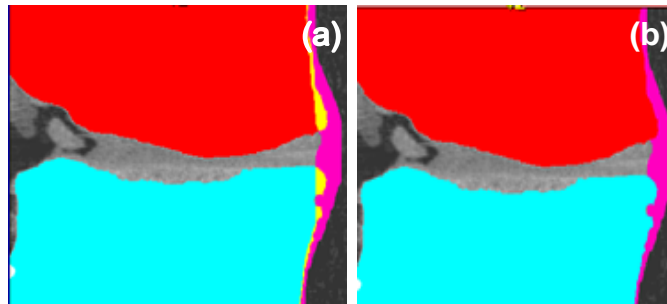
- The threshold operation was first applied iteratively over the whole image to determine the most appropriate values for capturing the ligament of interest i.e. either the ALL or PLL.
- The 'active thresholding tool' was then used with these values on individual image slices to create a mask over the ligament region on that slice. The procedure was repeated on every 5<sup>th</sup> slice over the bones area only (Figure 3.9). To save more time, the approach was also tried on every 20<sup>th</sup> slice and then on every 10<sup>th</sup> slice, but the post-processing steps that followed were found to be more time-consuming and labour intensive compared to the ones that followed painting on every 5<sup>th</sup> slice.
- A morphological close operation of 5 voxels in the direction of the slices was then performed on the ligament to join the painted segments resulting in a mask over both superior and inferior bone area.



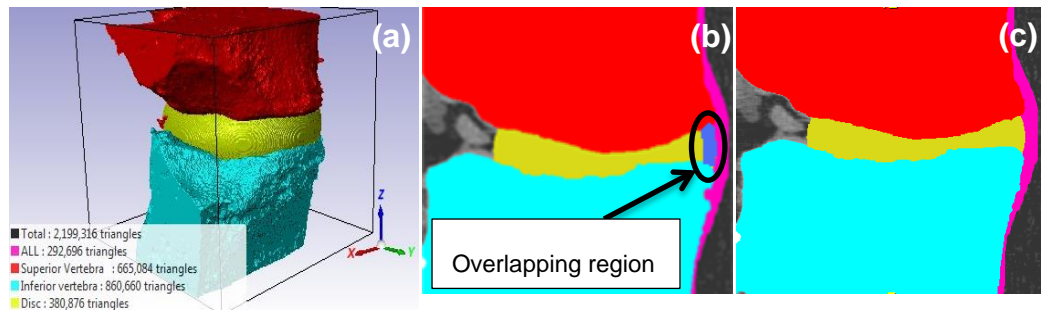
**Figure 3.9: ligament mask manually painted over every 5th slice of bone region only.**

- A further morphological close operation in the direction of the slices was then performed between the lower ligament slice of the superior vertebrae and the uppermost ligament slice of the inferior vertebrae to join the painted segments. This resulted in a mask representing the ligament over the disk region.

- Further segmentation was performed including the use of morphological close, cavity fill and floodfill functions, to obtain fully closed ligament masks with no holes or gaps.
- A 'subtract' Boolean operation was performed on the ligament and each vertebra in turn in order to remove any overlapping regions (yellow regions in Figure 3.10 (a)) between the ligament and the bones (Figure 3.10 (b)).
- An ellipsoid was created between the two bones to represent the disc, keeping the ellipsoid parameters within the boundaries of the bones as shown in Figure 3.11 (a) because the thickness of the ligament was shown to be very similar over the bone and the disc region (Section 3.3). Any overlapping region between this ellipsoid-disc mask and the ligament mask (blue region in Figure 3.11 (b)) was removed using Boolean operations, to cut away any remaining ligament mask from the disc region, thus preserving the disc mask while reducing the ligament mask (Figure 3.11 (c)). This creation of an ellipsoid mask was only required in the case of the ALL because the anterior aspect of disc is curved in reality, therefore it was important to reflect this shape in the ligament mask. Whereas, in the case of the PLL, the creation of an ellipsoid was not required because the posterior aspect of the vertebra and the disc region are flat. Here, it was found that a morphological close operation resulted in an accurate representation of the PLL shape.



**Figure 3.10: segmentation of ligament (a) before and (b) after the application of 'Boolean operations' whereby the yellow regions show the overlapping regions between the bones and the ligament.**



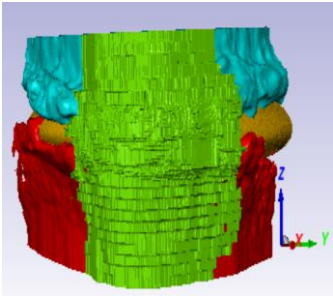
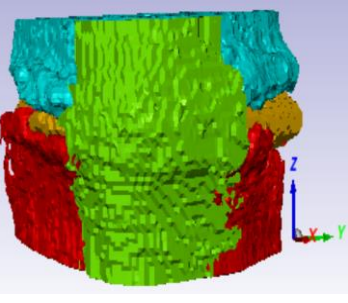
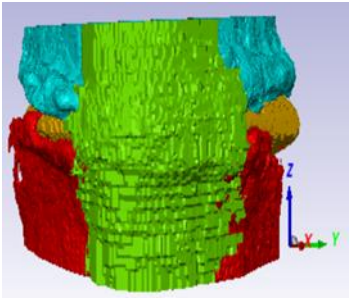
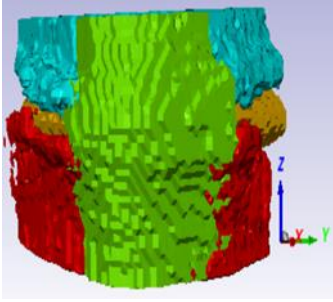
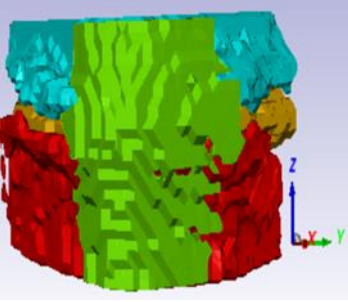
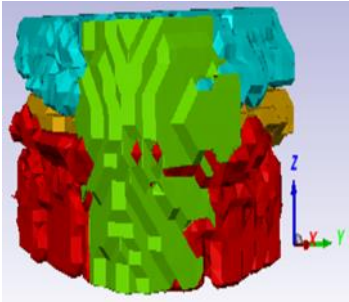
**Figure 3.11: (a) creation of an oval shape between the superior and inferior vertebrae to represent disc, (b) the overlapping region (blue area) between the disc and the ligament, (c) final ligament mask after using ‘Boolean operations’ to remove the unwanted region.**

### 3.5 Image Downsampling

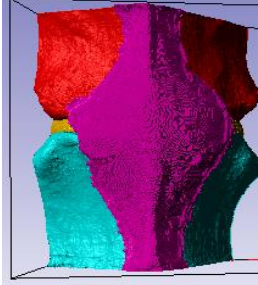
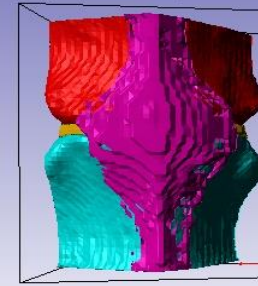
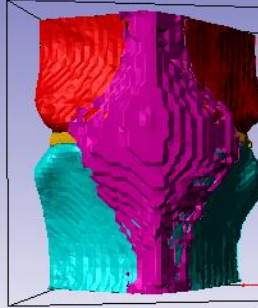
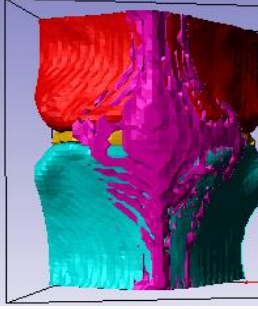
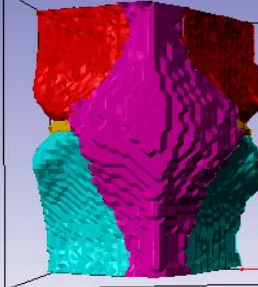
The segmented images were then down-sampled to an optimum resolution at which image pixel-size could be reduced without losing the detail of the ligament. The downsampling operation was performed to help govern the size of the finite element mesh and to speed up subsequent processes in ScanIP. The optimum was established by down-sampling the image from its original resolution of 0.074 mm to a set of resolutions between 0.1 and 1 mm, in increments of 0.1 mm, and comparing the mask on the ligament visually. A resolution of 0.6 mm was found to be the optimum because it was the lowest resolution to which the image could be down-sampled before there were visual discontinuities in the overall shape of the ligament. An example of this is shown in Table 3.3.

A number of different downsampling methods were also investigated using built-in algorithms within the software. The ‘majority wins’ interpolation was found to be the most optimum (see Table 3.4) because it had the least effect on the overall volume of the ligament, which was of greater importance in this study than the bone or disc in the overall behaviour of the model. However, the down-sampling procedure still resulted in severe discontinuities in the voxels, especially in the ligament (Figure 3.12). The down-sampled images were dilated and smoothed using built-in features to remove the discontinuities, hence pre-smoothing the image prior to the creation of a mesh. The final 3-D segmented models of the ALL and PLL are illustrated in Figure 3.13 (a) and (b) respectively, at the point prior to meshing. Visual comparison back to the underlying image showed that after these procedures, the mask was a good fit to the ligament boundaries.

**Table 3.3: An example of image downsampling from original resolution of 0.074mm to how the optimum of 0.6mm was arrived at.**

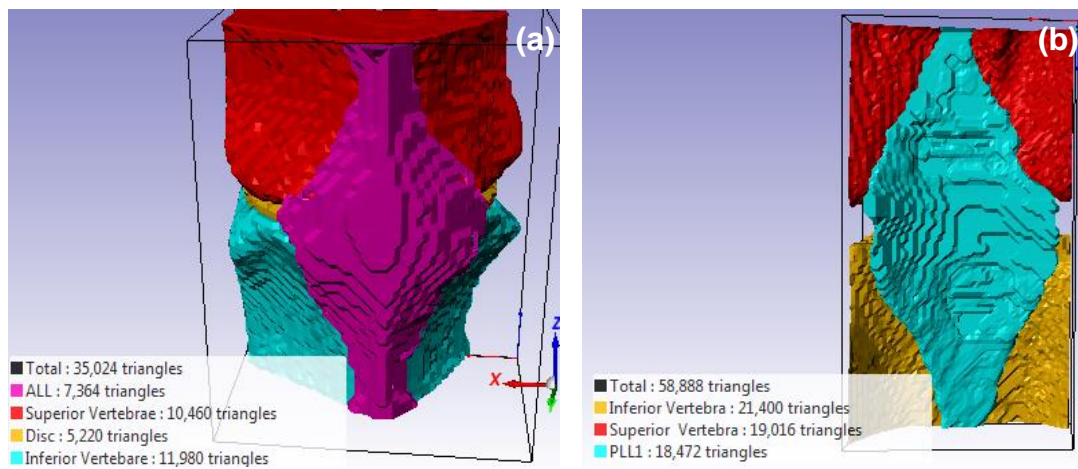
Original Image	0.2mm Resolution	0.4mm Resolution
		
0.6mm Resolution	0.7mm Resolution	0.8mm Resolution
		

**Table 3.4: The various downsampling algorithms along with the volume of ligament and the final model generated by each.**

Method	Volume of ligament (mm <sup>3</sup> )	Downsampled masks
<b>None (pre-downsampling)</b>	421.841	
<b>Linear</b>	237.194	
<b>Nearest Neighbour</b>	247.799	
<b>Partial Volume Effect</b>	132.585	
<b>Majority Wins</b>	407.352	



**Figure 3.12: Discontinuities in the ligament mask as a result of downsampling.**



**Figure 3.13: Final 3-D volume of the masks after dilate and smoothing tools have been applied, showing (a) the ALL, superior vertebra, inferior vertebra and disc, (b) the PLL with superior and inferior vertebrae.**

## **3.6 Finite Element Method Development**

The methodology for developing an FE model of the longitudinal ligaments was initially developed from the images of a FSU where the ALL was tested (Chapter 2). Sensitivity analyses were initially carried out on simple linear elastic material models of the ALL with both idealised rectangular geometry and a more realistic representation of the geometry, to test how the geometry, boundary conditions and applied load could be best simplified to represent the experimental setup accurately. The finite element mesh size was also examined. In addition, a series of non-linear material models (as described in Chapter 1, Section 1.2.7) were applied to the model to decide which material models were suitable. Combining the best choice of boundary conditions, loading and material model, a methodology was hence devised for generating specimen-specific models of the ligaments that could then be used to determine the material properties as described in Section 3.7.

The devised methodology was then also applied to a model of the PLL exported from ScanIP to demonstrate that the methodology could be replicated and would be appropriate for other ligamentous tissues.

### **3.6.1 Sensitivity Analysis**

Four different sensitivity studies were carried out to develop a methodology that best represented the experimental setup in order to derive the material properties of the ligaments.

- i. Study I – sensitivity to dimensions
- ii. Study II – sensitivity to boundary conditions
- iii. Study III – mesh sensitivity
- iv. Study IV – choice of material models

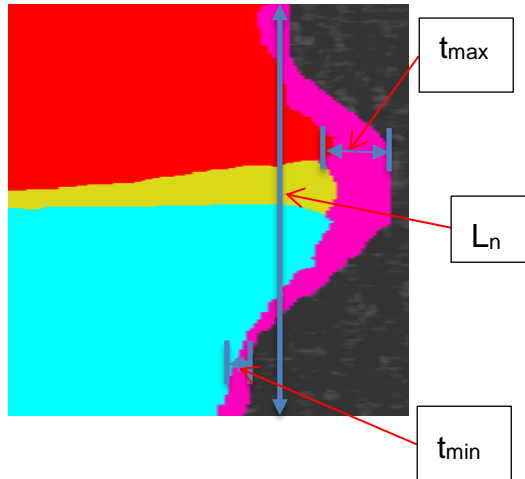
#### **3.6.1.1 Study I - Sensitivity to Dimensions**

The aim of this study was to determine how the geometry, i.e. the dimensions and shape of the ligament, affect the overall behaviour of the ligament. Two rectangular models, with idealised ligament geometry, and a third model based on the specimen image data were developed. All three models had the same total length and same average cross-sectional area. The rectangular models were compared to simplified theoretical calculations based on one-dimensional assumptions to understand if the change in physical dimensions affected the output of the model. The results obtained from all three models were also compared against each other to quantify the difference in predicted stiffness, if any, that was caused by the geometric simplifications.



### Model Geometry:

For the two idealised rectangular models (Rec\_A and Rec\_B), parameters were derived from a lateral view of the masked image of the ligament in ScanIP (Figure 3.14 and Table 3.5); these included the length ( $L_n$ ), maximum and minimum thickness ( $t_{max}$  and  $t_{min}$  respectively). From the mask volume and length, an average area was also determined.



**Figure 3.14: Sagittal view through segmented microCT image showing the measurements used for the development of the equivalent rectangular models ( $L_n$  = length,  $t_{max}$  = maximum thickness,  $t_{min}$  = minimum thickness).**

**Table 3.5: Geometric parameters used for the development of idealised rectangular models of ligament.**

Volume ( $V$ , mm <sup>3</sup> )	Length ( $L_n$ , mm)	Maximum Thickness ( $t_{max}$ , mm)	Minimum Thickness ( $t_{min}$ , mm)	Average Area ( $A$ , mm <sup>2</sup> )
124.1	23.49	1.31	0.17	5.22

The two models were built to represent the two extremes of the ALL thickness. The length used for both models was the same, with the thicknesses as given in Table 3.5 and the widths were calculated as follows:

For thickest model, Rec\_A;  $W_A = 3.97$  mm

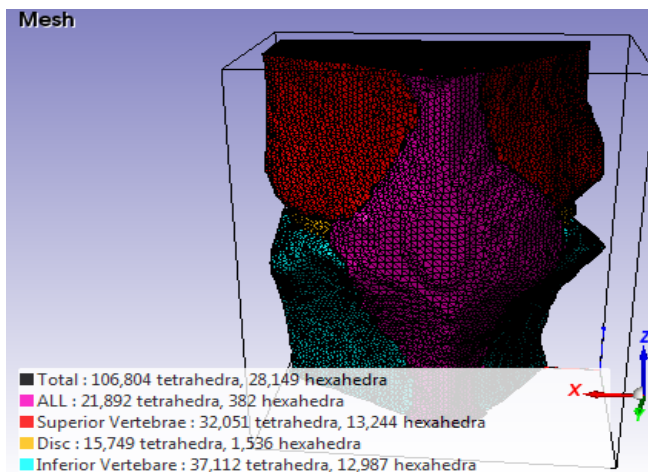
For thinnest model, Rec\_B;  $W_B = 31.46$  mm

The realistic geometry model, Real\_A, was obtained as a result of segmentation and downsampling in ScanIP (Section 3.4 and Section 3.5).

### Mesh:

The models, Rec\_A and Rec\_B, were both meshed using hexahedral elements while Real\_A was meshed in ScanIP employing the ScanIP meshing tool with

in-built meshing algorithm, +FE Grid, which converted the segmented masked regions of the FSU directly into an FE volumetric mesh. This resulted in meshes comprising 4-node tetrahedral and 8-node hexahedral linear elements. Figure 3.15 shows the full meshed model. Surfaces were also defined at the two extremes of the model i.e. the top and the bottom surface to be used for the application of load and possible boundary conditions. The models were exported from the ScanIP as FE input files for Abaqus. The meshed vertebrae were then deleted in Abaqus to leave only the model of the ligament, still containing the definitions of the surfaces, that was used in this study.



**Figure 3.15: Final meshed model of ALL ready to be exported.**

### **Material Properties:**

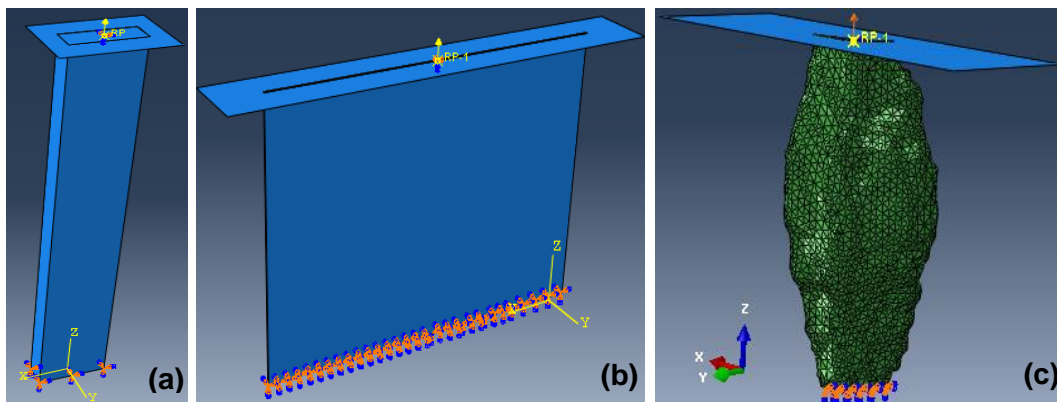
Although the ligament behaves in a non-linear elastic manner, an isotropic linear elastic material model was used for this initial study to simplify the material behaviour before a more realistic representation of material behaviour was devised. To describe a linear-elastic model in Abaqus, two independent material parameters, the Young's modulus ( $E$ ) and Poisson's ratio ( $\nu$ ), were required. The Young's modulus was taken as typical value of 0.4 GPa from Chapter 2 and the Poisson's ratio was assumed at 0.3 based on literature (Tusang et al., 2009).

### **Boundary Conditions and Applied Load:**

Figure 3.16 shows the boundary conditions (BCs) and load applied to the models. The bottom surface was fully encastre, i.e. constrained in all degrees of freedom, to stop any movement in order to represent the fixed inferior vertebra in the materials testing machine (Chapter 2, Section 2.3.4, and Figure 2.4). The top was fixed such that it was allowed to move in the upward direction only i.e. in the direction of the applied load to represent the movement of the

superior vertebra in upward direction only due to the application of the tensile load in the experiment.

All three models, Rec\_A and Rec\_B and Real\_A, were subjected to an upward concentrated force of 400 N. The force was applied to the top surface of ligament through a rigid plate created in tied contact and placed centrally over the top surface of the ligament. This was a simplified representation of the tensile load applied in the experimental setup as described in Chapter 2 (Section 2.3.4). The application of load via a plate tied directly to the surface was found to be easier as it distributes the load applied over the entire surface that it is tied to, compared to applying the loads to each individual node over the surface.



**Figure 3.16: Boundary conditions and loads applied to models (a) Rec\_A, (b) Rec\_B and, (c) Real\_A.**

### Theoretical Analysis of Rectangular Models:

Both the rectangular models were developed using the same cross-sectional area and length, with the same modelling parameters, therefore, if the models were under perfect uniaxial stress, then both should extend by the same amount. The displacement was calculated using Equation 3.1, assuming uniaxial stretch, and compared to the displacement from the models in the direction of the stretch (U3) given in Table 3.6;

$$\sigma = F/A = 0.4/5.22 = 0.766 \text{ kN/mm}^2$$

$$E = \sigma/\epsilon$$

$$\Rightarrow \Delta L = (\sigma \times L)/E = 4.45 \text{ mm}$$

[eq. 3.1]

Where,

$\sigma$  = stress

F = total force applied to the ligament

A = cross-sectional area of the ligament

E = Young's modulus

$\epsilon$  = strain

$L$ ,  $\Delta L$  = original length, change in length

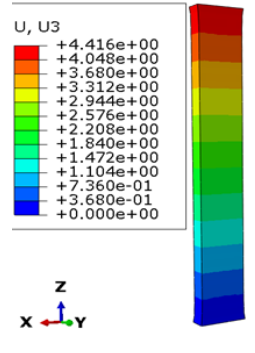
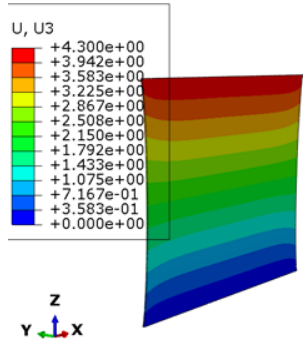
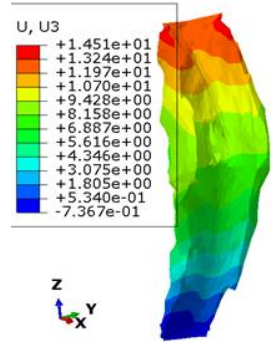
### Results:

The results obtained in the form of contour plots for all three models (Rec\_A, Rec\_B and Real\_A) are presented in Table 3.6. The results are only presented for the direction in which the force was applied, z-displacement ( $U_3$ ). The x (width) and y (thickness) displacements are difficult to interpret due to shape and orientation of ligament.

The theoretical displacement in the direction of the force applied was found to be 4.45 mm. The displacement for both Rec\_A (4.42 mm) and Rec\_B (4.30 mm) were very similar to the theoretical value, however, Rec\_A gave results closer to the theoretical results assuming uniaxial stretch.

The realistic geometry model, Real\_A, resulted in a  $U_3$  displacement of 14.5 mm which was over three times higher than both the theoretical calculations and the rectangular model outputs.

**Table 3.6: Contour plots obtained for Rec\_A, Rec\_B and Real\_A alongside the scale in mm showing displacement in the direction of stretch ( $U_3$ )**

Model	Rec_A	Rec_B	Real_A
Displacement in the direction of stretch ( $U_3$ /mm)			

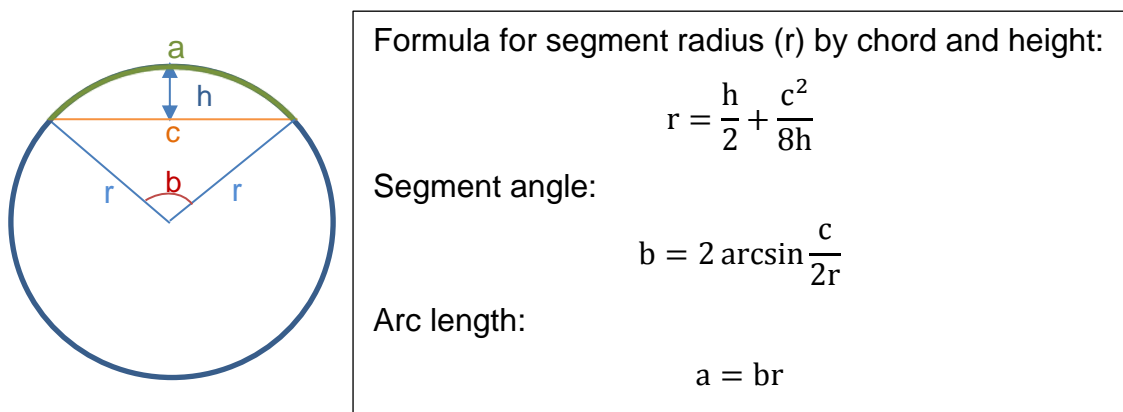
### Discussion:

The study indicated that the behaviour of ligaments in the modelled regime, i.e. in extension, is sensitive to the geometry used. There are two possible irregularities in the real ligament due to its:

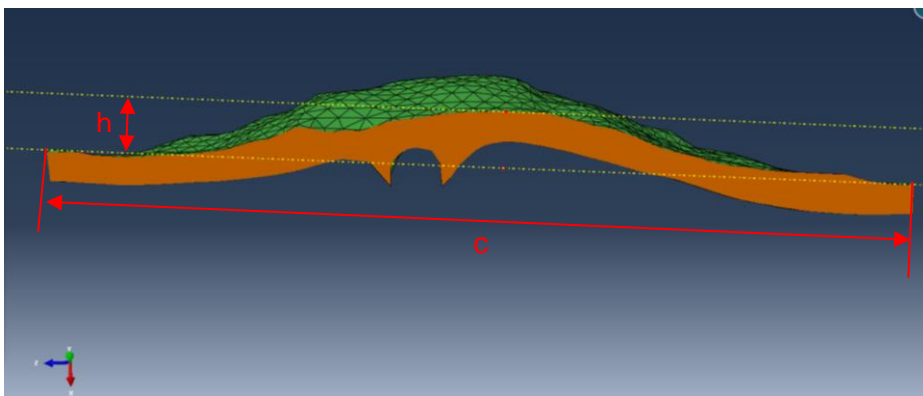
1. irregular cross-sectional area and
2. curved shape (curved in several different directions).

Although it is difficult to separate these two factors from the results, an approximation of the curvature along the length of the ligament could be made to evaluate its effects. When the real ligament is stretched without any contact

with the bone, it will straighten out. Assuming it to be an arc (Figure 3.17) then its length (a) (i.e. the length of the ligament prior to stretching), can be worked using the expressions given in Figure 3.17. The dimensions of ligament from the realistic model used in this study were measured as shown in Figure 3.18. This gives a chord length (c) of about 23 mm (See Table 3.5) and curve height (h) of ~1.6 mm, resulting in the initial length of the ligament (a) being ~23.3 mm. This means that theoretically a displacement of 0.3 mm could be applied purely to straighten it out, prior to causing any axial strain within the material. However, this displacement is small compared to the amount the ligament actually stretched by (14mm - see Table 3.6, U3 for Real\_A); therefore, it can be seen that the curvature alone cannot explain the disparity with the rectangular models, and the irregular cross-section must also play an important part.



**Figure 3.17: Expressions to theoretically calculate the approximate length of ligament (a) post-stretching, assuming it to be part of a circle.**



**Figure 3.18: Lateral view of a meshed ligament in Abaqus to measure the curved distance between top and bottom of ligament i.e. length of ligament (c) and difference between the ends and middle of the ligament (perpendicular distance between lines) i.e. curve (h) of ligament. The green region shows the meshed anterior side of the ligament.**

**Conclusion:**

The irregular shape of the ligament i.e. the varying cross-section as well as the irregular curved shape of ligament, is an important consideration while modelling its overall behaviour hence a simplified geometry could not be used to derive the material properties of the ligament.

### 3.6.1.2 Study II – Sensitivity to Boundary Conditions

The aim of this study was to test the sensitivity of the ligament behaviour to the boundary conditions (BCs) applied. Two models with different lengths but same width and thickness were developed and differing boundary conditions were applied. The work was carried out on rectangular models for the ease of modelling and subsequent meshing. The results in the form of displacement in the direction of stretch were compared between both models in order to quantify the differences, if any, made by varying the way the boundary conditions were applied and also to see if the realistic ligament model could be simplified by reducing it to just the region corresponding to the disc. This formed the basis of subsequent modelling on the realistic geometry.

#### **Model Geometry:**

Two rectangular models were developed, a long rectangular model with the same dimensions as Rec\_A (Rec\_C) and a short rectangular model which had the same length as the section of ligament between the vertebrae (Rec\_D).

#### *Long-Rectangular model (Rec\_C)*

In reality, the longitudinal ligaments are attached to the superior and inferior vertebrae and disc on one side while they are free on the other. In the experiments reported in Chapter 2, the force was applied to the ligament via the stiffer superior-vertebra bone while the inferior-vertebra, attached to the bottom section of the ligament, was held in place, leaving the central region (corresponding to the attachment to the disc) free, so this is the main region of stretch. A schematic representation of this is shown in Figure 3.19 (a). To represent these conditions in model Rec\_C, a discrete rigid plate was generated and placed centrally, in tied contact with the upper region of the model corresponding to the attachment region of the superior vertebra (Figure 3.19 (b)). The dimensions of the plate were kept slightly bigger than this surface of the ligament to ensure the full surface was attached.

#### *Short-Rectangular model (Rec\_D)*

The length of the region corresponding to the attachment of the disc was measured from ScanIP and a rectangular model, Rec\_D, with the same thickness and width as model Rec\_A but new height (corresponding to the disc length) was generated.

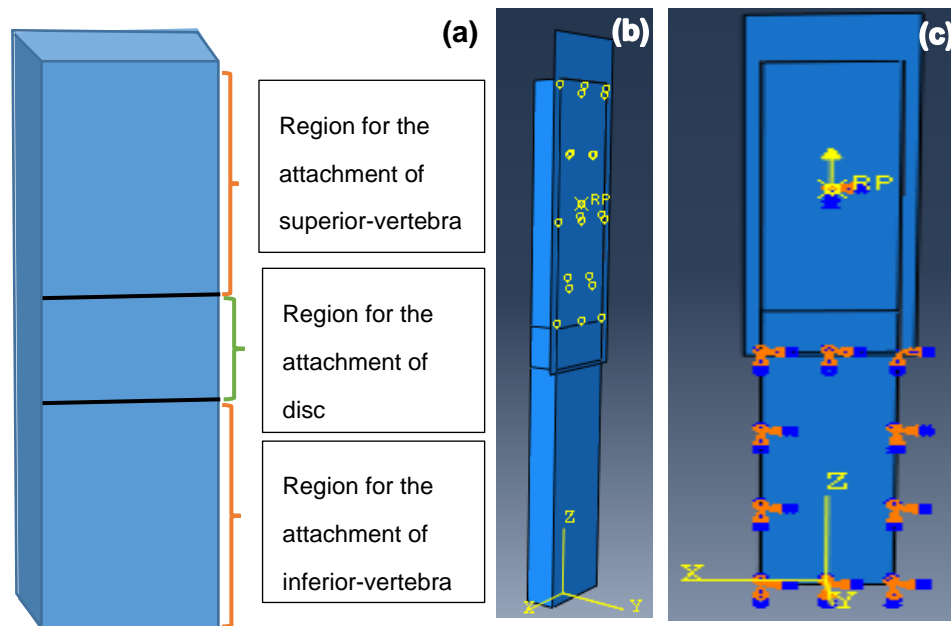
### Material Properties:

The same isotropic linear elastic material model, as previously used in study I, was used for both models in order to make the results comparable between the models.

### Boundary Conditions and Load Applied:

#### *Rec\_C*

An encastre constraint was set on the surface of the lower section which represented the area covered by the inferior vertebra to replicate the attachment with the inferior vertebra. The middle section which represents the area covered by disc was left free as in the experiment. The load was applied centrally on the plate in the upward direction to represent the load applied to the ligament, in reality, via the superior vertebra. The plate was restricted to move in the upward direction only. The model is represented in Figure 3.19 (c).



**Figure 3.19: Schematic of the Rec\_C model boundary conditions. (a) Ligament with bone and disc attachment regions identified, (b) image of model with side-plate tied to the top region, (c) front view of model with BCs and load.**

#### *Rec\_D*

The same BCs and load were applied to model Rec\_D as applied to the initial simplified rectangular model, Rec\_A. That is, encastre boundary conditions were applied to the bottom end of the model Rec\_D to stop any movement, while the top was allowed to move only in the direction of the applied load. The load was applied to the top surface of the model through a rigid plate created in

tied contact and placed centrally over the top surface. The same load of 400N, as previously used for Study I, was applied to both the models.

**Mesh:**

For Rec\_C, the model was meshed using same number of hexahedral elements as for Rec\_A. For Rec\_D, the model was meshed using same number of hexahedral elements as were present in the disc region of the model Rec\_A.

**Results:**

The results obtained are presented in Table 3.7. The results for model Rec\_C showed that the section of the ligament left free i.e. the region that corresponds to the attachment of the disc experienced higher strains, as expected.

**Analysis:**

Comparing the results of Rec\_D with Rec\_C (Table 3.7) showed that the overall behaviour was similar with similar contours observed in the free (stretched) section of ligament in both cases. However, the displacements were found to be very different in the two cases. The displacement U3 obtained for Rec\_C (0.756 mm) was found to be higher than the displacement obtained for Rec\_D (0.321 mm). Moreover, Rec\_D shows close to constant U3 displacement across the thickness while Rec\_C exhibits big differences in displacement between its anterior and posterior sides. This is due to the way the load was acting on the two models; in Rec\_C, it was effectively pulling just one edge of the middle section of the ligament, whereas in Rec\_D, the force was applied across the full width.

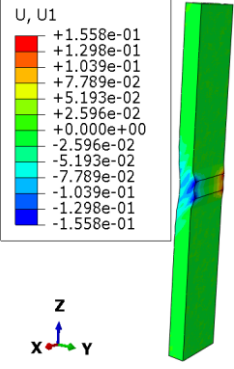
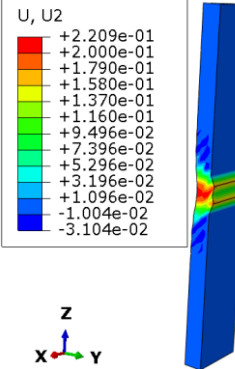
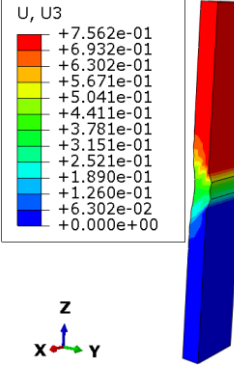
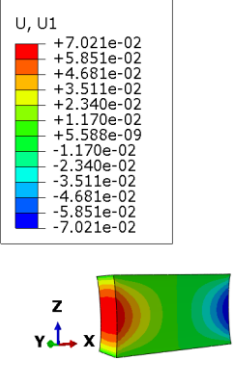
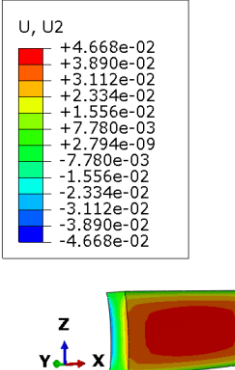
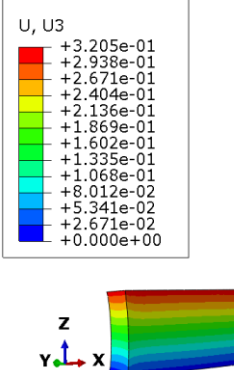
**Conclusion:**

The study showed that changing the boundary conditions from simplified to more realistic ones varied the loading applied in all directions which ultimately affected the overall stretch of the ligament in the principal direction. This indicated that the application of realistic boundary conditions is required to represent the true behaviour of the ligaments in order to derive the material properties of ligament accurately.

This study also showed that the use of only the middle section is not suitable for modelling the behaviour of the full ligament, therefore the realistic-geometry model of the ligament would have to capture the entire height of the ligament.



**Table 3.7: The displacements in the x (U1), y (U2) and z (U3) directions obtained for Rec\_C and Rec\_D showing that the greatest variation occurs over the section corresponding to the disc region.**

<p>Displacement- Rec_C (mm)</p>	<p>U, U1</p>  <p> <math>+1.558e-01</math>  <math>+1.298e-01</math>  <math>+1.039e-01</math>  <math>+7.789e-02</math>  <math>+5.193e-02</math>  <math>+2.596e-02</math>  <math>+0.000e+00</math>  <math>-2.596e-02</math>  <math>-5.193e-02</math>  <math>-7.789e-02</math>  <math>-1.039e-01</math>  <math>-1.298e-01</math>  <math>-1.558e-01</math> </p> <p>Z X Y</p>	<p>U, U2</p>  <p> <math>+2.209e-01</math>  <math>+2.000e-01</math>  <math>+1.790e-01</math>  <math>+1.580e-01</math>  <math>+1.370e-01</math>  <math>+1.160e-01</math>  <math>+9.496e-02</math>  <math>+7.396e-02</math>  <math>+5.296e-02</math>  <math>+3.196e-02</math>  <math>+1.096e-02</math>  <math>-1.004e-02</math>  <math>-3.104e-02</math> </p> <p>Z X Y</p>	<p>U, U3</p>  <p> <math>+7.562e-01</math>  <math>+6.932e-01</math>  <math>+6.302e-01</math>  <math>+5.671e-01</math>  <math>+5.041e-01</math>  <math>+4.411e-01</math>  <math>+3.781e-01</math>  <math>+3.151e-01</math>  <math>+2.521e-01</math>  <math>+1.890e-01</math>  <math>+1.260e-01</math>  <math>+6.302e-02</math>  <math>+0.000e+00</math> </p> <p>Z X Y</p>
<p>Displacement- Rec_D (mm)</p>	<p>U, U1</p>  <p> <math>+7.021e-02</math>  <math>+5.851e-02</math>  <math>+4.681e-02</math>  <math>+3.511e-02</math>  <math>+2.340e-02</math>  <math>+1.170e-02</math>  <math>+5.588e-09</math>  <math>-1.170e-02</math>  <math>-2.340e-02</math>  <math>-3.511e-02</math>  <math>-4.681e-02</math>  <math>-5.851e-02</math>  <math>-7.021e-02</math> </p> <p>Z Y X</p>	<p>U, U2</p>  <p> <math>+4.668e-02</math>  <math>+3.890e-02</math>  <math>+3.112e-02</math>  <math>+2.334e-02</math>  <math>+1.556e-02</math>  <math>+7.780e-03</math>  <math>+2.794e-09</math>  <math>-7.780e-03</math>  <math>-1.556e-02</math>  <math>-2.334e-02</math>  <math>-3.112e-02</math>  <math>-3.890e-02</math>  <math>-4.668e-02</math> </p> <p>Z Y X</p>	<p>U, U3</p>  <p> <math>+3.205e-01</math>  <math>+2.938e-01</math>  <math>+2.671e-01</math>  <math>+2.404e-01</math>  <math>+2.136e-01</math>  <math>+1.869e-01</math>  <math>+1.602e-01</math>  <math>+1.335e-01</math>  <math>+1.068e-01</math>  <math>+8.012e-02</math>  <math>+5.341e-02</math>  <math>+2.671e-02</math>  <math>+0.000e+00</math> </p> <p>Z Y X</p>

### 3.6.1.3 Study III – Mesh Sensitivity

The aim of this study was to analyse the sensitivity of the material to the type and size of mesh used and obtain a minimum mesh size that could be used for all the FE models.

#### **Model Geometry, Boundary Conditions, Loads and Material Properties:**

The study was carried out on a simpler model that was found to represent the experimental behaviour closely i.e. model Rec\_C with the same boundary conditions and loads as previously used in Section 3.6.1.2. The same isotropic linear elastic material model, as previously used in Study I was used. The realistic geometry was not used because it is difficult to control the mesh size in ScanIP where there is a complex shape involved, as one can only limit the maximum element size. Since each model will have different geometry, the aim of mesh convergence was to look at a generic case that could then be applied as a maximum size across all models. Moreover, in re-meshing the model in ScanIP, the capture of the geometry also changes (with finer features being captured at higher resolutions), and this is also affected by the underlying image voxel size (Jones & Wilcox, 2007), so there are two factors changing: the geometrical representation and the number of nodes (degrees of freedom). The Rec\_C model has a regular geometry, it is not based on image data and the shape does not change with increasing mesh size, so the effects of the number of degrees of freedom can be isolated; it was therefore deemed most suitable for this study.

#### **Element Type:**

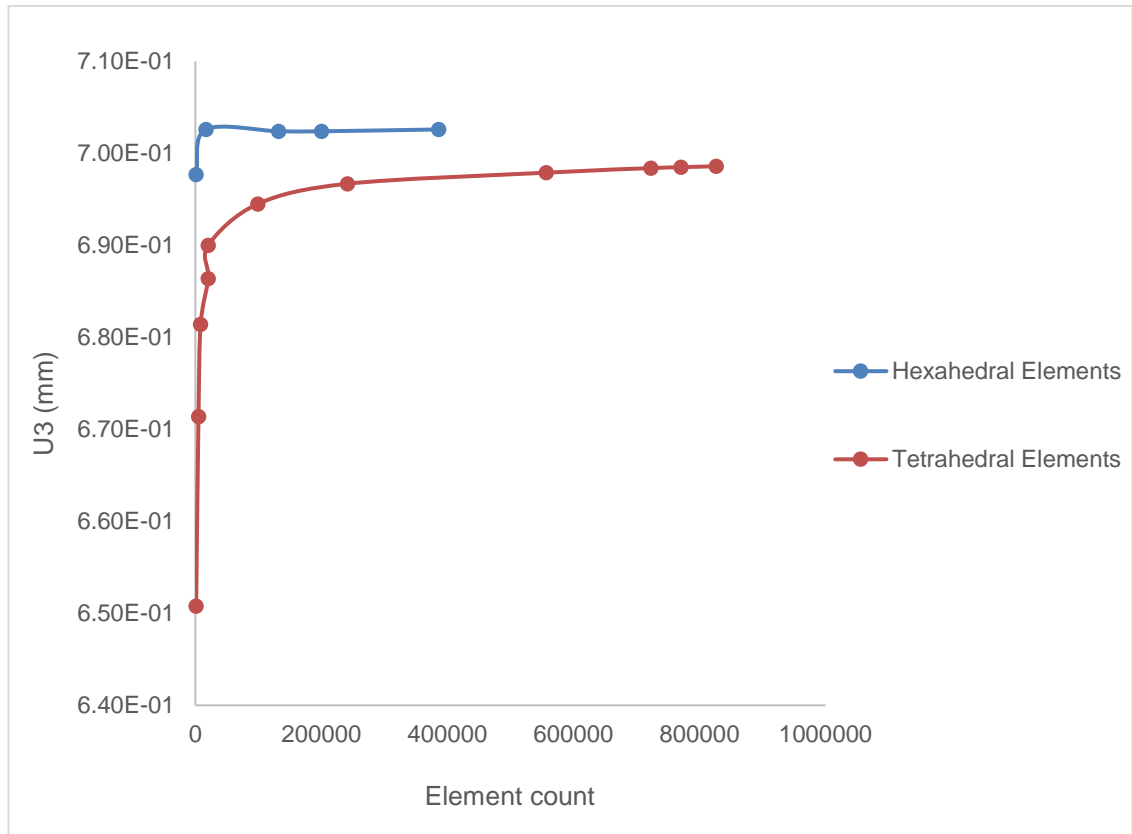
Tetrahedral elements are best for modelling complex geometry due to their ability to conform to irregular shapes with little distortion. However, the space generated by tetrahedral elements typically requires 4–10 times more elements than a hexahedral mesh to obtain the same level of accuracy (Cifuentes & Kalbag, 1992; Weingarten, 1994), implying that hexahedral elements are more efficient. Different orders of both types of elements are available with the higher order elements requiring more sophisticated shape functions, however, higher order means more integration points and hence an increasing computational cost (ABAQUS, 2014). The in-built meshing tool in ScanIP uses a mixture of 4-node tetrahedral and 8-node hexahedral linear elements to achieve a compromise in accuracy and computational cost. Both these element types were explored to find the optimum mesh size that would be used in further modelling.

**Mesh Size:**

Both hexahedral and tetrahedral elements were generated on the Rec\_C model with increasing number of elements (mesh size). The output of interest was the displacement in the direction of stretch (U3) since this was the only parameter used and compared to experimental data in the subsequent analysis within this thesis. For both types of elements, the mesh size was increased until solution convergence for the output of interest was achieved.

**Results and Analysis:**

The results obtained for both element types were plotted on the same graph (Figure 3.20). It can be seen that the hexahedral and tetrahedral element types converge to very similar displacement (respectively ~0.703 mm and ~0.698 mm - less than 1% difference). Since tetrahedral elements are stiffer (Carl, et al., 2006), for a given applied load, one would expect a smaller displacement for the tetrahedral mesh as was seen in this case. Hexahedral elements as expected, converged at a lower element count of under 20,000 elements, as compared to the tetrahedral mesh where a steady increase in displacement was achieved until around 750,000 elements and there was still an increasing trend even at 850,000 elements. To translate the findings from this simple study to the FE analysis of realistic-geometry models, a maximum element size was required since this could be controlled in ScanIP, an error of less than 5% in the output was deemed acceptable, because other factors in the experiment would likely produce considerably higher errors than this, such as the simplification of the boundary conditions, hence having a highly converged mesh would not have a significant effect on the accuracy of the FE analysis. Using the output of the converged hexahedral mesh as the target, any models achieving a displacement above 0.668 mm would therefore be deemed adequate. For the tetrahedral mesh, this was achieved with greater than ~5000 elements for the Rec\_C model, equating to an element size of 0.5 mm or smaller.



**Figure 3.20: Mesh convergence study on simple rectangular model, showing the predicted U3 displacement (note: U3 scale does not start at zero) for models using hexahedral and tetrahedral elements.**

### Conclusion:

From this study, it was found that an element size of less than 0.5 mm would provide adequate convergence of the axial displacement for both tetrahedral and hexahedral elements. It is important to note here that the focus of this study has been only on displacement so if future studies have interest in other output fields e.g. stress or strain, then further convergence tests would be necessary.

### 3.6.1.4 Study IV - Choice of Material Model

The aim of this study was to test various material models available in the Abaqus software and identify the ones that best represent the experimental behaviour of the ligament.

### Model Geometry:

The study was carried out on the idealised rectangular representation of ligament due to the ease of model development and implementation. The model Rec\_C represented a reasonable representation of the BCs and load applied to the experimental system, however, this setup could not be replicated in the realistic-geometry FE model due to the irregular shape of the ligament

which meant it could not be tied with a straight side-plate. Therefore, the model was adapted to more closely represent how a real irregular shaped ligament could be modelled. This model, Rec\_E had the same geometry as Rec\_A and Rec\_C, but with the addition of a rectangular part, attached to the top region, to replicate the superior-vertebra. A schematic of the model is given in Figure 3.21 (a).

#### **Boundary Conditions and Load Applied:**

A load of 400N, as in previous tests, was applied to the rectangular part representing the vertebral bone via a rigid plate tied to the top surface of the idealised rectangular vertebra. This replicated the load applied to the ligament via the superior-vertebra. The BCs defined on other regions were the same as in the case of Rec\_C. The top plate in this case was restricted to move only in the direction of stretch. The model with boundary conditions and loads is represented in Figure 3.21 (b).

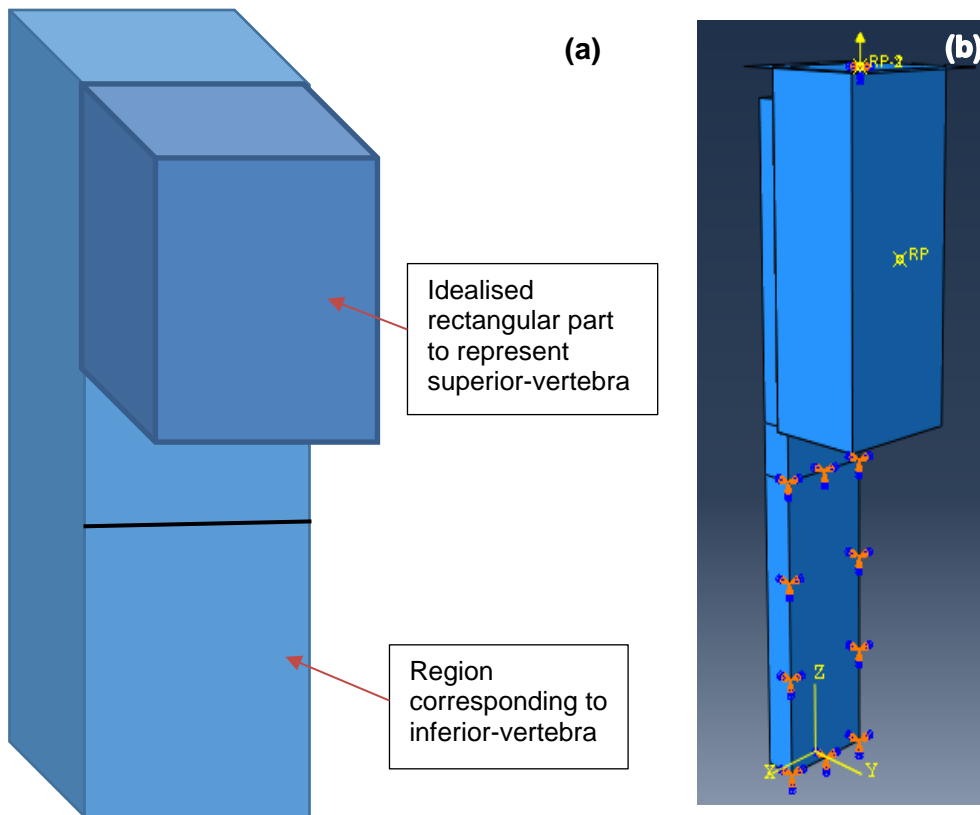
#### **Material Model:**

The idealised vertebra was made near-rigid by assigning it a linear elastic Young's modulus of 400 GPa i.e. 1000 times that of the ligament. This was to make sure that this structure represented the stiffer bone during the stretching of the ligament. A Poisson's ratio of 0.3 was applied to the bone.

The ligament was assigned different material models as described below:

- The linear elastic material model used in previous studies was applied to the ligament geometry in order to make a comparison with previous simplified models.
- The 'non-linear geometry' option in the finite element solver was turned on and the model was re-run to see the effects, if any, that this option had on the outputs. This option is an additional requirement for running hyperelastic or hyperfoam models and is optional for linear elastic models.
- A hyperelastic neo-Hookean model was evaluated because this model has been used previously in finite element modelling of knee ligaments (Chapter 1, Section 1.2.7).
- Two further hyperelastic models (Mooney-Rivlin and Ogden) were evaluated because they have also been shown to be effectively used in the modelling of ligaments (Chapter 1, Section 1.2.7).

- A hyperfoam material model which was shown to have a similar structure and response to the ligament (Chapter 1, Section 1.2.7) was also tested.



**Figure 3.21: (a) Schematic of ligament with idealised rectangular bone to represent superior-vertebra. (b) Rec\_E model with load applied to the reference point on top via a rigid plate and encastre BCs on the inferior vertebra and the restriction of the reference point at the top to move in the directions of the stretch only.**

Within the Abaqus software, the coefficients for both the hyperelastic and hyperfoam models could be determined directly from the input of the test-data in the form of nominal stress and nominal strain. The test data was obtained by using a typical load-extension data set from the experimental results, and the cross-sectional area and length used previously for the construction of the rectangular ligament models such as Rec\_A, assuming the ligament to behave as a uniform and uniaxial structure. This load-extension data was obtained from the same specimen as was used to generate the realistic-geometry model as well as the dimensions for the simple models. A Poisson's ratio of 0.3 was used to define the compressibility in each case.

Using the in-built algorithm within Abaqus, the material parameters for the hyperelastic and hyperfoam models were derived from the input test-data. A curve-fitting algorithm was used to gain the best fit to the inputs. The software outputted the predicted curve for each model alongside the input (test-data)

curve (Figure 3.22). The best-fit curve for each material model and the input experimental curve were then compared to see how accurately the material model could describe the curve based on the coefficients derived by the Abaqus software. The hyperfoam material model behaviour could not be predicted automatically from the input without simulation, because this option is not currently available in Abaqus. Therefore, this material model was directly applied to the FE model and the material parameters used by Abaqus were obtained from the .dat file of the FE model.

### **Implementation of Material Models:**

The material models which were found to closely follow the behaviour of the ligaments (see Figure 3.22) were then applied to the Rec\_E model and the results obtained, in the form of force-displacement behaviour, were compared against the experimental data. To extract this data, the time-displacement values over the reference-node where the load was applied were obtained. The time-displacement curve was converted into a force-displacement curve by multiplying the proportion of the time step by the applied load. The same procedure was repeated for the simulation of FE models with the hyperfoam material behaviour. This provided a means by which to examine if the material parameters could be derived by assuming the experimental data was a uniaxial test on a uniform geometry test-piece, or if the structure and geometry of the ligament meant the uniaxial assumption would be incorrect.

### **Results:**

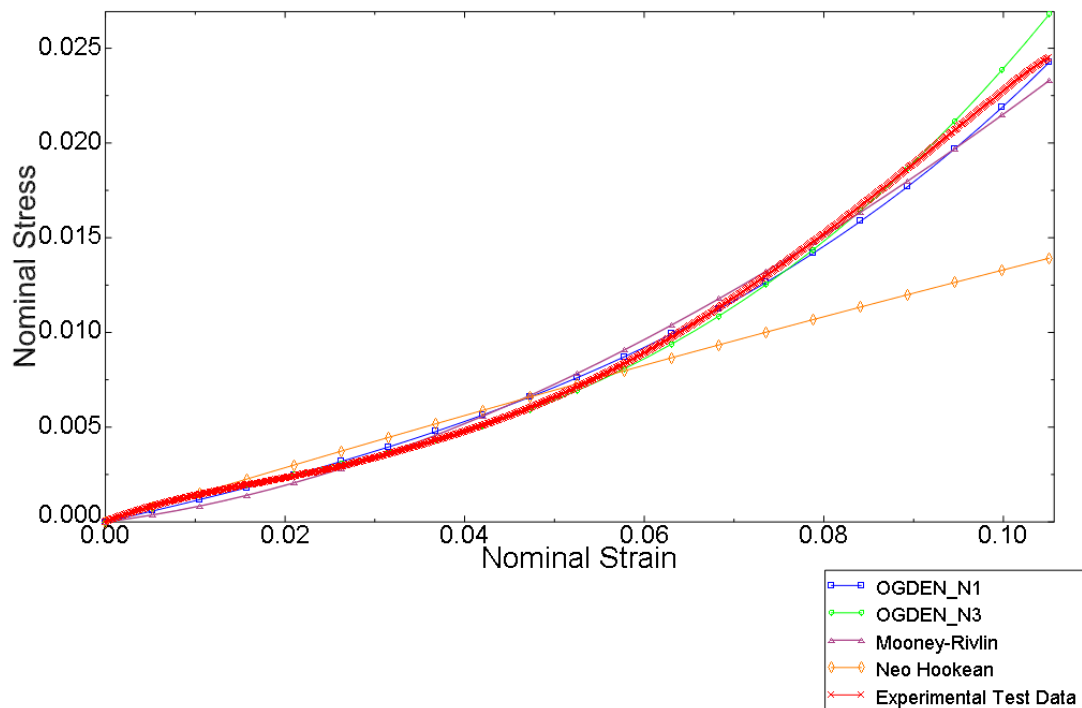
The linear elastic material model was unable to solve when the non-linear geometry option was not selected. The use of non-linear geometry option with the linear elastic model gave similar contours as were observed in the case of the Rec\_C model however, the local strains over the disc region as well as the displacements were higher in this case due to more realistic attachment to the upper vertebra being used.

When the hyperelastic Neo-Hookean model was applied to the experimental test data using the Abaqus curve-fitting algorithm, the resulting stress-strain curve showed similar behaviour to the linear elastic model (Figure 3.22) and did not fit the non-linear behaviour of ligament. Hence, this model was discarded as a potential representative of ligament behaviour.

The curve-fitting of the Mooney-Rivlin model by the Abaqus algorithm showed that it was able to represent the behaviour of ligament loosely (Figure 3.22), however when this material model was applied to the Rec\_E FE model, it did not converge and resulted in errors. Various geometric and meshing options

were examined, but the model was found to be too soft at low loads, causing large strains at very low stresses and excessive element distortion. Therefore, this model could not be used to represent the behaviour of ligament and hence it was also discarded as an option.

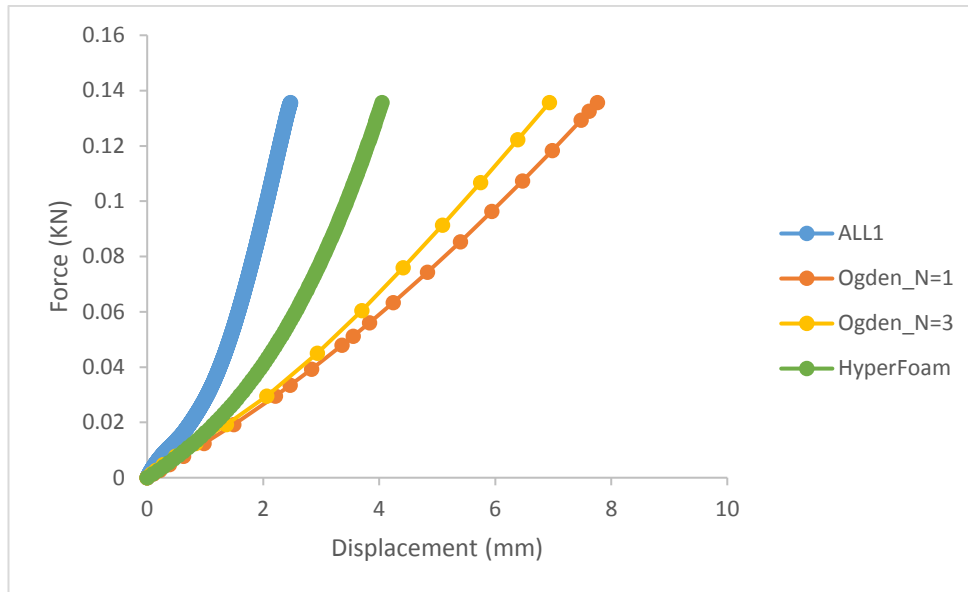
The curve-fitting of the Ogden models (N=1 and N=3) showed that the Ogden (N=3) model represented the behaviour of ligament quite accurately; the Ogden (N=1) model followed a similar characteristic shape but not as closely as Ogden (N=3) (Figure 3.22). The curves of both models had the same characteristic shape as the input but did not match it perfectly.



**Figure 3.22: Curve-fitting of different material models using the Abaqus software applied to data from an experimental specimen (Chapter 2). Both Ogden and Mooney-Rivlin models depicted similar behaviour to the experimental input. Neo Hookean behaved like a linear-elastic material and hence was discarded as an option for modelling the ligament behaviour.**

Using the values obtained through the curve-fitting algorithm in Abaqus and applying them to the Rec-E FE model yielded the force-displacement curves that are presented alongside the experimental force-displacement curve in Figure 3.23. It was found that the models were successful in representing the characteristic shape of the load-displacement curve of the ligament however, the resulting values deviated considerably from the experimental curve used as input data. This difference was attributed to the idealised geometry of ligament used in this study as the model considers a uniform cross-sectional area and length whereas the experimental data is for an irregular shaped ligament.





**Figure 3.23: Comparison of FE force-displacement curves from all material models with the experimental force-displacement curve.**

### **Conclusion:**

This study showed that the Neo Hookean model was unable to represent the non-linear behaviour of the ligament and hence was discarded. Other hyperelastic models i.e. the Mooney-Rivlin and Ogden appeared promising during evaluation as they both depicted the non-linear behaviour of ligaments quite closely. However, the Mooney-Rivlin model was unable to operate at the given stresses and hence was also discarded as an option for modelling the ligament behaviour. Both the Ogden models (N=1 and N=3) and the hyperfoam model resulted in load-displacement curves which matched the overall shape of the ligament curve, however all the FE model resulting values deviated from the experimental values. This was attributed to the non-uniaxial stress state in the FE model, indicating that the realism of the model is an important factor in deriving the material properties. Therefore, further work focussed on FE models with the realistic geometry of the ligament along with the Ogden (N=1 and N=3) and hyperfoam material models.

### **3.6.2 Summary**

From the sensitivity studies, it was identified that the realistic geometry of the ligament is needed, moreover, the level of element density and the most appropriate material models to consider were determined.

### **3.7 Final Methods of FE Modelling**

Based on the outcomes of the sensitivity studies, finite element models of both ALL and PLL were generated to derive the mechanical properties of the ligaments from the experimental data. The model geometry, boundary conditions, applied loads and material models were all chosen such that the resulting model represented the experimental setup as accurately as possible. This section presents the final modelling method for both ALL and PLL.

#### **3.7.1 FE Modelling of the ALL**

From the results of the sensitivity studies, it was found that the ALL model outputs were sensitive to the geometry and boundary conditions and that these should be represented as realistically as possible to give a solution closer to the experimental results.

##### **Model Geometry**

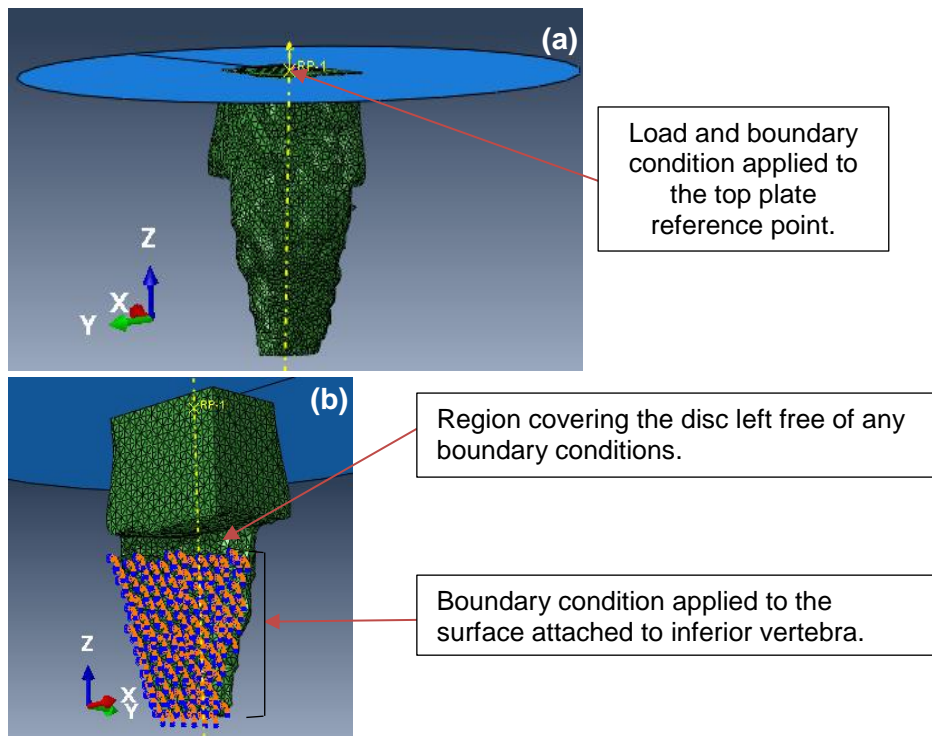
A model of ligament with realistic geometry and with both superior and inferior vertebra attached (Section 3.6.1.1) that resulted from segmentation and meshing was subsequently exported from ScanIP as an .inp file. The inferior vertebra was then removed, leaving the surface definition on the ligament that was attached to this section that could be used for the application of a boundary condition.

##### **Boundary Conditions and Load Applied**

A load of 400N was applied to the superior vertebral section via a rigid plate tied centrally to the top surface of the idealised vertebra. This replicated the load applied to ligament via the stiffer superior vertebra. The surface region representing the area covered by inferior-vertebra was assigned an encastre boundary condition to replicate the attachment, while the middle section which represented the area spanning the disc was left free. The model with boundary conditions and loads are shown in Figure 3.24.

##### **Material Model**

The section of vertebra was given the same material parameters as were used for the idealised vertebra in the previous studies (Section 3.6). For the ALL itself, the material models and their parameters are described in Section 3.8.



**Figure 3.24: shows (a) anterior and (b) posterior view of a realistic ligament (ALL) model in Abaqus with the load and boundary conditions highlighted.**

### 3.7.2 FE Modelling of the PLL

#### Model Geometry:

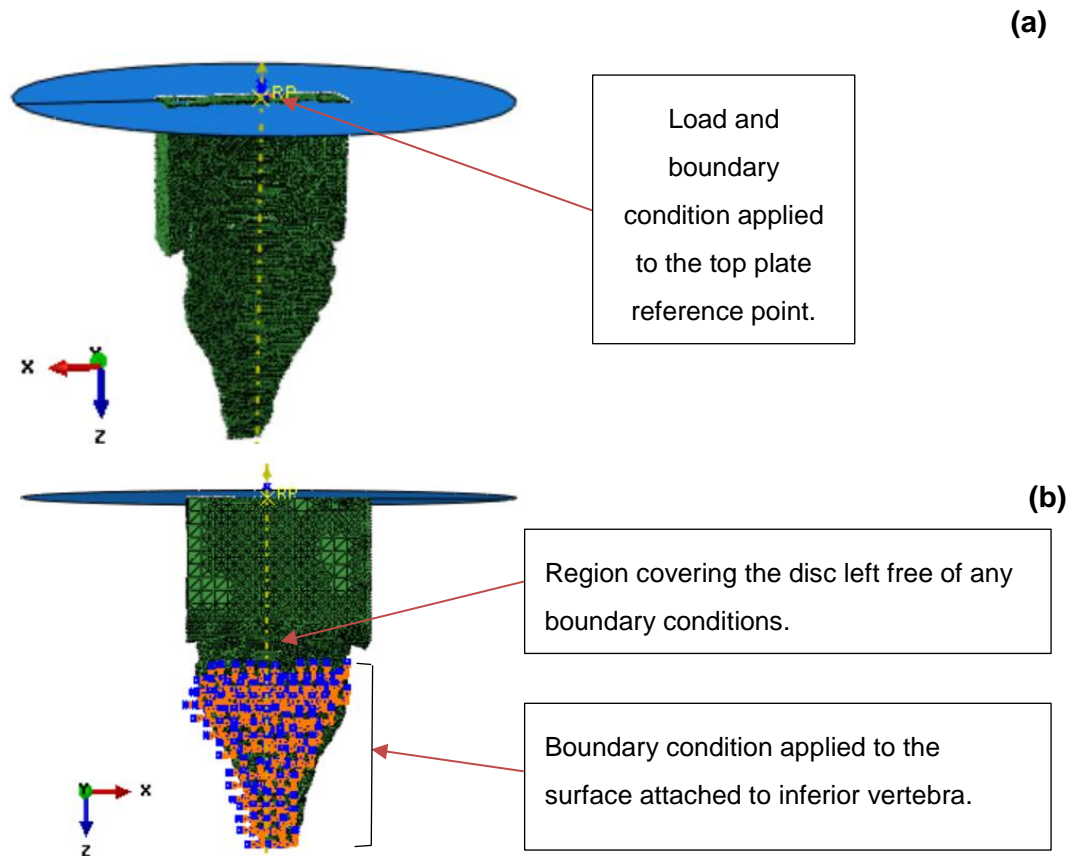
Based on the method developed for FE modelling of the ALL, a model of the PLL was also developed (Figure 3.25) from the images of one of the specimens tested experimentally, with the realistic geometry and with both superior and inferior vertebra attached. The same process was used for segmentation (Section 3.4 and Section 3.5), meshing and subsequent exportation from ScanIP as an .inp file. The inferior vertebra was then removed, leaving the surface definition on the ligament that was attached to this section that could be used for the application of a boundary condition.

#### Boundary Conditions and Load Applied:

Again, a load of 400N was applied to the superior vertebral section via a rigid plate tied centrally to the top surface of the idealised vertebra. This replicated the load applied to ligament via the stiffer superior-vertebra. The surface region representing the area covered by inferior-vertebra was assigned an encastre boundary condition to replicate the attachment, while the middle section which represented the area covered by disc was left free to represent the loose attachment to the disc. The model with boundary conditions and loads is shown in Figure 3.25.

### Material Model:

The section of vertebra was given same material parameters as were used for the idealised vertebra in the previous ALL model. Both the Ogden and hyperfoam models were then applied to this realistic-geometry model using the load-displacement data for the respective specimen recorded experimentally.



**Figure 3.25: (a) Anterior and (b) posterior view of the PLL model in Abaqus with the load and boundary conditions highlighted.**

## 3.8 Initial Results for the ALL Model with Material Data derived by Assuming Uniform Uniaxial Conditions

### Introduction

The ALL model described in Section 3.7.1 was evaluated using the material properties derived using the curve-fitting algorithm in Abaqus assuming a uniaxial test on a uniform test-piece.

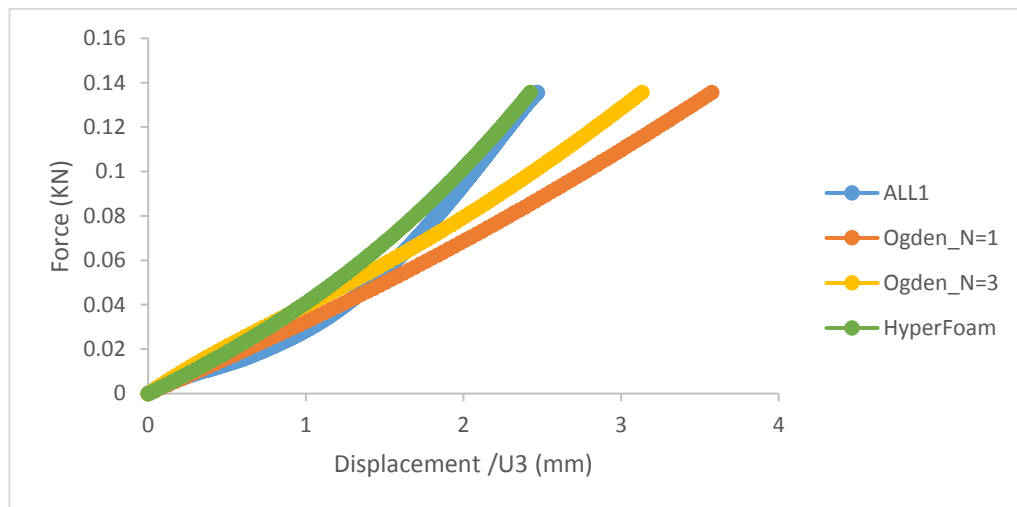
### Methods

The realistic representation of the ALL from Section 3.7.1 was adapted with the material models derived as per the last sensitivity test (Section 3.6.1.4). Both the Ogden (N=1 and N=3) and hyperfoam models were applied in turn to this realistic-geometry model and the resulting behaviour, in the form of the force-

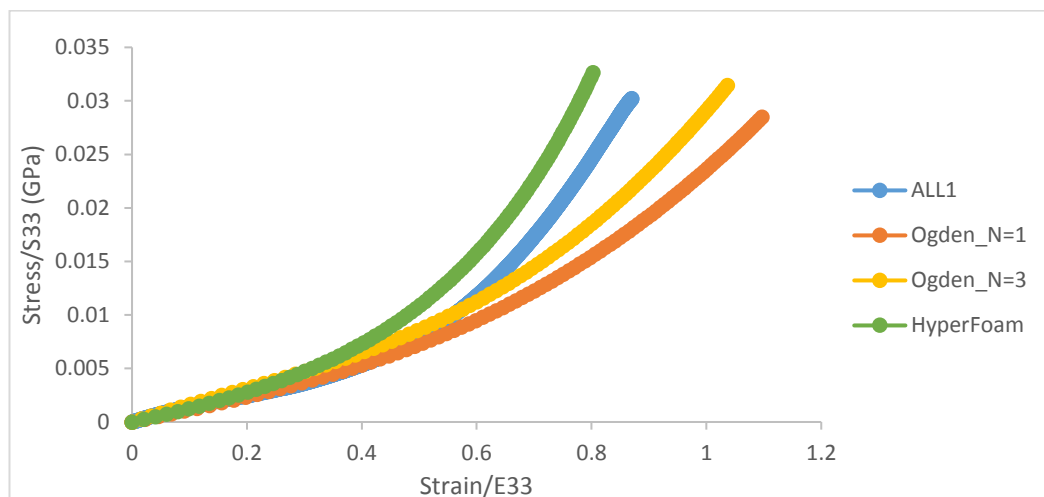
displacement curve, was compared against the corresponding experimental data. The displacement was taken from the reference-node where the load was applied, to most closely match to the experimentally-measured displacement.

## Results

The results obtained in the case of each model, in the form of the overall force-extension plot and a stress-strain plot in the direction of the stretch on an element in the middle of the free region of the ligament (i.e. region covering the disc region) are presented in Figure 3.26 and Figure 3.27.



**Figure 3.26: Comparison between experimental input for a specimen of ALL (ALL1) and FE model results from all three material models in the form of force-displacement curves in the direction of the stretch.**



**Figure 3.27: Comparison between experimental input for a specimen of ALL (ALL1) and FE models results for a single element in the form of stress-strain curves in the direction of the stretch. The stress-strain curves were obtained from the same element in all three models located on the surface of the middle section the ligament i.e. the section covering the disc region.**

The material parameters obtained by the in-built curve fitting algorithm in Abaqus for all three material models for a given force-displacement data as input are presented in Table 3.8.

**Table 3.8: Material coefficient values obtained for the various material models used for modelling ALL.**

Material model	Ogden (N=1)			Ogden (N=3)			hyperfoam		
Material Coefficients	$\mu$ (GPa)	$\alpha$	D (GPa <sup>-1</sup> )	$\mu$ (GPa)	$\alpha$	D (GPa <sup>-1</sup> )	$\mu$ (GPa)	A	v
N = 1	0.00375	4.22	245	-0.599	1.17	161	0.00407	4.07	0.3
N = 2				0.288	1.73	0			
N = 3				0.316	0.55	0			

**Discussion:**

The resulting curves from applying the different material models all had the characteristic shape but did not match the exact values of the experimental data, as was observed in the case of Rec\_E. This was attributed to the fact that the experimental data used as input i.e. nominal stress and nominal strain were derived using a uniform nominal mean cross-sectional area and mean length, whereas the realistic ligament geometry used for this model has a non-uniform cross sectional area.

**Conclusion:**

It was found that deriving the material properties from assumed uniaxial stress-strain behaviour and then applying these back into a more realistic model did not give results that matched the experiment, it is clear that the only way to derive the properties would be to 'reverse engineer' them from the models, hence, this will be discussed in more detail in Section 3.9.

### 3.9 Method of Tuning the Material Properties

The aim of this study was to devise a method of optimising the material coefficients in order to find values of material coefficients that accurately represent the behaviour of individual ligaments. The method was first devised using an ALL specimen, but such that it could be consistently applied to any force-displacement data set obtained for any specimen of ALL or PLL.

The material model parameters computed by Abaqus initially for each material model were iteratively changed until a best fit to the corresponding experimental load-displacement data was found. This procedure was only

applied to Ogden (N=1) and hyperfoam material models. The Ogden (N=3) required nine different material coefficients, which meant it would not have been possible to determine unique values using the manual method devised.

### 3.9.1 Theoretical Considerations

This aim of this section is to show how the varying material parameters are expected, theoretically, to affect the load-displacement curve. The procedure is presented firstly using Ogden (N=1) as an example.

The initial shear modulus ( $\mu_0$ ) and the initial bulk modulus ( $K_0$ ) for hyperelastic material are related to each other via Equation 3.2 (Hollenstein, 2008), which relates them to the Poisson's ratio ( $\nu$ ). Equation 3.2 was combined with the other form of initial bulk modulus given in Table 1.11 for the Ogden material to derive Equation 3.3. Since the initial shear modulus is also shown to be directly related to the material coefficient  $\mu$  (Table 1.11), therefore, Equation 3.3 can be re-written generally in terms of the material coefficients for the Ogden model (Eq. 3.4). This gives a direct relationship between the two coefficients ( $\mu$  and  $D$ ). Hence, the coefficients  $D$  and  $\mu$  are directly related to the compressibility of the material and changing either one will (automatically) inversely change the other one. Therefore, only the effect of variation of  $\mu$  and  $\alpha$  is considered in this section.

$$K_0 = \frac{2\mu_0(1+\nu)}{3(1-2\nu)} \quad [\text{eq. 3.2}]$$

$$\Rightarrow \mu_0 = \frac{3(1-2\nu)}{D(1+\nu)} \quad [\text{eq. 3.3}]$$

$$\Rightarrow \mu = \frac{3(1-2\nu)}{D(1+\nu)} \quad [\text{eq. 3.4}]$$

Where,

$\nu$  = Poisson's ratio, which was assumed to be 0.3

In order to directly examine the role of  $\alpha$  and  $\mu$  and determine the effects of varying either, the strain energy density functions were used to derive a function relating stress and strain for a simple 1D case. A further assumption of incompressibility was made here in order to reduce the complexity of the equations for this 1D example. The adaptation of strain energy density function for Ogden (N=1) (Chapter 1, Table 1.11), i.e.  $i=1$ , is given as:

$$U = \frac{2\mu}{\alpha^2} (\bar{\lambda}_1^\alpha + \bar{\lambda}_2^\alpha + \bar{\lambda}_3^\alpha - 3) + \frac{1}{D} (J - 1)$$

Where,  $\bar{\lambda}_i$  are the modified principal stretches related to the principal stretch as;  $\bar{\lambda}_i = \lambda_i \cdot J^{-\frac{1}{3}}$ .

For the 1D case, only  $\lambda_i = \lambda$  is relevant. Also for an incompressible material we have,  $\lambda_2 = \lambda_3 = \frac{1}{\sqrt{\lambda}}$ . Since  $J = \lambda_1 \lambda_2 \lambda_3 = 1$ ;

$$\Rightarrow U = \frac{2\mu}{\alpha^2} \left( \lambda^\alpha + 2\lambda^{-\frac{\alpha}{2}} - 3 \right)$$

The second Piola Kirchoff stretch i.e. stress (S) in 1D case is given by;

$$S = \frac{\partial U}{\partial E} = \frac{\partial U}{\partial \lambda} \frac{\partial \lambda}{\partial E}$$

Where, E = Green Lagrange deformation i.e. strain and is related to stretch in 1D case as;

$$\begin{aligned} E &= \frac{1}{2}(\lambda^2 - 1) \\ \Rightarrow \frac{\partial E}{\partial \lambda} &= \lambda \quad \text{and} \quad \lambda = (2E + 1)^{\frac{1}{2}} \\ \Rightarrow S &= \frac{\partial U}{\partial E} = \frac{\partial U}{\partial \lambda} \frac{\partial \lambda}{\partial E} = \frac{\partial U}{\partial \lambda} \frac{1}{\lambda} \\ &= \frac{2\mu}{\alpha} \left( \lambda^{\alpha-1} - \lambda^{-\frac{\alpha}{2}-1} \right) \frac{1}{\lambda} \\ &= \frac{2\mu}{\alpha} \left( \lambda^{\alpha-2} - \lambda^{-\frac{\alpha}{2}-2} \right) \\ &= \frac{2\mu}{\alpha} \left[ ((2E + 1)^{\frac{1}{2}})^{\alpha-2} - ((2E + 1)^{\frac{1}{2}})^{-\frac{\alpha}{2}-2} \right] \\ \Rightarrow S &= \frac{2\mu}{\alpha} \left[ (2E + 1)^{\frac{\alpha-2}{2}} - (2E + 1)^{-\frac{\alpha}{4}-1} \right] \quad [\text{eq. 3.5}] \end{aligned}$$

Where,

S and E are the stress and strain, respectively.  $\frac{2\mu}{\alpha}$  is related to the gradient of the curve whereas  $\left(\frac{\alpha-1}{2}\right)$  and  $\left(-\frac{\alpha}{4} - 1\right)$  are the exponents. It is noted that the second (subtracted) exponential term in Equation 3.5 gets smaller as alpha increases, so only the first term can be considered. This shows that  $\mu$  will alter the gradient by a uniform amount throughout, whereas alpha as an exponent will have greater effects at higher strains. This is explored in further detail in the next section with realistic values of mu and alpha.

Similarly, for the hyperfoam model, the material coefficient 'β' is completely defined by the Poisson's ratio which was kept the same for all models.

Moreover, the strain energy density function for the hyperfoam model for a simple 1D case and an incompressible material will be the same as derived above for Ogden (N=1) model, so will result in the same stress and strain function. Therefore, the effect of variation of material parameters  $\mu$  and  $\alpha$  would be the same as presented above for Ogden (N=1) model.

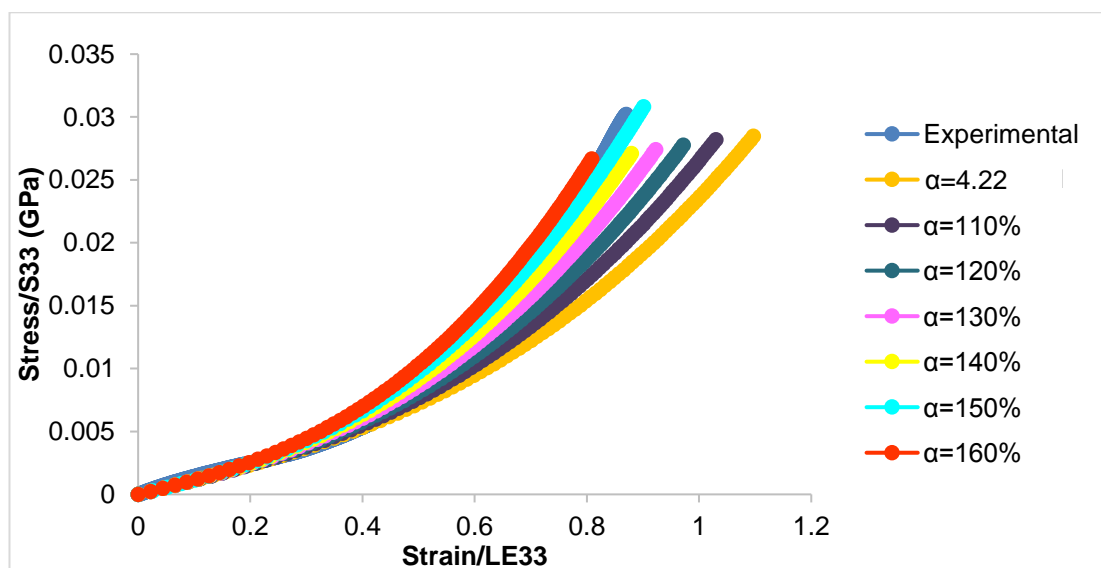


### 3.9.2 Effect of Varying Input Parameters

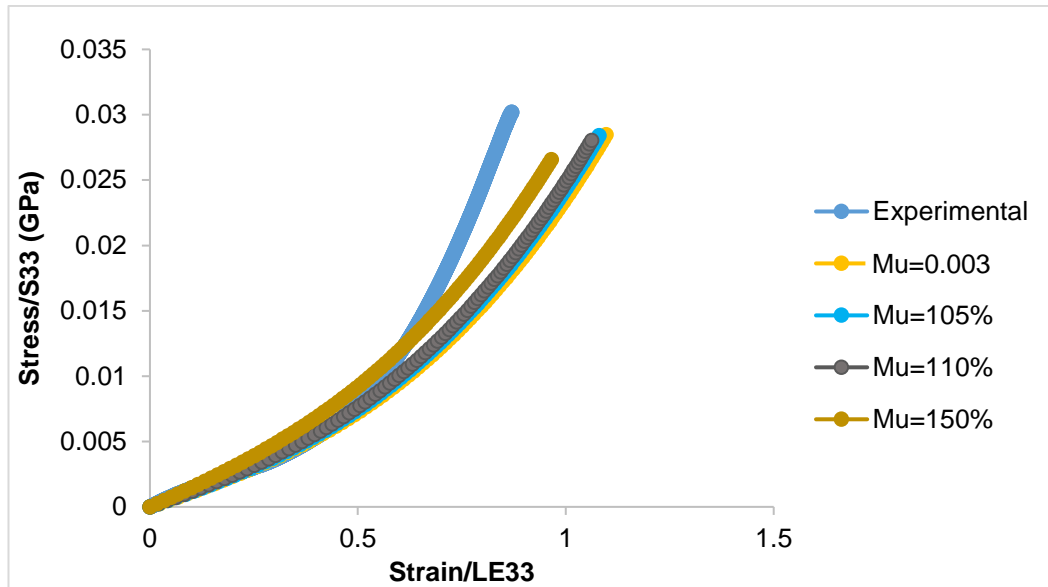
The aim of this study was to examine how variations in the input parameters affect the outputs. The material coefficients initially computed by the curve-fitting routine in Abaqus (see Table 3.8) were individually varied, in turn, while keeping the rest of the coefficients at the original values to determine the effect on the outputs. The results were plotted in terms of stress/strain on the same element each time.

Firstly, for Ogden ( $N=1$ ),  $\alpha$  was increased in increments of 10% from its original value and the results were plotted. Since the coefficients  $D$  and  $\mu$  are related as described previously (Section 3.9.1), therefore,  $\mu$  was then varied to determine its effect on the overall behaviour of the curve, and  $D$  was calculated accordingly using Equation 3.4.

The results obtained from this initial variation of material coefficients on the overall shape of force-displacement curve are presented in Figure 3.28 and Figure 3.29. The results showed that  $\alpha$  controls the amount of curvature i.e. the shape of the curve, causing differences in the gradient at the higher strains, while  $\mu$  rotates the curve around the origin, i.e. it has an effect on the gradient throughout the whole curve, as expected (see Section 3.9.1).



**Figure 3.28: Comparison between the experimental input and FE model results with the variation of  $\alpha$  in increments of 10% from its original value of 4.22.**

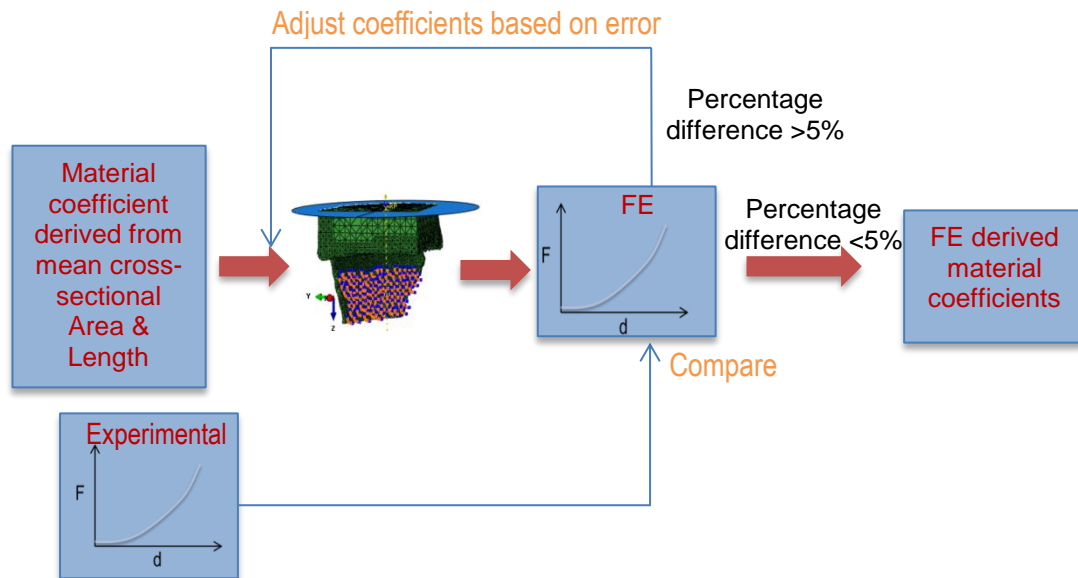


**Figure 3.29: Comparison between the experimental input and FE model results with the variation of  $\mu$  from its original value of 0.00375 GPa.**

It is important to note that different experimental curves result in different material parameters as the parameters are derived from the experimental input data. So any change in experimental curve will be reflected in the values of material parameters. Also the parameters have greater effect on different parts of the curves so if there is change in the values of overall curve then the material parameters will all be altered.

### 3.9.3 Parameter Tuning Methods

A flow chart of the procedure for material parameters tuning is presented in Figure 3.30. The same procedure was followed for both Ogden ( $N=1$ ) and hyperfoam model however, the material parameters for both models were different, therefore the chosen order of the parameter tuning for each material model was also different. The method was developed using a model of an ALL specimen as an example and was later applied to a model of a PLL specimen.

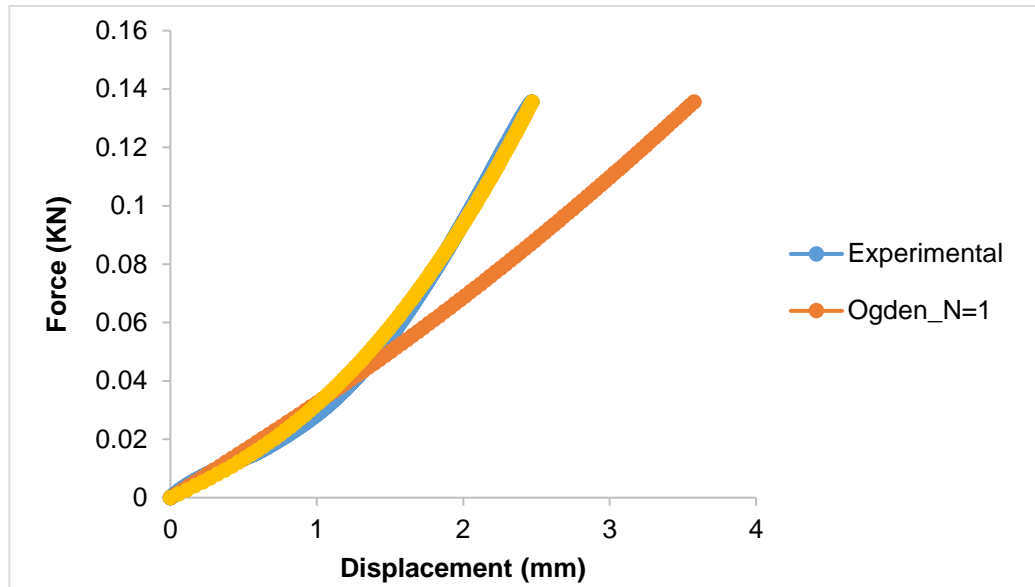


**Figure 3.30: Flowchart describing the general process for material tuning.**

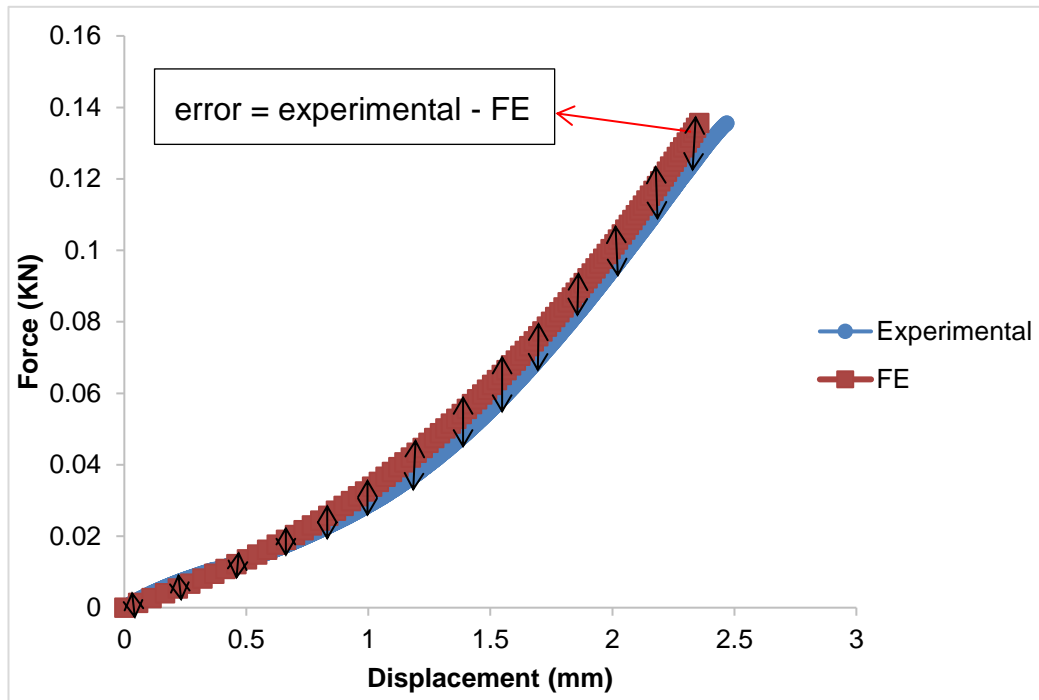
*Material Tuning for Ogden (N=1):*

As described in flowchart (Figure 3.30), the material coefficients initially computed by Abaqus (see Table 3.8) were used as a first 'guess'. By observing the difference between the original FE curve (i.e. Ogden\_N=1 curve) and the experimental curve (see Figure 3.26), it was evident that the curvature needed to be increased while giving lower stress values in the initial toe region of the curve, therefore an increase in  $\alpha$  but a decrease in  $\mu$  would give a solution closer to the original experimental curve. However, changing  $\mu$  would change  $D$ , as described in Section 3.9.1. Therefore, each time a new value of  $\mu$  was implemented, a corresponding  $D$  value was computed and updated. This procedure of tuning the material behaviour was evaluated in the form of load-displacement curves to make a like-with-like comparison with original load-displacement curve used as an input to the model.

Several different combinations of  $\mu$  and  $\alpha$  were tried and the ones for which the resulting computational (FE) curve visually appeared closer to the experimental curve (Figure 3.31) were quantified to decide on the one with least difference between both curves. This quantification involved resampling the FE curve to match its displacement values to the experimental curve and then finding the relative mean percentage difference between both (Figure 3.32 and Eq. 3.6). This was implemented via a custom written Matlab script (Matlab (R2014a)).



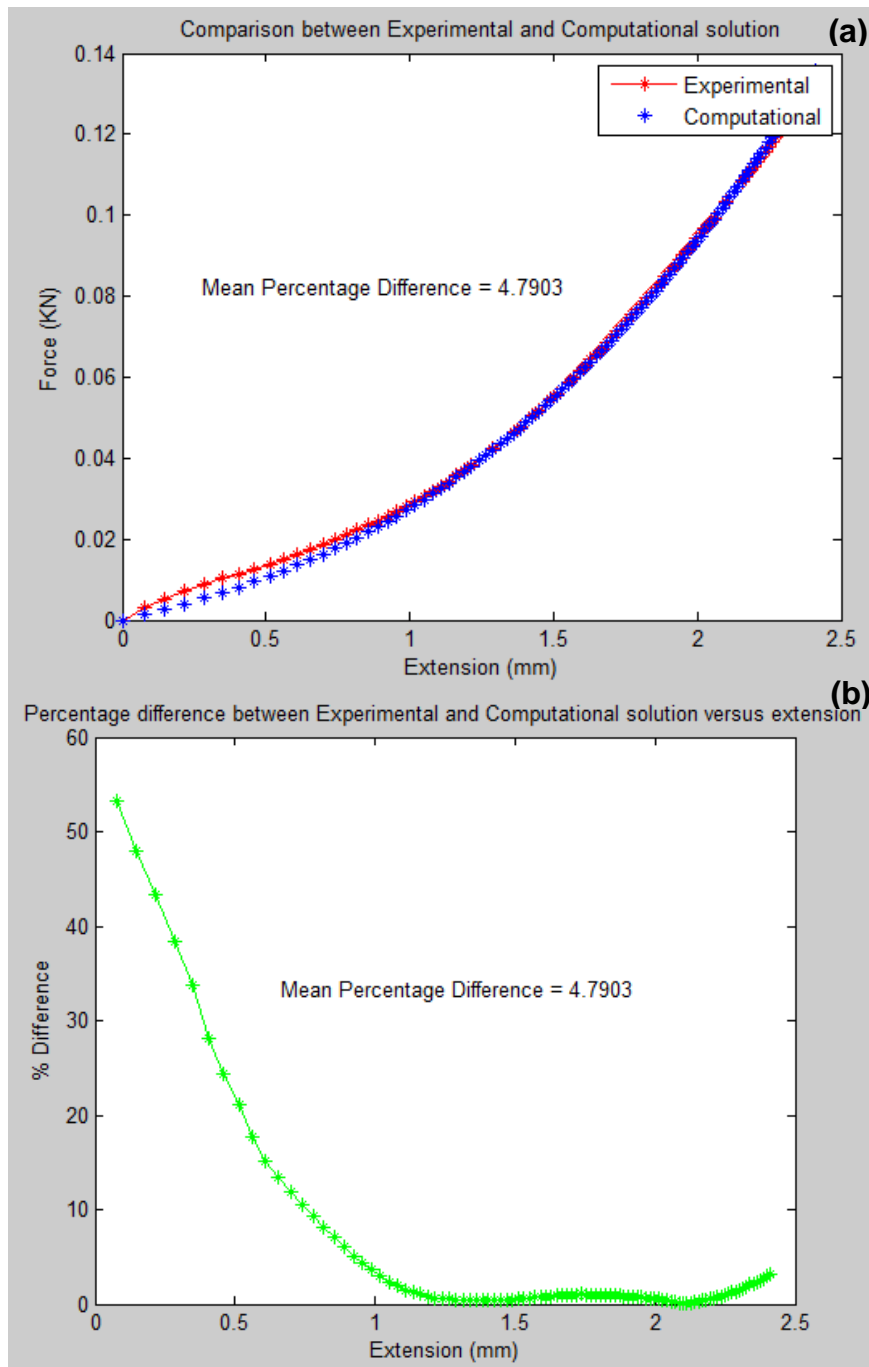
**Figure 3.31: The visually-best-matched force-displacement curve for Ogden (N=1) material tuning for the ALL model.**



**Figure 3.32: The method of finding the error between experimental input and FE output.**

$$\text{Mean difference (\%)} = \frac{\sum \left( \frac{|\text{error}|}{\text{experimental}} \right)}{n} * 100\% \quad [\text{eq. 3.6}]$$

The process of material tuning was implemented until the difference between the input and the output became less than 5%. An example of plots of input and closest matched output with mean percentage difference, obtained from Matlab are given in Figure 3.33.



**Figure 3.33: (a) example of plots obtained from matlab comparing the input and closest matched output along with (b) a plot of mean percentage difference between inputs and outputs for a model of ALL.**

*Material Tuning for the hyperfoam model:*

For the hyperfoam model, the material coefficient ' $\beta$ ' did not need to be tuned as it is completely defined by the same Poisson's ratio as described previously. Therefore, only  $\mu$  and  $\alpha$  were tuned in order to find a solution that best matched the experimental inputs. Both  $\mu$  and  $\alpha$  had similar effects on the behaviour of material model as was observed for both in the case of Ogden ( $N=1$ ). But since

$\mu$  is not dependent on  $D$  in the hyperfoam material tuning, both  $\mu$  and  $\alpha$  were varied until a best matched solution with a mean percentage difference of less than 5% was obtained.

### **3.9.4 Parameter Tuning Results**

This method of material tuning to optimise the material coefficients was then applied to the specimen of PLL (Figure 3.34) and the coefficients obtained were compared with the ALL material coefficients (Table 3.9). This shows that the method of specimen-specific modelling with material tuning developed on a specimen of ALL can be applied to other ligaments in order to derive the material coefficients representing the material behaviour.

Results show that the  $\mu$  value for the specimen of ALL was very similar between the Ogden and hyperfoam material models, whereas it was over twice as high in the Ogden model compared to the hyperfoam model for the specimen of PLL. However, the  $\alpha$  value for the Ogden material model was higher in both cases as compared to the hyperfoam material model. The value of  $\mu$  was an order of magnitude higher for the ALL than the PLL for both material models whereas  $\alpha$  was an order of magnitude lower.

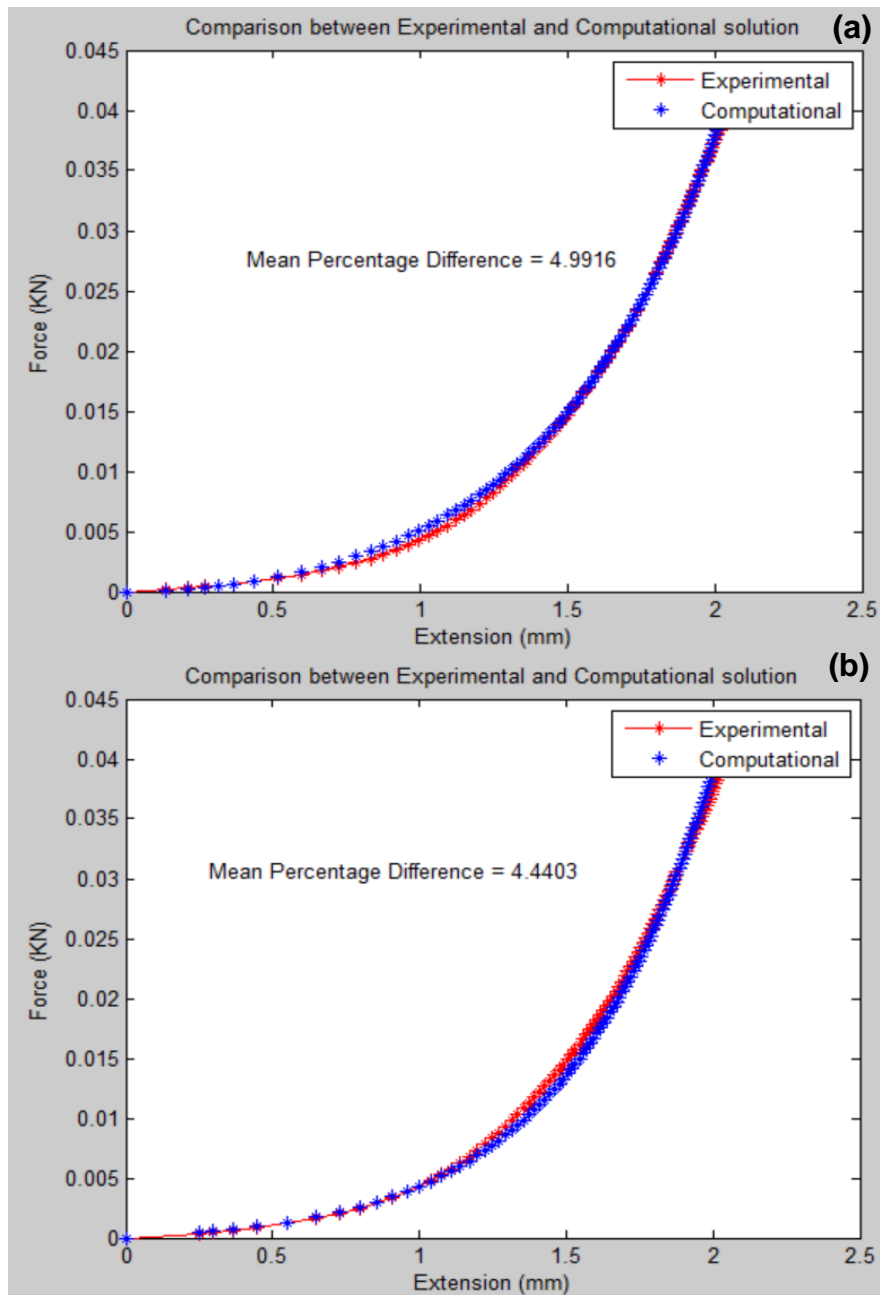


Figure 3.34: Plots obtained from matlab comparing the input and closest matched output for PLL, stating the mean percentage difference for (a) Ogden (N=1) and (b) hyperfoam material models.

Table 3.9: The final material coefficients obtained as a result of material tuning.

Material model	Ogden (N=1)			hyperfoam	
	$\mu$ (GPa)	$\alpha$	D (GPa <sup>-1</sup> )	$\mu$ (GPa)	$\alpha$
ALL	0.00263	8.23	351	0.00264	5.29
PLL	0.000227	46.4	4066	0.000620	10.6

### 3.10 Discussion

The aim of this chapter was to present the procedures that were used to develop a methodology for modelling the ovine spinal ligaments computationally. The methodology developed will be applied to human tissue in Chapter 4 in order to characterise the material properties of human spinal ligaments.

Firstly, a methodology for scanning the ligaments using  $\mu$ CT was developed, since the visualisation of soft tissue structures is always a challenging aspect of soft tissue imaging. This involved the use of NaI gel that was painted over the surface of the ligaments and then wiped off before scanning the FSU using  $\mu$ CT. The gel increased the visibility of the ligaments and made it easier for their subsequent segmentation in ScanIP. A study was carried out in order to find the concentration of gel that would help differentiate the ligaments from the background and bone. Four different concentrations were prepared and tested and the one that gave the optimum result such that it made ligaments appear brighter than the background but keeping them darker than the bone was selected as the optimum option for further scanning.

The gel made the ligaments distinguishable from the vertebral bone and the background, however, it was still hard to make a clear distinction between ligament and disc as they both have very similar structure and absorbance to x-rays in the scanned images. For this reason, two short studies were performed to determine if the thickness of the ligament in the disc region could be derived from the thickness in the bone region, in order to segment the ligaments accordingly. It was found that the thickness of ligament over both regions was very similar, hence the thickness over the disc region was assumed to be the same as the thickness measured over the vertebral regions for the purpose of segmentation and further analysis. The methods employed were not perfect but the similarity in thickness between regions was within the measurement error. If the ligament had a simple rectangular shape, one could estimate the difference in outcome from these measurement errors using the approximate proportions. However in reality, this is difficult to achieve because the ligament has an irregular shape. Moreover, the irregular shape of the ligament has been shown to play an important role in its mechanical performance (Section 3.6.1.1). Hence, it was difficult to assess in detail what effect any error in thickness, due to the local shape, would have on the results.

The segmentation of the bone was a straightforward process. However the segmentation of the ligaments was more challenging and was achieved via a combination of automated and manual segmentation. The procedure for



segmentation of the ligament was developed such that it was least time-consuming and easily transferrable to other specimens and different types of ligaments.

Four different sensitivity studies were carried out in order to understand how various modelling aspects affected the overall behaviour of the FE model. These aspects included dimensions, boundary conditions, mesh size and choice of material model. It was found that the behaviour of the ligaments in the modelled loading regime is sensitive to the geometry used, hence a simplified geometry could not be used to derive the material properties of the ligament, emphasising the importance of modelling the irregular shape of the ligament as accurately as possible. The study to test the effect of changing the boundary conditions from simplified to more realistic ones showed that the application of realistic boundary conditions are required to represent the true behaviour of ligament. Increasing the mesh size was shown to increase the accuracy of solution however an optimum mesh size was chosen that reduced the computational cost without compromising much on accuracy. The final chosen mesh is likely to give a displacement within 5% of the converged value. The convergence testing was only undertaken for displacement since this is the only parameter of interest in this study.

Both the Ogden models (N=1 and N=3) and the hyperfoam model were found to give the load-displacement curves with the same characteristic shape as the input load-displacement curve of the respective ligament. However even after tuning the material constants to fit the experimental stress-strain data, the resulting output behaviour deviated from the experimental input data. This was attributed to the uniform mean-cross sectional area and length used to derive the stress-strain data as an input to the model. The uniform geometric parameters did not represent the irregular shape of the ligament accurately which was reflected in the derived material parameters for each respective model, hence the discrepancies between inputs and outputs. In order to determine the material parameters that accurately represented the true behaviour of ligament, an iterative method was devised to optimise the material parameters. The iterative approach was first developed on the ALL and was later applied successfully to the PLL to not only obtain the material parameters for the PLL but also to show that the approach is transferrable to other ligaments.

In terms of material parameters, while the material models used are phenomenological and not based on the physical behaviour at the microstructural level, the results suggest that  $\mu$  would account more for the un-

crimping of the collagen (i.e. the toe region behaviour) and  $\alpha$  for the stretching of the relatively straightened out collagen fibres (i.e. on the more linear region at higher strains) (Section 3.9.1 and Section 3.9.2). If the  $\mu$  value is higher, this means that the material is stiffer in the toe-region as compared to the material with low  $\mu$ . Similarly, if the  $\alpha$  value is higher, this means that the material is stiffer in the linear-region as compared to the material with a low  $\alpha$  value. It is important to note that this stiffness is relative and care needs to be taken in comparing between material parameters ( $\mu$ ,  $\alpha$ ) and stiffness values ( $k_1$ ,  $k_2$ ), since the former are measures of the material itself and the latter take into account the dimensions as well. A comparison of material parameters between ALL and PLL showed that  $\mu$  for both Ogden ( $N=1$ ) and hyperfoam model is an order of magnitude lower for the PLL than the ALL whereas  $\alpha$  is higher for PLL in both cases. This implies that the ALL tissue is stiffer than the PLL tissue in the toe region whereas PLL tissue is stiffer in the linear region. Therefore the differences in the behaviour of the whole ligaments is not just due to their different geometries, but due to differences in the material properties themselves.

If the experimental bi-linear stiffness,  $k_1$  and  $k_2$ , for the same specimens (specimen 1:T2-3 for ALL and specimen 1:T4-5 for PLL) is considered (Chapter 2, Table 2.2 and Table 2.3), it can be seen that for the ALL ( $k_1 = 30$ ,  $k_2 = 82$ ), the ligament is stiffer but there is less of a difference between  $k_1$  and  $k_2$  than for the PLL ( $k_1 = 4$ ,  $k_2 = 41$ ), so one would expect that for the ALL,  $\mu$  would be higher (giving a higher initial gradient), but the exponent would be lower since there is not much change from  $k_1$  to  $k_2$ . Whereas for the PLL, the exponent must be higher as there is a bigger change from  $k_1$  to  $k_2$  as compared to ALL. This is exactly what is observed for  $\mu$  and  $\alpha$  for the ALL and PLL. It also shows that the use of a linear elastic model defined by either the toe-region or the linear region of the load-displacement curve would poorly reflect the complete behaviour. Because only one sample was modelled for each ligament, it is possible that what is observed is not a trend seen more universally with these ligaments, but a characteristic of that particular ligament sample, so this should be taken into account in interpreting the results.

A secondary aim of the study on varying input parameters (Section 3.9.2) was to gauge how sensitive the  $\mu$  and  $\alpha$  values obtained were to the experimental data. The curves in Figure 3.28 and Figure 3.29 show that a 10% change in  $\mu$  does not greatly affect the curve, but a 50% change has an impact, whereas for  $\alpha$ , a 20% change is quite considerable. This shows that changes of 20-50% in  $\alpha$  or  $\mu$  substantially change the curve, whereas the  $\alpha$  and  $\mu$  values between the ALL and PLL specimens were an order of magnitude different, so the author

can be confident that the differences in  $\alpha$  and  $\mu$  between the two specimens was not just due to experimental error.

In conclusion, the methods reported in this chapter were developed such that the processes could be used for specimen-specific modelling of the longitudinal ligaments on any specimen. The methodology developed in this chapter was applied to human tissue (as reported in Chapter 4) and the results obtained were then compared with the ovine tissue (Chapter 5).

## **Chapter 4**

### **Application of Experimental & Computational Methods to Human Longitudinal Ligaments**

#### **4.1 Introduction**

This chapter presents the adaptation and application of the methodologies developed in Chapter 2 and Chapter 3 to human ligaments to determine their properties. The first section presents the experimental methodology adapted to dissect and test human specimens, as well as the computational procedures adapted to model the ALL and PLL and evaluate their material properties. The second section presents the results obtained and a visual comparison with the ovine ligament tissue; a comparison with the literature on human data is also discussed.

#### **4.2 Methodology**

The methodology for dissection, testing and subsequent computational modelling of human tissue was adapted from Chapter 2 and Chapter 3. Thoracic sections of three frozen human cadaver spines were obtained with ethical approval (NHS National Research Ethics Service REC reference 15/YH/0096). Sections from T2-T11 were used for testing. The T1 and T12 vertebrae were not included due to their importance in other studies involving cervicothoracic and thoracolumbar junctions.

##### **4.2.1 Magnetic Resonance Imaging**

In order to characterise the soft tissues within the spinal segments more effectively prior to testing, an additional step was undertaken to image the specimens using magnetic resonance imaging (MRI).

Briefly, MRI employs strong magnetic fields and radio waves to produce images based on the behaviour of protons within hydrogen atoms. The axis about which each proton spins lines up in the same direction under a magnetic field. The radio waves are transmitted in short bursts to knock the protons out of alignment. The protons realign when the radio waves are turned off, sending out radio signals which are then picked up by the receiver. The protons belonging to different types of tissue realign at different speeds and hence produce distinct signals. These signals are combined to create images of the different tissues within that particular part of the body. Since MRI relies on

water content, soft tissues such as ligaments can be better visualised and differentiated, than under X-ray based systems such as CT where there is poor contrast between soft tissues. However, the image quality relies heavily on the sequence used, as well as the positioning of the specimen and additional coils, which requires experience and expertise.

The spine sections were defrosted and scanned under MRI prior to dissection and subsequent testing. The MR imaging was undertaken by Dr V. Nagitha Wijayathunga at the NIHR Leeds Musculoskeletal Biomedical Research Unit in a Siemens Magnetom Verio 3T scanner using a 2D-TSE-Sag-IW (2-dimensional turbo spin echo sagittal intermediate weight) sequence (TR = 3520 ms, TE = 12 ms).

#### **4.2.2 Dissection**

During dissection, visual inspection of the tissue was carried out in order to choose the specimens with least damage and assess the level of degeneration. A visual comparison with the ovine tissue was also made. Fifteen anterior sections of the FSUs were obtained from the three spines with seven specimens selected for testing the ALL and seven for the PLL. An initial examination of the spines showed visible damage in the anterior section with many cuts in the ALL. Also, anterior ossification of the discs was evident in certain regions resulting in it being impossible to test the ALL in these sections. Therefore, the specimens were always first evaluated for the feasibility of ALL testing, if not, they were assigned for testing the PLL. The specimens are listed in Table 4.1 according to the level of the spine and the ligament each specimen was tested for.

#### **4.2.3 Specimen preparation and testing**

The specimens were prepared and tested using the protocols described previously. Briefly, the specimens were potted (Chapter 2, Section 2.3.3) and scanned using  $\mu$ CT (Chapter 3, Section 3.2), then mechanically tested using the methodology described in Chapter 2, Section 2.4.3. The load-displacement curves obtained were cropped and bilinear stiffness values were obtained using the data analysis methods described in Chapter 2, Section 2.5.

**Table 4.1: List of specimens according to the level of the spine and the ligament tested alongside the gender and age for each donor.**

Spine	Gender, Age (yrs.)	Level	Ligament Tested
1	F, 90	T2-T3	<b>ALL</b>
		T4-T5	<b>ALL</b>
		T6-T7	<b>PLL</b> – cuts all across ALL
		T8-T9	<b>Discarded</b> – tested for PLL but a hole was made in error in the PLL while slicing through the disc
		T10-T11	<b>PLL</b> - the ALL was damaged with a big cut across the ALL over the disc region
2	M,86	T2-T3	<b>ALL</b>
		T4-T5	<b>ALL</b>
		T6-T7	<b>PLL</b> – cuts all across ALL
		T8-T9	<b>ALL</b>
		T10-T11	<b>PLL</b> – cuts all across ALL
3	M,83	T2-T3	<b>PLL</b> – cuts all across ALL
		T4-T5	<b>ALL</b>
		T6-T7	<b>ALL</b>
		T8-T9	<b>PLL</b> – cuts all across ALL
		T10-T11	<b>PLL</b> – visible ossification on right anterior side of the disc

#### 4.2.4 Computational Modelling

The  $\mu$ CT image data was used to segment and build FE models of all specimens in ScanIP and Abaqus respectively as described in Chapter 3, Section 3.4. The same process was followed as previously (Figure 3.30) with initial values for the material models derived by assuming the ligament was a uniaxial structure using a mean cross-sectional area and length obtained from ScanIP and using the in-built parameter-fitting algorithm in Abaqus (see Chapter 3, Section 3.8). This resulted in the initial values for the material

parameters for each respective specimen for both the Ogden and hyperfoam models used previously. The values were then iterated until the FE force-displacement curves best fitted the experimental data (see Chapter 3, Section 3.9.3). This was undertaken for both material models (Ogden and hyperfoam) for each ligament in order to obtain the parameters that best described the behaviour of the respective ligament. The parameters were considered optimised when the percentage errors (Equation 3.6) between experimental input and FE output reduced to 5% or less. The parameters were compared between the two material models used, within and across different spines.

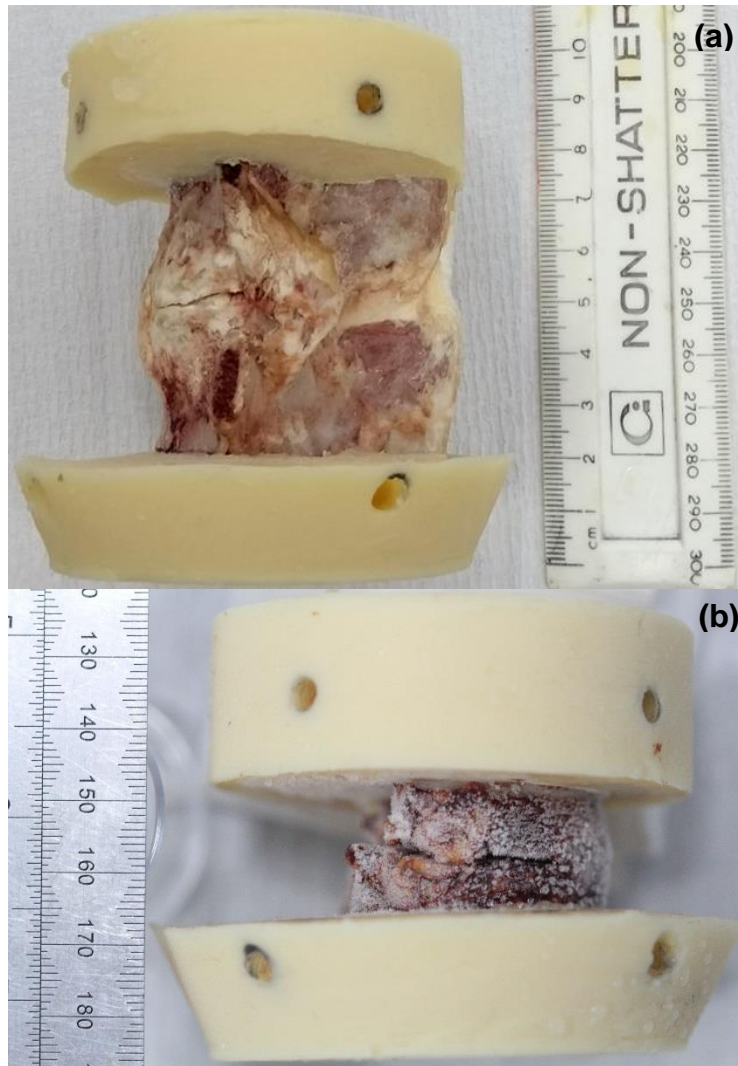
This process resulted in the generation of fourteen specimen-specific FE models. Each of these models was optimised for both the Ogden and the hyperfoam material models, each requiring 10-12 iterations to reach the required match to the experiment.

## **4.3 Results**

### **4.3.1 Comparison of Human and Ovine Thoracic Spine**

Visual examination of the human tissue revealed the similarities and differences between it and the ovine spine in terms of anatomy and level of degeneration. Both species were found to have very similar structures in terms of bony structures and ligament anatomy. The main difference observed was in the size, colour and general state of the tissues (Figure 4.1). The ovine FSUs were found to be almost double in height to that of the human FSUs. The main height difference was seen in the vertebrae, however human discs were also found to be thinner than the ovine discs. Slicing through the ovine discs presented white shiny annulus fibres that visually appeared healthy and hydrated (Figure 4.2(a)), whereas in case of human, the discs appeared dull and yellow-brown in colour (Figure 4.2 (b)), a characteristic of old discs due to the extra cross-links formed by the reaction between collagens and glucose (Adams & Roughley, 2006; DeGroot, et al., 2004). These extra cross-links have been shown to inhibit repair in old discs (Roughley, 2004) and probably leads to reduced tissue strength (Adams & Roughley, 2006). The ALL and PLL both appeared intact, hydrated and shinier in the ovine specimens whereas human ones appeared somewhat degenerated, dull and dehydrated. The PLL in the human specimens was found to be thinner than the ovine PLL, generally about half the thickness, whereas the ALL in the human specimens was found to be wider than the ovine (Figure 4.3 and 4.4). The ovine ALL had a thick but narrow band of fibres in the middle with very thin fibres spanning the anterior aspect of the FSU, whereas in the human specimens the middle thick band covered most

of the anterior aspect of the spine. The ovine ligaments were of a distinct whitish colour which was easier to distinguish from the bone and one could clearly draw a distinct boundary for all the thick and thin fibres. In contrast, with the human ligaments, it was hard to draw a clear boundary and the colour was more of a brown/red nature which was hard to distinguish from the bone and the surrounding muscles.



**Figure 4.1: Examples of the ovine (a) and human (b) cemented FSU illustrating the difference in height (cm).**



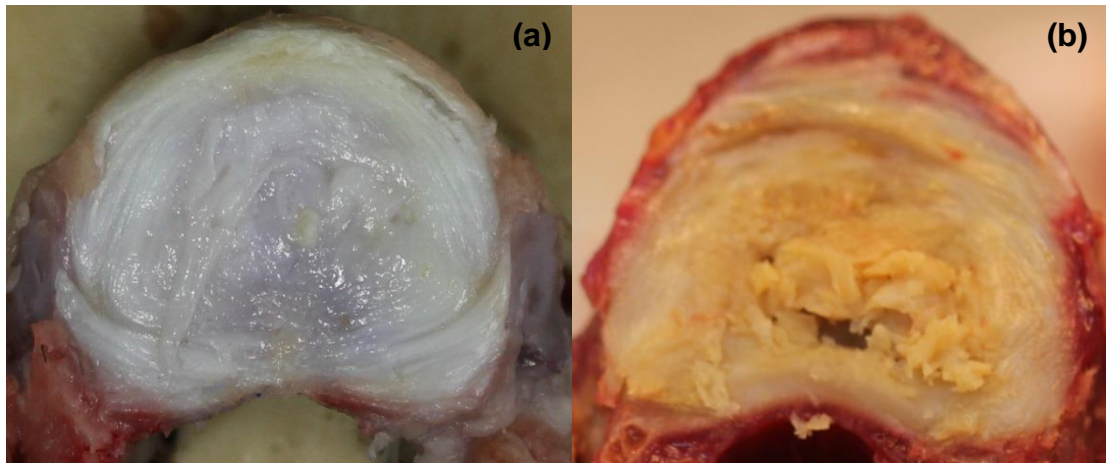


Figure 4.2: Examples of the (a) ovine and (b) human disc illustrating the difference in colour and appearance.

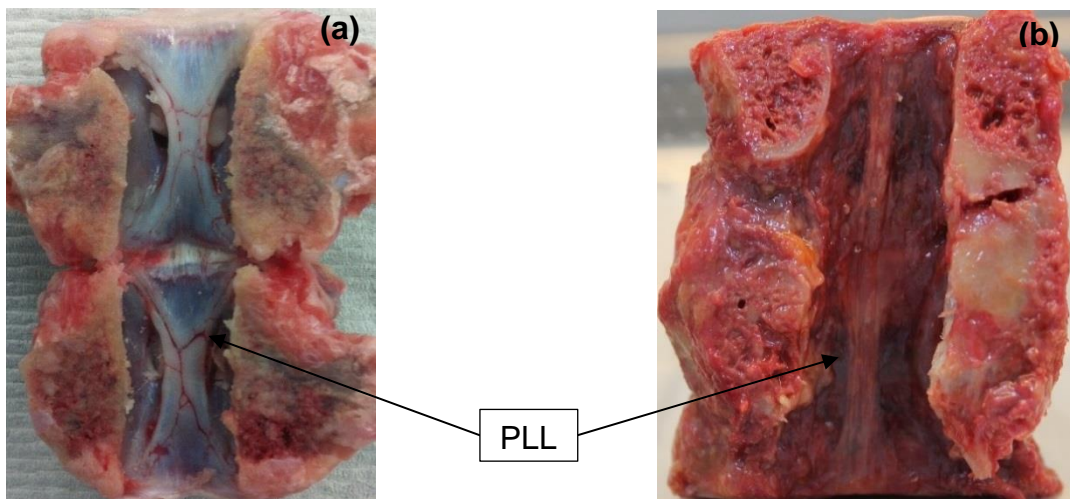


Figure 4.3: Photographs of the anterior spine following dissection through the spinal canal showing the differences in the appearance of the (a) ovine and (b) human PLL.

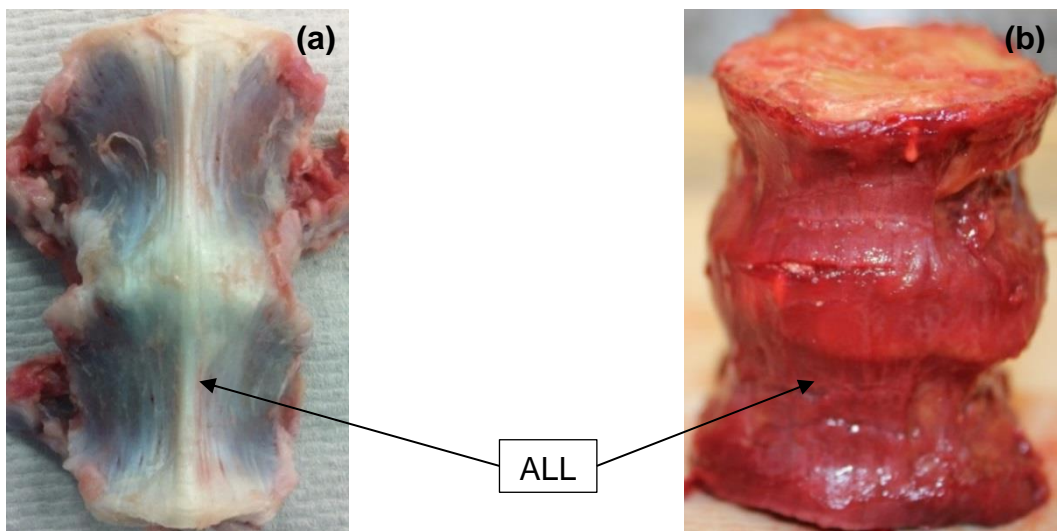
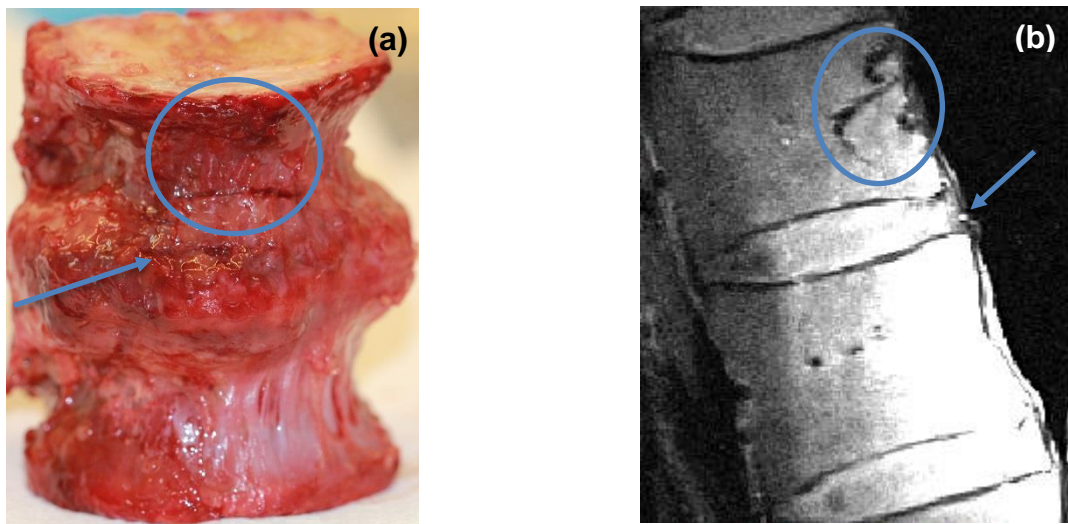


Figure 4.4: Photographs of the anterior spine showing differences in the appearance of (a) ovine and (b) human ALL.

### 4.3.2 Visual Observations, MRI and Photographic Images

Certain features were observed in the FSUs which might have an effect on the behaviour and the properties of the ligaments. Some of the features which were observed during inspection were also evident on the MRI. There were also certain features which were seen on the MRI which could not be observed by visual inspection alone, such as the protrusion of bones and discs which leads to the stretching of the ligaments and could have an effect on their mechanical behaviour. The following section describes the features observed alongside the relevant photographic and MR images.

As described previously (Section 4.2.2), the ALL in all three spines had cuts in various places which made a number of specimens unsuitable to be tested for the ALL. These cuts could also be visualised in the MRI images (Figure 4.5).

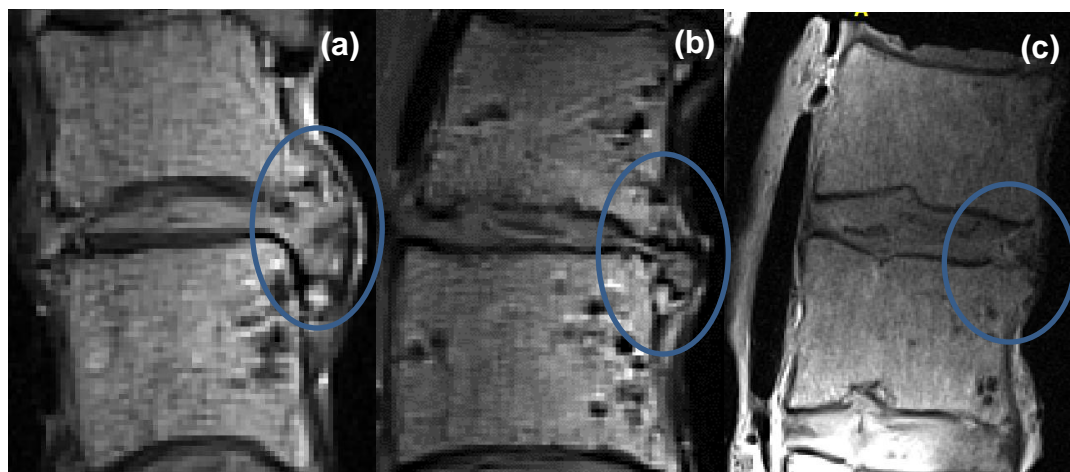
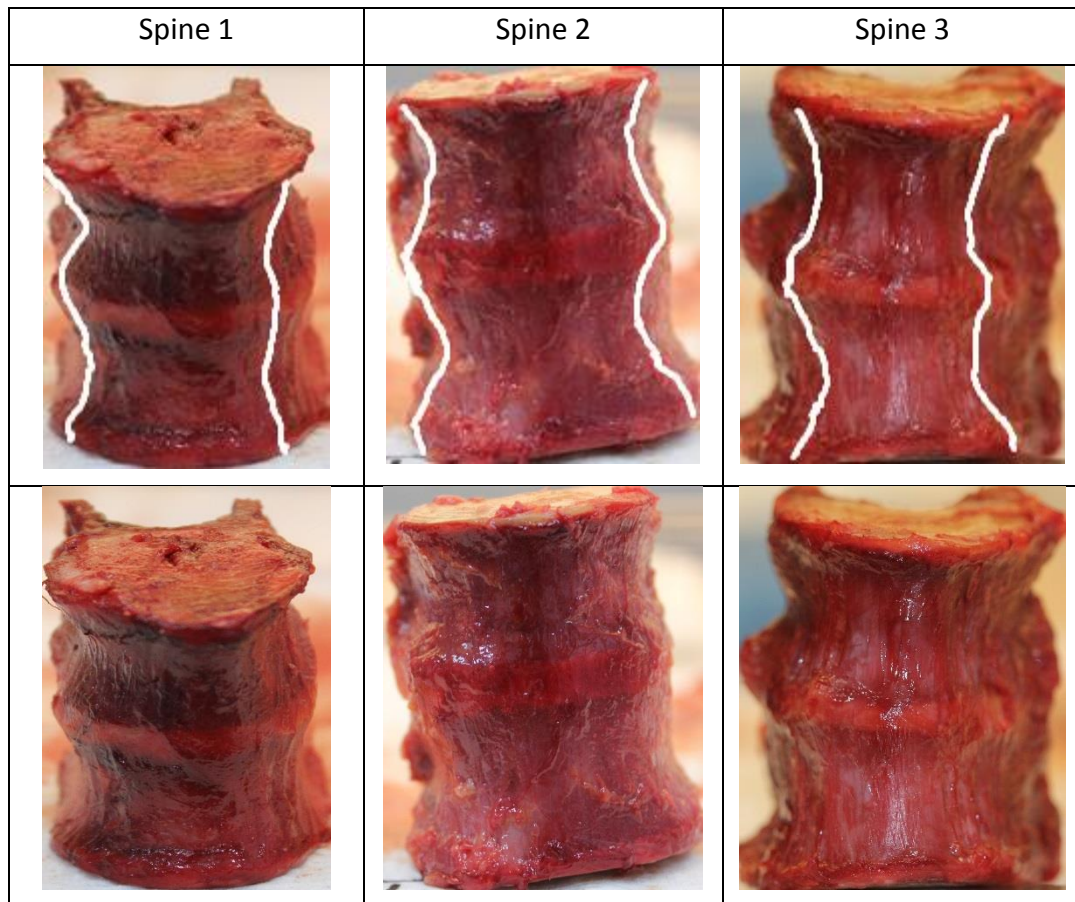


**Figure 4.5: Comparison of (a) photographic (anterior view) and (b) MRI image (sagittal view) showing the damage to the specimen (circled area) as well as cuts in the ALL (superimposed arrows) for a specimen (2:T10-11) chosen to be tested for the PLL.**

The ALL in Spine 1 appeared thinner than the other two spines; for Spine 3 it appeared the thickest (Table 4.2). This is evident in the table with the vascular network showing through the thinner ALL in the Spine 1 specimen. This might have implications on the behaviour of the ALL related to these spines.

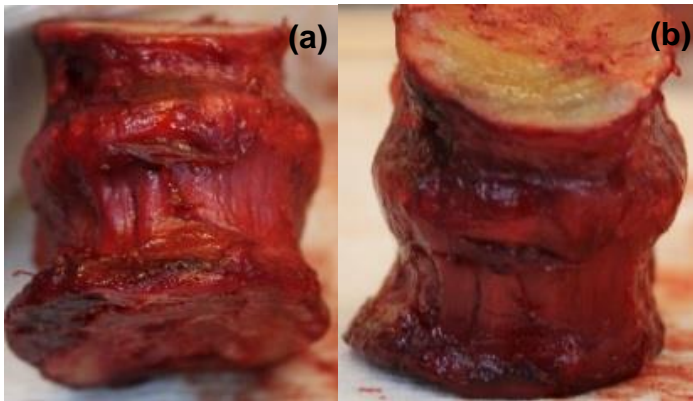
The MRI images for three specimens of Spine 1 i.e. 1:T2-3 (Figure 4.6 (a)), 1:T4-5 (Figure 4.6 (b)) and 1:T10-11 (Figure 4.6 (c)) showed disc and bony protrusions on MRI. This probably causes stretching in the ligaments and might have an effect on their mechanical behaviour. Spine 1:T10-11 also had cuts in the ALL with ossification visible on the right anterior side of the of the spine, significant in the disc region. The PLL appeared to be very thin and withered.

**Table 4.2: Differences in the thickness of the ALL across the three spines with white lines drawn over the images of specimens (row 1) to highlight the edges of the ligament while the unaltered images are presented in 2<sup>nd</sup> row showing that Spine 3 have the thickest and Spine 1 the thinnest ALL.**



**Figure 4.6: Sagittal view of three specimens of Spine 1 showing bone and disc protrusion in specimen (a) T2-3 and (b) T4-5 leading to stretching of the ALL, and specimen (c) T10-11 showing the fusion of disc and bone on the anterior side as a result of ossification.**

Bone compression was also observed in Spine 1:T6-7 (Figure 4.7) which led to the shortening of the vertebrae on the anterior side, and possible loosening of the ALL as well as stretching of the PLL.

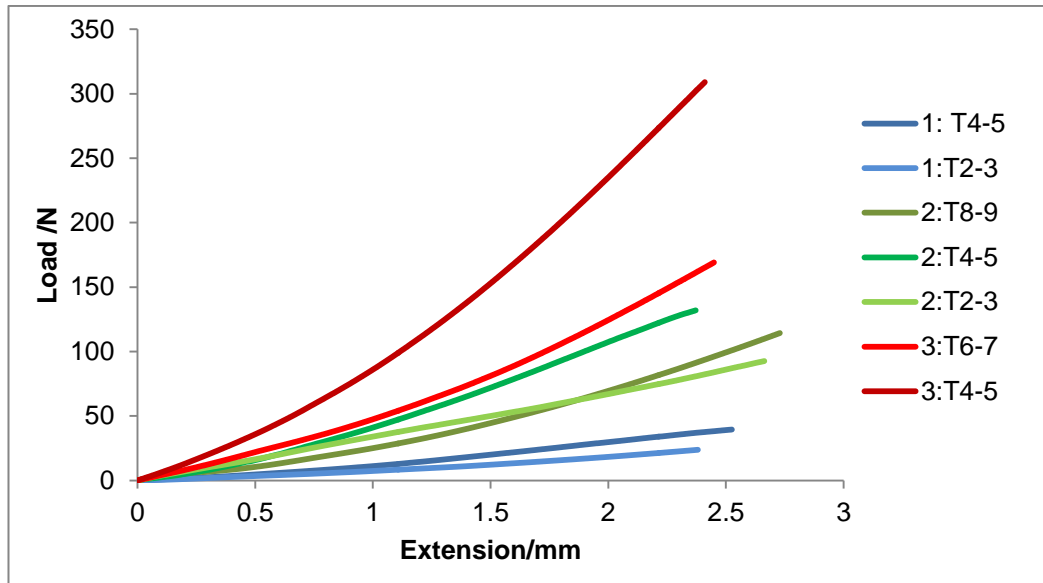


**Figure 4.7: (a) Anterior and (b) top-anterior view of the FSU (Spine 1:T6-7) showing bone compression leading to disc protrusion and bony infusion with the disc.**

### 4.3.3 Mechanical Testing

The load-displacement data obtained for each specimen was processed as described in Chapter 2, Section 2.5 and the results for the ALL and PLL were plotted separately (Figure 4.8 and Figure 4.9). It can be seen that all the curves followed the same basic shape but there was a large difference in gradients.

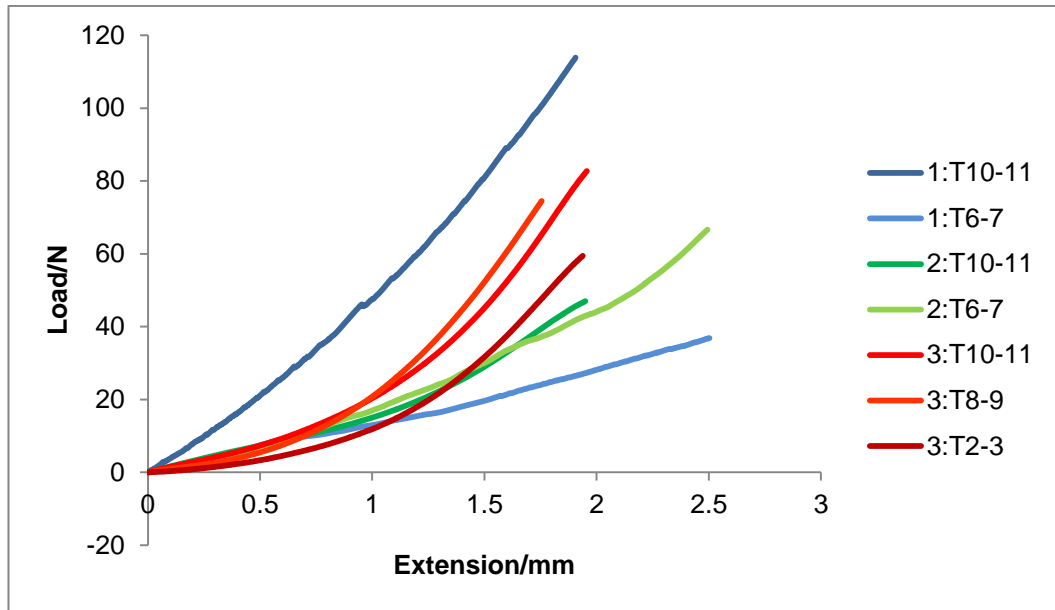
In order to make a comparison across different specimens, mean bilinear stiffness values for all the specimens were calculated using the data analysis method described in Chapter 2, Section 2.5. This gave the initial 'toe region' ( $k_1$ ) and final 'linear region' ( $k_2$ ) values, which are presented in Table 4.3 and Table 4.4 respectively. There was a lot of variability evident in both the toe region and the linear region across the different specimens of both ligaments. For the ALL, all the specimens belonging to the same spine had similar gradients i.e. the slopes are closer together for each spine, however no clear trends were seen for the PLL specimens. The inconsistency between spines and within specimens could be due to geometric as well as material variability which will be further explored in the next section. A further comparison of the  $k_2$  values with the stiffness values cited in the literature for human spinal ligaments is presented in Section 4.4.



**Figure 4.8: Post-processed load-displacement slopes for all the seven human specimens tested for ALL.**

**Table 4.3: The ‘toe region’ (k1) and ‘linear region’ (k2) stiffness values calculated by fitting least squares slopes to the post-processed load displacement curves of the ALL specimens. The level and the spine the specimen was obtained from are indicated in the specimen name.**

Specimen	Stiffness values for ALL (N/mm)	
	k1	k2
1: T2-3	7	13
1: T4-5	10	19
2: T2-3	34	39
2: T4-5	34	67
2: T8-9	25	55
3: T4-5	80	161
3: T6-7	47	88
<b>Mean ± S.D.</b>	<b>34 ± 25</b>	<b>63 ± 51</b>



**Figure 4.9: Post-processed load-displacement slopes for all the seven human specimens tested for PLL.**

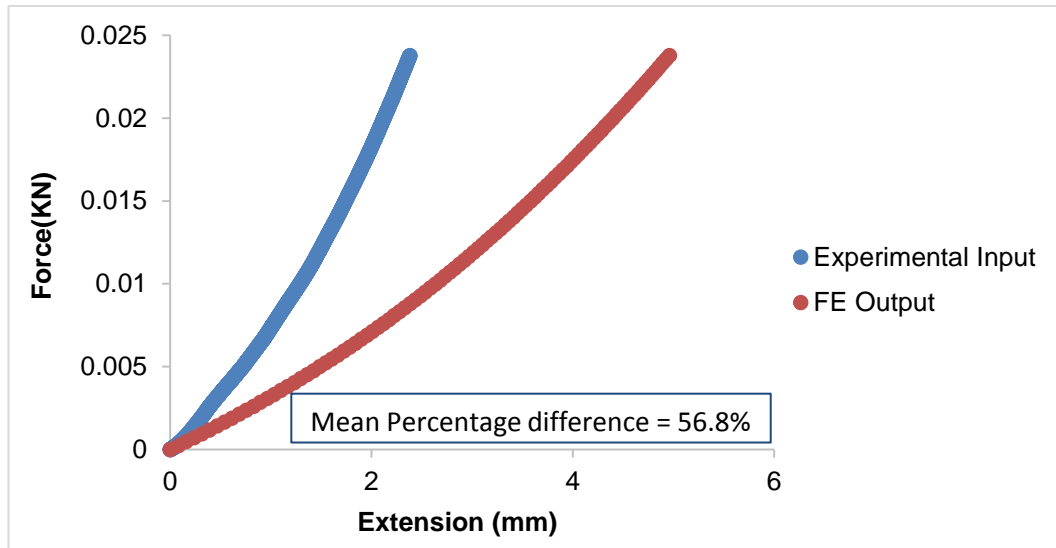
**Table 4.4: The ‘toe region’ (k1) and ‘linear region’ (k2) stiffness values calculated by fitting least squares slopes to the post-processed load displacement curves of the PLL. The level and the spine the specimen was obtained from are indicated in the specimen name.**

Specimen	Stiffness values for PLL (N/mm)	
	k1	k2
1: T6-7	13	17
1: T10-11	45	72
2: T6-7	16	31
2: T10-11	15	38
3: T2-3	10	55
3: T8-9	14	68
3: T10-11	19	71
<b>Mean ± S.D.</b>	<b>19 ± 12</b>	<b>50 ± 22</b>

### **4.3.4 FE modelling and material parameter tuning**

#### **4.3.4.1 Results using material property data derived under assumptions of uni-axial stress and uniform geometry**

A total of 14 specimen-specific FE models were generated to represent each of the experimental specimens. Ogden (N=1) and hyperfoam material models were fitted to the load-displacement data for each ligament using the curve-fitting algorithm in Abaqus. As explained in Chapter 3, these curve-fitting algorithms are based on the assumption of a uni-axial stress field and use the mean cross-sectional area and length. These derived material parameters for each specimen (i.e. prior to any further parameter optimisation) were then used as initial values for the material constants in the specimen-specific FE models of each FSU, and each model was then solved. An example of the resulting FE-predicted load-displacement curve is shown in Figure 4.10. This output data was then compared with the corresponding experimental force-displacement data that was used to derive the material parameter inputs for the respective ligament. The comparison was computed as percentage difference between the experimental input and FE output following the procedure described in Chapter 3, Section 3.9.3, and the results presented in Table 4.5. Again, it was seen that there were large errors between the experimental and FE data, following the same outcome as for the ovine specimens presented in Chapter 3. This showed that, as with the ovine specimens, the assumptions used for the derivation of the material properties in Abaqus (i.e. uniform cross-section and length, and a uniaxial applied stress (Chapter 3, Section 3.8) were also incorrect for the human specimens.



**Figure 4.10: An example of a comparison between the experimental input and resulting FE predicted force-extension behaviour using the Ogden material model for specimen 1:T2-3. The FE material parameters were determined using a mean cross-sectional area and length under the assumption of a uniaxial stress. The disparity in the resulting curves demonstrates that these assumptions were incorrect.**

**Table 4.5: Percentage difference between experimental input and specimen-specific FE-output using material parameters derived by the in-built Abaqus calibration code assuming mean cross-sectional area and length for all the specimens of ALL and PLL.**

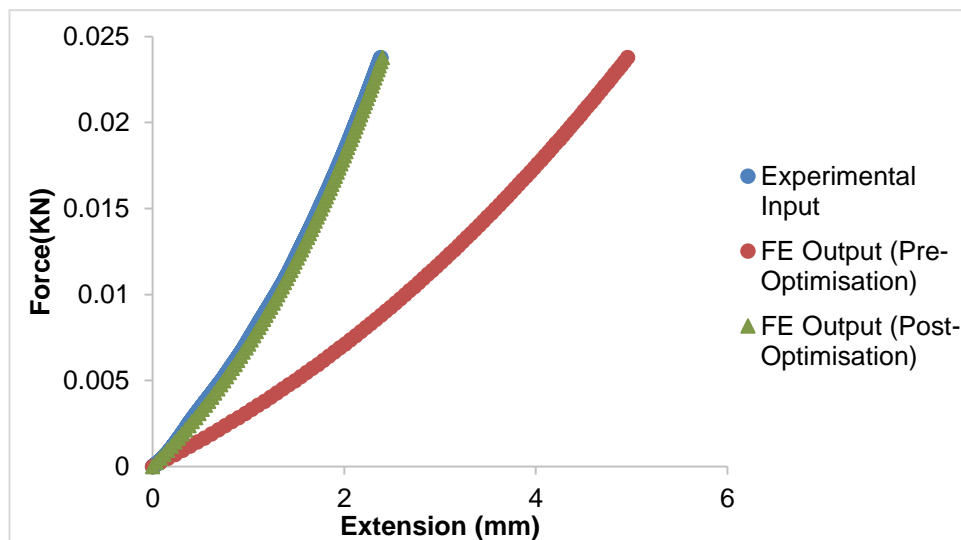
Specimen		Percentage Difference (%)	
		Ogden (N =1)	Hyperfoam
ALL	1: T2-3	56.8	45.7
	1: T4-5	35.4	12.9
	2: T2-3	36.8	19.5
	2: T4-5	56.5	36.5
	2: T8-9	15.5	20.1
	3: T4-5	73.1	65.7
	3: T6-7	97.9	49.2
PLL	1: T6-T7	8.5	3.3
	1: T10-T11	9.3	16.3
	2: T6-T7	28.5	12.2
	2: T10-T11	45.0	31.6
	3: T2-T3	64.1	34.4
	3: T8-T9	35.4	34.5
	3: T10-T11	47.2	29.2



#### 4.3.4.2 Results following material property calibration

The material parameters were then calibrated to obtain values that produced the best fit of the specimen-specific FE model output to the corresponding experimental curve as described in Section 4.2.3. The example shown in Figure 4.10 is presented again in Figure 4.11 with the addition of the final post-optimised FE slope derived from the FE model to illustrate the effect of the material calibration.

This procedure was applied to each of the specimen-specific models, in each case iterating the parameters to gain the best fit to the respective experimental data. The optimised parameters for both ALL and PLL are tabulated in Table 4.6.



**Figure 4.11: An example of a comparison of experimental input with pre-optimised and post-optimised FE outputs illustrating the effect of material calibration on Ogden material model for specimen 1:T2-3.**

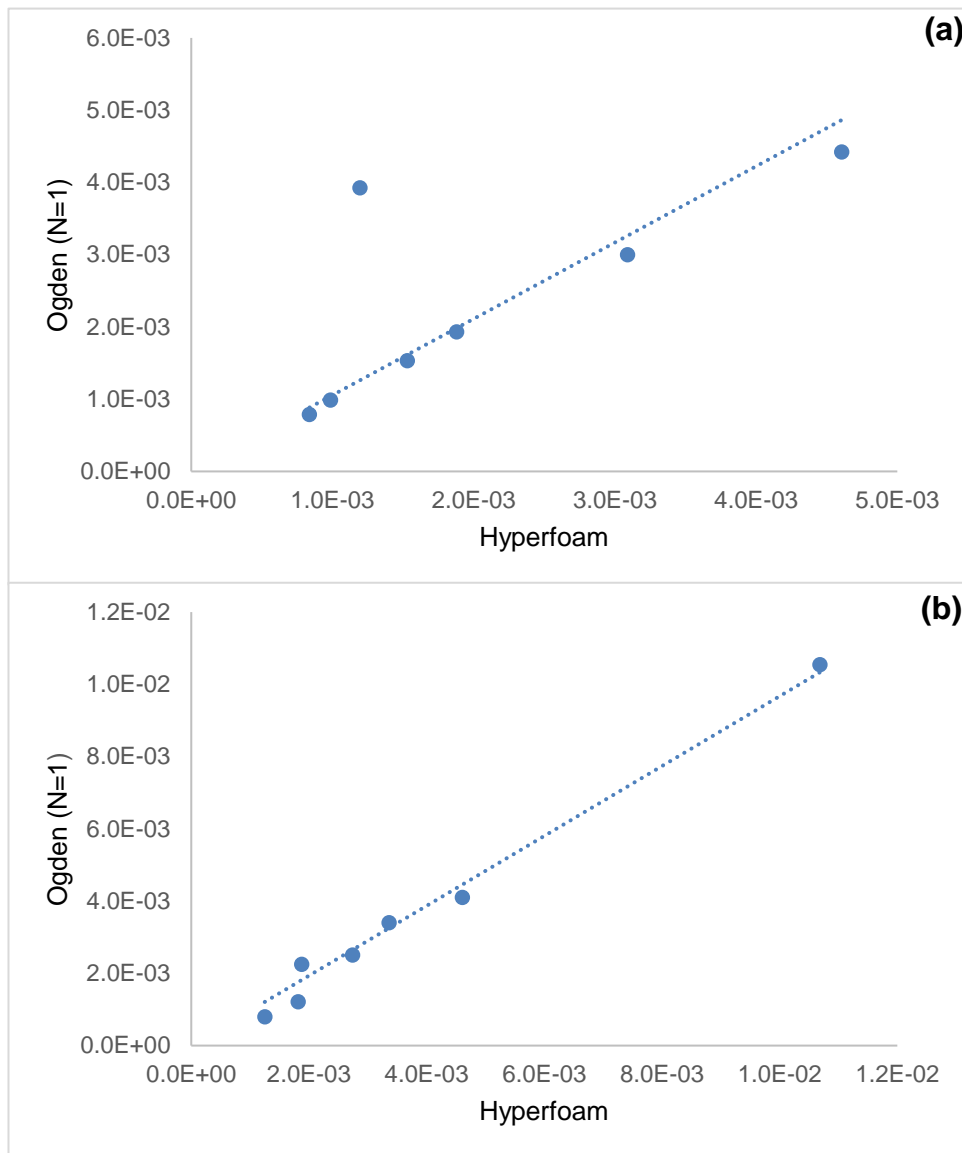
**Table 4.6: Calibrated material parameters for Ogden (N=1) and hyperfoam material models obtained as a result of the material optimisation procedure undertaken on the specimen-specific FE models by the author.**

Specimen		Ogden (N=1)			Hyperfoam	
		$\mu/\text{GPa}$	$\alpha$	$D/\text{GPa}^{-1}$	$\mu/\text{GPa}$	$\alpha$
ALL	1: T2-3	7.9E-04	9.4	1170	8.4E-04	5.9
	1: T4-5	9.9E-04	7.9	933	9.9E-04	5.3
	2: T2-3	1.9E-03	3.8	477	1.9E-03	2.7
	2: T4-5	3.0E-03	7.4	308	3.1E-03	4.6
	2: T8-9	1.5E-03	9.2	602	1.5E-03	5.9
	3: T4-5	4.4E-03	8.3	209	4.6E-03	5.2
	3: T6-7	3.9E-03	8.9	235	1.2E-03	5.8
PLL	1: T6-T7	4.1E-03	6.0	225	4.6E-03	4.4
	1: T10-T11	1.1E-02	9.7	88	1.1E-02	6.0
	2: T6-T7	2.3E-03	9.7	410	1.9E-03	6.6
	2: T10-T11	2.5E-03	15.0	369	2.7E-03	8.0
	3: T2-T3	7.9E-04	25.1	1167	1.2E-03	9.1
	3: T8-T9	1.2E-03	31.3	762	1.8E-03	11.6
	3: T10-T11	3.4E-03	24.1	272	3.4E-03	12.9

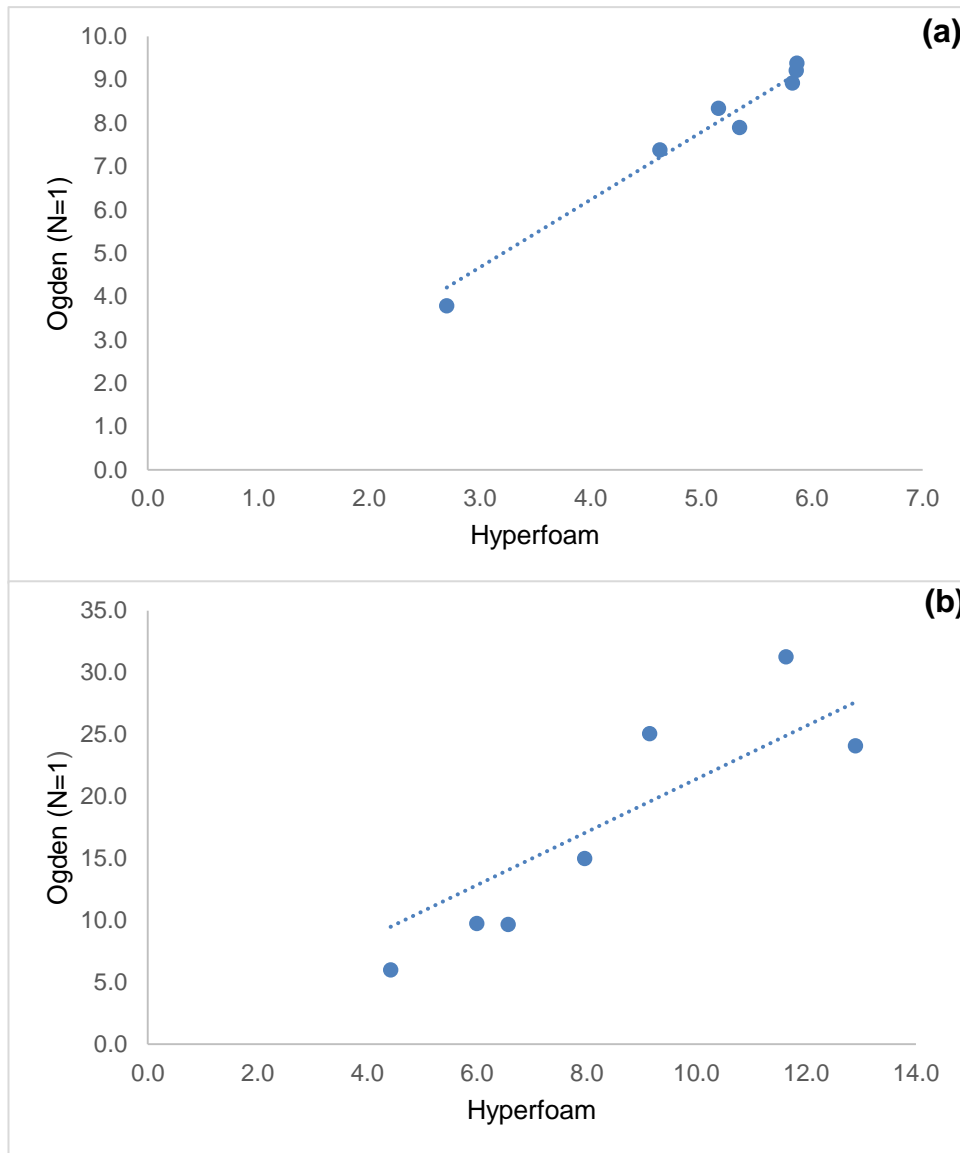
#### 4.3.5 Comparison of Material Models

As described previously, for the hyperfoam material model, the toe-region of the load-displacement slope is mainly controlled by  $\mu$  whereas the curvature is controlled by  $\alpha$  which in turn changes the gradient in the region that corresponds to the experimental 'linear zone'. Similarly, for the Ogden (N=1) material model, the toe region is controlled by both  $\mu$  and  $D$  whereas the curvature is controlled by  $\alpha$ . But since  $\mu$  is directly related to  $D$  for a given Poisson's ratio as assumed here (Equation 3.4, Chapter 3), altering either would automatically change the value of the other. Hence, here only the effects of  $\mu$  will be discussed when considering the toe region for the Ogden (N=1) material model.

In addition, it was found that the values for  $\mu$  and  $\alpha$  for the two material models were relatively well correlated for both the ALL and PLL, as shown in Figure 4.12 and Figure 4.13. Hence, only the Ogden (N=1) material model will be discussed in the subsequent comparisons between coefficients and across spines and levels.



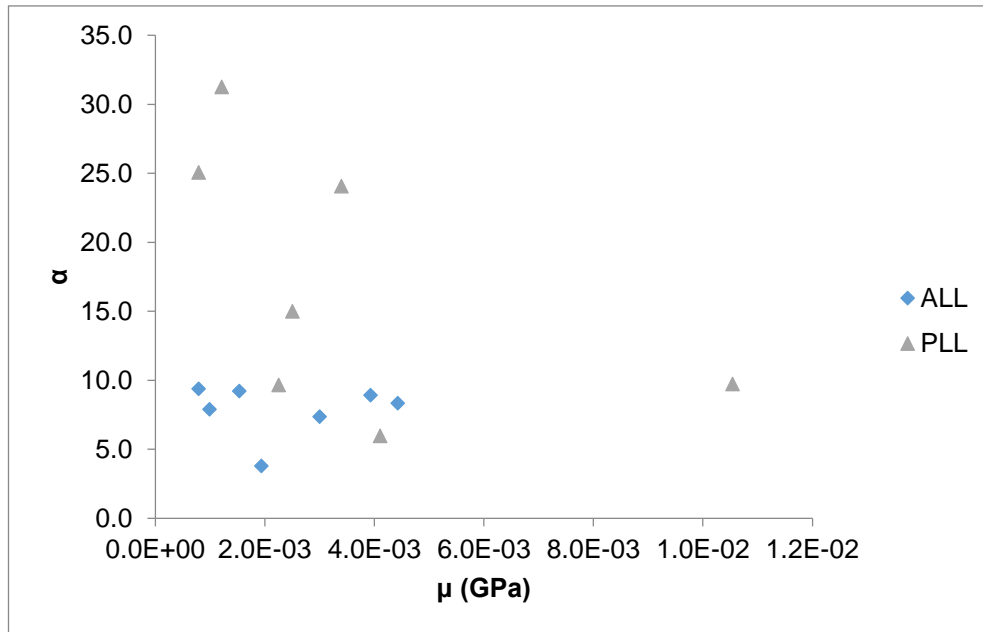
**Figure 4.12: Graphical comparison of the material coefficient  $\mu$  for both (a) ALL and (b) PLL derived using the two material models, showing that they are very similar hence either material model could be used for further analysis.**



**Figure 4.13: Graphical comparison of the material coefficient  $\alpha$  for both (a) ALL and (b) PLL derived using the two material models showing that they are related hence either material model could be used for further analysis.**

#### 4.3.6 Comparison between Coefficients

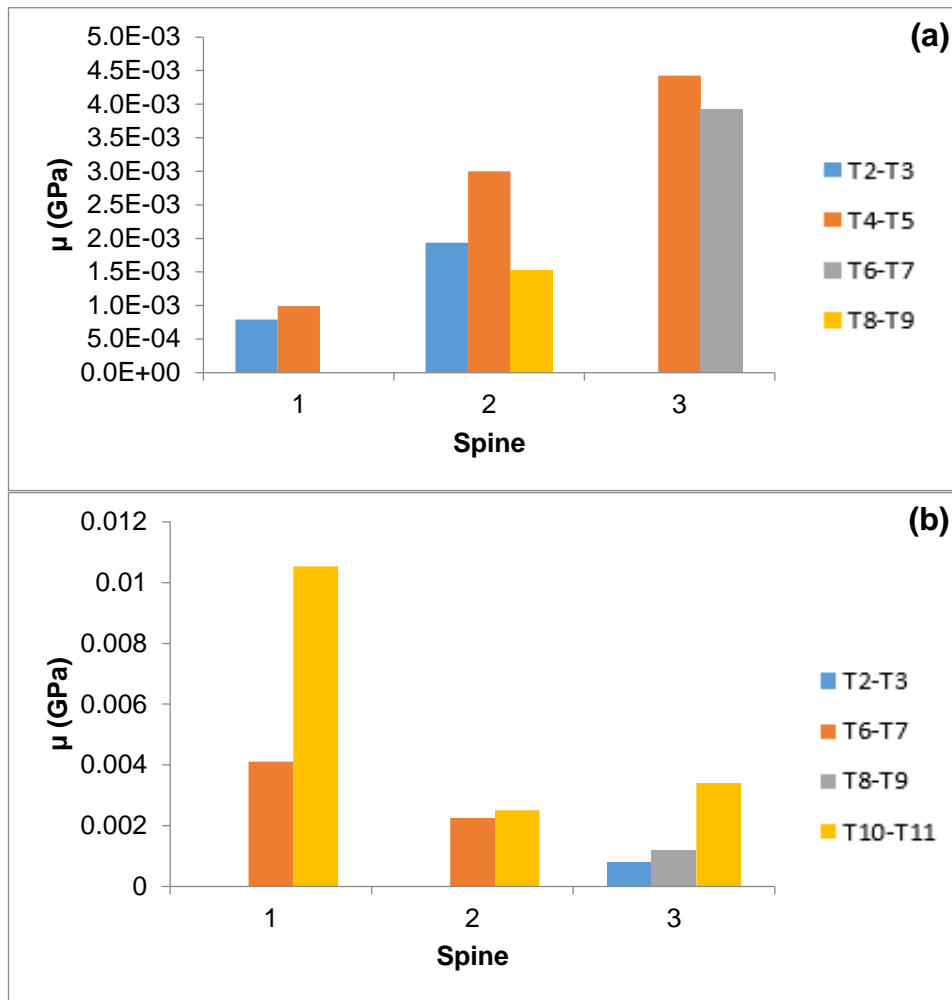
The material coefficients for Ogden (N=1) were plotted against each other (Figure 4.14) to examine if there was any relationship between the two. The graph illustrates that no clear relationship between the two can be drawn, hence both coefficients will be discussed in the following sections.



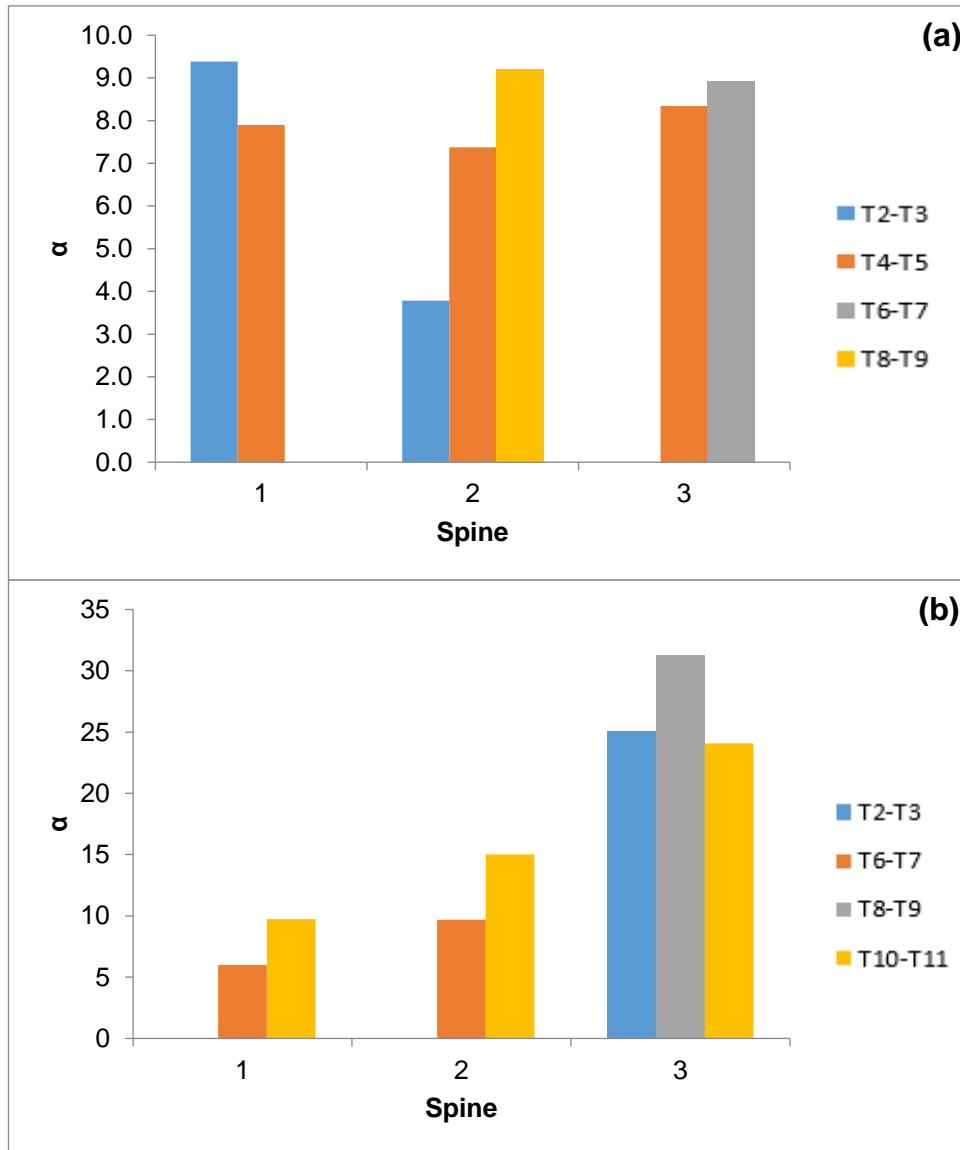
**Figure 4.14: Material coefficients plotted against each other for Ogden (N=1) material model. The figure illustrates that both coefficients are not related and hence both have to be discussed in further analysis.**

#### 4.3.7 Comparison by spine and by level

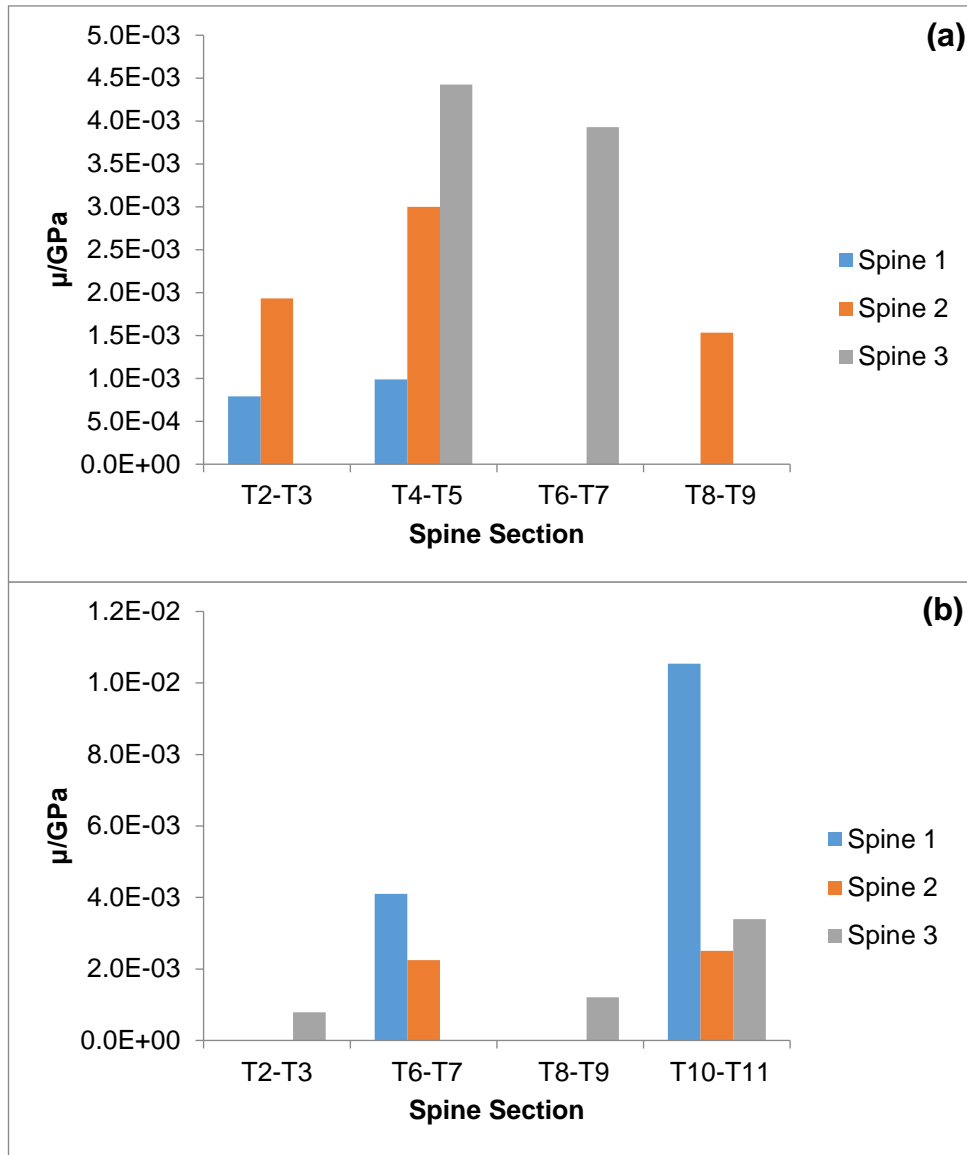
The material coefficients for each ligament group were plotted in groups of their respective spine (Figure 4.15 and Figure 4.16) and also by level (Figure 4.17 and Figure 4.18) to visualise the differences. Although there is not enough data to perform a statistical analysis, however, from the graphs, there was a large spread in values of both  $\alpha$  and  $\mu$  across the PLL and ALL. There were no clear trends for each ligament group; for example, the  $\mu$  value for the ALL was highest in Spine 3 whereas for the PLL, it was highest in Spine 1. Similarly, the  $\alpha$  value for the ALL did not vary much across different spines while for the PLL, it was highest in Spine 3. In some cases, there was more difference between spines than between levels (see Figure 4.15a and Figure 4.16b) and there were no clear trends seen between levels (Figure 4.17 and Figure 4.18).



**Figure 4.15: Comparison of  $\mu$  for Ogden (N=1) for (a) ALL and (b) PLL specimens by spine (left to right is from upper to lower levels). In the case of the ALL, there were bigger differences between spines than within each spine.**

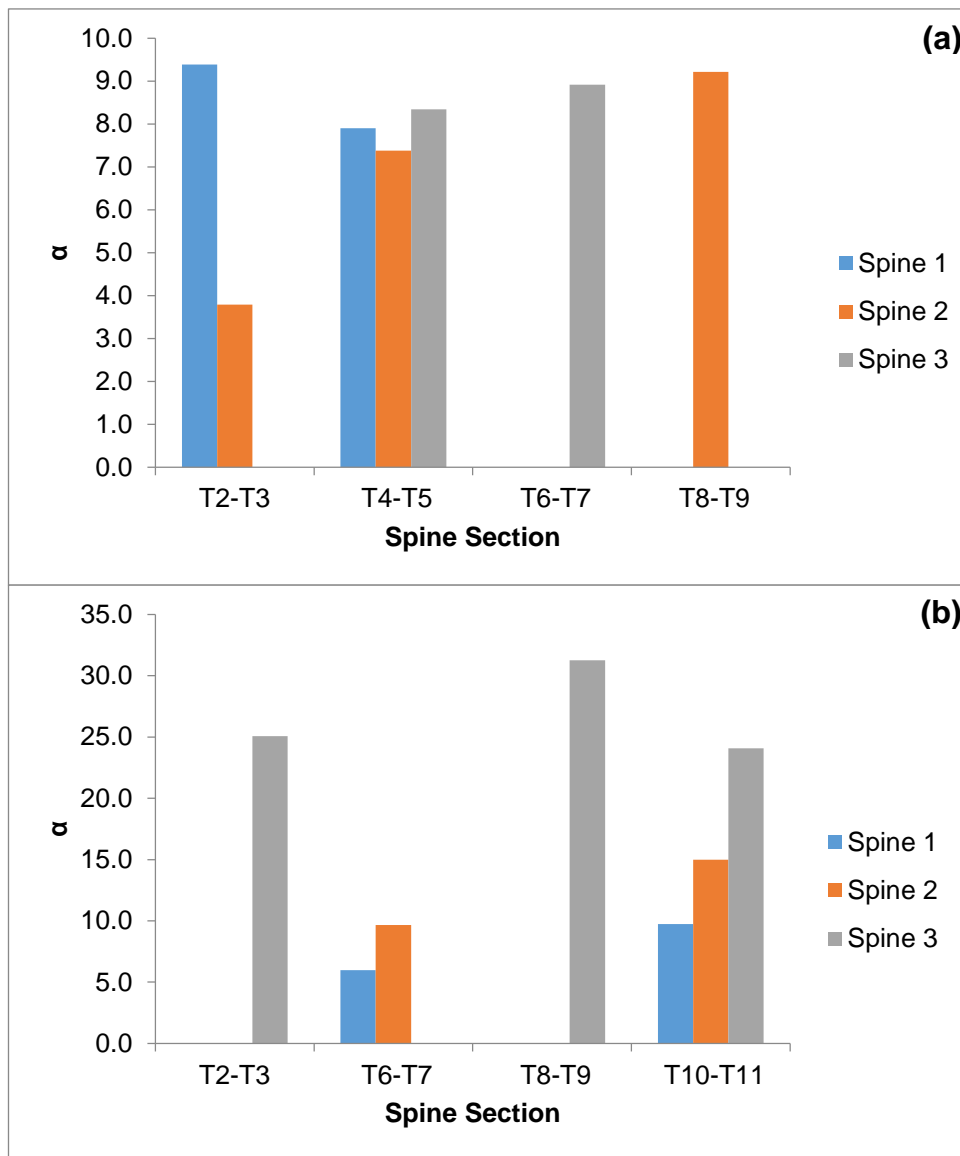


**Figure 4.16: Comparison of  $\alpha$  for Ogden (N=1) for (a) ALL and (b) PLL specimens by spine (left to right is from upper to lower levels). In the case of the PLL, there are bigger differences between spines than within each spine.**



**Figure 4.17: Comparison of  $\mu$  for Ogden (N=1) for (a) ALL and (b) PLL specimens by level showing big differences across individuals but no clear trends between levels are evident.**





**Figure 4.18: comparison of  $\alpha$  for Ogden (N=1) for (a) ALL and (b) PLL specimens by level showing big differences across individuals in the case of PLL but no clear trends between levels are evident.**

#### 4.3.8 Comparison with other computational data

To the authors knowledge no study has published hyperelastic material data, in terms of material parameters, for spinal ligaments hence a direct comparison with the material parameters obtained as a result of this study is not possible. It is, however, possible to compare the Young's modulus values used in other studies with an equivalent modulus at a given strain derived from the hyperelastic equations used here.

Equation 3.5 (Chapter 3) was differentiated to obtain an expression for the stress-strain gradient to make comparisons to the Young's modulus documented in other studies (Equation 4.1).

$$dS/d\epsilon = \frac{2\mu}{\alpha} \left[ \left( \frac{\alpha-2}{2} \right) (2\epsilon + 1)^{\frac{\alpha-4}{2}} - \left( 2 \left( -\frac{\alpha}{4} - 1 \right) (2\epsilon + 1)^{-\frac{\alpha}{4}-2} \right) \right] \quad [\text{eq. 4.1}]$$

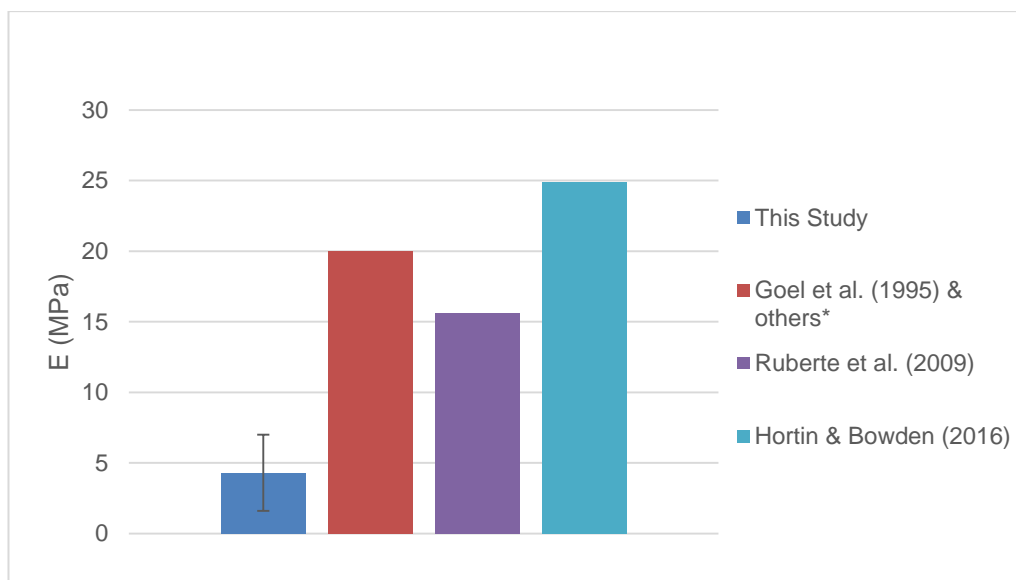
The majority of computational modelling studies have represented the behaviour of the ligaments up until the end of their linear regions with some using only a single linear region at all strains (Chapter 1, Section 1.2.6). To make comparisons with the literature, the strain at the end of linear region was used. This provided a comparison at the highest strain the ligaments would likely experience in vivo. Chazal et al. (1985) determined strain at the end of linear region for the ALL as 12% while a value of 20% strain has been documented for PLL to be within the physiological range and at the end of linear region (Ruberte et al., 2009)). These values were used in Eq.4.1 along with the material parameters for each individual ligament, and the resulting stress-strain gradients are presented in Tables 4.7 and 4.8. The average gradients for both ALL and PLL was also deduced and was compared with the Young's Modulus data from the simple computational models (Chapter 1, Table 1.9) in the linear range. The comparisons are presented in Figure 4.19 & Figure 4.20.

**Table 4.7: Estimated values of the stress-strain gradient at 12% strain (E) from the material parameters for all the specimens of ALL (n=7).**

Specimen	$\mu$ (MPa)	$\alpha$	E (MPa)
1: T2-T3	7.9E-04	9.4	1.6
1: T4-T5	9.9E-04	7.9	1.8
2: T2-T3	1.9E-03	3.8	3.0
2: T4-T5	3.0E-03	7.4	5.2
2: T8-T9	1.5E-03	9.2	3.0
3: T4-T5	4.4E-03	8.3	8.1
3: T6-T7	3.9E-03	8.9	7.5
Average $\pm$ S.D.			4.3 $\pm$ 2.7

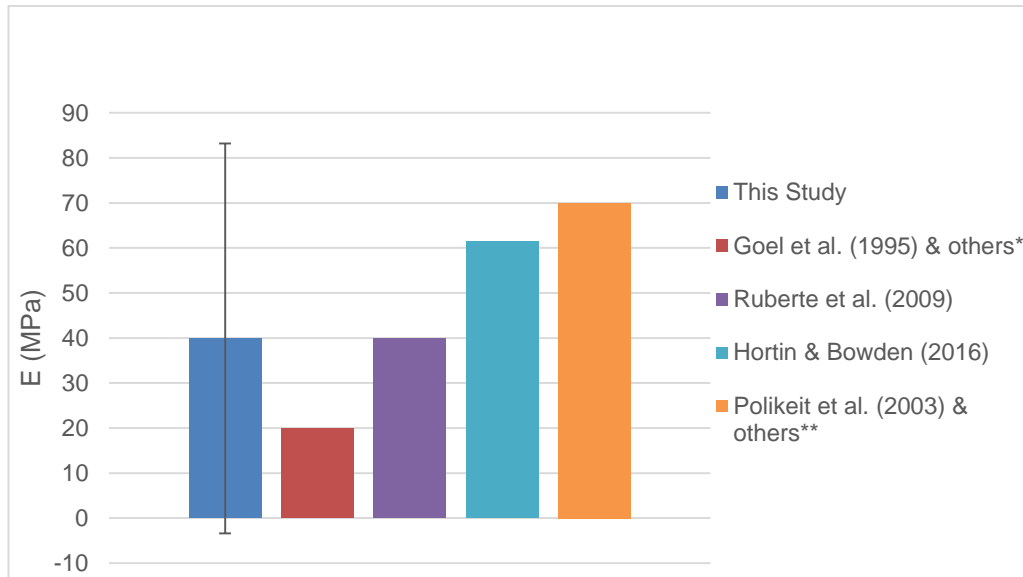
**Table 4.8: Estimated values of the stress-strain gradient at 20% strain (E) from the material parameters for all the specimens of PLL (n=7).**

Specimen	$\mu$ (MPa)	$\alpha$	E (MPa)
1: T6-T7	4.1E-03	6.0	5.9
1: T10-T11	1.1E-02	9.7	25.3
2: T6-T7	2.3E-03	9.7	5.4
2: T10-T11	2.5E-03	15.0	14.3
3: T2-T3	7.9E-04	25.1	25.3
3: T8-T9	1.2E-03	31.3	111.6
3: T10-T11	3.4E-03	24.1	91.6
Average $\pm$ S.D.			39.9 $\pm$ 43.3



**Figure 4.19: Comparison of Young's modulus (E) between the average value of ALL from the current study and the data cited by computational studies.**

\*others include; Lee & Teo (2005), Polikeit et al. (2003), Lee & Teo (2004), Sylvestre et al. (2007), Bowden et al. (2008), Tsuang et al. (2009), Moramarco et al. (2010)



**Figure 4.20: Comparison of Young's modulus (E) between the average value of PLL from the current study and the data cited by computational studies.**

\*others include; Lee & Teo (2005), Tsuang et al. (2009)

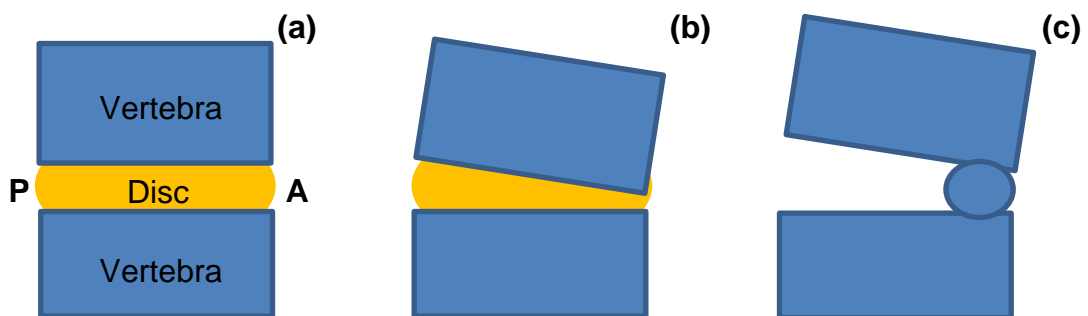
\*\*others include; Lee & Teo (2004), Sylvestre et al. (2007), Bowden et al. (2008)

## 4.4 Discussion

### 4.4.1 Discussion of Experimental Results and Visual Observations

This chapter presented the procedures adapted to characterise the human ALL and PLL. The results alongside visual observations and possible causes is discussed below. The testing was carried out on thoracic regions of human cadaveric spines and the results were presented as load-displacement curves for each ligament (Figure 4.8 and Figure 4.9). The curves all followed the same basic shape but there were large differences in the gradients. Both Figures 4.8 and 4.9 show that there were generally larger differences between the spines than within each spine because the curves for each spine mostly lie next to each other. There was one outlier to these observations: specimen T10-11 from Spine 1 showed a considerably higher stiffness than all other PLL specimens. This specimen was found to have anterior ossification as well as big cuts in the ALL and its MRI scans showed bony protrusions into the disc space (see Figure 4.6 (C)). This would suggest that the two vertebrae were self-fusing together and could potentially imply that the attached ligament on the anterior side i.e. the ALL had become redundant and was wasting away. The PLL on the other hand could have been subjected to greater loads as the hardening on the anterior side might result in an anterior pivoting under flexion and greater stretch of the posterior side (see Figure 4.21), and hence the PLL

has to be stiffer to compensate. The fusion of vertebrae have been shown to be related to many underlying conditions, including degeneration of discs as a result of old age or trauma. Fusion due to both organic means (Benzel, 2012) or as a result of surgery (Srinivas, et al., 2016; Lee & Choi, 2015), has been shown to result in regions of increased stress and strain in segments adjacent to the fused segments. This indicates a change in the load distribution following fusion, and since ligaments play a role in providing stability to the spine alongside facets (Sharma, et al., 1995) and discs, an imbalance due to changing any of the stabilising structures will alter the role of the other two (Ng, et al., 2003). Moreover, anterior ossification can be related to diseases such as the idiopathic skeletal hyperostosis (Resnick, et al., 1975) which mainly affects the thoracic spine, or ankylosing spinal hyperostosis (Forestier & Lagier, 1971). While a specific diagnosis from the evidence seen for Spine 1 is not possible, it is important to note that these diseases are known to be associated with spinal enthesopathy, a phenomenon related to ossification of paraspinal ligaments (Nakhoda & Greene, 2016). If the anterior ossification observed in the Spine 1 specimens is associated with any of the diseases mentioned above, then the ossification of the PLL is also quite possible, which would result in an increased stiffness. This could potentially be another reason for the stiffer PLL.



**Figure 4.21: A schematic illustration of anterior flexion in healthy FSU and in degenerated FSU due to anterior ossification. (a) illustrates an FSU of an healthy individual in a resting state with posterior (P) and anterior (A) side labelled; (b) illustrates the same healthy FSU when the individual bends forward; there would be anterior disc compression with the centre of rotation located towards the middle of the disc; (c) illustrates an individual with anterior ossification that leads to anterior pivoting of the vertebra during forward flexion, resulting in greater stretching of the structures at the posterior.**

The anterior ossification that leads to bone and disc protrusions is also evident in two other specimens of Spine 1, which were both used for testing the ALL. Both these specimens show very low stiffness values and the ALL was thinner

than in the other two spines (e.g. Table 4.2), which would corroborate the theory stated above about the ALL having become redundant.

The tables of bilinear stiffness (Table 4.3 and 4.4) show that the value of  $k_2$  is generally double or higher than the  $k_1$  value, however for the Spine 1 specimens, this does not hold true and there is a little difference between the  $k_1$  and  $k_2$  values. This could be due to the ossification and bony protrusions that led to the over-stretching of the ligament, which could potentially cause the ligaments to operate in the linear region with the collagen fibres already straightened. In the ALL, this is likely due to the over exertion caused by bone protrusions anteriorly, and to PLL, due to the overextension and/or secondary-ossification discussed above. This is especially true in the case of Spine 1:T6-7 (see Figure 4.7) whereby bone compression led to misalignment of spine and PLL potentially stretched beyond its normal limits to keep the spine in place.

#### **4.4.2 Discussion of Finite Element Modelling**

The FE modelling of ligaments provides further evidence for the idea previously established in Chapter 3 (see Section 3.8) that the assumption of a uniform mean cross-sectional area and length, and a resulting uniaxial stress state, cannot be used to derive the properties of the ligament accurately. As shown in Table 4.5, using these assumptions led to large differences between experimental output and FE output. There could be a number of other factors causing discrepancies between the FE predictions and experimental data, such as variations in dimensions and boundary conditions, or errors due to the mesh size used (Chapter 3, Section 3.6.1)., however, these discrepancies will be small as efforts were made to ensure that the geometry used and boundary conditions applied were realistic (Chapter 3). Moreover, it was ensured that the mesh size used was defined by the optimum mesh size established in Chapter 3, Section 3.6.1.3. Therefore it seems likely the majority of the difference is due to the assumption of uniform geometry and uniaxial stress.

The optimisation procedure undertaken subsequently resulted in the final FE outputs being very close to the experimental outputs, with the accepted percentage difference of 5% or less between the two outputs being achieved in all cases. To the best of our knowledge, this is the first FE study showing that a uniform cross-sectional area and length cannot be used to represent the accurate behaviour of ligaments. However, in FE modelling of knee ligaments, a comparison between springs and geometrically accurate ligaments has been carried out (Beidokhti, et al., 2017). They built two models; one with one-dimensional spring elements, as a way of simplifying the geometry, and the other with three-dimensional continuum elements based on segmentation and

found more accurate contact outcome variables with the continuum modelling approach. Although the springs used in that study were not directly comparable to the uniform geometry assumptions used here, the study provides further evidence of the importance of modelling geometrically accurate ligaments.

#### 4.4.3 Comparison and Analysis of Material Parameters

The hyperfoam or Ogden model optimised values provided a numerical way of capturing the difference between the experimental curves, as the two coefficients influence different parts of the curve;  $\mu$  influences the toe-region whereas  $\alpha$  influences the curvature, as previously described in Chapter 3 (Section 3.9.2 & 3.9.3). If the slope has greater curvature (that is, has a higher exponential), it is due to the  $\alpha$  value being higher and if its initial gradient is higher, then the  $\mu$  value is higher. Hence, one can deduce the relative shape of the load-displacement slope for a specimen from the material coefficients and vice versa. For example, the values of  $\mu$  for the ALL specimens for Spine 3 are larger than for the other two spines (see Figure 4.15) because the toe region of these specimens has a higher gradient (see Figure 4.8). Whereas the  $\alpha$  value for all these specimens are very similar because the curvature across all these specimens is very similar in what would be classed as the 'linear zone' of the slope. The main difference in  $\alpha$  is seen in specimen 2:T2-3 (Figure 4.16), displaying the lowest value, because it has a very low curvature and maintains a low gradient in the 'linear zone' (Figure 4.8). In the case of the PLL, the value of  $\mu$  is highest for specimens of Spine 1 (See Figure 4.15) because the specimens have higher toe region than the others, especially specimen 1:T10-11 (Figure 4.17) which was steeper than all the other PLL specimens (Figure 4.9). Similarly, the  $\alpha$  value for Spine 3, in the case of the PLL, has higher values than the other two spines because the curvature of the load-displacement slopes of these specimens is greater than the others.

It is important to remember that the models used are all phenomenological hence the resulting material coefficients do not have direct physical meaning as described previously (Chapter 1, Section 1.2.7; Chapter 3, Section 3.10). However, as described, their effect is seen in different parts of the load-displacement curve. Since we know that different components of the ligament e.g. elastin content, collagen content, amount of collagen crimping etc. affect the load-displacement slope (Chapter 1, Section 1.2.4.1), some comparisons between the tissue composition and structure and the two variables can be made but it must be noted that it is not a one-to-one mapping because there are only two material variables as opposed to multiple tissue variables. Based on the above, it could be hypothesised that the collagen fibres straightening out

and taking the load dominates the behaviour of  $\alpha$  since collagen dominates at higher strains once it straightens out, whereas for  $\mu$ , the elastin is taking more of the load as it dominates at low strains. However, there is no clear distinction between the two variables and their relevance to the tissue structures. Even if we just consider the collagen, there are several different factors that can affect the shape of the slope such as the amount of collagen will affect the overall gradient once all the fibres uncrimp, while the variability in crimping will affect how quickly the gradient changes i.e. if all the crimps straighten at the same strain, then there would be a very sudden change in gradient, compared to a more gradual curve if different crimps straightened at different strains. Since the best exponential fit accommodates both of these factors, they cannot be differentiated. For example, it was observed that Spine 3 specimens (red curves in the Figure 4.8 and Figure 4.9) had the highest stiffness overall for both ligaments. This spine was also found to have the highest  $\alpha$  value in the case of PLL than the other two spines. The  $\alpha$  value for ALL for this spine is in the higher spectrum compared to other ALL specimens. If the microstructure of these ligaments is influenced by the material parameters in the same manner as described above, then the ligaments of this spine, especially the PLL, probably have either a higher amount of collagen fibres and/or the fibres are stiffer once un-crimped. If the same also holds true for Spine 1 which was found to have highest  $\mu$  for PLL specimens but lowest for ALL, then the PLL would have adapted to the anterior ossification observed in these specimens, as discussed above, and have higher amount of collagen fibres or the fibres are more crimped. Or else if the PLL has not adapted and is stiff due to secondary ossification, as described above, then the higher  $\mu$  value is influenced by the ossified structure. ALL specimens for Spine 1, on the other hand, with lowest  $\mu$  values, also have the lowest stiffness values supporting the visual observation about the ligaments becoming redundant due to anterior ossification of the disc. So the collagen fibres have either stretched beyond their capacity and are working in the liner region or the amount of elastin in these ligaments have reduced immensely. This also shows the differences amongst individual spines due to a disease or inherent difference in the tissue microstructure. Such speculations can only be supported by a histological analysis, which is beyond the scope of this study. This helps illustrate the point about the material models being phenomenological, i.e. they do not have any physical relevance and purely simulate the mechanical behaviour. The models might give an indication about the structural relevance in a healthy state but would not be able to predict true relevance in a diseased state such as ossification.



The values of the material coefficient  $\mu$  obtained for all the specimens are very similar between the two material models (see Table 4.6). The values for  $\alpha$  however are different but are mostly of the same order of magnitude in both cases (see Table 4.6). Graphical representation of this is presented in Figure 4.12 and 4.13. However, for both models, the coefficients are not related to each other (Figure 4.14) so it is not possible to derive one from the other. This is not surprising given that different material factors affect each coefficient (as discussed previously), and would not necessarily vary in the same way from specimen to specimen.

#### **4.4.4 Variability across Individual Spines and Spinal Levels**

As with the stiffness values, a comparison of material coefficients across the three spines (Figure 4.15 and Figure 4.16) and across different levels (Figure 4.17 and Figure 4.18) showed that there are bigger differences between spines than there are between levels. The differences between spines is discussed in detail above in relation to the material parameters. No clear trends are evident between levels and one cannot comment if moving along the length of the spine has any significant effect on the material properties of the ligament. This might be because this study is restricted to thoracic region where the spine is held in place and the motions are restricted by the rib cage, hence the differences along the length are not very evident. If the study were performed over a longer length with the inclusion of either the cervical or the lumbar region where there are greater differences in loading and range of motion (Chapter 2, Section 2.7.1), then more trends may have been evident. In the lumbar spine for example, where there is greater curvature, there will be differences from one vertebrae to another in the articulation and because the motions are not restricted. This has been shown in a recent study by Putzer et al. (2016) who found that the lumbar spine kinematics have a trend towards increased lower lumbar flexion.

The big differences observed between the three spines show that each individual is different to the others and places emphasis on the importance of specimen-specific modelling. Although it is difficult to determine the exact properties of each ligament for each individual without having to perform an elaborate study like this, however, the state of the spine and the tissue as observed through an MRI scan of the individual can give an indication of what category it falls under. For example, physical inspection of Spine 1 revealed right anterior ossification. This was seen on MRI scan as bone and disc protrusions showing that the ligaments are stretched in those regions. Even if the ligaments had adapted and were no longer under a greater stress due to

this increased stretch around the protrusions. When the disc was dissected during the testing, this removed more strain than in the normal disc state. Therefore, regardless of where on the stress-strain curve the ALL usually operates (in a stretched or adapted state), the start of the test would have been moved further to the left (towards a lower strain) than normal, which could explain why the specimens tested for the ALL showed a lower stiffness than the specimens from other spines (Table 4.3). The PLL in these regions would also have to be stiffer as discussed above. Specimen 1:T10-11 displays this higher stiffness in the PLL, however, specimen 1:T6-7 displays quite a low stiffness comparatively (Table 4.4), assuming the above hypothesis holds true. This can be attributed to the bone compression evident in this specimen (Figure 4.7) which might have already caused damage to the PLL hence the low stiffness. This shows that although some evidence on the ligament properties can be gleaned from the MRI, it may not always be possible to predict likely properties because of damage or overstretching that is not visible.

#### **4.4.5 Comparison with Published Human Data**

The main aim of this section was not only to characterise the human spinal ligaments but also to compare the data obtained with the published human data. To the author's knowledge, no data has been published on the material parameters of spinal ligaments, which could be directly compared with the material coefficients obtained in this study. As previously discussed in Chapter 1 (Section 1.2.7), hyperelastic material models have been used to model other joints and ligaments in the human body however, a comparison with the material parameters used in those studies would not be appropriate since large differences are observed even between the ALL and PLL. For this reason, it was only possible to compare an equivalent modulus at a given strain from this study with Young's modulus values cited in previous computational modelling studies. (Section 4.3.8). The comparison shows that the Young's modulus for the ALL averaged from this study is lower than the values used by computational modelling researchers whereas the value for PLL lies approximately in the middle of what is used by these researchers. The majority of these computational studies used the experimental data cited in literature to work out the material properties for ligaments. Some refer to other computational studies as a reference, and following the trail leads to the same experimental studies as the others. The differences observed are due to the differences in the experimental procedures used to generate the data in respective studies. The study by Pintar et al. (1992) was found to be the original source of data for most studies (Goel et al. (1995), Lee & Teo (2005), Polikeit et al. (2003), Lee & Teo (2004), Sylvestre et al. (2007), Bowden et al.

(2008), Ruberte et al. (2009), and Tsuang et al. (2009)). The other sources of data cited were traced back to the study by Chazal et al. (1985) (Polikeit et al. (2003), Lee & Teo (2004), Sylvestre et al. (2007), Hortin & Bowden et al. (2016)). The experimental studies cited stiffness values which were manipulated by the researchers alongside the geometric properties i.e. cross-sectional area and length, to derive the Young's modulus.

Some studies used different sources for obtaining the data for different ligaments e.g. Polikeit et al. (2003) used a Young's modulus of 20 MPa for the ALL from Pintar et al. (1992), but 70 MPa for the ALL which was derived from Chazal et al (1985). Some studies referenced back to the same experimental study but cited different modulus values. For example, Ruberte et al. (2009) cited 15.6 MPa for the ALL whereas Polikeit et al. (2003) cited 20 MPa, although both referenced back Pintar et al. (1992). While these differences may be due to the difference in the level of FSU used, there is a lot of ambiguity in how the Young's modulus values were derived. Regardless of how the modulus values were derived, the values used previously for the ALL are all considerably higher than the stress-strain gradient derived from the steepest physiological portion of the stress-strain curve in any of the specimens tested here. This could be because of the differences in specimens, spinal levels etc. as discussed in detail below, but it may also suggest that the modulus has previously been overestimated. The assumptions made about uniform geometry to convert the published stiffness into a Young's modulus could be likely reason for this overestimation, as is shown by this study. Nevertheless, it is difficult to know whether any overestimation of the ALL properties would have changed the study outcomes, because no sensitivity tests were undertaken.

In order to make direct comparisons between the original experimental data and the current study, the two most cited experimental studies by the computational modellers i.e. Chazal et al. (1985) and Pintar et al. (1992) were also analysed. The study by Chazal et al. (1985) could not be compared for two reasons; they did not publish stiffness data to allow us to make direct comparisons, and, they tested the ligaments individually as opposed to keeping them in situ (current study) which has been shown to bring about differences in the results as discussed previously in detail in Section 1.2.5.4.

Pintar et al. used the data from Myklebust et al. (1988) who performed a study on 41 fresh human male cadavers with a mean age of 67 years (ranging from 30-89 years). Whole ligament stiffness values were cited, but only in terms of  $k_2$  as the toe region was neglected. The authors tested ligaments at each level

in isolation, *in situ*, and all the supporting structures except the ligaments to be evaluated were sectioned through. Pintar et al. (1992) analysed the data on specimens of the lumbar region of the spines from the above study and presented the mean stiffness (slope of the least-squares fit line) values of the linear portion of the force-deformation curve. The values published for ALL ( $33 \pm 15.7$  N/mm;  $n=25$ ) and PLL ( $20.4 \pm 11.9$  N/mm;  $n=21$ ) were both found to be less stiff than the ones obtained for human ALL ( $63 \pm 51$  N/mm) and PLL ( $50 \pm 22$  N/mm) in this study. An un-paired t-test was carried out to see if the stiffness values were significantly different between the two studies for both ALL and PLL. The data was assumed to meet the requirements for an unpaired t-test, i.e. that there were no outliers and the data was normally distributed, since it was not possible to access the raw data from this study. It was found that there was a significant difference ( $P < 0.05$ ) between the means of stiffness values of ALL for the two studies whereas no significant difference was found between the means of the stiffness values obtained for the PLL from the two studies. It is important to note that the specimens are not fully independent, as several specimens came from the same spine.

There could be a number of reasons for the differences in the mean stiffness values including the testing regime, the regions tested (thoracic or lumbar), the tissue storage method and the age, gender and fitness level of individual, which are each discussed below.

#### *Regional differences*

Our study was performed on the thoracic region whereas the published data was obtained from lumbar region, therefore, the differences in the stiffness might be due to the difference in the regions. To author's knowledge no study is published on intra-individual differences between spinal ligaments mechanics from different regions. However, Weiler et al. (2012) performed a study on human intervertebral discs (IVD) in order to analyse the amount of degenerative changes in different spine levels in humans from different ages. They found the cervical and thoracic disc specimens showed significantly less degenerative changes compared to the lumbar region (Weiler, et al., 2012). If the same is true for the spinal ligaments then this could also explain some of the stiffness differences between the two studies. Some differences in ALL structure at varying regions of the vertebral column were illustrated by Bogduk (1997) and Bannister et al. (1996). Bogduk (1997) found that the ALL was not associated with any of the prevertebral muscles in the thoracic region and therefore, stood alone. This shows functional differences in the ligament over the length of spine. Bannister et al. (1996) reported that ALL is thicker and

narrower in the thoracic region as compared to the other regions, and broadens as it travels caudally. These differences likely alter the cross sectional area and hence stiffness if the material properties remain constant. Further comparison of dimensions in different regions is hampered by the huge differences in the values reported (see Chapter 1, Table 1.9) depending on the method of measurement used, as described previously in Chapter 1, Section 1.2.5.1.1 and Section 1.2.6.7.

### *Age differences*

The specimens in this study were obtained from cadavers with mean age of 86 years, which is higher than the mean age (67 years) of the published data. This could be another likely reason for differences seen in stiffness as the mechanical properties of the spine have been found to deteriorate with increasing age (Nachemson & Evans, 1968; Tkaczuk, 1968; Neumann, et al., 1994; Pintar, et al., 1998; Neumann, et al., 1992; Iida, et al., 2002). The ligament properties have been shown to correlate with the bone mineral content (Neumann, et al., 1994; Pintar, et al., 1998) which is known to decline after the age of 50 due to the onset of osteoporosis (Kanis, et al., 1994) therefore a change in their mechanical properties is inevitable. Moreover, the ligament properties are closely related to the collagen content present which decreases with age, resulting in a decline in material properties such as their strength and the ability to withstand deformation (Cowin & Doty, 2007). Tkaczuk, (1968) carried out testing on lumbar ALL and PLL and found a decrease in failure force, stress, and elongation with increasing age. Nachemson et al., (1968) also found the modulus of elasticity and failure stress in lumbar LF to go down by a factor of four between the ages of 20 to 80 years. A similar aging effect on ligament failure stress was observed by Chazal et al., (1985). This shows that with increasing age both the elasticity and the collagen content decreases which ultimately will result in a decreased elongation and failure force. However, these studies were carried out on sections of ligaments as opposed to our study, hence evaluating the material properties but not the total stiffness of the ligaments. The stiffness is related to both the modulus as well as the dimensions, so although the modulus was shown to decrease in these studies there might be counteracting changes in geometry (e.g. ligament thickening) which will give an overall increase in stiffness with age. Neumann et al., (1994) has shown greater effects of increased cadaver age, and decreased vertebral mineral content on isolated lumbar ALL specimens at slow elongation rates with stiffness varying by as much as 5 times across regions. They found increased stiffness at mid-substance whereas a decreased stiffness was found at the insertion point of the ligament compared to younger

specimens. This shows that aging affects different regions of ligaments in different ways (Neumann, et al., 1994). If slow elongation rates are used, the mid-substance of the ligaments is exploited whereas the low stiffness and failure at the insertion points at faster loading rate might be a result of mechanical integrity of the Sharpey's fibre insertions or the underlying layer of bone, or both, during aging as hypothesised by Neumann et al. (1994 (Cowin & Doty, 2007)). This might explain why studies carried at a comparatively higher loading rate to this study (Myklebust, et al., 1988; Iida, et al., 2002) have found the elastic stiffness of ligaments to decrease with increasing age; if there was a progressive pulling out of the Sharpey's fibres even before failure.

#### *Differences in testing regimes*

The testing regimes of both studies; this study and the study by Pintar et al. (1992), were the same in terms of the ligaments being tested in situ and all the supporting structures except the ligament to be evaluated were sectioned. However, the loading rates in both cases were very different with Pintar et al. (1992) using a faster rate of 600 mm/min compared to 1 mm/min used in this study. As described previously (Chapter 2, Section 2.7), an increase in loading rate has been shown to increase the stiffness in cervical spinal ligaments in similar isolated bone-ligament-bone samples (Butler, et al., 1988; Mattucci, et al., 2012; Trajkovski, et al., 2014). If the same is true for the lumbar spine, then the published stiffness by Pintar et al. (1992) would be lower if the tests were to be carried out at a slower loading rate of 1 mm/min. However, Pintar et al. (1998) carried out compressive loading on whole cervical spines and found that the loading rate effects decreased with increasing age. The interaction between loading rate and age was thought to be attributed to the degradation of bone with age since most failures occurred in the bone. This may also affect ligament properties, as ALL and PLL properties have been shown to correlate with bone mineral content in the vertebrae, which goes down with age (Neumann, et al., 1994) as discussed previously, and so the loading rate effect might not make a significant difference to the values obtained for elderly specimens because the aging effects overrides other effects.

#### *Differences due to storage method*

The published data was obtained from fresh specimens whereas the data in this study was obtained from frozen specimens that have gone through a number of freeze-thaw cycles before the testing. Freezing specimens on the day of retrieval with subsequent dissection and testing on a later day has been shown to not affect the behaviour of ligaments adversely (Chapter 1, Section 1.2.5.4). However, since the specimens in this study had unavoidably gone

through a number of freeze-thaw cycles, despite efforts to reduce water loss, this could have caused dehydration of the tissue hence resulting in a stiffening of the ligaments.

The large standard deviations in this study are an indication of just how variable the tissue is from one individual to another. It is therefore quite likely that these two studies simply represent different samples taken from the natural range across different spinal levels and age distributions, and hence both the studies are equally valid.

The differences in stiffness values due to biological variability and aging effects are an inevitable consequence of cadaveric research but the differences due to testing regimes can be controlled. Hence a comparison of the human and ovine data obtained as a result of testing carried out in the same manner is conducted in Chapter 5.

#### **4.4.6 Conclusion**

In conclusion, this chapter has presented new data on the behaviour of the thoracic longitudinal ligaments, including parameters for material models that represent its non-linear behaviour for the first time. It is apparent that these properties are highly variable from one person to another, which poses challenges for representing the behaviour in finite element models of the spine.

## Chapter 5 Discussion

### 5.1 Introduction

This chapter brings together all the key results obtained from this work and discusses their meaning in a wider context. The limitations of the work are also discussed, followed by some suggestions for future work. The chapter ends with final concluding statements to emphasise the key points and the significance of this work.

Overall from this work, a new method has been developed to mechanically characterise the spinal ligaments using a combined experimental and computational approach. The method was successfully applied to the longitudinal ligaments, namely the anterior longitudinal ligament (ALL) and posterior longitudinal ligament (PLL), but has the potential to be replicated on the other ligaments of the spine. The method was developed on ovine spines and was successfully applied to human spines resulting in new data on the mechanical properties of both ovine and human ALL and PLL.

In the literature (Chapter 1, Section 1.2.6), the spinal ligaments have been characterised either by their overall mechanical behaviour (i.e. stiffness), or by the underlying material behaviour (most commonly measured through a Young's modulus). The stiffness is useful in understanding the relative effects of the different ligaments, such as in the larger scale models of the spine where ligaments are represented by springs or truss elements. Whereas the material properties are useful in understanding the effects of differences in the material composition of the ligaments, and in FE models where the ligaments are represented as solid structures.

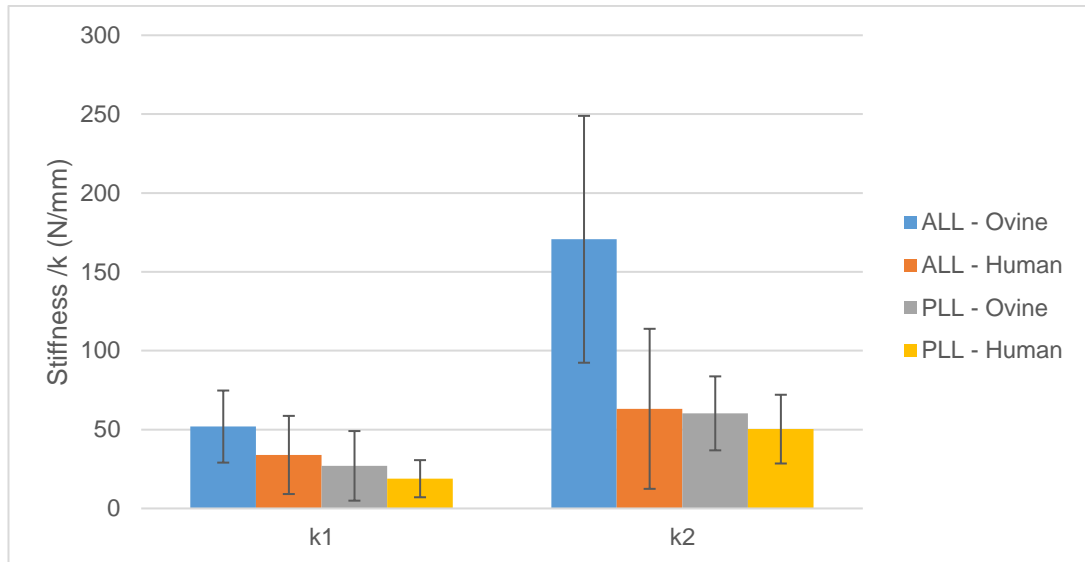
Both the ovine and human specimens were found to have stiffness values higher than those cited in literature (see Chapters 2 and 4). A comparison of both human and ovine stiffness values in relation to each other is presented in the next section. Moreover, a poor agreement was found between the material parameters derived from FE models and the initial values derived by assuming uniaxial behaviour, that is, assuming uniform cross-sectional area and length (see Chapters 3 and 4). The material parameter values for the human spine were found to be more consistent within each spine than between spines (see Chapter 4). The material parameters obtained for both human and ovine specimens are also compared in the following section.



## 5.2 Comparison of the stiffness values for human and ovine longitudinal ligaments

It was clear from the experimental data that both ovine (Chapter 2) and human ligaments (Chapter 4) exhibited a non-linear load-displacement relationship. Therefore, in order to make comparisons, a bi-linear model was employed as had been used previously in the literature (Chapter 1, Section 1.2.6). Figure 5.1 shows a comparison of the toe-region ( $k_1$ ) and linear-region ( $k_2$ ) stiffness values between the human and ovine species for both the ALL and PLL.

Overall, the ovine ligaments were both found to be higher in stiffness than the human ligaments, with the ALL being stiffer than the PLL. The main function of the ligaments is to resist tensile loads and to restrict the range of motion of the spine within specific limits (Chapter 1, Section 1.2.1.5). The ALL and PLL span the anterior and the posterior aspect of the spine protecting the spinal cord during hyperextension and hyperflexion, respectively. Both the ligaments experience different amounts of loading as well as varied range of motions (Chazal, et al., 1985; Pintar, et al., 1992; Myklebust, et al., 1988), so it is not surprising that their stiffness values differ. These differences between ALL and PLL could be due to the differences in their sizes, their underlying material properties, or both. In terms of their sizes, during dissection, a visual comparison suggested the ALL to be almost double the thickness of the PLL in both human and ovine specimens. This difference was also reported previously, with the cross sectional areas (CSAs) of the ALL and PLL in the literature (presented in Chapter 1, Table 1.9), ranging from 22.4 - 65.5 mm<sup>2</sup> for the ALL, and only 5 - 25.7 mm<sup>2</sup> for the PLL. If the material properties are assumed to be similar across the two ligaments, and in this study the gauge length was also similar (i.e. the distance across the dissected disc), then the difference in the CSA between the two will result in higher stiffness for the ALL. The ratio between the ALL and PLL stiffness values seen in this study fall within the ratio of cross-sectional areas reported in the literature, suggesting that the stiffness differences could be entirely due to geometry. However, in reality, some differences were also found in the material properties as discussed in the next section.



**Figure 5.1: Comparison of mean bilinear stiffness for human (n=7x2) and ovine (n=6x2) ALL and PLL.**

A one-way analysis of variance (ANOVA,  $p < 0.05$ , post-hoc Fisher's least significant difference) was performed to statistically compare the stiffness between human and ovine ALL and PLL specimens. Four separate ANOVAs were performed to compare ALL and PLL toe-region and linear-region stiffness respectively. The results are presented in Table 5.1. A statistically significant difference was found only between the human and ovine ALL linear region stiffness. The difference could be due to the additional bending that the anterior ligaments have to undergo in the case of the relatively straight ovine spine, due to the body mass pulling downwards. Whereas in the human, the body weight is anterior to the spine so it is pulling the body forward, meaning the ligaments and muscles in the posterior of the spine would be expected to be more in tension than at the anterior of the spine. This has also been analysed by Smit, T.H. (2002) who believed the ventral part of the ovine trunk is stretched under its own weight, while the dorsal part is compressed. This compressive force is thought to be resisted by the spine itself whereas the stretching is counterbalanced by the tensile structures such as the muscles and the ligaments in order to maintain the spinal alignment against gravitational forces (Smit, 2002). He also found the quadruped trunk to be subjected to high extension moments on the posterior column during gallop, indicating a possible explanation for the stiffer ALL in the ovine spine.

**Table 5.1: Results of ANOVA performed to compare the stiffness between human and ovine ALL and PLL specimens separately for the toe-region (K1) and linear-region (K2) stiffness.**

Specimen Stiffness category	P-Value
ALL_K1	0.204
ALL_K2	0.0122
PLL_K1	0.424
PLL_K2	0.447

As the ligaments tend to be in pre-tension in situ, they are more likely to be operating in the linear-region of the load-displacement curve during loading. The higher linear-region stiffness (Figure 5.1) in the ovine ALL potentially has repercussions if researchers are using the ovine spine as an experimental animal model for spine research, since this is the region of the load-displacement curve with greatest difference between the ovine and human spines. For example, spinal stabilization devices have been tested in live ovine models to evaluate their performance (Gunzburg, et al., 2009; Tichota, et al., 2009). If the ligaments are stiffer, then they are likely to hold the components in place, increasing the stability while reducing the risk of component movement compared to the human spine. This means that spinal components which are approved for clinical trial or for human use as a result of the success of testing in an ovine model (in devices where the longitudinal ligaments are retained) could be less successful in humans because the stabilizing forces provided by the human longitudinal ligaments will be smaller. It should be noted, though, that the bending stiffness of the spine is dependent on other factors such as the cross-sectional area of the attaching vertebrae, which is greater for lumbar human vertebrae than for ovine (Wang, et al., 2016; Wilke, et al., 1997). The smaller size of the ovine vertebrae might counteract the higher stiffness of their ligaments which means the effect of the stiffer ligaments on the overall segment stiffness might not be as dominant as anticipated. Another confounding factor is that ovine vertebrae, like other quadrupeds, are known to have higher bone densities than human vertebrae (Aerssens, et al., 1998; Nafei, et al., 2000) indicating that they are subject to greater axial compression stress and hence are believed to be stiffer and stronger than human (Smit, 2002). Indeed, a study by Smit et al. (2000) found that lumbar vertebrae of goats were approximately as strong as humans lumbar vertebrae despite having only 25% of the cross-sectional area. Moreover, Hauerstock et al. (2001) measured axial loads in the live ovine lumbar spines and found that the

vertical stresses in the ovine exceeded those in the human (Wilke, et al., 1999) by a factor of 1.2 to 2.4 in a variety of daily activities. The vertebrae in ovine spines will likely deform less under axial loads and moments due to their higher stiffness (adding to the segment stiffness) as well as providing better support for implant fixation due to their higher strength. The higher loads that the ovine spine are subjected to are likely due to the greater muscle forces needed to counterbalance the bending moments that the horizontal trunk has to sustain (Smit, 2002). These muscle forces also add to compress the segment, increasing its stiffness. It is difficult to unpick the role of these individual components, but it seems likely that the stiffer anterior ligaments combined with stiffer, stronger vertebrae and greater supporting muscle forces will provide a stronger mechanical hold on spinal implants than the human spine. Therefore, these distinctive interspecies differences, including the ligament properties, should be borne in mind in preclinical testing when making a transition from the ovine model to humans.

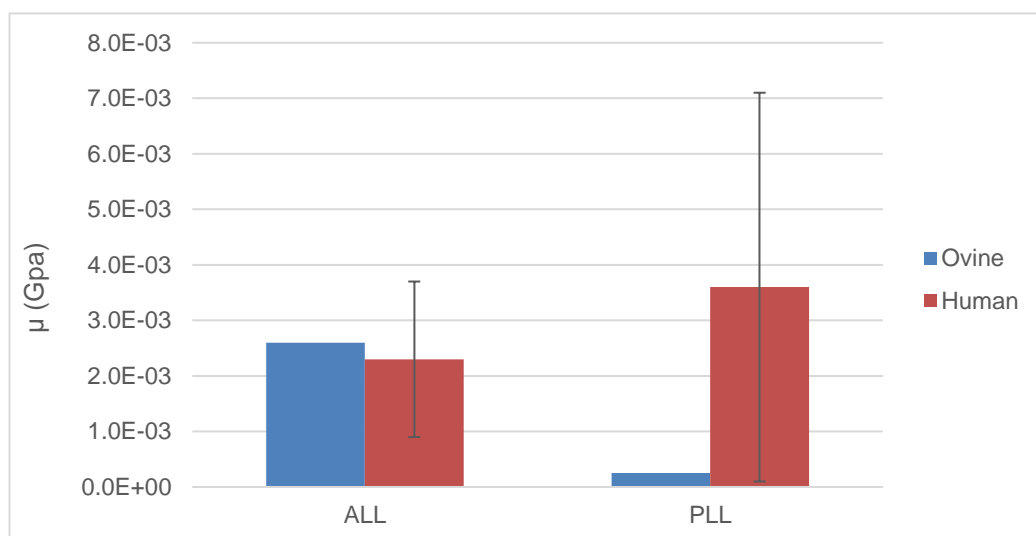
### **5.3 Comparison of the material parameters of human and ovine ligaments**

In order to derive material constants for the ligaments, it was necessary to generate specimen-specific finite element models of the ligament and bony attachments. This procedure was first developed for the ovine spines, but since it was time-consuming to undertake, it was only applied to one PLL and one ALL specimen as a proof of concept. It was then applied to all the human specimens tested, requiring the construction of 14 specimen-specific models which were each iteratively changed to obtain the best fit to the corresponding experimental data. Two material models, hyperfoam and Ogden ( $N = 1$ ) were used to describe the behaviour of the ligaments. For making comparisons between species, either material model could be used since the parameters for both were found to be quite similar to each other (see Figure 4.12 and 4.13). Furthermore, the material parameter  $\mu$  is directly related to  $D$  (Equation 3.3, Chapter 3) therefore, altering either would automatically change the value of other. Hence, for the purpose of this discussion, we can neglect  $D$  and assume that for the Ogden ( $N=1$ ) material model, the toe-region is influenced mostly by  $\mu$ , while the later, more linear, region is influenced primarily by  $\alpha$ . Figure 5.2 and Figure 5.3 presents a comparison of both material parameters for the two species.

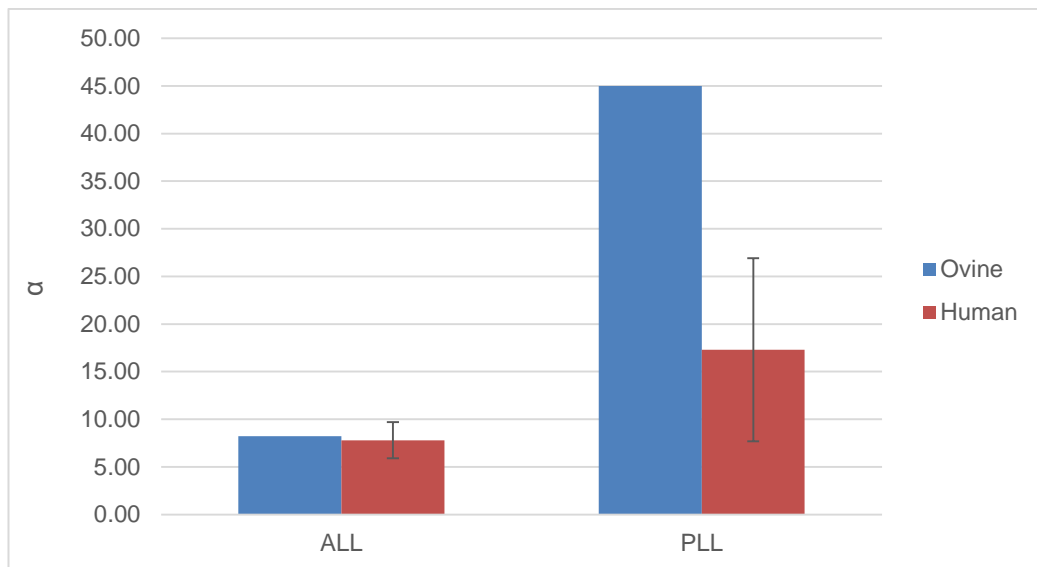
This comparison should be treated with some caution. The material parameters for both the ligaments, the ALL and PLL, for the human specimens (showed a

lot of variability across the different spines (see Chapter 4), which is seen in the large error bars observed in the figures. Moreover, unlike the experimental stiffness values, for the material parameters only one ovine specimen for each ligament was characterised (see Chapter 3), making the comparison even less robust and meaning inferential statistical evaluation was not possible.

The figures show that, given the variability, both the material parameters appear to be very similar in terms of the ALL for the two species, whereas a large difference can be observed in terms of the PLL. Specifically, the  $\mu$  values for both the ALL and PLL ovine specimens fall within the 95% range of the respective human data (i.e. less than two standard deviations from the mean). Whereas, the  $\alpha$  value for only the ovine ALL falls within the 95% range of the human ALL. For the PLL, the ovine material parameter  $\alpha$  differs by more than two standard deviations of the mean of the human value. The difference could be due to the difference in the level of the specimens used or due to the differences in the structural composition of the ligaments themselves. For the human samples, the PLL specimens were mainly from level T6 and above, whereas the ovine specimen used was from level T2-3. The ovine PLL specimen had lower  $\mu$  but a higher  $\alpha$  than the mean human values which might mean the composition of PLL in the ovine specimen had a higher elastin content than the human PLL or maybe the collagen fibrils in the human PLL are more crimped compared to the ovine PLL. Further specimens would be required to undertake a more thorough investigation of these differences. A histological analysis and comparison of the ovine and human ligaments structure would benefit such a speculation, however, to authors knowledge no study has been published that helps support this.



**Figure 5.2: Comparison of material parameter  $\mu$  between human (n=7x2) and ovine ALL and PLL with the standard deviation error bars.**



**Figure 5.3: Comparison of material parameter  $\alpha$  between human (n=7x2) and ovine ALL and PLL.**

#### 5.4 Comparison with the literature on other ligaments

To author's knowledge, no studies have been published that compare the material parameters between human and ovine spinal ligaments. Therefore, a direct comparison of material parameters obtained as a result of this study is not possible. However, Asgari & Rashedi (2018) recently published a study implementing hyperelastic constitutive models on four different knee ligaments. The authors made a comparison between the human and ovine ligament properties to evaluate the suitability of usage of ovine specimens for testing of knee interventions and devices as an alternative for human specimens. They carried out tensile testing on individual samples of ovine knee ligaments and curve-fitted the data using an optimization algorithm to three constitutive models, including an Ogden (3rd order) model as well as Yeoh and Fung–Demiray models, to derive the material parameters/coefficients. The material parameters were then compared with the coefficients of constitutive models of human knee ligaments obtained from two different studies in literature (Wan, et al., 2015; Arnoux, et al., 2002). The results showed that the Ogden model was the best at fitting closely to the experimental-behaviour of the ligaments, and there were huge variations in the results of the coefficients for the other two constitutive models. This reflects the results seen here in terms of showing the effectiveness of using Ogden model for simulating the behaviour of ligamentous soft tissue. The paper also demonstrates the importance of specimen-specific FE models with the implementation of constitutive material behaviour because the inaccuracy in results due to the assumed geometric parameters in calculating initial nominal stress and strain in individual ligament

samples (as described in Chapter 1, Section 1.2.5.4), can be eliminated. Moreover, from the above studies, the human ligament study by Wan et al. (2015) used a comparatively similar strain-rate (10 mm/min) to the ovine study (20 mm/min) and resulted in analogous material parameters, as opposed to the study by Arnoux et al. (2002) who used very high strain rate (1.98 m/s). This demonstrates the importance of using similar strain-rates for comparative testing across species such as the one used in this study. While the Asgari & Rashedi (2018) study provides material coefficients for the knee ligaments, from the current work, it is clear that these cannot be readily converted to determine the overall ligament stiffness because the stiffness requires additional physical attributes, such as the non-uniform cross-sectional area and length, whereas the material properties are dictated purely by the shape of the stress-strain curve.

In terms of the comparison of stiffness, and discounting the study by Arnoux et al. (2015) due to the large difference in strain rate, between the other two studies with comparatively similar strain-rates, the ovine knee ligaments were found to be slightly less stiff than the human. This is the opposite to what was found in this study on the spinal ligaments, but there are many differing factors in the knee. A direct comparison between the aforementioned study and the current work cannot be made, since there were many differences in the testing procedures and data acquisition. It is, however, interesting to note that the material parameters,  $\alpha$  and  $\mu$ , for the anterior cruciate ligament (ACL) from the Ogden model were roughly of the same order of magnitude to those of the ALL and PLL from the current study.

Two other studies which have characterised the human ACL at the same strain rate of 1/s have reported a lot of variability in the tangent modulus, i.e. the terminal slope of the nominal stress versus nominal strain response curve (Noyes & Grood, 1976; Chandrashekar, et al., 2006). This had been attributed to the sensitivity of the tangent modulus to discrepancies associated with the method of strain measurement and uncertainties in strain determination, e.g. difficulty in deciding the initial length of the ligament because of its non-uniform structure (McLean, et al., 2015). It has also been attributed to the differences in age and gender of the specimens. This shows the importance of keeping the methodology consistent when making interspecies as well as intra-species comparisons. It also shows the advantage of specimen-specific modelling to derive the data for the particular specimen to reduce the error associated with testing regime and data acquisition. All three studies above used different pre-loads (pre-strain) which had inevitable effects on the differences observed in the resulting parameters. Also, it shows the benefit of in-situ modelling where

the ligament are in the state of pre-stress that they would be in vivo. This eliminates the error caused by inaccurate implementation of this important factor at low stresses, as described previously in Chapter 1, Section 1.2.6.5.

In a geometrically accurate model of the ligament such as in the current study, assigning the material properties with uniform cross sectional area and length is analogous to modelling the ligaments as spring elements whereby the spring elements assumes a uniform geometry. A plethora of computational studies have been performed to model the behaviour of knee ligaments as bundles of point-to-point, tension-only, nonlinear spring elements. Most of these studies focussed on modelling the global behaviour of the knee joint (Harris, et al., 2016; Halonen, et al., 2016; Ali, et al., 2017; Fitzpatrick, et al., 2014; Yoon, et al., 2010) so the prediction of accurate strains within the ligament structure was not considered imperative. The studies where the aim of model was to focus on characterising the biomechanics of ligament itself or where the interactions between ligaments and surrounding tissues were imperative, importance was given to the geometric realism of the ligament (Mootanah, et al., 2014; Westermann, et al., 2013; Song, et al., 2004; Ramaniraka, et al., 2005). Since the structure of the ligament is non-uniform, as shown by the current work and many other published studies, modelling it as uniform spring elements covering approximately the same area as the real ligament is unlikely to be completely representative. To author's knowledge, only one study has been published recently that directly compares geometric modelling approaches in ligament between two separate subject-specific finite element knee models (Beidokhti, et al., 2016). One model was developed with 1D non-linear, tension-only spring elements (bundles) while the other one was modelled using 3D nonlinear solid elements using transversely isotropic material using the Holzapfel–Gasser–Ogden model. The ligament properties in both the models were initially inputted from literature values and were then optimised using knee motion data validated against cadaveric experimental tests. The authors found that both optimised models were able to follow the experimental translations in flexion, however, the anatomically accurate model was in better agreement with the experimentally measured translations. This shows that optimising the material parameters can achieve behaviour that closely matches the experimental kinematics, but the anatomically accurate structure with optimised mechanical behaviour will be better at simulating the full biomechanics of the joint. The study also showed the importance of implementing specimen-specific test data for optimisation, because employing the properties directly from the literature was shown to provide incorrect solutions.



In summary, the most comparable work on other ligaments in the body is almost wholly in the knee. While direct comparisons with the current study are not possible, it is interesting that the same material model (Ogden) has proved effective and that the same specimen-specific approaches are being shown to be necessary to derive the material properties accurately.

## **5.5 Limitations and future work**

### **5.5.1 Limitations**

A number of limitations have been identified in the experimental and computational analyses conducted throughout this work:

- A relatively small number of specimens were used in this work hence based on the results of this study, we cannot make any definite statements about the whole population.
- Although it had initially been planned to derive properties for both ligaments of each specimen, and so they were tested with sequential removal of the other tissues, this was not possible within the timeframe of the study, due to the need to develop image-based FE models to derive accurate properties. Also building true-to-life FE models of both the ligaments would require modelling of the disc as well, which would have added further complexity to the model. However the image and experimental data was collected and could be used in subsequent studies.
- A limited age range was used for the human specimens which all came from elderly cadavers; this limits the significance of the results since we can only make speculations about how the young specimens would behave in comparison to our data.
- Only the thoracic region of the spine was used in this study which is held in place by the rib cage, restricting its motion. Hence, there were more differences observed between spines than within spines. If the study were to be performed on longer spinal sections including the cervical or lumbar regions, than it may be possible to observe trends within spines.
- The human specimens had to go through a number of freeze/thaw cycles before being used. This might have affected the properties of the soft tissues involved. Although there is some evidence that the tensile properties of ligaments appear to remain unaffected by freezing (Mathews & Ellis, 1968; Nordwall, 1973), it cannot be ruled out.
- The tissue had to be used in its untreated state, hence no histology was performed prior to testing and since specimens were tested to failure, it

would be difficult to determine the undamaged structure from post-test histology, which might have helped in making any relations between the composition of the tissue and its material parameters. This could have helped in developing compositional differences, if any, between the ALL and PLL and between the human and ovine ligaments.

- A significant proportion of this study was spent on the development of a technique for characterising the ligaments, including a large amount of preliminary testing to make it repeatable. Although a workable solution was achieved, the technique developed for the image segmentation is time consuming, with a combination of hand and manual segmentation, because of the irregular shape of ligaments and with the change in the thickness of the fibres.
- Although in-situ testing is better than full extraction of ligaments for maintaining the pre-load, the results in Chapter 2 suggest that there can still be changes in length due to disc hydration. Keeping the discs hydrated to the same amount is another major challenge, especially without the ligaments over-swelling.
- The computational models developed in this study were only calibrated against experimental results obtained for the same specimens under axial tension. Therefore, the image based specimen specific approach should be considered validated only under these conditions. Moreover, care should be taken when applying the same approach to model experimental boundary conditions that deviate from the ones used in this study.

### **5.5.2 Future recommendations**

There are a few suggested directions for the future development of this work. To address a number of the limitations, testing more specimens would be required. An early focus should be to develop a method that could be more rapidly applied. This includes developing automated methods for segmentation and material optimisation which are the two most time-consuming aspects of the FE part of the work. Once achieved, the datasets from this project could be further analysed to derive properties for the other ligament in each test, plus properties for all of the ovine specimens (not just one). The technique could then be performed on longer sections of the spine including cervical, thoracic and the lumbar regions to establish any trends within spine. Studies could also be undertaken across wider population including young and middle age as well as elderly specimens to establish the differences, if any, that aging has on the mechanical characteristics of the ligaments.

Furthermore, a histological analysis of the ligament structure for both human and ovine spines would be useful to establish a relationship, if any, between the material parameters and the ligament composition. Such a study would help distinguish if the differences in the ligament stiffness between the two species exist due to differences in structural composition or differences in their physical geometry. Also, such a study can also help differentiate if the ligaments have any change in their structural composition due to a diseased state of corresponding tissues, such as ossification of discs.

Moreover, the Holzapfel-Gasser-Ogden model, which was recently used successfully to model the anisotropic behaviour of the spinal ligaments (Hortin & Bowden, 2016) could be explored further. However, the authors implemented the material model on ligaments which were modelled as tension-only shell elements with constant cross-sectional areas. The results presented in this thesis indicate that the non-uniform shape and cross-sectional area are fundamental aspects of modelling the true behaviour of ligaments. Thus, combining the material model from Hortin & Bowden with the approach developed in this study could produce more true-to-life results.

## **5.6 Conclusion**

To the author's knowledge this is the first study to characterize ovine spinal longitudinal ligaments and compare them with the human. The combined experimental and computational approach developed in this study to determine the material properties of the spinal ligaments marks a step change from the current state-of-art and will enable the mechanical contribution of the ligaments to be more realistically represented in future FE models. In addition to the methodology development itself and derivation of the longitudinal ligament properties, the outcomes of this study also demonstrated that (i) a specimen-specific image-based approach needs to be applied to derive the elastic properties of the spinal longitudinal ligaments due to their non-uniform shape and cross-sectional area; and (ii) there are differences between the stiffness values of human and ovine longitudinal ligaments, particularly for the ALL. This may have implications for the use of ovine models for preclinical testing of products such as spinal stabilisation devices. These differences should be borne in mind alongside other factors that affect the segment stiffness to ensure there is not a more favourable mechanical environment with increased stability compared to the human spine.

The approaches developed in this study can go on to be applied more widely to determine the properties of a greater range of spinal ligamentous tissue and provide more realistic data for future computational models.

## List of References

ABAQUS, 2011. *ABAQUS Documentation*, Providence, RI, USA: Dassault Systèmes.

ABAQUS, 2014. *Solid (continuum) elements*. [Online] Available at: <https://www.sharcnet.ca/Software/Abaqus/6.14.2/v6.14/books/usb/default.htm?startat=pt06ch28s01alm01.html> [Accessed 15 07 2018].

Abraham, A. C. et al., 2011. Hyperelastic properties of human meniscal attachments. *J Biomech*, 44(3), pp. 413-418.

Aerssens, J., Boonen, S., Lowet, G. & Dequeker, J., 1998. Interspecies difference in bone composition, density and quality; Potential implications for in vivo bone research. *Endocrinology*, Volume 139, pp. 663-670.

Ali, A. A. et al., 2017. Combined Measurement and Modeling of Specimen-Specific Knee Mechanics for Healthy and ACL-deficient Conditions. *J Biomech*, Volume 57, pp. 117-124.

Anton, 2011. *Circular segment*. [Online] Available at: <https://planetcalc.com/1421/> [Accessed 23 08 2018].

Arnoux, P. J., Chabrand, P., Jean, M. & Bonnoit, J., 2002. A visco-hyperelastic model with damage for the knee ligaments under dynamic constraints. *Comput Methods Biomech Biomed Eng*, 5(2), pp. 167-174.

Asazuma, T., Stokes, I., Moreland, M. & Suzuki, N., 1990. Intersegmental spinal flexibility with lumbosacral instrumentation: An in vitro biomechanical investigation. *Spine*, Volume 15, pp. 1153-1158.

Aspden, R., 1992. Review of the functional anatomy of the spinal ligaments and the lumbar erector spinae muscles. *Clinical anatomy*, Volume 5, pp. 372-387.

Autodesk Inc., 2014. *Hyperfoam Material Properties*. [Online]  
Available at: <https://knowledge.autodesk.com/support/simulation-mechanical/learn-explore/caas/CloudHelp/cloudhelp/2014/ENU/SimMech/files/GUID-FAE1B469-B1E7-4F1B-94F4-2A627634E7EB-htm.html>

[Accessed 07 03 2018].

Banton, R., 2012. Biomechanics of The Spine. *Journal of The Spinal Research Foundation*, 7(2), pp. 12-20.

Beidokhti, H. N. et al., 2016. *Subject-specific knee ligaments modeling approaches in finite element analysis: 1d and 3d*. Lyon, 22nd Congress of the European Society of Biomechanics.

Bellini, C. et al., 2007. Biomechanics of the lumbar spine after dynamic stabilisation. *J Spinal Diord Tech*, 20(6), pp. 423-429.

Benjamin, M., Evans, E. & Copp, L., 1986. The histology of tendon attachments to bone in man. *J Anat*, Volume 149, pp. 89-100.

Beomkeun, K., Lee, S. B., Lee, J. & et al., 2012. A comparison among Neo-Hookean model, Mooney-Rivlin model, and Ogden model for chloroprene rubber. *International Journal of Precision Engineering and Manufacturing*, 13(5), pp. 759-764.

Bernick, S. & Cailliet, R., 1982. Vertebral end-plate changes with aging of human vertebrae. *Spine*, 7(2), p. 97.

Bevan, S., 2012. *The Impact of Back Pain on Sickness Absence in Europe*. [Online]

Available at: [http://www.theworkfoundation.com/DownloadPublication/Report/313\\_The%20Impact%20of%20Back%20Pain%20on%20Sickness%20A](http://www.theworkfoundation.com/DownloadPublication/Report/313_The%20Impact%20of%20Back%20Pain%20on%20Sickness%20A)

[Accessed 06 05 2014].

Blumenthal, S. et al., 2005. A prospective, randomised, multicenter food and drug administration investigational device exemptions study of lumbar total disc replacement with the CHARTIE artificial disc versus lumbar fusion: Part I: Evaluation of clinical outcomes. *Spine*, 30(14), pp. 1565-75.

Bogduk, N., 2005. *Clinical anatomy of the lumbar spine and sacrum*. 4th ed. s.l.:Elsevier Ltd.

Bogduk, N., 2012. *Clinical and radiological anatomy of the lumbar spine*. London ed. London: Elsevier Health Sciences.

Bowden, A. et al., 2008. Quality of motion considerations in numerical analysis of motion restoring implants of the spine. *Clinical Biomechanics*, Volume 23, pp. 536-544.

Bowden, A. et al., 2008. Quality of motion considerations in numerical analysis of motion restoring implants of the spine. *Clinical Biomechanics*, Volume 23, pp. 536-544.

Carl, J., Müller-Hoeppe, D. & Meadows , M., 2006. *Comparison of Tetrahedral and Brick Elements for Linear Elastic Analysis*, Denver: University of Colorado Boulder.

Chandrashekar, N., Mansouri, H. & Slauterbeck, J., 2006. Sex-Based Differences in the Tensile Properties of the Human Anterior Cruciate Ligament. *J Biomech*, 39(16), pp. 2943-2950.

Chazal, J. et al., 1985. Biomechanical properties of spinal ligaments and a histological study of the supraspinal ligament in traction. *J. Biomechanics*, 18(3), pp. 167-176.

Cheng, T. & Gan, R. Z., 2008. Mechanical properties of anterior malleolar ligament from experimental measurement and material modeling analysis. *Biomech Model Mechanobiol*, 7(5), p. 387–394.

Chen, S.-H.et al., 2009. Biomechanical comparison between lumbar disc arthroplasty and fusion. *Medical Engineering & Physics*, Volume 31, pp. 244-253.

Cheung, J., Zhang, M. & Chow, D., 2003. Biomechanical responses of the intervertebral joints to static and vibrational loading: a finite element study. *Clin Biomech*, Volume 18, pp. 790-799.

- Cifuentes, A. O. & Kalbag, A., 1992. A performance study of tetrahedral and hexahedral elements in 3-D finite element structural analysis. *Finite Elem Anal Des*, 12(3-4), p. 313–318.
- Cooper, R. & Misol, S., 1970. Tendons and ligament insertion. A light and electron microscope study. *J Bone Joint Surg*, 52(A), pp. 1-20.
- Coric, D. & Mummaneni, P., 2007. Nucleus replacement technologies. *Jornal of neurosurgery: Spine*, 8(2), pp. 115-120.
- Cramer, G. D. & Darby, S., 2014. *Clinical Anatomy of the Spine, Spinal Cord, and ANS*. 3rd ed. s.l.:Elsevier Health Sciences.
- Dai, C. et al., 2015. Construction of finite element model and stress analysis of anterior cruciate ligament tibial insertion. *Pak J Med Sci.*, 31(3), p. 632–636.
- Dhafer, Y., Kwon, T. -H. & Schroeder, M., 2010. The Effect of Connective Tissue Material Uncertainties on Knee Joint Mechanics under Isolated Loading Conditions. *J Biomech*, 43(16), p. 3118–3125.
- Dorlot, J., Ait Ba Sidi, M., Tremblay, G. & Drouin, G., 1980. Load elongation behaviour of the canine anterior cruciate ligament. *J Biomech Eng*, Volume 102, pp. 190-193.
- Dumas, G., Beaudoin, L. & Drouin, G., 1987. In situ mechanical behaviour of posterior spinal ligaments in the lumbar region. An in vitro study. *J. Biomechanics*, 20(3), pp. 301-310.
- Edgar, M. & Ghadially, J., 1976. Innervation of the lumbar spine. *Clin Orthop*, Volume 115, pp. 35-41.
- Eidelson, S., 2012. *Spinal ligaments and tendons*. [Online] Available at: <http://www.spineuniverse.com/anatomy/spinal-ligaments-tendons> [Accessed 02 04 2013].
- Ellis, B., Lujan, T., Dalton, M. & Weiss, J., 2006. Medial collateral ligament insertion site and contact forces in the ACL-deficient knee. *J. Orthop. Res.*, 24(4), pp. 800-810.



Emory University, 1997. *The Vertebral Column and Spinal Cord*. [Online] Available at: <http://www.emory.edu/ANATOMY/AnatomyManual/back.html> [Accessed 17 07 2014].

Farfan, H. et al., 1970. The effects of torsion on the lumbar intervertebral joints: The role of torsion in the production of disc degeneration. *J Bone Joint Surg*, Volume 52A, p. 468.

Fitzpatrick, C. K., Komistek, R. D. & Rullkoetter, P. J., 2014. Developing simulations to reproduce in vivo fluoroscopy kinematics in total knee replacement patients. *J Biomech*, 47(10), pp. 2398-2405.

Francois, R., 1975. Ligament insertions into the human lumbar vertebral body. *Acta Anat*, Volume 91, pp. 467-480.

Freeman, B. & Davenport, J., 2006. total disc replacement in the lumbar spine: A systematic review of the literature. *Eur Spine J*, Volume 15, pp. 439-47.

Fung, Y., 1993. *Biomechanics: mechanical properties of living tissues*. 2nd ed. New York: Springer-Verlag.

Gan, R. Z., Yang, F., Zhang, X. & Nakmali, D., 2011. Mechanical properties of stapedial annular ligament. *Med Eng Phys*, 33(3), pp. 330-339.

Gillespie, K. & Dickey, J., 2004. Biomechanical role of lumbar spine ligaments in flexion and extension: determination using a parallel linkage robot and a porcine model. *Spine*, Volume 29, pp. 1208-1216.

Giori, N., Beaupre, G. & Carter, D., 1993. Cellular shape and pressure may mediate mechanical control of tissue composition in tendons. *J Orthop Res*, 11(4), pp. 581-591.

Goel, V., Monroe, B., Gilbertson, L. & Brinckmann, P., 1995a. Interlaminar shear stresses and laminae separation in a disc - Finite element analysis of L3-L4 motion segment subjected to axial compressive loads. *Spine*, 20(6), pp. 689-698.

Goel, V., Ramirez, S., Kong, W. & Gilbertson, L., 1995b. Cancellous bone Young's modulus variation within the vertebral body of a ligamentous lumbar

spine – application of bone adaptive remodelling concepts. *Journal of Biomechanical Engineering*, Volume 117, pp. 266-271.

Gray, H., 1944. *Anatomy, descriptive and applied*. 28th ed. London: Longmans, Green & Co.

Guan, Y. et al., 2006. Validation of a clinical finite element model of the human lumbosacral spine. *Medical and Biological Engineering and Computing*, 44(8), pp. 633-641.

Gunzburg, R., Fraser, R. D., Moore, R. & Vernon-Roberts, B., 1993. An experimental study comparing percutaneous discectomy with chemonucleolysis. *Spine (Phila Pa 1976)*, 18(2), pp. 218-226.

Gunzburg, R. et al., 2009. Effect of a novel interspinous implant on lumbar spinal range of motion. *Eur Spine J*, 18(5), p. 696–703.

Gunzburg, R. et al., 2009. Effect of a novel interspinous implant on lumbar spinal range of motion. *Eur Spine J.*, 18(5), p. 696–703.

Haer, T. et al., 1992. Instantaneous axis of rotation as a function of the three columns of the spine. *Spine*, 17(6), pp. 149-154.

Halonen, K. S. et al., 2016. Optimal graft stiffness and pre-strain restore normal joint motion and cartilage responses in ACL reconstructed knee. *J Biomech*, 49(13), pp. 2566-2576.

Harris, M. D. et al., 2016. A Combined Experimental and Computational Approach to Subject-Specific Analysis of Knee Joint Laxity. *J Biomech Eng*, 138(8), p. 0810041–0810048.

Hasberry, S. & Pearcy, M., 1986. Temperature dependence of the tensile properties of interspinous ligaments of sheep. *J Biomed Eng*, Volume 8, pp. 62-66.

Hashemi, J., Chandrashekar, N. & Slauterbeck, J., 2005. The Mechanical Properties of the Human Patellar Tendon are Correlated to its Mass Density and are Independent of Sex. *Clinical Biomechanics*, Volume 20, pp. 645-652.

Hauerstock, D., Reindl, R. & Steffen, T., 2001. Telemetric measurement of compressive loads in the sheep lumbar spine. *Transactions of the 47th Annual Meeting of the Orthopaedic Research Society*, Volume 26, p. Article 391.

Herbert, A. et al., 2016. Bi-linear mechanical property determination of acellular human patellar tendon grafts for use in anterior cruciate ligament replacement. *J Biomech.*, 49(9), p. 1607–1612.

Heuer, F. et al., 2007. Stepwise reduction of functional spinal structures increase range of motion and change lordosis angle. *Journal of Biomechanics*, Volume 40, pp. 271-280.

Hickey, D. & Hukins, D., 1979. Effects of methods of preservation on the arrangement of collagen fibrils in connective tissue matrices: an x ray diffraction study of annulus fibrosus. *Connective Tissue Res*, Volume 6, pp. 223-228.

Hirsch, C., 1955. The reaction of intervertebral discs to compression forces. *J. bone joint surg.*, Volume 37A, p. 1188.

Hirsch, C., Ingelmark, B. & Miller, M., 1963. The anatomic basis of low back pain. *Acta Orthop Scand*, Volume 33, pp. 1-17.

Hollenstein, M., 2008. *Mechanical Characterization of soft materials: Comparison between different experiments on synthetic materials*, Zurich: Center of Mechanics, ETH.

Hortin, M. S. & Bowden, A. E., 2016. Quantitative comparison of ligament formulation and pre-strain in finite element analysis of the human lumbar spine. *Comput Methods Biomech Biomed Engin*, 19(16), pp. 1505-1518.

Hughes, D. et al., 1990. Comparison of structure, mechanical properties, and functions of lumbar spinal ligaments. *Spine*, 15(8), pp. 787-795.

Hukins, D. & Aspden, R., 1985. Compositions and properties of connective tissues. *Trends in biochem. Sci.*, Volume 10, pp. 260-264.

Hukins, D. et al., 1990. Comparison of structure, mechanical properties and functions of lumbar spinal ligaments. *Spine*, Volume 15, pp. 787-795.

Ivanov, A., Kiapour, A., Ebraheim, N. & Goel, V., 2009. Lumbar fusion leads to increases in angular motion and stress across sacroiliac joint. *Spine*, 34(5), pp. E162-E169.

Ivanov, A., Kiapour, A., Ebraheim, N. & Goel, V., 2009. Lumbar fusion leads to increases in angular motion and stress across sacroiliac joint. *Spine*, 34(5), pp. E162-E169.

Jackson, H. & Winkelmann, R., 1966. Nerve endings in the human lumbar spinal column and related structures. *J Bone Joint Surg*, Volume 48A, p. 1272.

Jemiolo, S. & Turtletaub, S., 2000. Parametric model for a class of foam-like isotropic hyperelastic materials. *J. Appl. Mech.*, 67(2), pp. 248-254.

Jones, A. C. & Wilcox, R. K., 2007. Assessment of factors influencing finite-element vertebral predictions. *J. Biomech. Eng*, Volume 129, p. 898–903.

Kandziora, F. et al., 2001. Comparison Between Sheep and Human Cervical Spines: An Anatomic, Radiographic, Bone Mineral Density, and Biomechanical Study. *Spine*, 26(9), pp. 1028-1037.

Kiapour, A. et al., 2014. Finite Element Model of the Knee for Investigation of Injury Mechanisms: Development and Validation. *J Biomech Eng.*, 136(1), p. 0110021–01100214.

Kim, Y., 2007. Finite element analysis of anterior lumbar interbody fusion. *Spine*, 32(23), pp. 2558-2568.

Kirby, M., Sikoryn, T., Hukins, D. & Aspden, R., 1989. Structure and mechanical properties of the longitudinal ligaments and ligamentum flavum of the spine. *J. Biomed Eng*, Volume 11, pp. 192-196.

Kotani, Y. et al., 1996. The role of spinal instrumentation in augmenting lumbar posterolateral fusion. *Spine (Phila Pa 1976)*, 21(3), pp. 278-287.

Kumar, N. & Venkateswara Rao, V., 2016. Hyperelastic Mooney-Rivlin model: determination and physical interpretation of material constants. *MIT International Journal of Mechanical Engineering*, 6(1), pp. 43-46.

- Lee, K. & Teo, E., 2004. Poroelastic analysis of lumbar spinal stability in combined compression and anterior shear. *Spinal Disord Tech*, 17(5), pp. 429-438.
- Lee, K. & Teo, E., 2005. Material sensitivity study on Lumbar motion segment (L2-L3) under sagittal plane loadings using probabilistic method. *Spinal Disord Tech*, 18(2), pp. 163-170.
- Levangie, P. K. & Norkin, C. C., 2011. *Joint Structure and Function: A Comprehensive Analysis*. 5th ed. Philadelphia: F.A.Davis Company.
- Li, G., Kanamori, A. & Woo, S., 1999. A validated three-dimensional computational model of a human knee joint. *ASME J Biomech Eng*, 121(6), pp. 657-662.
- Limbirt, G., Taylor, M. & Middleton, J., 2004. Three-dimensional finite element modelling of the human ACL: simulation of passive knee flexion with a stressed and stress-free ACL. *Journal of Biomechanics*, 37(11), pp. 1723-1731.
- Little, J. & Khalsa, P., 2005. Material Properties of the Human Lumbar Facet Joint Capsule. *J Biomech Eng.*, 127(1), pp. 15-24.
- Liu, X. & Zhang, M., 2013. Redistribution of knee stress using laterally wedged insole intervention: Finite element analysis of knee-ankle-foot complex.. *Clin Biomech (Bristol, Avon)*, 28(1), pp. 61-67.
- Martins, P., Natal Jorge, R. M. & Ferreira, A., 2006. A comparative study of several material models for prediction of hyperelastic properties: Application to silicone-rubber and soft tissues. *Strain*, 42(3), pp. 135-147.
- Masharawi, Y. et al., 2008. Vertebral body shape variation in the thoracic and lumbar spine: characterization of its asymmetry and wedging. *Clinical Anatomy*, 21(1), pp. 46-54.
- Mathews, L. & Ellis, D., 1968. Viscoelastic properties of cat tendon: effect of time after death and preservation by freezing. *J Biomech*, Volume 1, pp. 65-71.
- Matyan, J., Anton, M., Shrive, N. & Frank, C., 1995. Stress governs tissue phenotype at the femoral insertion of the rabbit MCL. *J Biomech*, 28(2), pp. 147-157.

McLean, S. G., Mallett, K. F. & Arruda, E. M., 2015. Deconstructing the anterior cruciate ligament: what we know and do not know about function, material properties and injury mechanics. *J Biomech Eng*, 137(2), pp. 020906-020906-19.

Micheau, A. & Hoa, D., 2009. *Anatomical diagrams of the spine and back*. [Online]

Available at: <http://www.imaios.com/en/e-Anatomy/Spine/Spine-diagrams> [Accessed 17 07 2014].

Mommersteeg, T. et al., 1996. Characterisation of the mechanical behaviour of human knee ligaments: a numerical-experimental approach. *J Biomech*, 29(2), pp. 151-160.

Mooney, M., 1940. A theory of large elastic deformation. *Journal of Applied Physics*, 11(9), p. 582–592.

Moore, K. L. & Dalley, A. F., 1999. *Clinically Oriented Anatomy*. 4th ed. s.l.:Lippincott Williams & Wilkins.

Moore, R., Osti, O., Vernon-Roberts, B. & Fraser, R., 1992. Changes in endplate vascularity after an outer annulus tear in the sheep. *Spine*, Volume 17, pp. 874-878.

Mootanah, R. et al., 2014. Development and validation of a computational model of the knee joint for the evaluation of surgical treatments for osteoarthritis. *Comput Methods Biomech Biomed Engin*, 17(13), p. 1502–1517.

Moramarco, V., del Palomar, A., Pappalettere, C. & Doblare, M., 2010. An accurate validation of a computational model of a human lumbosacral segment. *Journal of Biomechanics*, Volume 43, pp. 334-342.

Mosekilde, L., 1993. vertebral structure and strength In vivo and In vitro. *Calcified Tissue International*, 53(Supplement 1), pp. S121-126.

Myklebust, J. et al., 1988. Tensile strength of spinal ligaments. *Spine*, Volume 13, pp. 526-531.

Nachemson, A. & Evans, J., 1968. Some mechanical properties of the third human lumbar interlaminar ligament. *J. Biomechanics*, Volume 1, pp. 221-220.

Nachemson, A. & Morris, J., 1964. In vivo measurements of intradiscal pressure. *J. Bone Joint Surg*, Volume 46, p. 1077.

Nafei, A., Danielsen, C. C., Linde, F. & Hvid, I., 2000. Properties of growing trabecular ovine bone. Part I: Mechanical and physical properties. *J Bone Joint Surg Br*, Volume 82, pp. 910-920.

Nagel, D. A. et al., 1991. A paradigm of delayed union and nonunion in the lumbosacral joint. A study of motion and bone grafting of the lumbosacral spine in sheep. *Spine (Phila Pa 1976)*, 16(5), pp. 553-559.

Naveh, G. et al., 2014. Direct microCT imaging of non-mineralized connective tissues at high resolution.. *Connect Tissue Res.*, 55(1), pp. 52-60.

Niepel, G. & Sitaj, S., 1979. Enthesopathy. *Clinics in rheumatic diseases*, Volume 5, pp. 857-871.

Nordwall, A., 1973. Studies in idiopathic scoliosis. *Acta Orthop Scand*, Volume Suppl 150.

Noyes, F. et al., 1984. Biomechanical analysis of human ligament grafts used in knee-ligament repairs and reconstructions. *J Bone Joint Surg*, 66(A), pp. 344-352.

Noyes, F. R. & Grood, E. S., 1976. The Strength of the Anterior Cruciate Ligament in Humans and Rhesus Monkeys. *J Bone Jt Surg Am*, 58(8), pp. 1074-1082.

Noyes, F., Torvik, P., Hyde, W. & Lelucas, M., 1974. Biomechanics of ligament failure. II . An analysis of immobilisation, exercise and reconditioning effects in primates.. *J Bone Joint Surg*, 56(A), pp. 1406-1418.

NuChiro, 2011. *A disc that matters*. [Online] Available at: <http://nuchiro.wordpress.com/2011/04/18/a-disc-that-matters/> [Accessed 17 07 2014].

Ogden, R., 1997. *Non-Linear Elastic Deformations*. Mineola, NY, Dover.

Ogden, R., Saccomandi, G. & Sgura, I., 2004. Fitting hyperelastic models to experimental data. *Computational Mechanics*, Volume 34, pp. 484-502.

Ogden, R. W., 1972. Large Deformation Isotropic Elasticity - On the Correlation of Theory and Experiment for Incompressible Rubberlike Solids. *Proceedings of the Royal Society of London. Series A, Mathematical and Physical*, 326(1567), pp. 565-584.

PainNeck.com, 2010. *Symptoms of Cervical Facet Joint Disease (Osteoarthritis)*. [Online]

Available at: <http://www.painneck.com/facet-joint-disease-symptoms>  
[Accessed 17 07 2014].

Panagiotacopoulos, N., Pope, M., Block, R. & Krag, M., 1987. Water content in human intervertebral discs. Part II. Viscoelastic behaviour. *Spine*, Volume 12, p. 918.

PANAGOS, A., 2015. *The 10 secrets about your amazing ligaments*. [Online]  
Available at: <http://healthcareextreme.com/2015/12/09/the-10-secrets-about-your-amazing-ligaments/>  
[Accessed 11 01 2018].

Panjabi, M., 1995. The Stabilizing System of the Spine. Part I. Function, Dysfunction, Adaptation, and Enhancement. *Journal of Spinal Disorders*, 5(4).

Panjabi, M., Goel, V. & Takata, K., 1982. Physiological strains in the lumbar spinal ligaments. *Spine*, 7(3), pp. 192-203.

Panjabi, M., Hausfeld, J. & White, A., 1978. *Experimental determination of thoracic spine stability*. s.l., Orthopaedic Research Society Proceedings.

Panjabi, M., Krag, M. H. & Goel, V., 1981. Technique for measurement and description of three dimensional six degree-of-freedom of a body joint with application to human spine. *J Biomech*, Volume 14, pp. 447-460.

Panjabi, M., White, A. & Johnson, R., 1975. Cervical spine mechanics as a function of transection of components. *J Biomech*, Volume 8, p. 327.

Panjabi, M. et al., 1978. Stability of the cervical spine under tension. *J Biomech*, Volume 11, pp. 189-197.

Panjani, M., Goel, V. & Takata, K., 1982. Physiologic strains in the lumbar spinal ligaments. An in vitro biomechanical study. *Spine*, 7(3), p. 192.



Park, H. -S. et al., 2010. A knee-specific finite element analysis of the human anterior cruciate ligament impingement against the femoral intercondylar notch. *J Biomec*, 43(10), p. 2039–2042.

Pech, P., Bergstrom, K., Rauschninh, W. & Haughton, V., 1987. Attenuation values, volume changes and artifacts in tissue due to freezing. *Acta Radiol*, Volume 28, pp. 779-782.

Pederson, H., Blunck, C. & Gardner, E., 1956. The anatomy of the lumbosacral posterior rami and menengial branches of spinal nerves with an experimental study of their function. *J Bone Joint Surg*, Volume 38A, p. 377.

Pena, E., Calvo, B., Martinez, M. A. & Doblare, M., 2005. A three-dimensional finite element analysis of the combined behavior of ligaments and menisci in the healthy human knee joint. *J Biomech*, 39(9), p. 1686–1701.

Penning, L. & Wilmlink, J., 1986. *Posture dependent compression of lumbar dural sac and emerging root sheaths through facet hypertrophy: a dynamic CT-myelographic study..* Dallas, 12th Annual meeting of the international society for the study of the lumbar spine.

Petter, C., 1933. Methods of measuring the pressure of the intervertebral disc. *The Journal of Bone and Joint Surgery*, Volume 15, pp. 365-368.

Pintar, F. et al., 1992. Biomechanical properties of human lumbar spine ligaments. *J. Biomechanics*, 25(11), pp. 1351-1356.

Polikeit, A., Nolte, L. & Ferguson, J., 2003. The effect of cement augmentation on the load. *Spine*, 28(10), pp. 991-996.

Pollintine, P., Dolan, P., Tobias, J. H. & Adams, M. A., 2004. Intervertebral disc degeneration can lead to 'stress-shielding' of the anterior vertebral body: a cause of osteoporotic vertebral fracture?. *Spine*, Volume 29, pp. 774-782.

Pollintine, P., Przybyla, A. S., Dolan, P. & Adams, M. A., 2004. Neural arch load-bearing in old and degenerated spines. *J. Biomechanics*, Volume 37, pp. 197-204.

Posner, I., White, A., Edwards, T. & Hayes, W., 1980. *A biomechanical analysis of the clinical stability of the lumbar and lumbosacral spine*. New Orleans, Annual Meeting of the International Society for Study of the Lumbar Spine.

Prasad, P., King, A. & Ewing, C., 1974. The role of articular facets during +Gz acceleration. *J. appl. mech*, Volume 41, p. 321.

Putz, R. & Müller-Gerbl, M., 1996. The vertebral column--a phylogenetic failure? A theory explaining the function and vulnerability of the human spine. *Clin Anat.*, 9(3), pp. 205-212.

Qiu, T.-X., Tan, K.-W., Lee, V.-S. & Teo, E.-C., 2006. Investigation of thoracolumbar T12-L1 burst fracture mechanism using finite element model. *Med Eng Phy*, Volume 28, pp. 656-664.

Ramaniraka, N. A., Terrier, A., Theumann, N. & Siegrist, O., 2005. Effects of the posterior cruciate ligament reconstruction on the biomechanics of the knee joint: a finite element analysis. *Clin Biomech (Bristol, Avon)*, 20(4), pp. 434-442.

Rivlin, R. S., 1948. Large Elastic Deformations Isotropic Materials. IV. Further Developments of the General Theory. *Philosophical Transactions of the Royal Society A*, 241(835), pp. 379-397.

Rohlmann, A., Zander, T. & Bergmann, G., 2006. Spinal loads after vertebral fractures treated by vertebroplasty or kyphoplasty. *Eur Spine J.*, Volume 15, pp. 1255-1264.

Ruberte, L., Natarajan, R. & Andersson, G., 2009. Influence of single-level lumbar degenerative disc disease on the behavior of the adjacent segments. *Journal of Biomechanics*, Volume 42, pp. 341-348.

Scapinelli, R., 1989. Morphological and functional changes of the lumbar spinous processes in the elderly. *Surgical and Radiologic Anatomy*, 11(2), pp. 129-133.

Schmidt, H. et al., 2007. Application of a calibration method provides more realistic results for a finite element model of a lumbar spinal segment. *Clinical Biomechanics*, Volume 22, pp. 377-384.

- Shahzad, M., Kamran, A., Siddiqui, M. Z. & et al., 2015. Mechanical Characterization and FE Modelling of a Hyperelastic Material. *Material Research*, 18(5), pp. 918-924.
- Sharma, M., Langrana, N. & Rodriguez, J., 1995. Role of ligaments and facets in lumbar spinal stability.. *Spine (Phila Pa 1976)*, 20(8), pp. 887-900.
- Sheng, S.-R. et al., 2010. Anatomy of large animal spine and its comparisons to the human spine: a systematic review. *Eur Spine J*, Volume 19, pp. 46-56.
- Shim, V., Liu, J. & Lee, V., 2005. A technique for dynamic tensile testing of human cervical spine ligaments. *Experimental Mechanics*, Volume 46, pp. 77-89.
- Sikoryn, T. & Hukins, D., 1988. Failure of the longitudinal ligaments of the spine. *J Mat Sci Lett*, Volume 7, pp. 1345-1349.
- Silva, M., Wang, C., Keaveny, T. & Hayes, W., 1994. Direct and computed-tomography thickness measurements of the human lumbar vertebral shell and end-plate. *Bone*, 15(4), pp. 409-414.
- Silva, M., Wang, C., Keaveny, T. & Hayes, W., 1994. Direct and computed-tomography thickness measurements of the human lumbar vertebral shell and end-plate.. *Bone*, 15(4), pp. 409-414.
- Skedros, J. G., 1994. Collagen fiber orientation in skeletal tension/compression systems: A potential role of variant strain stimuli in the maintenance of cortical bone organization. *J Bone Miner Res*, Volume 9, p. S251.
- Slater, R., Nagel, D. & Smith, R. L., 1988. Biochemistry of fusion mass consolidation in the sheep spine. *J Orthop Res*, 6(1), pp. 138-144.
- Smith, L. et al., 2011. Degeneration and regeneration of the intervertebral disc: lessons from development. *Dis Model Mech.*, 4(1), pp. 31-41.
- Smit, T. H., 2002. The use of a quadruped as an in vivo model for the study of the spine – biomechanical considerations. *Eur. Spine J*, Volume 11, p. 137–144.
- Smit, T., Van Dijk, M., Arnoe, M. & Wuisman, P., 2000. The mechanics of absorbable spinal cages perforating the endplates: an in vitro study.

*Transactions of the 46th Annual Meeting of the Orthopaedic Research Society*, 25(Article 349).

Song, Y. et al., 2004. A three-dimensional finite element model of the human anterior cruciate ligament: a computational analysis with experimental validation. *J Biomech*, 37(3), pp. 383-390.

Stillwell, D., 1956. The nerve supply of the vertebral column and its associated structures in the monkey. *Anat Rec*, Volume 125, p. 139.

Stromberg, D. & Wiederhielm, C., 1969. Viscoelastic description of a collagenous tissue in simple elongation. *J. appl. Physiol*, Volume 26, pp. 857-862.

Sylvestre, P.-L., Villemure, I. & Aubin, C.-E., 2007. Finite element modelling of the growth plate in a detailed spine model. *Medical and Biological Engineering and Computing*, Volume 45, pp. 977-988.

Tichota, R. et al., 2009. *A Biomechanical Study of a Limited Motion Device for Lumbar Posterior Stabilization in an Ovine Model*. Las Vegas, 55th Annual Meeting of the Orthopaedic Research Society.

Tkaczuk, H., 1968. Tensile properties of human lumbar longitudinal ligaments. *Acta Orthop. Scand.*, Volume Suppl. 115, p. 69 pp.

Tsuang, Y.-H. et al., 2009. Comparison of cage application modality in posterior lumbar interbody fusion with posterior instrumentation – A finite element study. *Medical Engineering and Physics*, Volume 31, pp. 565-570.

Urban, J. & Roberts, S., 2003. Degeneration of the intervertebral disc. *Arthritis Reseach & Therapy*, 5(3), pp. 120-130.

Urban, J., Roberts, S. & Ralphs, J., 2000. The nucleus of the intervertebral disc from development to degeneration. *American Zoology*, Volume 40, pp. 53-61.

Van Ee, C. A., Nightingale, R. W., Camacho, D. L. & Chancey, V. C., 2000. Tensile Properties of the Human Muscular and Ligamentous Cervical Spine. *44th Stapp Car Crash Conference*, Volume 44, pp. 85-102.

van Tulder, M., Tuut, M., Pennick, V. & et al., 2004. European Guidelines for the Management of Acute Nonspecific Low Back Pain in Primary Care. *Spine*, 14 June, 29(17), pp. E357-362.

Vazquez-Seoane, P. et al., 1993. Interference screw fixation of cervical grafts. A combined in vitro biomechanical and in vivo animal study. *Spine*, 18(8), pp. 946-954.

Viidiik, A., Sandqvist, L. & Magi, M., 1965. Influence of postmortal storage on tensile strength characteristics and histology of rabbit ligaments. *Acta Orthop. Scand.*, Volume Suppl. 79, p. 38 pp.

Von Forell, G. A. & Bowden, A. E., 2014. Biomechanical implications of lumbar spinal ligament transection. *Comput Methods Biomech Biomed Engin*, 17(15), pp. 1685-1695.

Wan, C. et al., 2015. An update on the constitutive relation of ligament tissues with the effects of collagen types. *J Mech Behav Biomed Mater*, Volume 50, pp. 255-267.

Wang, J., Shirazi-Adl, A. & Parnianpour, M., 2005. Search for critical loading condition of the spine- A meta analysis of a nonlinear viscoelastic finite element model. *Computer Methods Biomech Biomed Eng*, Volume 8, pp. 323-330.

Wang, Y., Liu, T., Song, L.-S. & al., e., 2016. Anatomical Characteristics of Deer and Sheep Lumbar Spines: Comparison to the Human Lumbar Spine. *Int. J. Morphol.*, 33(1), pp. 105-112.

Waters, R. & Morris, J., 1973. An in vitro study of normal and scoliotic interspinous ligaments. *J Biomechanics*, Volume 6, pp. 343-348.

Weiler, C. et al., 2012. Age-related changes in human cervical, thoracic and lumbar intervertebral disc exhibit a strong intra-individual correlation. *Eur Spine J.*, 21(6), p. 810–818.

Weingarten, V. I., 1994. The controversy over hex or tet meshing. *Mach. Des.*, Volume 66, pp. 74-78.

Weiss, J. & Gardiner, J., 2001. Computational modelling of ligament mechanics. *Critical Reviews in Biomedical Engineering*, 29(3), pp. 303-371.

Weiss, J. et al., 2005. Three-dimensional finite element modelling of ligaments: technical aspects. *Med Eng Phys*, Volume 27, pp. 845-861.

Weiss, J., Schauter, D. & Gardiner, J., 1996. Modelling contact in biological joints using penalty and augmented Lagrangian methods. *Proc ASME Winter Annual Meeting*, Volume BED-33, pp. 47-48.

Westermann, R. W., Wolf, B. & Elkins, J. M., 2013. Effect of Acl Reconstruction Graft Size on Simulated Lachman Testing: A Finite Element Analysis. *Iowa Orthop J.*, Volume 33, pp. 70-77.

White III, A. & Panjabi, M., 1990. *Clinical biomechanics of the spine*. 2nd Edition ed. Philadelphia, USA: Lippincott Williams & Wilkins.

White, A. & Panjabi, M., 1990. *Clinical Biomechanics of the Spine*. Philadelphia, PA: Lippincot.

Whyne, C., Hu, S. & Lotz, J., 2003. Burst fracture in the metastatically involved spine: development, validation and parametric analysis of a three-dimensional poroelastic finite-element-model. *Spine*, Volume 28, pp. 652-660.

Wilcox, R. et al., 2004. A dynamic investigation of the burst fracture process using a combined experimental and finite element approach. *Eur Spine J*, Volume 13, pp. 481-488.

Wilke, H., Claes, L., Schmitt, H. & Wolf, S., 1994. A universal spine tester for in vitro experiments with muscle force simulation. *European Spine Journal*, Volume 3, pp. 91-97.

Wilke, H. J. et al., 1999. New in vivo measurements of pressures in the intervertebral disc in daily life.. *Spine (Phila Pa 1976)*, 24(8).

Wilke, H. -J., Kettler, A. & Claes, L., 1997. Are sheep spines a valid biomechanical model for human spines?. *Spine (Phila Pa 1976)*., 22(20), pp. 2365-2374.

Wilke, H., Kettler, A., Wenger, K. & Claes, L., 1997. Anatomy of the sheep spine and its comparison to the human spine. *Anat Rec*, 247(4), pp. 542-555.

Williams, P. e., 1995. *Gray's Anatomy*. 38th ed. Edinburgh: Churchill Livingstone.

Wong, C., Gehrchen, P., Darvann, T. & Kiaer, T., 2003. Nonlinear finite-element analysis and biomechanical evaluation of the lumbar spine. *IEEE Transactions on Medical Imaging*, 22(6), pp. 742-745.

Woo, S.-Y. et al., 1983. Measurement of mechanical properties of ligament substance from a bone-ligament-bone preparation. *J Orthop Res*, Volume 1, pp. 22-29.

Woo, S.-Y. et al., 1987. The biomechanical and morphological changes in the medial collateral ligament healing of the rabbit after immobilisation and remobilisation. *J Bone Joint Surg*, 69(A), pp. 1200-1211.

Woo, S. L.-Y. & Buckwalter, J., 1988. *Injury and repair of the musculoskeletal soft tissues*. Park Ridge IL, American Academy of Orthopaedic Surgeons.

Woo, S.-Y., Weiss, J., Gomez, M. & Hawkins, D., 1990. Measurement of changes in ligament tension with knee motion and skeletal maturation. *ASME J Biomech Eng*, 112(1), pp. 46-51.

Yahia, L. & Drouin, G., 1990. Study of the hysteresis phenomenon in canine anterior cruciate ligaments. *J Biomed Eng*, Volume 12, pp. 57-62.

Yamamuro, T. et al., 1990. Replacement of the lumbar vertebrae of sheep with ceramic prostheses. *J Bone Joint Surg Br*, 72(5), pp. 889-893.

Yamashita, T. et al., 1996. A morphological study of the fibrous capsule of the human lumbar facet joint. *Spine (Phila Pa 1976)*, 21(5), pp. 538-543.

Yoganandan, N., Pintar, F. & Butler, J., 1989. Dynamic Response of Human Cervical Spine ligaments. *Spine*, 14(10), pp. 1102-1110.

Yoon, K. H. et al., 2010. Biomechanical evaluation of double bundle augmentation of posterior cruciate ligament using finite element analysis. *Clini Biomech*, 25(10), pp. 1042 - 1046.

Yoshida, M. et al., 1992. Hypertrophied ligamentum flavum in lumbar spinal-canal stenosis—pathogenesis and morphologic and immunohistochemical observation. *Spine*, Volume 17, pp. 1353-1360.

Yu, J. et al., 2007. Microfibrils, elastic fibres and collagen fibres in the human intervertebral disc and bovine tail disc. *Journal of Anatomy*, Volume 210, pp. 460-471.

Zapata-Cornelio, F. Y. et al., 2017. Methodology to Produce Specimen-Specific Models of Vertebrae: Application to Different Species. *Ann Biomed Eng*, p. Ann Biomed Eng.

Zhang, L., Yang, G., Wu, L. & Yu, B., 2010. The biomechanical effects of osteoporosis vertebral augmentation with cancellous bone granules or bone cement on treated and adjacent nontreated vertebral bodies: a finite element evaluation. *Clinical Biomechanics*, 25(2), pp. 166-172.



## **Appendix A**

### **Conference Abstracts**

The work in this thesis has been presented at the following international conferences:

- EUROMECH Colloquia: Advanced Experimental Methods in Tissue Biomechanics, 12 – 16 February 2017, Burg Warberg, Germany
- ORS 2017 Annual Meeting, 19 – 22 March 2017, San Diego, USA

## A.1 Abstract for EUROMECH Colloquia

### Mechanical Characterisation of Spinal Ligaments using Finite Element Analysis

A. Bint-E-Siddiq<sup>1\*</sup>, V.N. Wijayathunga<sup>1</sup>, M. Mengoni<sup>1</sup>, A.C. Jones<sup>1</sup>, R.K. Wilcox<sup>1</sup>

<sup>1</sup>Institute of Medical & Biological Engineering, School of Mechanical Engineering, University of

Leeds, Leeds, UK

\*mnabes@leeds.ac.uk

#### Introduction

The spinal ligaments provide passive stability to spine, particularly the anterior longitudinal ligament (ALL) plays a major mechanical role within the physiological range of motion in extension [1]. Previous studies have developed linear [2] or bilinear material [3] properties for the ALL directly from force-displacement data, using mean values for cross sectional area and length. The aim of this study was to uniquely combine experimental and computational approaches to mechanically characterise the ligamentous spinal structures using a specimen-specific modelling approach.

#### Methods

**Experimental work:** Three human thoracic spines, obtained with ethical approval, were dissected into functional spinal units (FSUs) with the posterior elements removed and imaged under micro computed tomography ( $\mu$ CT), using a radiopaque gel painted onto the surface of the ligaments to aid in visualising the structure. The specimens were carefully sectioned through the disc to leave only the ALL intact. A tensile testing machine (3365, Instron, UK) was used to test the FSUs under displacement-controlled tension (Fig. 1) to obtain load displacement data.

**Computational work:** The  $\mu$ CT image data from each FSU was exported to an image processing package (Scan IP, Simpleware, UK). Using a combination of thresholding, morphological closing & dilation, smoothing, and manual segmentation, the ALL and bone were segmented and used to generate a specimen-specific finite element (FE) model of the ligament and bony attachments. Ogden Hyper-elastic material model was used to represent the ligament behaviour, making a first guess of the parameters for the material models, using mean cross sectional area (CSA) and length (L), with the assumption that ligament is a uniaxial structure and iteratively changing those parameters until a best fit to the experimental load-displacement data was found (Table 1).

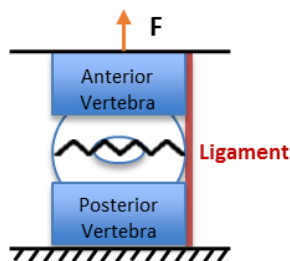


Fig. 1: Experimental setup

Table 1 : Hyper-elastic material model constants.

Specimen	Pre-optimisation			Post-optimisation		
	Mu/GPa	alpha	D/GPa <sup>-1</sup>	Mu/GPa	alpha	D/GPa <sup>-1</sup>
1: T2-3	3.9E-04	6.3	2339	7.9E-04	9.4	1170
1: T4-5	7.4E-04	5.6	1244	9.9E-04	7.9	933
2: T2-3	1.4E-03	3.0	682	1.9E-03	3.8	477
2: T4-5	1.6E-03	5.1	559	3.0E-03	7.4	308
2: T8-9	1.5E-03	6.6	602	1.5E-03	9.2	602
3: T4-5	1.5E-03	4.9	596	4.4E-03	8.3	209
3: T6-7	1.8E-03	6.2	522	3.9E-03	8.9	235

#### Results

Results from experimental tests showed the characteristic non-linear behaviour of the ALL. There was poor agreement between the material parameters derived from FE models and those derived by assuming a mean CSA and L. Therefore taking into account the geometry of the specimen, through calibration of a finite element model, has a substantial effect on derived material properties. The material parameter values were found to be more consistent within spine than between spines.

#### Conclusion

This work demonstrates that a specimen-specific image-based approach needs to be applied to derive the elastic properties of the ligaments. The study marks a step change from the current state-of-art where ligament properties are derived from widely varying data in literature, and will enable the mechanical contribution of the ligaments to be more realistically represented in future FE models.

#### References

- [1] Sharma M., et al. *Spine (Phila Pa 1976)*, 20(8): 887-900, 1995
- [2] Tsuang Y.-H., et al. *MED ENG PHYS*, 31: 565-570, 2009
- [3] Moramarco V., et al. *JBiomech*, 43: 334-342, 2010

## A.2 Abstract for ORS

### Characterisation and Comparison of Human and Ovine Spinal Ligaments

Ayesha Bint-E-Siddiq<sup>1</sup>, Vithanage N. Wijayathunga<sup>1</sup>, Marlène Mengoni<sup>1</sup>, Alison C. Jones<sup>1</sup>, Ruth K. Wilcox<sup>1</sup>

<sup>1</sup>Institute of Medical and Biological Engineering, School of Mechanical Engineering, University of Leeds, Leeds, UK

**Disclosures:** Ayesha Bint-E-Siddiq (N), Vithanage N. Wijayathunga (N), Marlène Mengoni (N), Alison C. Jones (N), Ruth K. Wilcox (N)

**INTRODUCTION:** Ovine spine models are commonly employed in preclinical research studies as a precursor to clinical trials for the evaluation of interventions and devices. The spinal ligaments provide passive stability to the spine, particularly the anterior longitudinal ligament (ALL) and posterior longitudinal ligament (PLL) play a major mechanical role within the physiological range of motion in extension and flexion respectively [1]. Anatomically, the vertebral geometry of ovine spine has been shown to be favourably comparable with that of human [2, 3]. However, limited studies have been conducted to characterise the mechanical properties of ovine spinal ligaments to justify the use of ovine spine as an alternative model for the human spine. Moreover, previous studies have derived linear [4] or bilinear [5] material properties for the ALL and PLL directly from force-displacement data, using mean values for cross sectional area (CSA) and length (L), and these values have been used extensively in finite element models of the spine for the analysis of clinical interventions [4, 6]. The aim of this study was to develop a methodology to test and compare the stiffness of human and ovine spinal ligaments and to uniquely combine experimental and computational approaches to mechanically characterise the ligamentous spinal structures using a specimen-specific finite element (FE) modelling approach.

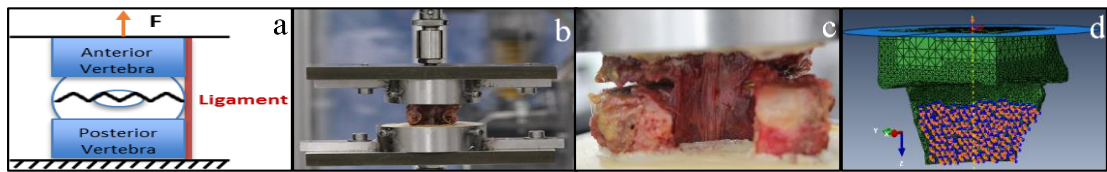
**METHODS:** Thoracic section of three ovine and three human spines, obtained with ethical approval, were dissected into functional spinal units (FSUs). These were imaged under micro computed tomography ( $\mu$ CT) with the posterior elements removed and a radiopaque gel painted onto the surface of the ligaments to aid in visualising the morphology. The FSUs were carefully sectioned through the disc to leave only either the ALL or the PLL intact (Fig 1 (a)). A tensile testing machine ( $\pm 500$ N Load cell, 3365, Instron, UK) was used to test the FSUs under displacement-controlled tension (Fig. 1 (b)) to obtain load-displacement data. A systematic data analysis method [7] was used in order to consistently extract the stiffness of the ligaments giving initial 'toe region' ( $k_1$ ) and final 'linear region' ( $k_2$ ) values. In order to derive the material properties of the human ALL, the  $\mu$ CT image data from each FSU was analysed with an image processing package (Scan IP, Simpleware, UK) to segment the ligament and bone and a specimen-specific FE model of the ligament and bony attachments was generated (Fig. 1 (d)). The Ogden hyperelastic material model was used to represent the ligament behaviour and boundary conditions representing the experimental setup were applied (Abaqus, SIMULIA, US). Initial values for the material model were derived using mean CSA and L. The material model parameters for each specimen were then iteratively changed until a best fit to the corresponding experimental load-displacement data was found.

**RESULTS:** The experimental load-displacement data showed the characteristic non-linear behaviour of ligaments for both the ALL and PLL, with the ALL being stiffer and stronger. Values for  $k_1$  and  $k_2$  for the ovine ALL and PLL ( $n=6$  each) and human ALL and PLL ( $n=7$  each) are shown in Fig. 2. There was a statistically significant difference ( $p<0.05$ ) between the human and ovine linear region stiffness. There was poor agreement between the material parameters derived from FE models and the initial values derived by assuming uniaxial behaviour (Table 1). The material parameter values were found to be more consistent within each spine than between spines.

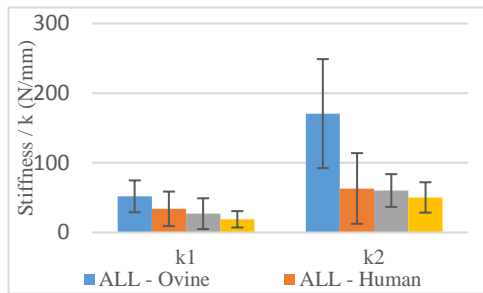
**DISCUSSION:** The main aim of this study was not only to characterise the spinal ligaments but also to compare the stiffness data obtained across ovine and human specimens. Whilst there was considerable variation in the results, the stiffness of the ALL for ovine specimens was found to be higher than for the human specimens. This may have implications for the use of ovine models for preclinical testing of devices such as spinal stabilisation devices, where the greater stiffness may increase the stability and reduce the risk of component movement compared to the human spine. Therefore, the differences in the material properties between human and ovine ligaments should be borne in mind when making a transition from the ovine model to the human spine. A methodology for characterizing the mechanical properties of spinal ligaments was also developed and applied to the ALL. This work demonstrates that a specimen-specific image-based approach needs to be applied to derive the elastic properties of the ligaments due to its non-uniform shape and cross-sectional area. To the author’s knowledge this is the first study to characterize ovine spinal ligaments and compare them with the human.

**SIGNIFICANCE:** This work demonstrates the mechanical differences, in terms of stiffness, between ovine and human spinal ligaments, which might have implications on the use of ovine for pre-clinical testing. The study marks a step change from the current state-of-art where ligament properties are derived from widely varying data in literature, and will enable the mechanical contribution of the ligaments to be more realistically represented in future FE models.

**REFERENCES:** [1] Sharma et al., Spine (Phila Pa 1976), 1995. 20(8):p.887-900. [2] Wilke et al., Spine, 1997. 22(20):p.2365-2374. [3] Mageed et al., Lab Anim Res, 2013. 29(4):p.183-189. [4] Tsuang et al., Med Eng Phys, 2009. 31:p.565-570. [5] Moramarco et al., JBiomech, 2010. 43:p.334-342. [6] Bellini et al., J Spinal Disord Tech, 2007. 20(6):p.423-429. [7] Herbert et al., JBiomech, 2016. 49(9):p.1607-1612. [8] Ogden et al., Proc. R. Soc. Lond., 1999. 455(A):p.2861-2877.



**Figure 1: Experimental setup: schematic of lateral view (a), posterior view (b), stretched ligament (c), and the computational Model (d).**



**Figure 2: Comparison of Mean Bilinear Stiffness for ALL and PLL.**

**Table 1: Material model constants for the human ALL.**

Specimen	Assuming constant CSA and L			Derived from FE model		
	Mu/GPa	alpha	D/GPa <sup>-1</sup>	Mu/GPa	alpha	D/GPa <sup>-1</sup>
1: T2-3	3.9E-04	6.3	2339	7.9E-04	9.4	1170
1: T4-5	7.4E-04	5.6	1244	9.9E-04	7.9	933
2: T2-3	1.4E-03	3.0	682	1.9E-03	3.8	477
2: T4-5	1.6E-03	5.1	559	3.0E-03	7.4	308
2: T8-9	1.5E-03	6.6	602	1.5E-03	9.2	602
3: T4-5	1.5E-03	4.9	596	4.4E-03	8.3	209
3: T6-7	1.8E-03	6.2	522	3.9E-03	8.9	235